OBJECT POSITIONING TECHNIQUES: PERFORMANCE ANALYSIS AND EFFICIENT SOLUTIONS

A Dissertation

presented to

the Faculty of the Graduate School

at the University of Missouri

In Partial Fulfillment

of the Requirements for the Degree

Doctor of Philosophy

---

by

Liyang Rui

Dr. Dominic K. C. Ho, Dissertation Supervisor

Dec 2015

The undersigned, appointed by the Dean of the Graduate School, have examined the dissertation entitled:

OBJECT POSITIONING TECHNIQUES:
PERFORMANCE ANALYSIS AND EFFICIENT SOLUTIONS

presented by Liyang Rui,
a candidate for the degree of Doctor of Philosophy and hereby certify that, in their opinion, it is worthy of acceptance.

Dr. Dominic K. C. Ho

Dr. Henry Zhihai He

Dr. Justin Legarsky

Dr. Yi Shang

ACKNOWLEDGMENTS

I would like to gratefully acknowledge everyone who made this dissertation possible. First I would like to sincerely thank my supervisor, Dr. Dominic K.C. Ho, for his priceless and invaluable guidance in my academic research. I have learned a lot from him on signal processing theory, research skills and how to manage time efficiently. I also have learned from him on being an cautious, careful, and responsible person. Under his guidance, I have published a few high-quality research papers and successfully presented my work in some worldwide famous conferences.

I would also like to express my sincere gratitude to my committee members Dr. Zhihai He, Dr. Justin Legarsky, and Dr. Yi Shang. Thank you for your invaluable time for reviewing my dissertation and important feedback for polishing this dissertation. I would like to thank all of my labmates, Ming Sun, Le Yang, Zhenhua Ma, Shanjie Chen, Yue Wang, and Bo-Yu Su, for your valuable suggestions of my research in the last five years.

At last, I would like to thank my parents and my girlfriend, Leanna. Without your support, I would not be able to finish this dissertation.

TABLE OF CONTENTS

LIST OF TABLES

Table Page

LIST OF FIGURES

Figure Page

ABSTRACT

Object positioning is an important research which has been applied in many application areas for decades. Usually, a number of spatially separated observers capture a set of range or angle based measurements, and then estimate the object location based on the measurements. The problem is not trivial because of the high non-linearity between the measurements and the object position. The performance of a localization system mainly depends on two factors. One is the measurement type and the other is the estimator which explores the non-linear measurement equations to estimate the object position. This research investigates the positioning techniques from these two aspects.

First, we analyze the localization performance of the common positioning approaches, such as time of arrivals (TOA), time differences of arrival (TDOA) and angle of arrivals (AOA). We theoretically derive the biases of their Maximum Likelihood (ML) object location estimates resulted from the Gaussian measurement noise and observer position errors. The derived formulas show that the two types of errors contribute inter-related bias components unless they are independent and identically distributed (IID). The bias behaviors of the three positioning approaches are contrasted and the geometric conditions under which the location bias becomes zero are elaborated. The effectiveness of the developed results for bias compensation in improving the performance of object tracking is illustrated. The study is then extended to elliptic positioning, which is recently received attentions because of its asynchronous operation capability. We characterize its performance with respect to TDOA based on the Cramer-Rao Lower Bound (CRLB) and the bias of the ML ob-

ject location estimate under Gaussian measurement noise as well as transmitter and observer position errors. When the observer positions are controllable, we derive its optimum observer placement to improve the localization accuracy. Its performance study is demonstrated by simulation.

Second, we propose efficient solutions for three challenging positioning problems. The basic idea is to use parameter transformation and multi-stage processing to convert the original non-linear estimation problem into multiple sequential linear estimation problems. One example is the joint localization and synchronization problem in a wireless sensor network (WSN) when Gaussian beacon position and clock uncertainties are present. Two computationally efficient closed-form algorithms are developed to explore the time stamp information from message exchanges within the WSN. One is for the case without message exchanges among the sensor nodes and the other is with the exchanges. The proposed algorithms are proved by theoretical analysis and simulations to reach the CRLB accuracy for the sensor node positions and the clock parameters over the mild error region. The second problem addressed is the multistatic sonar localization when the uncertainties in the signal propagation speed and the transmitter and receiver positions are present. The proposed efficient algorithms for this problem obtains the hybrid CRLB over the mild error region as shown by the analysis and simulation. The last problem is for object localization in the relay network. Comparing to traditional problems, additional ambiguity exists because the measurements are collected along time without the knowledge of their corresponding relays. A Markov Chain Monte Carlo method, Metropolis-Hastings algorithm, is applied to solve the measurement association problem to avoid the high computation burden in the traditional brute-force method. The ML object location estimate is

iteratively obtained by the alternating minimization principle. The proposed method has shown good performance under the mild noise level in the simulation.

Chapter 1

Introduction

1.1 Background and Motivation

Object positioning is a fundamental problem in many application areas such as radar [1, 2, 3], sonar [4, 5], wireless communications [6, 7] and wireless sensor networks (WSNs) [8, 9, 10]. The general localization approach is to obtain certain measurements by a number of spatially separated observers and then determine the unknown object position by solving the set of measurement equations.

The common measurement types are time of arrivals (TOAs) [8, 11], elliptic measurement, time differences of arrival (TDOAs) [12, 13, 14], and angle of arrivals (AOAs) [8, 15]. The TOA positioning has been widely used in wireless communication and WSN localization, where the object to be located is synchronized with the observers and interchanges messages with them [16]. Two-way ranging used in radar and Ultra-wideband (UWB) localization [1, 8] can eliminate the synchronization re-

quirement. In the absence of measurement noise, the TOAs are proportional to the distances between the object and the observers up to a constant propagation speed. Each TOA induces a circular locus, which is centered at the observer, for the object. The intersection of all circles gives the object position estimate.

Unlike TOA, the elliptic positioning employs an extra transmitter to locate the object. It can work in either synchronous or asynchronous manner. Synchronous elliptic (SE) positioning is adopted in multistatic radar [1, 3], MIMO radar [17, 18], radio communications [19] and UWB network localization [20] where the transmitter and observers are synchronous. Many techniques, e.g. [16], are available to obtain the SE time measurements, which is equal to the time delay from the transmitter via the object to the observer. Asynchronous elliptic (AE) positioning has been applied to sonar [4] and UWB localization [20] with numerous successes. It is very flexible in the sense that no synchronization between the transmitter and an observer, or among the observers is needed. The time measurement in this case is the arrival time difference between the indirect signal reflected/relayed from the object and the direct signal from the transmitter. It can be obtained simply by auto-correlating the signal at a receiver [16], or by estimating the indirect and direct arrival times with respect to a local receiver clock and subtracting them [20]. The asynchronous mode is an important advantage of elliptic positioning over TOA and TDOA [4, 20, 21]. The measurements in SE and AE trace out ellipsoids. Each transmit-receive pair corresponds to an ellipsoid and their intersection yields the object position estimate.

TDOA is mostly used for passive and non-cooperative positioning where it is not possible to synchronize the observers with the signal source (e.g., the object in the TOA positioning) [4, 19, 20]. It requires the observers be synchronized in order to

obtain accurate arrival time difference between two received signals [16]. When there is no measurement noise, the TDOA forms a hyperbolic surface with foci at the two related observers and the intersection of hyperboloids fixes the object position.

Rather than observing distance information, AOA positioning is a type of angle based 2 dimensional (2D) localization method. It measures the angle from the object to the observer. The object lies at the intersection of the angle lines from the observers. The AOA measurement can be obtained by using calibrated sensor arrays or directional antennas employed by the observers.

All of the aforementioned measurements are nonlinear with respect to the unknown object position. In the past few decades, many algorithms have been proposed to exploit those nonlinear measurements and estimate the object location. Perhaps, the maximum likelihood estimator (MLE) [22] is the most well known one because of its asymptotic efficiency. Usually, it is realized by gradient based iterative procedure [8, 23], which has a potential divergence drawback [24]. To avoid carefully picking the initial guess in MLE, the closed-form multi-stage processing estimators have been developed. The first one [25] was proposed to solve the TDOA positioning and is well known for its optimum performance. It has been extended to TOA [26], joint TDOA / frequency differences of arrival (FDOA) [27], and elliptic [19] positionings. They are all shown to be optimum for Gaussian noise. Furthermore, the recent work [28] extended the multi-stage processing estimator to address additional uncertainties in the localization problem, such as observer position errors.

These positioning approaches have different complexities and accuracies and one may be preferable than the others depending on the applications and environment. Fundamental investigation on their performance attracts numerous interests over the

past few decades [7, 8, 15, 29]. The performance is usually characterized by the Mean-square error (MSE) [22] which is the expectation of the sum of the squared differences between the coordinates of an object position estimate and the actual. It is the superposition of the variance and the bias square. When the noise level is small, the variance dominates and the bias is negligible. The Cramer-Rao Lower Bound (CRLB) sets fundamental limits on estimation accuracy since it gives the best achievable accuracy on the variance of any linear unbiased estimator [22]. The CRLBs of th e four positioning approaches under Gaussian measurement noise has been derived in [7, 8, 15, 20]. [29] compared the CRLBs of TOA and TDOA when all TOA measurement noises are independent and identically distributed (IID). It demonstrated that TDOA is inferior to the TOA. The authors in [7] considered this comparison under non-IID measurement error condition. The CRLB of AOA was derived in [15] and served as a benchmark to evaluate the performance of its Maximum Likelihood (ML) object position estimator. [8] studied the CRLBs of TOA and AOA in the WSN localization problem. The references [30, 31, 32] used the CRLBs to find the optimum localization geometries of TOA, TDOA and AOA positionings. The derived geometries provide the minimum achievable MSEs for their corresponding positioning approaches when the bias is negligible. All of these works analyzed the localization performance based on CRLB and neglected the bias in the object position estimate, which has been demonstrated to be a non-negligible issue when several successive sets of measurements are obtained even if the noise power is small, such as UWB localization [33] and tracking [34, 35, 36]. To prevent the performance degradation caused by bias, [37] applied the constrained least-squares estimators for TOA and TDOA positionings while [33] eliminated the bias of the classic location

estimator [25] by the total least-squares technique. Ho [13] developed two advanced methods over [33], BiasSub and BiasRed, where BiasSub subtracts the expected bias from the object position estimate, and BiasRed imposes a quadratic constraint on the expanded parameter space to decrease the bias. Gavish and Weiss [15] derived the theoretical biases of the MLE and the Stansfield estimator in the AOA positioning. They concluded the Stansfield estimator has a much larger amount of bias than the MLE. A bias compensation method in MLE was proposed in [38], where the expected bias was derived through combining Taylor series expansion and Jacobian matrix utilization. It has been shown having good performance in TOA positioning, but is limited to the independent Gaussian measurement noise only. Apart from the research in the engineering field, some statisticians have investigated the bias of the MLE for a general estimation problem [39, 40, 41, 42]. Their methods were generalized in [43, 44] for geodetic and geophysical data analysis. These studies are not from an engineering point of view and may not be easy to apply. Also, the optimum geometries for the positioning approaches in [30, 31, 32] are based on the CRLB only while the bias under these "optimal" geometries is still unknown. This motivates us to theoretically analyze and compare the bias behaviors of TOA, TDOA and AOA positionings. The elliptic positioning is relatively less investigated comparing to TOA and TDOA. The performance characterization of the elliptic positioning with respect to TDOA, in terms of CRLB and bias, are necessary because they both have been implemented in [4, 5, 19, 20]. Furthermore, the optimum geometry in the elliptic positioning is an interesting question to be addressed.

Recently, the classic closed-form multi-stage processing method has been extended to solve the problem of joint localization and synchronization of sensor nodes in a

WSN [45, 46]. The two proposed methods show promising performance when beacon positions and clocks are perfectly known. In practice, they may contain uncertainties even when they are equipped with GPS technology. Zheng and Wu [47] applied the generalized total least-squares (GTLS) [48] algorithm to take into account the beacon uncertainties. Its performance, however, is not able to achieve CRLB. It is developed to localize and synchronize one sensor with multiple beacons and does not use message exchanges among the sensor nodes. It also ignores the improvements that can be gained from the message exchanges of the sensor nodes with the same beacons because they will encounter the same uncertainties in the beacon positions and clock values. Furthermore, GTLS requires computationally demanding eigen-decomposition which could be prohibitive in some applications. These problems drive us to find accurate and efficient closed-form algorithms.

The elliptic positioning approach has been widely applied in multistatic sonar system [4, 5, 49, 50, 51]. The currently proposed algorithms [17, 19, 20, 21, 52] are for the radar and WSNs which are not appropriate for the multistatic sonar localization problem because of the complex ocean environments. One challenge is that the floating receivers tend to drift with the currents and their available positions are not accurate. The transmitter positions often have uncertainties as well, such as in the case of airborne multistatic sonar where the sensors are deployed from an aircraft. The traditional studies [4, 49, 50] considered the position uncertainties but ignored the uncertainty of the acoustic signal propagation speed [53, 54] in the underwater environment, which is another important factor to be considered [5, 51]. The researches [5, 51, 55, 56] derived the object position estimate by utilizing the statistical knowledge of the signal propagation speed. They are not applicable when

the statistical model of the signal propagation speed is not accurate or even not known. [57, 58, 59] investigated the TDOA localization problem with unknown signal propagation speed and developed joint estimation algorithms of the object position and propagation speed. The performance, however, is not optimum. Efficient closed-form estimator for multistatic sonar localization is not available in literature.

In the harsh indoor environment, range and angle measurement accuracies may be dramatically deteriorated due to the non light of sight (NLOS) channels [60]. The UWB signal offers attractive abilities to resolve multipath and provide highly accurate range measurements. Many methods have been published to detect the NLOS channel [61, 62]. However, only a few works focus on the benefit by exploring the information embedded in the indirect transmission paths [63, 64]. In [63, 64], the UWB localization systems which only have one anchor are proposed. They use the known floor plan to define the set of signal reflection points as virtual anchors. In addition to the direct measurement, the indirect range measurements, which are from the anchor through the virtual anchors to the object, are used to estimate the object position. Meissner, et al, further extended their work to the object tracking case [65]. The idea has been validated by real world experiments [66]. Similar ideas have been applied in the UWB relay networks to enhance the localization coverage by introducing the relay nodes as secondary active anchors [67, 68, 69]. All of the above methods assume the object and the anchor are well clock synchronized. Also, the number of virtual anchors or relays are not large so that it is not hard to associate the indirect range measurement to its corresponding virtual anchors or relays. Decarli [70] proposed a grid search algorithm to solve them under the ML criterion. However, its computation burden and estimation accuracy significantly depend on the grid resolution.

1.2 Contributions of the Research

The contributions of this research are five-folds.

First, it analytically studies the bias for the ML object location estimate of TOA, TDOA and AOA positioning approaches under Gaussian noise. The study considers a practical and generalized scenario where both measurement noise and observer position errors are present. The effects of measurement noise and observer position error on the overall bias are contrasted. The bias behaviors of the three positioning approaches are compared and the geometries which result in zero location bias are derived. The analysis results indicate that the geometries that yield zero bias will also achieve minimum variance. Furthermore, the applicability of the developed theoretical results to compensate the bias is validated in a multiple observer object tracking problem when both measurement noise and observer position errors are present.

Second, the performance of elliptic localization is fundamentally investigated with respect to the TDOA positioning. Both SE and AE positioning systems are evaluated through the CRLB analysis under Gaussian noise. The study is comprehensive by taking into account the transmitter and receiver position errors as well as measurement noise. The effect of sensor position errors to the performance of different types of elliptic positioning is theoretically analyzed and evaluated by simulation. To complement the CRLB study, we also evaluate the bias of ML object position estimate of elliptic positioning. The investigation is further advanced to the optimum receiver placement analysis with respect to a single transmitter that minimizes the localization error.

Third, the problem of jointly locating and synchronizing multiple sensor nodes in a WSN is addressed. We have developed computationally attractive closed-form solu-

tions for the problem. The main idea is to introduce auxiliary variables and nonlinear transformations to form pseudo linear equations that can be solved globally and efficiently through weighted least-squares (WLS) minimization. Multi-stage processing is used to exploit the auxiliary variables to refine the unknowns to be estimated. The solutions do not require initialization and are shown to guarantee the CRLB accuracy under IID Gaussian measurement noise and beacon uncertainties.

Fourth, the optimum localization of an object using multistatic sonar in the presence of uncertainties in the transmitter and receiver positions, as well as in the signal propagation speed is addressed. Two estimators were developed when using the time measurements, one is with the statistical knowledge of the propagation speed and the other is without. They have closed-forms and are derived through parameter transformation and multi-stage processing. Analysis shows that they achieve the hybrid CRLB performance in Gaussian noise over the small error region. The two estimators were extended to include the bearing measurements to improve the localization accuracy. Simulations collaborate the theoretical performance of the proposed estimators.

Fifth, we have developed an efficient solution to the relay network localization problem based on iterative minimization method. It solves the measurement association problem and object location estimation iteratively. The Metropolis-Hastings algorithm is employed to simulate the probability distribution of the measurement association plan and avoid the huge computation burden in the brute force method. The MLE is applied to estimate the object position given the measurement association results. The performance of the proposed algorithm has been shown to be close to the CRLB accuracy for Gaussian noise over the small error region.

1.3 Content Organization

The rest Chapters are organized as follows. Chapter 2 introduces preliminary concepts of positioning approaches and location estimators. Chapter 3 presents the investigation of the bias behaviors of the TOA, TDOA and AOA positionings. Chapter 4 fundamentally investigates the performance of elliptic positioning, both synchronous and asynchronous, with respect to TDOA positioning. The proposed closed-form solutions for joint localization and synchronization of multiple sensor nodes in a WSN are presented in Chapter 5. Chapter 6 proposes efficient algorithms to locate an object using the multistatic sonar. Chapter 7 discusses the solution for the relay network localization problem. Chapter 8 summarizes the research.

Chapter 2

Preliminary

2.1 Common Positioning Approaches

We shall consider the localization scenario, which consists of one transmitter at $\mathbf{t}^o$, N receivers at $\mathbf{s}_j^o$, $j = 1, 2, \ldots, N$, and one object to be located at unknown location $\mathbf{u}^o$ as shown in Fig. 2.1. The conditions for multiple transmitters will be explained in Chapters 4. The position vectors $\mathbf{t}^o$, $\mathbf{s}_j^o$ and $\mathbf{u}^o$, $j = 1, 2, \ldots, N$, are all length K Cartesian coordinate vectors, where $K = 2$ for 2D or 3 for 3D localization.

The true transmitter and receiver positions are unknown and their noisy corrupted values are available that

$$\mathbf{t} = \mathbf{t}^o + \mathbf{n}_\mathbf{t}, \qquad \mathbf{s}_j = \mathbf{s}_j^o + \mathbf{n}_{\mathbf{s}_j}\,, \qquad j = 1, 2, \ldots, N\,. \tag{2.1}$$

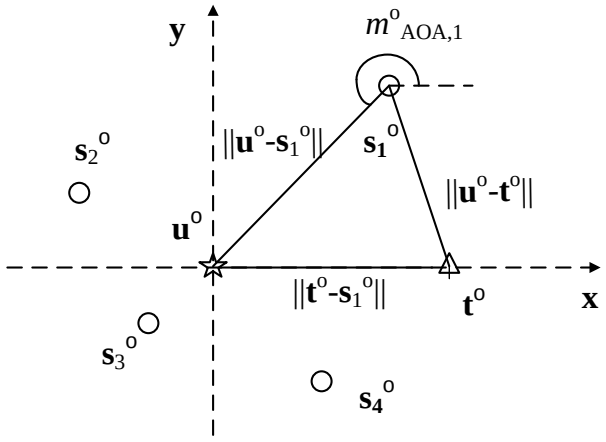

Figure 2.1: An example of typical localization geometry.

Collecting all the receiver positions as a single vector gives

$$\mathbf{s} = \left[\, \mathbf{s}_1^T \,,\, \mathbf{s}_2^T \,,\, \cdots \,,\, \mathbf{s}_N^T \,\right]^T = \mathbf{s}^o + \mathbf{n_s} \,, \tag{2.2}$$

where $\mathbf{s}^o = \left[\, \mathbf{s}_1^{oT}, \mathbf{s}_2^{oT}, \cdots, \mathbf{s}_N^{o\,T} \,\right]^T$. In (2.1) and (2.2), $\mathbf{n_t}$ and $\mathbf{n_s}$ are the vectors of transmitter and receiver position errors. We assume that they are independent with each other and follow Gaussian distributions with zero mean and covariance matrices $\mathbf{Q_t}$ and $\mathbf{Q_s}$ respectively.

Generally, the measurements obtained by the observers can be expressed as a generic vector form

$$\mathbf{m} = \mathbf{m}^o + \mathbf{n_m} \,, \tag{2.3}$$

where $\mathbf{m}^o$ is the vector of true measurement values and $\mathbf{n_m}$ is the noise vector which is assumed to be zero mean Gaussian with covariance matrix $\mathbf{Q_m}$ and independent of $\mathbf{n_t}$ and $\mathbf{n_s}$.

The positioning approaches considered in this research are TOA, elliptic positioning, TDOA (hyperbolic) and AOA. For the range based approaches, we shall use time and range measurements interchangeably in the following until ambiguity occurs because they are differed by a known scaling factor of signal propagation speed.

2.1.1 TOA Positioning

The jth element in the TOA measurement vector $\mathbf{m}_{\mathrm{TOA}}$ relates the object and the receiver j by

$$m_{\mathrm{TOA},j} = m^o_{\mathrm{TOA},j} + n_{\mathrm{TOA},j} = ||\mathbf{u}^o - \mathbf{s}^o_j|| + n_{\mathrm{TOA},j}, \qquad j = 1, 2, \ldots, N, \quad (2.4)$$

where $||*||$ denotes the Euclidean norm. Note that the object directly communicates with the receivers in the TOA positioning and no transmitter is employed.

2.1.2 Elliptic Positioning

Depending on whether the transmitter and receivers are synchronous or not, we have the SE positioning and the AE positioning.

SE Positioning

The SE measurement vector is denoted by $\mathbf{m}_{\mathrm{SE}}$, whose element values are related to the object location $\mathbf{u}^o$ through

$$m_{\mathrm{SE},j} = m^o_{\mathrm{SE},j} + n_{\mathrm{SE},j} = ||\mathbf{u}^o - \mathbf{t}^o|| + ||\mathbf{u}^o - \mathbf{s}^o_j|| + n_{\mathrm{SE},j}, \quad j = 1, 2, \ldots, N. \quad (2.5)$$

Each $m^o_{\mathrm{SE},j}$ creates an ellipsoid with foci at $\mathbf{t}^o$ and $\mathbf{s}^o_j$ that traces out the possible locations of the object.

Another set of measurements available in the SE system is the direct propagation times from the transmitter to the receiver j [19, 20], $j = 1, 2, \ldots, N$. This extra set is denoted by $\bar{\mathbf{m}}_{\mathrm{SE}}$ whose element values are

$$\bar{m}_{\mathrm{SE},j} = \bar{m}^o_{\mathrm{SE},j} + \bar{n}_{\mathrm{SE},j} = ||\mathbf{t}^o - \mathbf{s}^o_j|| + \bar{n}_{\mathrm{SE},j}\ , \qquad j = 1, 2, \ldots, N\,. \tag{2.6}$$

It is reasonable to assume $\mathbf{m}_{\mathrm{SE}}$ and $\bar{\mathbf{m}}_{\mathrm{SE}}$ are independent.

The extra measurement $\bar{\mathbf{m}}_{\mathrm{SE}}$ does not depend on the object position $\mathbf{u}^o$ and it is irrelevant if the transmitter and receiver positions are accurate. In the presence of transmitter and receiver position errors, however, $\bar{\mathbf{m}}_{\mathrm{SE}}$ enhances the localization performance and this will be illustrated in the Chapter 4.

AE Positioning

The measurement vector in this case is $\mathbf{m}_{\mathrm{AE}}$, whose element values have parametric form with the object position $\mathbf{u}^o$ as

$$m_{\mathrm{AE},j} = m^o_{\mathrm{AE},j} + n_{\mathrm{AE},j} = ||\mathbf{u}^o - \mathbf{t}^o|| + ||\mathbf{u}^o - \mathbf{s}^o_j|| - ||\mathbf{t}^o - \mathbf{s}^o_j|| + n_{\mathrm{AE},j}\ , \quad j = 1, 2, \ldots, N\,. \tag{2.7}$$

From (2.5) to (2.7), the SE and AE measurements are related by [4, 20]

$$\mathbf{m}_{\mathrm{AE}} = \mathbf{m}_{\mathrm{SE}} - \bar{\mathbf{m}}_{\mathrm{SE}}\,. \tag{2.8}$$

Typically, the time interval between the arrivals of the direct and reflected/relayed

signals is long enough so that the measurement noise components $\mathbf{n}_{\mathrm{SE}}$ and $\bar{\mathbf{n}}_{\mathrm{SE}}$ are uncorrelated [4, 20, 71]. Hence

$$\mathbf{Q}_{\mathrm{AE}} = \mathbf{Q}_{\mathrm{SE}} + \bar{\mathbf{Q}}_{\mathrm{SE}}\,, \tag{2.9}$$

meaning that AE measurement is noisier than SE, where $\mathbf{Q}_{\mathrm{SE}}$, $\bar{\mathbf{Q}}_{\mathrm{SE}}$ and $\mathbf{Q}_{\mathrm{AE}}$ are the covariance matrices of $\mathbf{n}_{\mathrm{SE}}$, $\bar{\mathbf{n}}_{\mathrm{SE}}$ and $\mathbf{n}_{\mathrm{AE}}$ respectively.

Each AE measurement traces out the same ellipsoid as an SE measurement for the possible object locations when noise is absent. In the presence of noise, the AE ellipsoid is perturbed more than the SE ellipsoid, leading to possibly less localization accuracy than SE positioning.

2.1.3 TDOA Positioning

Without loss of generality, let us choose receiver 1 as the reference for time difference. The TDOA measurement vector $\mathbf{m}_{\mathrm{H}}$ is jointly obtained using the received signals at all receivers whose jth element is

$$m_{\mathrm{H},j} = m^o_{\mathrm{H},j} + n_{\mathrm{H},j} = ||\mathbf{u}^o - \mathbf{s}^o_{j+1}|| - ||\mathbf{u}^o - \mathbf{s}^o_1|| + n_{\mathrm{H},j}\,, \quad j = 1\,,2\,,\ldots\,,N-1\,, \tag{2.10}$$

where $n_{\mathrm{H},j}$ is the TDOA measurement noise at the $(j+1)$th receiver. Each $m^o_{\mathrm{H},j}$ defines a hyperboloid with foci at $\mathbf{s}^o_{j+1}$ and $\mathbf{s}^o_1$ for the object location.

2.1.4 AOA Positioning

The AOA measurement of the object at receiver j with respect to the x-axis is

$$m_{\text{AOA},} = m^o_{\text{AOA},j} + n_{\text{AOA},j} = \arccos\left(\frac{\left(\mathbf{u}^o - \mathbf{s}^o_j\right)^T}{||\mathbf{u}^o - \mathbf{s}^o_j||}\boldsymbol{\rho}_x\right) + n_{\text{AOA},j},\ \ j = 1\,,\,2\,,\,\ldots\,,\,N\,, \tag{2.11}$$

where $\boldsymbol{\rho}_x = [\,1,\,0\,]^T$ is the unit vector along the x-axis.

2.2 Common Estimators

2.2.1 MLE

In general, the principle of MLE is to select the set of parameter values $\boldsymbol{\gamma}^o$ that maximizes the likelihood function of a set of fixed measurement data $\mathbf{h}$ under a specific statistical model. Suppose the statistical relationship between $\mathbf{h}$ and $\boldsymbol{\gamma}^o$ satisfies the additive Gaussian model which is

$$\mathbf{h} = \mathbf{g}\left(\boldsymbol{\gamma}^o\right) + \mathbf{n}, \tag{2.12}$$

where $\mathbf{g}\left(*\right)$ is the nonlinear function relating $\mathbf{h}$ and $\boldsymbol{\gamma}^o$ in the absence of noise and $\mathbf{n}$ is the random noise following zero mean Gaussian with covariance matrix $\mathbf{Q}$. The ML estimate $\hat{\boldsymbol{\gamma}}$ satisfies $\hat{\boldsymbol{\gamma}} = \arg\min\left(J\left(\boldsymbol{\gamma}\right)\right)$, where $J\left(\boldsymbol{\gamma}\right) \triangleq \left(\mathbf{h} - \mathbf{g}\left(\boldsymbol{\gamma}\right)\right)^T \mathbf{Q}^{-1}\left(\mathbf{h} - \mathbf{g}\left(\boldsymbol{\gamma}\right)\right)$. Clearly $\hat{\boldsymbol{\gamma}}$ satisfies

$$\mathbf{p}\left(\hat{\boldsymbol{\gamma}}\right) = \left.\frac{\partial J\left(\boldsymbol{\gamma}\right)}{\partial \boldsymbol{\gamma}}\right|_{\gamma=\hat{\boldsymbol{\gamma}}} = \mathbf{0}\,. \tag{2.13}$$

where $\mathbf{0}$ is the zero column vector with the same length of $\boldsymbol{\gamma}^o$. (2.13) is an important property of the MLE which will be used in the next Chapter.

The ML estimate of $\boldsymbol{\gamma}^o$ can be solved by many ways [22]. The research here investigates the property of the ML estimate and supposes it has been properly obtained.

2.2.2 WLS

Suppose the relationship function $\mathbf{g}(*)$ in (2.12) is linear that it can be rewritten as

$$\mathbf{n} = \mathbf{h} - \mathbf{G}\boldsymbol{\gamma}^o. \tag{2.14}$$

The WLS solution of $\boldsymbol{\gamma}^o$ is [22]

$$\hat{\boldsymbol{\gamma}} = \left(\mathbf{G}^T\mathbf{W}\mathbf{G}\right)^{-1}\mathbf{G}^T\mathbf{W}\mathbf{h}. \tag{2.15}$$

The optimum weighting matrix is given by $\mathbf{W} = \left(\mathrm{E}\left(\mathbf{n}\mathbf{n}^T\right)\right)^{-1}$, where $\mathrm{E}(*)$ represents the expectation computation of $*$. The resulting covariance matrix of the WLS parameter estimate is

$$\mathrm{cov}\left(\hat{\boldsymbol{\gamma}}\right) = \left(\mathbf{G}^T\mathbf{W}\mathbf{G}\right)^{-1}. \tag{2.16}$$

The WLS method (2.15) and (2.16) is equivalent to the MLE in the linear estimation problem (2.14). However, most positioning problems are nonlinear. Hence, the WLS cannot be directly applied to solve the positioning problem. It will be an important component of the multi-stage methods proposed in the following Chapters.

2.3 Common Performance Measures

2.3.1 CRLB

The CRLB provides the best achievable accuracy on the variance of any linear unbiased estimator [22]. Assume the probability density function of a data vector $\mathbf{h}$ on the unknown vector $\boldsymbol{\gamma}^o$, $p(\mathbf{h};\, \boldsymbol{\gamma}^o)$, satisfies $\mathrm{E}\left(\frac{\partial \ln p(\mathbf{h};\boldsymbol{\gamma}^o)}{\partial \boldsymbol{\gamma}^o}\right) = \mathbf{0}$, for all $\boldsymbol{\gamma}^o$. The covariance matrix of any unbiased estimate of $\boldsymbol{\gamma}^o$ follows the inequality that

$$\mathrm{cov}\,(\hat{\boldsymbol{\gamma}}) \succeq \mathrm{CRLB}_{\boldsymbol{\gamma}}, \tag{2.17}$$

where $\succeq$ stands for positive semi-definite and the term $\mathrm{CRLB}_{\boldsymbol{\gamma}}$ is the inverse of Fisher Information Matrix (FIM) which is defined by

$$\mathrm{FIM}_{\boldsymbol{\gamma}} = -\mathrm{E}\left(\frac{\partial \ln p\,(\mathbf{h};\, \boldsymbol{\gamma}^o)}{\partial \boldsymbol{\gamma}^o \partial \boldsymbol{\gamma}^{oT}}\right). \tag{2.18}$$

Given (2.18), the FIM of the general measurement model (2.12) can be derived as

$$\mathrm{FIM}_{\boldsymbol{\gamma}} = \left(\frac{\partial \mathbf{g}(\boldsymbol{\gamma}^o)}{\partial \boldsymbol{\gamma}^{oT}}\right)^T \mathbf{Q}^{-1} \frac{\partial \mathbf{g}(\boldsymbol{\gamma}^o)}{\partial \boldsymbol{\gamma}^{oT}}, \tag{2.19}$$

The CRLB is the inverse of the formula (2.19).

2.3.2 Bias

In statistics, the bias of an estimator is the difference between the expected value of its estimate $\hat{\boldsymbol{\gamma}}$ and the true value of the parameter to be estimated $\boldsymbol{\gamma}^o$, which can be

summarized as

$$\mathbf{b}_{\boldsymbol{\gamma}} = \mathrm{E}\left(\hat{\boldsymbol{\gamma}}\right) - \boldsymbol{\gamma}^{o}. \tag{2.20}$$

The bias in (2.20) depends not only on the positioning approaches, but also the estimation algorithm applied to solve the measurement functions. This research mainly focuses on the bias of the MLE since it is asymptotically efficient and has been widely used in solving the object localization problems.

Chapter 3

Bias Analysis of MLE in TOA, TDOA and AOA Positionings

This Chapter investigates the bias of the ML object location estimate under Gaussian noise in the TOA, TDOA and AOA positionings. First, both measurement noise and sensor position errors are considered [27]. Their effects on the overall bias will be contrasted. Insights about the influences of different positioning approaches on the bias will be elaborated. We next develop the geometric conditions between the object and receivers in which if satisfied could result in zero location bias. Finally, we demonstrate the applicability of the developed theoretical results to compensate the bias in a multiple sensor object tracking problem. The elliptic positioning will be analyzed in the next Chapter. We use the MLE here because it is often fundamentally used as a benchmark for estimation performance.

3.1 Bias Analysis

We shall start from the generic measurement model (2.3) and re-express it as

$$\mathbf{m} = \mathbf{m}^o(\boldsymbol{\gamma}^o) + \mathbf{n}_\mathbf{m}, \tag{3.1}$$

where the vector $\mathbf{m}^o(\boldsymbol{\gamma}^o)$ represents the functional relationship of the expected measurement vector in terms of $\boldsymbol{\gamma}^o$ and $\boldsymbol{\gamma}^o = \left[\, \mathbf{u}^{oT}, \mathbf{s}^{oT} \,\right]^T$ is the parameter vector containing the unknown object and receiver positions. Note that the transmitter is not used in the three positioning approaches used in this Chapter.

Stacking the noisy receiver position vector (2.2) and (3.1) together gives a convenient single vector representation which satisfies (2.12)

$$\mathbf{h} = \mathbf{g}(\boldsymbol{\gamma}^o) + \mathbf{n},$$

where $\mathbf{h} = \left[\, \mathbf{m}^T, \mathbf{s}^T \,\right]^T$, $\mathbf{g}(\boldsymbol{\gamma}^o) = \left[\, \mathbf{m}^o(\boldsymbol{\gamma}^o)^T, ([\, \mathbf{O}_{KN\times K}, \mathbf{I}_{KN} \,]\, \boldsymbol{\gamma}^o)^T \,\right]^T$. The noise vector $\mathbf{n} = \left[\, \mathbf{n}_\mathbf{m}^T, \mathbf{n}_\mathbf{s}^T \,\right]^T$ has covariance matrix $\mathbf{Q} = \mathrm{diag}(\, \mathbf{Q}_\mathbf{m}, \mathbf{Q}_\mathbf{s} \,)$.

We shall use small noise analysis to simplify the bias investigation. In other words, only the noise components up to second order will be maintained and the noise terms of order higher than second will be ignored.

3.1.1 Bias of the MLE

Based on (2.13) in Section 2.3.1, the Taylor series expansion of $\mathbf{p}(\hat{\boldsymbol{\gamma}})$ at $\boldsymbol{\gamma}^o$ is

$$\begin{aligned}\mathbf{p}(\hat{\boldsymbol{\gamma}}) =& \mathbf{p}(\boldsymbol{\gamma}^o) + \sum_{i=1}^{K(N+1)} \frac{\partial \mathbf{p}(\boldsymbol{\gamma}^o)}{\partial \gamma_i} \left(\hat{\gamma}_i - \gamma_i^o\right) + \frac{1}{2} \sum_{i,j=1}^{K(N+1)} \frac{\partial^2 \mathbf{p}(\boldsymbol{\gamma}^o)}{\partial \gamma_i \partial \gamma_j} \left(\hat{\gamma}_i - \gamma_i^o\right) \left(\hat{\gamma}_j - \gamma_j^o\right) \\ &+ \frac{1}{6} \sum_{i,j,k=1}^{K(N+1)} \frac{\partial^3 \mathbf{p}(\boldsymbol{\gamma}^o)}{\partial \gamma_i \partial \gamma_j \partial \gamma_k} \left(\hat{\gamma}_i - \gamma_i^o\right) \left(\hat{\gamma}_j - \gamma_j^o\right) \left(\hat{\gamma}_k - \gamma_k^o\right) + \cdots ,\end{aligned} \tag{3.2}$$

where $\frac{\partial \mathbf{p}(\boldsymbol{\gamma}^o)}{\partial \gamma_i}$ represents $\left.\frac{\partial \mathbf{p}(\boldsymbol{\gamma})}{\partial \gamma_i}\right|_{\boldsymbol{\gamma}=\boldsymbol{\gamma}^o}$, and similarly for $\frac{\partial^2 \mathbf{p}(\boldsymbol{\gamma}^o)}{\partial \gamma_i \partial \gamma_j}$ and $\frac{\partial^3 \mathbf{p}(\boldsymbol{\gamma}^o)}{\partial \gamma_i \partial \gamma_j \partial \gamma_k}$. The term $\hat{\gamma}_i$ is the ith elements of the vector $\hat{\boldsymbol{\gamma}}$, $i = 1, 2, \ldots, K(N+1)$. Let us denote the ith element of $\mathbf{p}(\boldsymbol{\gamma}^o)$ as $p_i(\boldsymbol{\gamma}^o)$. Re-expressing (3.2) in terms of the entire vector $\boldsymbol{\gamma}$ and truncating $\mathbf{p}(\hat{\boldsymbol{\gamma}})$ to the second order term under the small noise approximation give

$$\mathbf{p}(\hat{\boldsymbol{\gamma}}) \simeq \mathbf{p}(\boldsymbol{\gamma}^o) + \frac{\partial \mathbf{p}(\boldsymbol{\gamma}^o)}{\partial \boldsymbol{\gamma}^T} \left(\hat{\boldsymbol{\gamma}} - \boldsymbol{\gamma}^o\right) + \frac{1}{2} \begin{bmatrix} \left(\hat{\boldsymbol{\gamma}} - \boldsymbol{\gamma}^o\right)^T \left(\frac{\partial^2 p_1(\boldsymbol{\gamma}^o)}{\partial \boldsymbol{\gamma} \partial \boldsymbol{\gamma}^T}\right) \left(\hat{\boldsymbol{\gamma}} - \boldsymbol{\gamma}^o\right) \\ \vdots \\ \left(\hat{\boldsymbol{\gamma}} - \boldsymbol{\gamma}^o\right)^T \left(\frac{\partial^2 p_{K(N+1)}(\boldsymbol{\gamma}^o)}{\partial \boldsymbol{\gamma} \partial \boldsymbol{\gamma}^T}\right) \left(\hat{\boldsymbol{\gamma}} - \boldsymbol{\gamma}^o\right) \end{bmatrix}. \tag{3.3}$$

Using (2.13) in (3.3), rearranging and taking the expectation yield the bias

$$\mathbf{b}_{\boldsymbol{\gamma}} = \mathrm{E}\left(\hat{\boldsymbol{\gamma}} - \boldsymbol{\gamma}^o\right) \simeq -\mathrm{E}\left(\left(\frac{\partial \mathbf{p}(\boldsymbol{\gamma}^o)}{\partial \boldsymbol{\gamma}^T}\right)^{-1} \mathbf{p}(\boldsymbol{\gamma}^o)\right) - \mathrm{E}\left(\left(\frac{\partial \mathbf{p}(\boldsymbol{\gamma}^o)}{\partial \boldsymbol{\gamma}^T}\right)^{-1} \mathbf{q}(\boldsymbol{\gamma}^o)\right), \tag{3.4}$$

where $\mathbf{q}(\boldsymbol{\gamma}^o)$ denotes the second order term in (3.3). Appendix A.1 evaluates the expectation computation in (3.4) under the small noise condition and reduces it to

$$\mathbf{b}_{\boldsymbol{\gamma}} \simeq -\frac{1}{2} \mathrm{FIM}_{\boldsymbol{\gamma}}^{-1} \boldsymbol{\nabla}_{\boldsymbol{\gamma}}^T \mathbf{Q}_{\mathbf{m}}^{-1} \mathbf{k}, \tag{3.5}$$

where $\boldsymbol{\nabla}_{\boldsymbol{\gamma}} = [\, \boldsymbol{\nabla}_{\mathbf{u}},\, \boldsymbol{\nabla}_{\mathbf{s}} \,] = \partial \mathbf{m}^o(\boldsymbol{\gamma}^o)/\partial \boldsymbol{\gamma}^T$.

Recall the term $\mathrm{FIM}_{\boldsymbol{\gamma}}$ is the FIM of $\boldsymbol{\gamma}^o$ (2.19). $\mathrm{FIM}_{\boldsymbol{\gamma}}$ and the vector $\mathbf{k}$ are

$$\mathrm{FIM}_{\boldsymbol{\gamma}} = \boldsymbol{\nabla}_{\boldsymbol{\gamma}}^T \mathbf{Q}_{\mathbf{m}}^{-1} \boldsymbol{\nabla}_{\boldsymbol{\gamma}} + \mathrm{diag}\left(\mathbf{O}_{K\times K},\, \mathbf{Q}_{\mathbf{s}}^{-1} \right), \tag{3.6a}$$

$$\mathbf{k} = [\, k_1,\, k_2,\, \cdots,\, k_L \,]^T, \;\; k_i = \mathrm{tr}\left(\frac{\partial^2 m_i^o(\boldsymbol{\gamma}^o)}{\partial \boldsymbol{\gamma} \partial \boldsymbol{\gamma}^T} \mathrm{FIM}_{\boldsymbol{\gamma}}^{-1} \right), \tag{3.6b}$$

where $\mathrm{tr}(*)$ represents the trace operation. L is the number of measurements that $L = N$ for TOA and AOA and $L = N - 1$ for TDOA.

The first K elements of (3.5) give the bias of $\hat{\mathbf{u}}$. Express $\mathrm{FIM}_{\boldsymbol{\gamma}}$ as a 2×2 block matrix and apply the block matrix inverse lemma [72] give

$$\mathrm{FIM}_{\boldsymbol{\gamma}} = \begin{bmatrix} \mathrm{FIM}_{\boldsymbol{\gamma},\mathbf{uu}} & \mathrm{FIM}_{\boldsymbol{\gamma},\mathbf{us}} \\ \mathrm{FIM}_{\boldsymbol{\gamma},\mathbf{us}}^T & \mathrm{FIM}_{\boldsymbol{\gamma},\mathbf{ss}} \end{bmatrix} = \begin{bmatrix} \boldsymbol{\nabla}_{\mathbf{u}}^T \mathbf{Q}_{\mathbf{m}}^{-1} \boldsymbol{\nabla}_{\mathbf{u}} & \boldsymbol{\nabla}_{\mathbf{u}}^T \mathbf{Q}_{\mathbf{m}}^{-1} \boldsymbol{\nabla}_{\mathbf{s}} \\ \boldsymbol{\nabla}_{\mathbf{s}}^T \mathbf{Q}_{\mathbf{m}}^{-1} \boldsymbol{\nabla}_{\mathbf{u}} & \boldsymbol{\nabla}_{\mathbf{s}}^T \mathbf{Q}_{\mathbf{m}}^{-1} \boldsymbol{\nabla}_{\mathbf{s}} + \mathbf{Q}_{\mathbf{s}}^{-1} \end{bmatrix}. \tag{3.7a}$$

$$\mathrm{FIM}_{\boldsymbol{\gamma}}^{-1} = \begin{bmatrix} \mathrm{FIM}_{\mathbf{u}}^{-1} & -\mathrm{FIM}_{\mathbf{u}}^{-1} \mathrm{FIM}_{\boldsymbol{\gamma},\mathbf{us}} \mathrm{FIM}_{\boldsymbol{\gamma},\mathbf{ss}}^{-1} \\ -\left(\mathrm{FIM}_{\boldsymbol{\gamma},\mathbf{us}} \mathrm{FIM}_{\boldsymbol{\gamma},\mathbf{ss}}^{-1} \right)^T \mathrm{FIM}_{\mathbf{u}}^{-1} & \mathrm{FIM}_{\mathbf{s}}^{-1} \end{bmatrix}, \tag{3.7b}$$

where $\mathrm{FIM}_{\mathbf{u}}^{-1} = \left(\mathrm{FIM}_{\boldsymbol{\gamma},\mathbf{uu}} - \mathrm{FIM}_{\boldsymbol{\gamma},\mathbf{us}} \mathrm{FIM}_{\boldsymbol{\gamma},\mathbf{ss}}^{-1} \mathrm{FIM}_{\boldsymbol{\gamma},\mathbf{us}}^T \right)^{-1}$ and $\mathrm{FIM}_{\mathbf{s}}^{-1} = \mathrm{FIM}_{\boldsymbol{\gamma},\mathbf{ss}}^{-1} + \left(\mathrm{FIM}_{\boldsymbol{\gamma},\mathbf{us}} \mathrm{FIM}_{\boldsymbol{\gamma},\mathbf{ss}}^{-1} \right)^T \mathrm{FIM}_{\mathbf{u}}^{-1} \mathrm{FIM}_{\boldsymbol{\gamma},\mathbf{us}} \mathrm{FIM}_{\boldsymbol{\gamma},\mathbf{ss}}^{-1}$. Putting (3.7b) back to (3.5) yields the bias formula of the ML object position estimate

$$\mathbf{b}_{\mathbf{u}} = -\frac{1}{2} \mathrm{FIM}_{\mathbf{u}}^{-1} \boldsymbol{\nabla}_{\mathbf{u}}^T \left(\mathbf{Q}_{\mathbf{m}} + \boldsymbol{\nabla}_{\mathbf{s}} \mathbf{Q}_{\mathbf{s}} \boldsymbol{\nabla}_{\mathbf{s}}^T \right)^{-1} \mathbf{k} \tag{3.8}$$

It is apparent in (3.5), (3.6) and (3.8) that the computation of bias requires the first and second derivatives of measurement function $\mathbf{m}^o(\boldsymbol{\gamma}^o)$. Different measure-

ment types have different forms of the first and second derivatives, yielding different amounts of $\mathbf{b_u}$. The derivatives of the three measurement types are summarized in the Appendix A.2 in (A.12), (A.14) and (A.16).

Next, we are interested to separate the bias components from $\mathbf{n_m}$ and $\mathbf{n_s}$. $\mathrm{FIM}_{\mathbf{u}}^{-1}$ in (3.7b) can be expanded as, after using the matrix inversion lemma [22],

$$\mathrm{FIM}_{\mathbf{u}}^{-1} = \mathrm{FIM}_{\boldsymbol{\gamma},\mathbf{uu}}^{-1} + \mathrm{FIM}_{\boldsymbol{\gamma},\mathbf{uu}}^{-1}\mathrm{FIM}_{\boldsymbol{\gamma},\mathbf{us}}\mathrm{FIM}_{\mathbf{s}}^{-1}\mathrm{FIM}_{\boldsymbol{\gamma},\mathbf{us}}^{T}\mathrm{FIM}_{\boldsymbol{\gamma},\mathbf{uu}}^{-1}. \tag{3.9}$$

Substituting (3.7b) and (3.9) into (3.5) and simplifying yield

$$\mathbf{b_u} = \mathbf{b_{u,m}} + \mathbf{b_{u,s}}. \tag{3.10}$$

The first component $\mathbf{b_{u,m}}$ is the bias resulted from the measurement noise $\mathbf{n_m}$ that

$$\mathbf{b_{u,m}} = -\frac{1}{2}\mathrm{FIM}_{\boldsymbol{\gamma},\mathbf{uu}}^{-1}\nabla_{\mathbf{u}}^{T}\mathbf{Q}_{\mathbf{m}}^{-1}\mathbf{k_m} \tag{3.11}$$

where $\mathbf{k_m} = [\, k_{\mathbf{m},1},\, k_{\mathbf{m},2},\, \cdots,\, k_{\mathbf{m},L}\,]^T$ and $k_{\mathbf{m},i} = \mathrm{tr}\left(\frac{\partial^2 m_i^o(\boldsymbol{\gamma}^o)}{\partial\mathbf{u}\partial\mathbf{u}^T}\mathrm{FIM}_{\boldsymbol{\gamma},\mathbf{uu}}^{-1}\right)$.

The second component $\mathbf{b_{u,s}}$ is the additional amount of bias caused by the receiver position errors. The expression of $\mathbf{b_{u,s}}$ is quite tedious and is given in (A.18) of Appendix A.3. Note that $\mathbf{b_{u,s}}$ not only depends on the receiver position covariance matrix, but also on the measurement noise covariance through $\mathrm{FIM}_{\boldsymbol{\gamma},\mathbf{uu}}$, $\mathrm{FIM}_{\boldsymbol{\gamma},\mathbf{us}}$ and $\mathrm{FIM}_{\boldsymbol{\gamma},\mathbf{ss}}$. As a result, the bias of the object position estimate does not follow the superposition of the bias from measurement noise and position error individually, unless under some specific cases as will be demonstrated in the next subsection.

Next, we shall use (3.5) to analyze the biases of the three positioning approaches.

3.1.2 Bias for TOA, TDOA and AOA

The evaluation of bias is tedious. To make the investigation manageable, the analysis below considers a specific form of the receiver position covariance matrix where their position errors are independent and the error in each coordinate of a given receiver is IID. In other words, $\mathbf{Q_s} = \widetilde{\mathbf{Q}}_\mathbf{s} \otimes \mathbf{I}_K$, where $\widetilde{\mathbf{Q}}_\mathbf{s} = \text{diag}\left(\sigma^2_{\mathbf{s}_1}, \sigma^2_{\mathbf{s}_2}, \cdots, \sigma^2_{\mathbf{s}_N}\right)$, $\otimes$ represents the Kronecker product operation. This kind of receiver position covariance occurs in practice [27, 73]. The bias expressions for the TOA, TDOA and AOA positionings are given in Appendix A.4. They are applicable for any positive definite measurement noise covariance matrix $\mathbf{Q_m}$.

To gain some insights on the bias behaviors of the three localization approaches, let us further assume the signals observed by the receivers have the same signal-to-noise ratio and the measurement noise is IID. An example for such a situation to occur is when the object is at an equal distance from all receivers [8]. We also restrict the receiver position covariance to be proportional to an identity.

With $\mathbf{Q_m} = \sigma^2_{\text{TOA}}\mathbf{I}_N$ and $\mathbf{Q_s} = \sigma^2_\mathbf{s}\mathbf{I}_{KN}$, the bias of TOA (A.21) becomes

$$\mathbf{b}_{\mathbf{u},\text{TOA}} = \left(\mathbf{P}^T_{\mathbf{u},\mathbf{s}}\mathbf{P}_{\mathbf{u},\mathbf{s}}\right)^{-1}\mathbf{P}^T_{\mathbf{u},\mathbf{s}}\mathbf{k}_{\text{TOA}}, \tag{3.12}$$

where

$$\begin{aligned} k_{\text{TOA},j} =& k_{\text{TOA},\mathbf{m},j} + k_{\text{TOA},\mathbf{s},j} = \frac{\sigma^2_{\text{TOA}}}{2||\mathbf{u}^o - \mathbf{s}^o_j||}\text{tr}\left(\mathbf{P}^\perp_{\mathbf{u}^o,\mathbf{s}^o_j}\left(\mathbf{P}^T_{\mathbf{u},\mathbf{s}}\mathbf{P}_{\mathbf{u},\mathbf{s}}\right)^{-1}\right) \\ &+ \frac{\sigma^2_\mathbf{s}}{2||\mathbf{u}^o - \mathbf{s}^o_j||}\left(K - 1 + \text{tr}\left(\mathbf{P}^\perp_{\mathbf{u}^o,\mathbf{s}^o_j}\left(\mathbf{P}^T_{\mathbf{u},\mathbf{s}}\mathbf{P}_{\mathbf{u},\mathbf{s}}\right)^{-1}\right)\right), \end{aligned} \tag{3.13}$$

$j = 1, 2, \ldots, N$, and $\mathbf{P}^\perp_{\mathbf{u}^o,\mathbf{s}^o_j}$ and $\mathbf{P}_{\mathbf{u},\mathbf{s}}$ are defined below (A.13b) and (A.19c).

When $\mathbf{Q_m} = \sigma_{\mathrm{H}}^2 \mathbf{H}\mathbf{H}^T$ for hyperbolic positioning, (A.23) becomes

$$\mathbf{b}_{\mathbf{u},\mathrm{H}} = \left(\mathbf{P}_{\mathbf{u},\mathbf{s}}^T \mathbf{P}_{\mathbf{H}} \mathbf{P}_{\mathbf{u},\mathbf{s}}\right)^{-1} \mathbf{P}_{\mathbf{u},\mathbf{s}}^T \mathbf{P}_{\mathbf{H}} \boldsymbol{\kappa}_{\mathrm{H}}, \tag{3.14}$$

where $\mathbf{H}$ is defined below (A.22), $\mathbf{P_H}$ is the projection matrix onto the column space of $\mathbf{H}^T$ given by $\mathbf{P_H} = \mathbf{H}^T \left(\mathbf{H}\mathbf{H}^T\right)^{-1} \mathbf{H}$, and the elements of $\boldsymbol{\kappa}_{\mathrm{H}}$, $j = 1, 2, \ldots, N$, are

$$\begin{aligned} \kappa_{\mathrm{H},j} = \kappa_{\mathrm{H},\mathbf{m},j} + \kappa_{\mathrm{H},\mathbf{s},j} = {} & \frac{\sigma_{\mathrm{H}}^2}{2||\mathbf{u}^o - \mathbf{s}_j^o||} \mathrm{tr}\left(\mathbf{P}_{\mathbf{u}^o,\mathbf{s}_j^o}^{\perp} \left(\mathbf{P}_{\mathbf{u},\mathbf{s}} \mathbf{P}_{\mathbf{H}} \mathbf{P}_{\mathbf{u},\mathbf{s}}\right)^{-1}\right) \\ & + \frac{\sigma_{\mathbf{s}}^2}{2||\mathbf{u}^o - \mathbf{s}_j^o||} \left(K - 1 + \mathrm{tr}\left(\mathbf{P}_{\mathbf{u}^o,\mathbf{s}_j^o}^{\perp} \left(\mathbf{P}_{\mathbf{u},\mathbf{s}}^T \mathbf{P}_{\mathbf{H}} \mathbf{P}_{\mathbf{u},\mathbf{s}}\right)^{-1}\right)\right). \end{aligned} \tag{3.15}$$

For AOA, $\mathbf{Q_m} = \sigma_{\mathrm{AOA}}^2 \mathbf{I}_N$ and

$$\mathbf{b}_{\mathbf{u},\mathrm{AOA}} = \boldsymbol{\Psi}^{-1} \mathbf{T} \mathbf{P}_{\mathbf{u},\mathbf{s}}^T \mathbf{k}_{\mathrm{AOA}}, \tag{3.16}$$

where $\boldsymbol{\Psi} = \sum_{j=1}^{N} \left(\sigma_{\mathbf{s}}^2 + ||\mathbf{u}^o - \mathbf{s}_j^o||^2 \sigma_{\mathrm{AOA}}^2\right)^{-1} \mathbf{P}_{\mathbf{u}^o,\mathbf{s}_j^o}^{\perp}$ and the elements of $\mathbf{k}_{\mathrm{AOA}}$ are

$$k_{\mathrm{AOA},j} = -\frac{\sigma_{\mathrm{AOA}}^2 ||\mathbf{u}^o - \mathbf{s}_j^o||}{\left(\sigma_{\mathbf{s}}^2 + ||\mathbf{u}^o - \mathbf{s}_j^o||^2 \sigma_{\mathrm{AOA}}^2\right)^2} \mathrm{tr}\left(\boldsymbol{\Psi}^{-1} \mathbf{T} \boldsymbol{\rho}_{\mathbf{u}^o,\mathbf{s}_j^o} \boldsymbol{\rho}_{\mathbf{u}^o,\mathbf{s}_j^o}{}^T\right), \tag{3.17}$$

where $j = 1, 2, \ldots, N$, $\mathbf{T}$ is defined below (A.17b) and $\boldsymbol{\rho}_{\mathbf{u}^o,\mathbf{s}_j^o}$ below (A.13b).

Let us consider the bias of TOA and TDOA localizations. First, comparing (3.12)−(3.13) with (3.14)−(3.15) shows that the difference of the bias of TDOA from TOA is the presence of the matrix $\mathbf{P_H}$ caused by the difference operation (A.22). Second, both of them are inversely proportional to the distances from the object to the receivers. The bias is more significant for a near to receiver object than for a distant one. Third, they are separable as the direct sum of the bias from the measurement

noise and from the position errors, which is apparent in (3.13) and (3.15).

The bias behavior of AOA positioning is different from those of TOA and TDOA. The bias is directly proportional to the distance between the object and the receivers, which is evident by substituting $\mathbf{\Psi}$ into (3.17). A distant object will have a larger bias than a close object. Second, the bias resulted from data measurement noise and from receiver position errors are not separable. In fact, the bias reduces to zero if the measurement noise is zero since $k_{\mathrm{AOA},j}$ becomes zero, even if the position error is significant. However, bias remains if the receiver positions are accurate. Third, the bias is insensitive to the position error when the object is far from the receivers.

Besides the data measurement noise and receiver position error, the object/receiver geometry has significant influence on the bias of the three positioning approaches. We examine next if geometry exists where the localization bias can be zero.

3.2 Geometries of Zero Bias

The derivation of the geometries will be based on the formulae (3.12), (3.14) and (3.16) under the special noise situation used in the previous Section.

TOA

In (3.12), $\left(\mathbf{P}_{\mathbf{u},\mathbf{s}}^T\mathbf{P}_{\mathbf{u},\mathbf{s}}\right)^{-1}$ is positive definite and zero bias requires $\mathbf{P}_{\mathbf{u},\mathbf{s}}^T\mathbf{k}_{\mathrm{TOA}} = \mathbf{0}_K$, i.e.

$$\sum_{j=1}^{N} k_{\mathrm{TOA},j}\boldsymbol{\rho}_{\mathbf{u}^o,\mathbf{s}_j^o} = \mathbf{0}_K. \tag{3.18}$$

Putting (3.13) into (3.18) gives the condition

$$\sum_{j=1}^{N}\frac{1}{||\mathbf{u}^o-\mathbf{s}_j^o||}\mathrm{tr}\left(\mathbf{P}^{\perp}_{\mathbf{u}^o,\mathbf{s}_j^o}\left(\mathbf{P}^T_{\mathbf{u},\mathbf{s}}\mathbf{P}_{\mathbf{u},\mathbf{s}}\right)^{-1}\right)\boldsymbol{\rho}_{\mathbf{u}^o,\mathbf{s}_j^o}=\mathbf{0}_K,\ \sum_{j=1}^{N}\frac{1}{||\mathbf{u}^o-\mathbf{s}_j^o||}\boldsymbol{\rho}_{\mathbf{u}^o,\mathbf{s}_j^o}=\mathbf{0}_K. \tag{3.19}$$

TDOA

Following similar steps as in TOA approach, the conditions to achieve zero bias are

$$\sum_{j=1}^{N}\frac{1}{||\mathbf{u}^o-\mathbf{s}_j^o||}\mathrm{tr}\left(\mathbf{P}^{\perp}_{\mathbf{u}^o,\mathbf{s}_j^o}\left(\mathbf{P}^T_{\mathbf{u},\mathbf{s}}\mathbf{P}_{\mathbf{H}}\mathbf{P}_{\mathbf{u},\mathbf{s}}\right)^{-1}\right)\left(\boldsymbol{\rho}_{\mathbf{u}^o,\mathbf{s}_j^o}-\frac{1}{N}\sum_{i=1}^{N}\boldsymbol{\rho}_{\mathbf{u}^o,\mathbf{s}_i^o}\right)=\mathbf{0}_K, \tag{3.20a}$$

$$\sum_{j=1}^{N}\frac{1}{||\mathbf{u}^o-\mathbf{s}_j^o||}\left(\boldsymbol{\rho}_{\mathbf{u}^o,\mathbf{s}_j^o}-\frac{1}{N}\sum_{i=1}^{N}\boldsymbol{\rho}_{\mathbf{u}^o,\mathbf{s}_i^o}\right)=\mathbf{0}_K. \tag{3.20b}$$

AOA

The matrix term $\boldsymbol{\Psi}$ is positive definite and so does its inverse. Hence, to achieve the zero bias in (3.16), we require

$$\sum_{j=1}^{N}k_{\mathrm{AOA},j}\boldsymbol{\rho}_{\mathbf{u}^o,\mathbf{s}_j^o}=\mathbf{0}_K. \tag{3.21}$$

(3.21) is rather involved. If we restrict the object to be at equal distance to the receivers so that $||\mathbf{u}^o-\mathbf{s}_1^o||=||\mathbf{u}^o-\mathbf{s}_2^o||=\cdots=||\mathbf{u}^o-\mathbf{s}_N^o||$, it can be simplified to

$$\sum_{j=1}^{N}\mathrm{tr}\left(\left(\sum_{i=1}^{N}\mathbf{P}^{\perp}_{\mathbf{u}^o,\mathbf{s}_i^o}\right)^{-1}\mathbf{T}\boldsymbol{\rho}_{\mathbf{u}^o,\mathbf{s}_j^o}\boldsymbol{\rho}^T_{\mathbf{u}^o,\mathbf{s}_j^o}\right)\boldsymbol{\rho}_{\mathbf{u}^o,\mathbf{s}_j^o}=\mathbf{0}_K. \tag{3.22}$$

It turns out that the requirements (3.19), (3.20) and (3.22) of achieving zero bias are similar but more restricted than those for reaching minimum CRLBs when considering measurement noise only and under small error condition where the bias can be neglected [30, 31, 32]. The geometries that yield zero bias will also attain the smallest CRLBs. In particular, the uniform circular array for 2D localization will have zero bias for TOA, TDOA and AOA localization. Also, having receivers evenly spaced that span half of circle with the object at the centre will also yield zero bias for AOA. For 3D localization, uniform spherical array will result in zero bias for TOA and TDOA localizations.

3.3 Bias Compensation

In addition to understanding the bias behaviors of different positioning approaches and deriving the geometries with zero location bias, the bias expressions can be used to compensate bias to avoid its accumulation. We shall use object tracking as an example to illustrate. The extended Kalman filter (EKF) [74, 75] is a familiar and direct approach to handle the nonlinear measurement functions in tracking. It could become unstable with its state estimate seriously diverging from the true state in some scenarios [76]. An alternative is to obtain the ML object position estimates at different time instants and process them via the Kalman filter (KF) to deduce the tracking trajectory [35, 77], or to improve the location estimate when the object is stationary [78]. We shall use the derived expected amounts of bias to compensate the detrimental effect of bias accumulation in the KF object tracking.

Let us consider an object moving at constant velocity $\mathbf{v}^o$ whose position at time

instant l is $\mathbf{u}^o(l)$. The $2K \times 1$ state vector is

$$\boldsymbol{\gamma}^o_{\mathrm{KF}}(l) = \left[\, \mathbf{u}^o(l)^T,\, \mathbf{v}^{oT} \,\right]^T \tag{3.23}$$

and the dynamic equation is

$$\boldsymbol{\gamma}^o_{\mathrm{KF}}(l) = \mathbf{F}_{\mathrm{KF}}\boldsymbol{\gamma}^o_{\mathrm{KF}}(l-1) + \mathbf{B}_{\mathrm{KF}}\boldsymbol{\nu}, \tag{3.24}$$

where $\mathbf{F}_{\mathrm{KF}} = \begin{bmatrix} \mathbf{I}_K & T_{\mathrm{KF}}\mathbf{I}_K \\ \mathbf{O}_{K\times K} & \mathbf{I}_K \end{bmatrix}$, $\mathbf{B}_{\mathrm{KF}} = \left[\, \frac{T^2_{\mathrm{KF}}}{2}\mathbf{I}_K,\, T_{\mathrm{KF}}\mathbf{I}_K \,\right]^T$, T_{KF} is the observation interval and the $K \times 1$ process noise vector $\boldsymbol{\nu}$ is zero mean Gaussian with covariance matrix $\mathbf{Q}_{\boldsymbol{\nu}}$. The observation equation is

$$\hat{\mathbf{u}}(l) = \mathbf{H}_{\mathrm{KF}}\boldsymbol{\gamma}^o_{\mathrm{KF}}(l-1) + \mathbf{b}_{\mathbf{u}}(l) + \mathbf{n}_{\mathbf{u}}(l), \tag{3.25}$$

where $\mathbf{H}_{\mathrm{KF}} = [\mathbf{I}_K,\, \mathbf{O}_{K\times K}]$ and $\mathbf{n}_{\mathbf{u}}(l)$ is the zero-mean estimation noise of $\mathbf{u}(l)$. Since the MLE is asymptotically efficient, $\mathbf{n}_{\mathbf{u}}(l)$ is assumed to be Gaussian whose covariance matrix is denoted by $\mathbf{Q}_{\mathbf{u}}(l)$. The observation interval is expected to be sufficiently long and $\mathbf{n}_{\mathbf{u}}(l)$ is uncorrelated at different time instants.

We shall apply the standard KF to estimate the state vector. The prediction equations are

$$\hat{\boldsymbol{\gamma}}_{\mathrm{KF}}(l|l-1) = \mathbf{F}_{\mathrm{KF}}\hat{\boldsymbol{\gamma}}_{\mathrm{KF}}(l-1|l-1), \tag{3.26a}$$

$$\mathbf{Q}_{\boldsymbol{\gamma},\mathrm{KF}}(l|l-1) = \mathbf{F}_{\mathrm{KF}}\mathbf{Q}_{\boldsymbol{\gamma},\mathrm{KF}}(l-1|l-1)\mathbf{F}^T_{\mathrm{KF}} + \mathbf{B}_{\mathrm{KF}}\mathbf{Q}_{\boldsymbol{\nu}}\mathbf{B}^T_{\mathrm{KF}}, \tag{3.26b}$$

where $\hat{\boldsymbol{\gamma}}_{\mathrm{KF}}(l|l-1)$ is the predicted object state at l given all the ML position estimates from time instant 0 to $l-1$ and $\mathbf{Q}_{\boldsymbol{\gamma},\mathrm{KF}}(l|l-1)$ is the covariance matrix of $\hat{\boldsymbol{\gamma}}_{\mathrm{KF}}(l|l-1)$.

The update equations are:

$$\mathbf{y}_{\mathrm{KF}}(l) = \hat{\mathbf{u}}(l) - \mathbf{H}_{\mathrm{KF}}\hat{\boldsymbol{\gamma}}_{\mathrm{KF}}(l|l-1) - \mathbf{b}_{\mathbf{u}}(l), \tag{3.27a}$$

$$\mathbf{S}_{\mathrm{KF}}(l) = \mathbf{H}_{\mathrm{KF}}\mathbf{Q}_{\boldsymbol{\gamma},\mathrm{KF}}(l|l-1)\mathbf{H}_{\mathrm{KF}}^{T} + \mathbf{Q}_{\mathbf{u}}(l), \tag{3.27b}$$

$$\mathbf{K}_{\mathrm{KF}}(l) = \mathbf{Q}_{\boldsymbol{\gamma},\mathrm{KF}}(l|l-1)\mathbf{H}_{\mathrm{KF}}^{T}\mathbf{S}_{\mathrm{KF}}(l)^{-1}, \tag{3.27c}$$

$$\hat{\boldsymbol{\gamma}}_{\mathrm{KF}}(l|l) = \hat{\boldsymbol{\gamma}}_{\mathrm{KF}}(l|l-1) + \mathbf{K}_{\mathrm{KF}}(l)\mathbf{y}_{\mathrm{KF}}(l), \tag{3.27d}$$

$$\mathbf{Q}_{\boldsymbol{\gamma},\mathrm{KF}}(l|l) = \Big(\mathbf{I}_{2K} - \mathbf{K}_{\mathrm{KF}}(l)\mathbf{H}_{\mathrm{KF}}\Big)\,\mathbf{Q}_{\boldsymbol{\gamma},\mathrm{KF}}(l|l-1). \tag{3.27e}$$

The first K elements of $\hat{\boldsymbol{\gamma}}_{\mathrm{KF}}(l|l)$ in (3.27d) gives the filtered object position at time instant l.

The implementation of (3.27a) requires the true object position $\mathbf{u}^{o}(l)$ at time l to compute the bias $\mathbf{b}_{\mathbf{u}}(l)$ via (3.5). In practice, it is approximated using the predicted object position $\mathbf{H}_{\mathrm{KF}}\hat{\boldsymbol{\gamma}}_{\mathrm{KF}}(l|l-1)$. The covariance matrix $\mathbf{Q}_{\mathbf{u}}(l)$ in (3.27b) is assumed equal to the CRLB of the predicted object position $\mathbf{H}_{\mathrm{KF}}\hat{\boldsymbol{\gamma}}_{\mathrm{KF}}(l|l-1)$, where again the true position is replaced by the predicted location in the CRLB evaluation. These two approximations are reasonable due to the asymptotic efficiency of the MLE.

Next, the bias behaviors of the three positioning methods are evaluated and contrasted by simulation experiments. The effectiveness of bias compensation in the object tracking problem in the presence of both measurement noise and receiver position errors is also examined.

3.4 Simulation

The simulation scenario is in 2D for ease of illustration.

3.4.1 Bias Comparison

Six receivers are used to locate an object. Both the object and receivers are randomly allocated in a 500 m $\times$ 500 m area with uniform distribution in the Cartesian coordinates. Two constraints are imposed in the generation of a localization geometry. First, the distances between the object and receivers and each pair of receivers are greater than 20 m. Second, at least three receivers i, j and k satisfy

$$\langle \boldsymbol{\rho}_{\mathbf{u}^o,\mathbf{s}_i^o}, \boldsymbol{\rho}_{\mathbf{u}^o,\mathbf{s}_j^o} \rangle < 0.98, \quad \langle \boldsymbol{\rho}_{\mathbf{u}^o,\mathbf{s}_i^o}, \boldsymbol{\rho}_{\mathbf{u}^o,\mathbf{s}_k^o} \rangle < 0.98, \quad \langle \boldsymbol{\rho}_{\mathbf{u}^o,\mathbf{s}_j^o}, \boldsymbol{\rho}_{\mathbf{u}^o,\mathbf{s}_k^o} \rangle < 0.98, \quad i \neq j \neq k, \tag{3.28}$$

where $\langle \boldsymbol{\alpha}, \boldsymbol{\beta} \rangle$ represents the inner product of the vectors $\boldsymbol{\alpha}$ and $\boldsymbol{\beta}$. The first constraint is to ensure that the object and receivers are not too close to each other. The second constraint is to prevent co-linear object and receivers that would create degenerate localization scenario. Without the two constraints, extremely poor MLE performance could occur which will dominate the simulation results.

The covariance matrices of the TOA, TDOA and AOA measurements are $\eta\sigma^2_{\text{TOA}}\mathbf{I}_N$, $\eta\sigma^2_{\text{H}}\mathbf{H}\mathbf{H}^T$ and $\eta\sigma^2_{\text{AOA}}\mathbf{I}_N$ respectively, where $\sigma^2_{\text{TOA}} = \sigma^2_{\text{H}} = 1$ m^2, $\sigma^2_{\text{AOA}} = 10^{-4}$ rad^2 and η is the unitless coefficient for varying the noise power. The covariance matrix of the receiver positions is $\mathbf{Q}_{\mathbf{s}} = \sigma^2_{\mathbf{s}}\mathbf{I}_{KN}$. The MLE is implemented using the Gauss-Newton iteration that jointly estimate the object and sensor positions, where the true object and receiver locations are set as the initial guess.

In the first simulation, 100 random geometries are formed and 10,000 ensemble

runs are applied to each geometry to obtain the bias. The results shown are the bias-square averaged over the 100 random geometries. Fig. 3.1 shows the bias behaviors of the ML estimates when η increases and $\sigma_{\mathbf{s}}^2 = 1$ m^2. The simulation results match very well with the theoretical bias values. For the TOA and TDOA positionings, the bias is dominated by the receiver position uncertainties when the measurement noise power is small, $\eta < 10^{-0.5}$. As η increases, the influence of the measurement noise to the bias increases. The bias-square of TDOA positioning is nearly 100 times greater than TOA localization in this simulation. Unlike TOA and TDOA, the bias in AOA positioning always increases with η and the receiver position error does not dominate the bias even when the measurement noise is very small. This observation is consistent to the theoretical analysis in the Section 3.1.2. Note that when the measurement noise factor η is large, the threshold effect of MLE occurs [27].

Fig. 3.2 is the simulation results when η is fixed at 1 and $\sigma_{\mathbf{s}}^2$ varies. The observations for TOA and TDOA localizations are very similar to those in Fig. 3.1. For AOA localization, the bias nearly remains constant when $\sigma_{\mathbf{s}}^2$ increases. This bias behavior is what we expect from the theoretical analysis in Section 3.1.2.

To further understand the bias sensitivity with respect to the measurement and receiver position errors, Figs. 3.3−3.5 depict the histograms of theoretical bias-squares of the ML object position estimates in the three positioning approaches using (3.12), (3.14) and (3.16). In each case, the three bias values $\mathbf{b_u}$, $\mathbf{b_{u,m}}$ and $\mathbf{b_{u,s}}$ are contrasted. Note that from Section 3.1, $\mathbf{b_{u,s}}$ depends on receiver position errors in the TOA and TDOA localization and is unaffected by the measurement noise. This is not the case for AOA localization. The histograms are created using 100,000 random geometries and they are shown with respect to the bias after taking the logarithm of base 10.

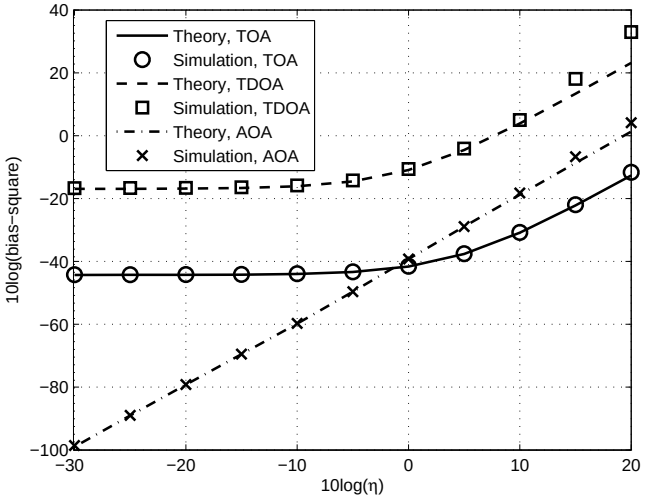

Figure 3.1: The bias behaviors of the ML object position estimates in TOA, TDOA and AOA localizations when $\sigma_{\mathrm{s}}^2 = 1\ \mathrm{m}^2$.

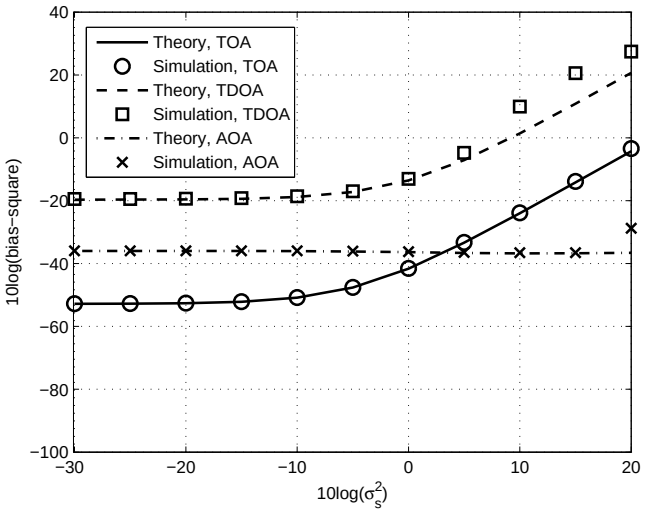

Figure 3.2: The bias behaviors of the ML object position estimates in TOA, TDOA and AOA localizations when $\eta = 1$.

The coefficient η is 1 and $\sigma_{\mathbf{s}}^2$ is 1 m^2. Fig. 3.3 shows that the receiver position uncertainties have higher possibility of causing more bias than the measurement noise in the TOA localization. In the TDOA localization, this is not as evident in Fig. 3.4. The histograms in Fig. 3.3 for TOA are more concentrated and towards the left compared to those of TDOA and AOA in Figs. 3.4 and 3.5. It implies that the bias behavior of TOA is less sensitive to the localization geometry than TDOA and AOA.

We next compare the bias-squares in TDOA and TOA localizations under same object/receiver geometry by taking the ratio. Fig. 3.6 depicts the histogram of the bias-square ratio of TDOA to TOA for the 100,000 geometries when only measurement noise is present ($\eta = 1$, $\sigma_{\mathbf{s}}^2 = 0$ m^2) and when only sensor position error is present ($\eta = 0$, $\sigma_{\mathbf{s}}^2 = 1$ m^2). In most geometries TDOA positioning has larger bias-square than the TOA positioning. Furthermore the shapes of the histograms are quite different for the two situations. It appears the bias-square of TOA localization is more sensitive to the receiver position uncertainties than the measurement noise compared to TDOA.

3.4.2 Bias Compensation

We adopt the receiver configuration from the real data experiment in [74]. As shown in Fig. 3.7, the positions of the 6 receivers are $[-190,\ 40]^T$ m, $[-190,\ -10]^T$ m, $[-10,\ 20]^T$ m, $[0,\ -20]^T$ m, $[190,\ 10]^T$ m, and $[180,\ -15]^T$ m. The object is initially at $[-200,\ 800]^T$ m and its true velocity is $\mathbf{v}^o = [2,\ 0]^T$ m/s. In every $T_{\mathrm{KF}} = 1$ s, TOA, TDOA or AOA measurements are acquired to track the location of the object. Their measurement covariance matrices have same structures in the Section 3.1.2 where $\sigma_{\mathrm{TOA}}^2 = 10^{2.5}$ m^2, $\sigma_{\mathrm{H}}^2 = 10^{-1}$ m^2 and $\sigma_{\mathrm{AOA}}^2 = 10^{-3.5}$ rad^2. The covariance matrix of the receiver position errors is $\mathbf{Q}_{\mathbf{s}} = \sigma_{\mathbf{s}}^2 \mathbf{I}_{KN}$, where $\sigma_{\mathbf{s}}^2 = 1$ m^2. The covariance

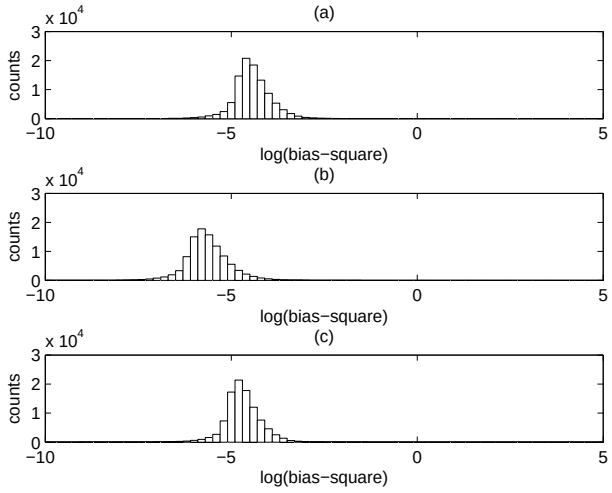

Figure 3.3: The histograms of log(bias-square) in TOA localization when $\eta = 1$ and $\sigma_{\mathbf{s}}^2 = 1$ m^2. (a) The total bias of object position estimate. (b) The bias caused by the measurement noise. (c) The bias caused by the receiver position errors.

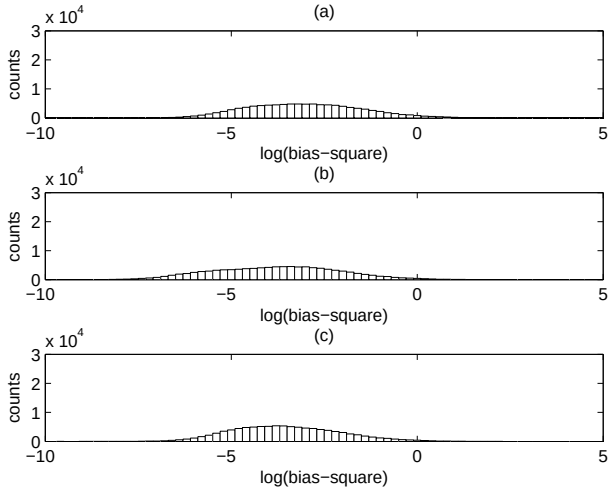

Figure 3.4: The histograms of log(bias-square) in TDOA localization when $\eta = 1$ and $\sigma_{\mathbf{s}}^2 = 1$ m^2. (a) The total bias of object position estimate. (b) The bias caused by the measurement noise. (c) The bias caused by the receiver position errors.

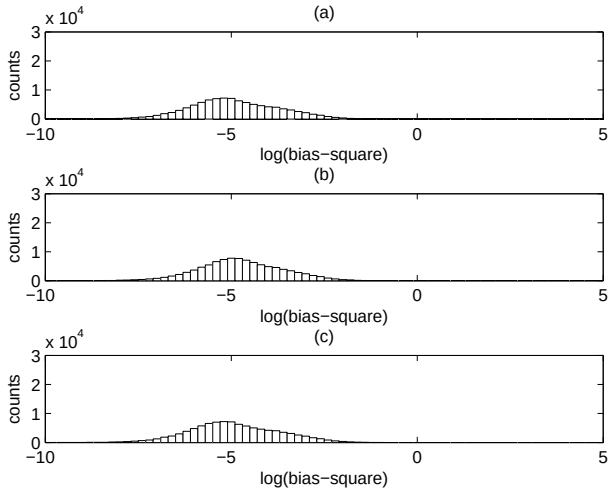

Figure 3.5: The histograms of log(bias-square) in AOA localization when $\eta = 1$ and $\sigma_{\mathbf{s}}^2 = 1$ m^2. (a) The total bias of object position estimate. (b) The bias caused by the measurement noise. (c) The bias created by the presence of receiver position errors.

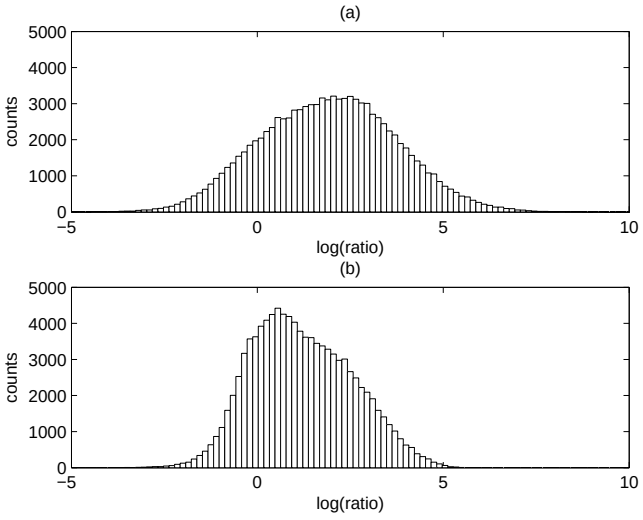

Figure 3.6: The histograms of the log(ratio) of the bias-square of TDOA localization to the bias-square of TOA for the 100,000 geometries. (a) Measurement noise present only ($\eta = 1$, $\sigma_{\mathbf{s}}^2 = 0$ m^2). (b) Observer position uncertainties present only ($\eta = 0$, $\sigma_{\mathbf{s}}^2 = 1$m^2).

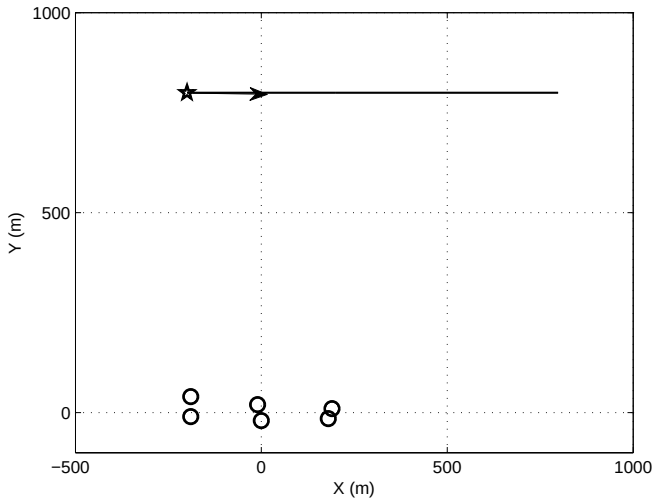

Figure 3.7: The geometry for object tracking, the pentagram denotes the initial object position and the circles are the receiver locations.

of state noise is $\mathbf{Q}_{\boldsymbol{\nu}}^2 = \sigma_{\boldsymbol{\nu}}^2 \mathbf{I}_K$, where $\sigma_{\boldsymbol{\nu}} = 10^{-3}$ m/s^2. For TDOA , the receiver at $[-190,\ 40]^T$ m is the reference sensor. The ensemble run number is 10,000.

Three types of trackers are compared in the simulation: the KF with bias compensation proposed in Section 3.3 (Type I), the KF without bias compensation (Type II) and the EKF which ignores the existence of receiver position error [74]. At time index l, the initial guess of the object position in the MLE is randomly drawn under Gaussian distribution with mean $\mathbf{u}^o(l)$ and covariance matrix 4CRLB of $\mathbf{u}^o(l)$. The EKF is initialized using the state $\boldsymbol{\gamma}_{\mathrm{KF}}(0) = \left[\hat{\mathbf{u}}(0)^T,\ \mathbf{0}_K^T\right]^T$, where $\hat{\mathbf{u}}(0)$ is the ML estimate of the object position at time 0. If the EKF is initialized farther away, our simulation indicates that it has difficulty in converging to the correct object track.

The performance of the three filters for TOA positioning as time increases are shown in Figs. 3.8 and 3.9 for position and velocity estimates. The bias compensation can effectively reduce the bias of the object state in the KF and prevents its

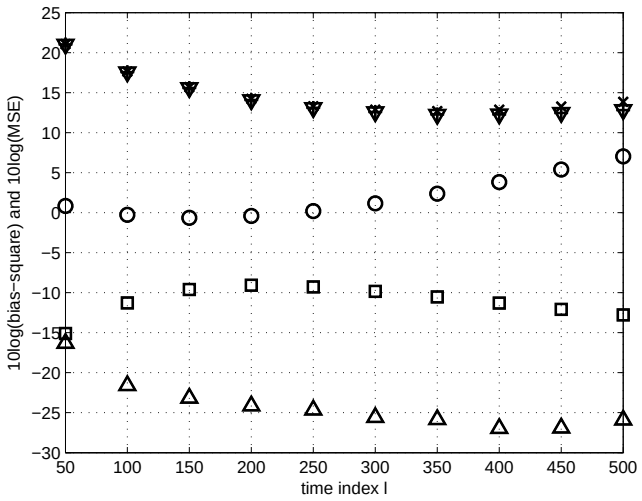

Figure 3.8: Comparison of position estimation accuracy for TOA measurements. The $\triangle$, $\bigcirc$ and $\square$ are the bias-squares using type I KF, type II KF and EKF respectively. The $\triangledown$, $\times$ and $+$ are the MSEs using type I KF, type II KF, and EKF respectively.

accumulation. Without bias compensation, the bias gradually increases and becomes significant compared to MSE. At $l = 500$, bias compensation results in nearly 1 dB improvement in the position MSE. The EKF does not show obvious bias accumulation and provides acceptable tracking accuracy in the simulation. Its bias, however, is about 10 dB higher compared to the bias of KF with bias compensation.

The results of the TDOA case are given in Figs. 3.10 and 3.11. The bias accumulation degrades the performance of KF (Type II) much worse than the TOA case. At $l = 250$, the position MSE of the KF (Type II) is already about 1 dB higher than KF (Type I) that has bias compensation. The influence of the bias further deteriorates the performance of the KF (Type II) as time increases. EKF does not perform well in the TDOA case because of the relatively large receiver position error relative to the measurement noise.

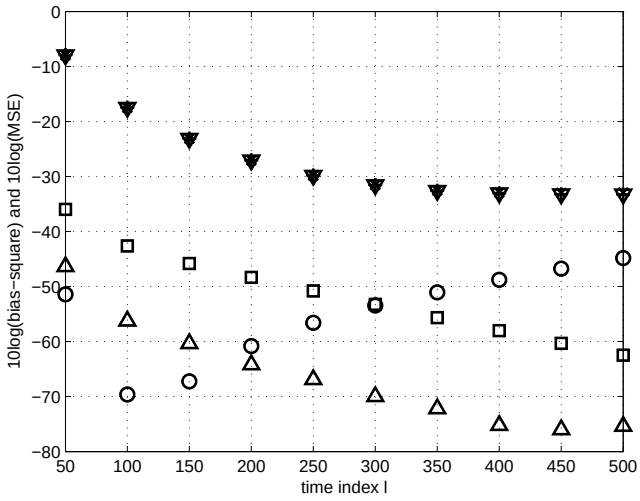

Figure 3.9: Comparison of velocity estimation accuracy for TOA measurements. The $\triangle$, $\bigcirc$ and $\square$ are the bias-squares using type I KF, type II KF and EKF respectively. The $\triangledown$, $\times$ and $+$ are the MSEs using type I KF, type II KF, and EKF respectively.

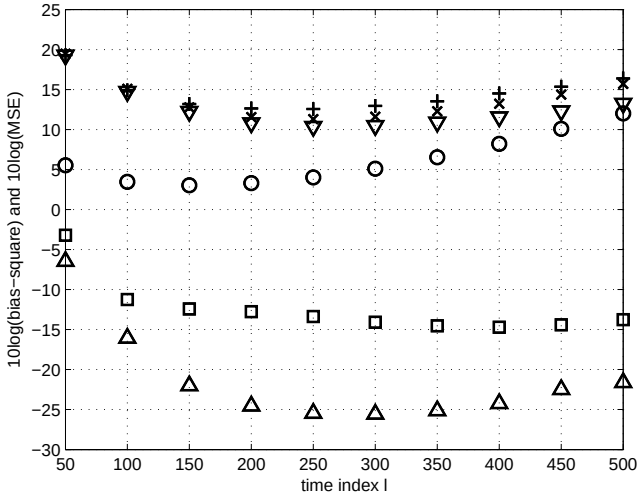

Figure 3.10: Comparison of position estimation accuracy for TDOA measurements. The $\triangle$, $\bigcirc$ and $\square$ are the bias-squares using type I KF, type II KF and EKF respectively. The $\triangledown$, $\times$ and $+$ are the MSEs using type I KF, type II KF, and EKF respectively.

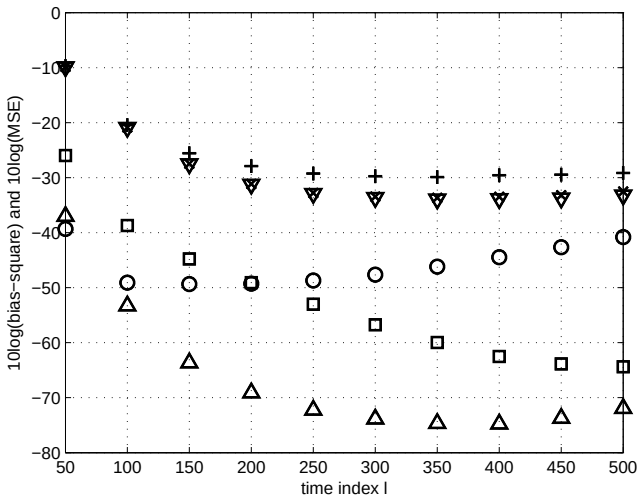

Figure 3.11: Comparison of velocity estimation accuracy for TDOA measurements. The $\triangle$, $\bigcirc$ and $\square$ are the bias-squares using type I KF, type II KF and EKF respectively. The $\triangledown$, $\times$ and $+$ are the MSEs using type I KF, type II KF, and EKF respectively.

Figs. 3.12 and 3.13 illustrate the performance for the AOA case. The observations are similar to those of the TOA and TDOA cases. To better assess the performance gain through bias compensation, Fig. 3.14 gives the amount of position MSE reduction in dB after and before bias compensation. The improvement is very apparent especially for the TDOA and AOA measurements.

Table 3.1 compares the computation times from Matlab for KF (Type I), KF (Type II) and EKF, where the values are relative to the time consumption of KF (Type II) for TOA measurements. KF (Type I) has only modest increase in complexity (no more than 15%) compared KF (Type II), which is due to the evaluation of the bias for its compensation. EKF takes much less computations since it does not require the ML estimate as KF (Type I) and KF (Type II) do. We applied the Gauss-Newton implementation with about 5 iterations to jointly obtain the ML estimates

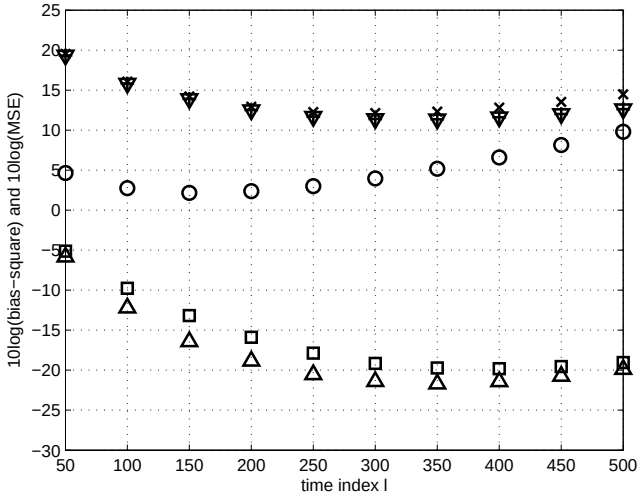

Figure 3.12: Comparison of position estimation accuracy for AOA measurements. The $\triangle$, $\bigcirc$ and $\square$ are the bias-squares using type I KF, type II KF and EKF respectively. The $\triangledown$, $\times$ and $+$ are the MSEs using type I KF, type II KF, and EKF respectively.

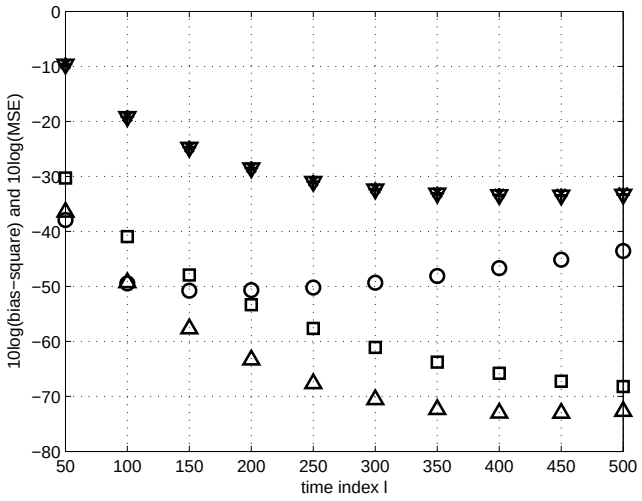

Figure 3.13: Comparison of velocity estimation accuracy for AOA measurements. The $\triangle$, $\bigcirc$ and $\square$ are the bias-squares using type I KF, type II KF and EKF respectively. The $\triangledown$, $\times$ and $+$ are the MSEs using type I KF, type II KF, and EKF respectively.

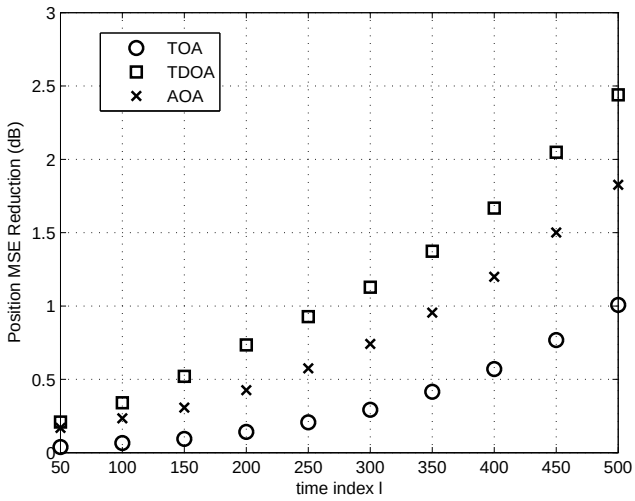

Figure 3.14: Reduction in MSE of the position estimates after bias compensation.

Measurement Type	KF (Type I)	KF (Type II)	EKF
TOA	1.13	1.00	0.06
TDOA	1.56	1.40	0.18
AOA	1.20	1.06	0.07

Table 3.1: Simulation times for KF (Type I), KF (Type II) and EKF relative to that of KF (Type II) with TOA measurements

of the object and sensor positions. The computation advantage of EKF, however, is outweighed by its non-robust and inadequate behaviors as shown in the simulations.

3.5 Conclusion

This Chapter performs an in-depth analysis of the bias in the ML object position estimate that is caused by data measurement noise and sensor position errors. The sensor position error is not equivalent to measurement noise in creating the bias. The bias components resulted from measurement noise and position errors are coupled,

unless for some specific case where the measurement noise and position errors are IID. The bias behaviors for TOA, TDOA and AOA localizations are analyzed. TOA and TDOA positionings have smaller bias for a distant than a near object. On the contrary, AOA positioning has larger bias for a distant object. While sensor position errors have considerable effects in increasing the location bias for TOA and TDOA positionings, the bias of AOA localization is relatively resilient to sensor position errors. On the average, TOA positioning has smaller bias than TDOA and AOA positionings under the same noise conditions. Occasionally, however, TDOA could have smaller bias than TOA for some localization geometries.

The geometric conditions that yield zero bias are derived. They are found to be similar but more restrictive than those that yield minimum variance. An application of the developed theoretical results to compensate for the bias in the object tracking problem is presented. The usefulness of the derived bias expressions and the importance of bias compensation are clearly demonstrated.

Chapter 4

Elliptic Positioning: Performance Study and Optimum Receiver Placement

This Chapter accomplishes a fundamental investigation on the performance of elliptic localization, both synchronous and asynchronous, with respect to the hyperbolic positioning, TDOA. The performance comparison is through the CRLB analysis under Gaussian noise. The transmitter and receiver position errors are taken into account in addition to measurement noise. To complement the CRLB study, we also evaluate the bias when the MLE is used. We advance the investigation further by deriving the optimum receiver placement with respect to a single transmitter that minimizes the localization error.

4.1 Elliptic Positioning Performance

The performance evaluation here is for small noise analysis such that the CRLB is adequate to indicate the best possible accuracy of a location estimate.

4.1.1 CRLB

We introduce the transmitter and receiver positions as nuisance variables so that the unknown parameter vector for the CRLB evaluation is $\boldsymbol{\gamma}^o = \left[\, \mathbf{u}^{oT}\,,\, \mathbf{t}^{oT}\,,\, \mathbf{s}^{oT}\,\right]^T$, where $\mathbf{t}^o$ and $\mathbf{s}^o$ are deterministic nuisance parameters. From the error models described in Chapter 2, the logarithm of the probability density function under $\boldsymbol{\gamma}^o$ is $\ln p(\mathbf{m}, \mathbf{t}, \mathbf{s}\,|\,\boldsymbol{\gamma}^o) = C - \frac{1}{2}(\mathbf{m}-\mathbf{m}^o)^T\mathbf{Q}_\mathbf{m}^{-1}(\mathbf{m}-\mathbf{m}^o) - \frac{1}{2}(\mathbf{t}-\mathbf{t}^o)^T\mathbf{Q}_\mathbf{t}^{-1}(\mathbf{t}-\mathbf{t}^o) - \frac{1}{2}(\mathbf{s}-\mathbf{s}^o)^T\mathbf{Q}_\mathbf{s}^{-1}(\mathbf{s}-\mathbf{s}^o)$, where C is a constant independent of $\boldsymbol{\gamma}^o$. The FIM by (2.18) is

$$\mathrm{FIM}_{\boldsymbol{\gamma}} = \boldsymbol{\nabla}_{\boldsymbol{\gamma}}^T\mathbf{Q}_\mathbf{m}^{-1}\boldsymbol{\nabla}_{\boldsymbol{\gamma}} + \mathrm{diag}\left(\,\mathbf{O}_{K\times K}\,,\,\mathbf{Q}_\mathbf{t}^{-1}\,,\,\mathbf{Q}_\mathbf{s}^{-1}\,\right)\,, \tag{4.1}$$

where $\boldsymbol{\nabla}_{\boldsymbol{\gamma}} = [\,\boldsymbol{\nabla}_\mathbf{u}\,,\,\boldsymbol{\nabla}_\mathbf{t}\,,\,\boldsymbol{\nabla}_\mathbf{s}\,] = \partial\mathbf{m}^o\,(\boldsymbol{\gamma}^o)/\partial\boldsymbol{\gamma}^T$.

The CRLB of $\mathbf{u}^o$ is the upper left $K\times K$ block of $\mathrm{FIM}_{\boldsymbol{\gamma}}^{-1}$. Invoking the partitioned matrix inversion formula and the Woodbury identity [22] to (4.1), we have

$$\mathrm{CRLB}_\mathbf{u} = \mathrm{FIM}_\mathbf{u}^{-1} \quad,\quad \mathrm{FIM}_\mathbf{u} = \boldsymbol{\nabla}_\mathbf{u}^T\left(\mathbf{Q} + \boldsymbol{\nabla}_\mathbf{t}\mathbf{Q}_\mathbf{t}\boldsymbol{\nabla}_\mathbf{t}^T + \boldsymbol{\nabla}_\mathbf{s}\mathbf{Q}_\mathbf{s}\boldsymbol{\nabla}_\mathbf{s}^T\right)^{-1}\boldsymbol{\nabla}_\mathbf{u}\,. \tag{4.2}$$

Furthermore, let us define the matrices

$$\mathbf{P}_{\mathbf{u},\mathbf{t}} = \mathbf{1}_N\boldsymbol{\rho}_{\mathbf{u}^o,\mathbf{t}^o}^T, \tag{4.3a}$$

$$\mathbf{P}_{\mathbf{t},\mathbf{s}} = \left[\, \boldsymbol{\rho}_{\mathbf{t}^o,\mathbf{s}_1^o} \,,\, \boldsymbol{\rho}_{\mathbf{t}^o,\mathbf{s}_2^o} \,,\, \cdots \,,\, \boldsymbol{\rho}_{\mathbf{t}^o,\mathbf{s}_N^o} \,\right]^T , \tag{4.3b}$$

$$\widetilde{\mathbf{P}}_{\mathbf{t},\mathbf{s}} = \mathrm{diag}\left(\boldsymbol{\rho}_{\mathbf{t}^o,\mathbf{s}_1^o} \,,\, \boldsymbol{\rho}_{\mathbf{t}^o,\mathbf{s}_2^o} \,,\, \cdots \,,\, \boldsymbol{\rho}_{\mathbf{t}^o,\mathbf{s}_N^o} \right)^T , \tag{4.3c}$$

where $\boldsymbol{\rho}_{\mathbf{u}^o,\mathbf{t}^o}$ and $\boldsymbol{\rho}_{\mathbf{t}^o,\mathbf{s}_j^o}$ are similarly defined with $\boldsymbol{\rho}_{\mathbf{u}^o,\mathbf{s}_j^o}$ below (A.13b). The partial derivatives $\boldsymbol{\nabla}_{\mathbf{u}}$, $\boldsymbol{\nabla}_{\mathbf{t}}$ and $\boldsymbol{\nabla}_{\mathbf{s}}$ can be expressed in term of the matrices in (4.3). Appendix B.1 contains the evaluations of the FIMs for SE, AE and hyperbolic localizations. We are now ready to examine the performance of elliptic localization.

Let

$$\mathbf{R} = \begin{bmatrix} \mathbf{Q}_{\mathrm{SE}} & \mathbf{O}_{N\times N} \\ \mathbf{O}_{N\times N} & \bar{\mathbf{Q}}_{\mathrm{SE}} \end{bmatrix} + \begin{bmatrix} \mathbf{P}_{\mathbf{u},\mathbf{t}} \\ -\mathbf{P}_{\mathbf{t},\mathbf{s}} \end{bmatrix} \mathbf{Q}_{\mathbf{t}} \begin{bmatrix} \mathbf{P}_{\mathbf{u},\mathbf{t}} \\ -\mathbf{P}_{\mathbf{t},\mathbf{s}} \end{bmatrix}^T + \begin{bmatrix} \widetilde{\mathbf{P}}_{\mathbf{u},\mathbf{s}} \\ \widetilde{\mathbf{P}}_{\mathbf{t},\mathbf{s}} \end{bmatrix} \mathbf{Q}_{\mathbf{s}} \begin{bmatrix} \widetilde{\mathbf{P}}_{\mathbf{u},\mathbf{s}} \\ \widetilde{\mathbf{P}}_{\mathbf{t},\mathbf{s}} \end{bmatrix}^T \tag{4.4}$$

and $\mathbf{P}_{\mathbf{R}} = \left[\, \mathbf{P}_{\mathbf{u},\mathbf{s}}^T + \mathbf{P}_{\mathbf{u},\mathbf{t}}^T \,,\, \mathbf{O}_{K\times N} \,\right]^T$, where $\mathbf{P}_{\mathbf{u},\mathbf{s}}$ and $\widetilde{\mathbf{P}}_{\mathbf{u},\mathbf{s}}$ are defined below (A.19c). After some direct algebraic manipulations, the FIMs can be expressed as

$$\mathrm{FIM}_{\mathbf{u},\mathrm{SE_f}} = \mathbf{P}_{\mathbf{R}}^T \mathbf{R}^{-1} \mathbf{P}_{\mathbf{R}} \,, \tag{4.5a}$$

$$\mathrm{FIM}_{\mathbf{u},\mathrm{SE}} = \mathbf{P}_{\mathbf{R}}^T \mathbf{L}_{\mathrm{SE}} \left(\mathbf{L}_{\mathrm{SE}}^T \mathbf{R} \mathbf{L}_{\mathrm{SE}} \right)^{-1} \mathbf{L}_{\mathrm{SE}}^T \mathbf{P}_{\mathbf{R}} \,, \tag{4.5b}$$

$$\mathrm{FIM}_{\mathbf{u},\mathrm{AE}} = \mathbf{P}_{\mathbf{R}}^T \mathbf{L}_{\mathrm{AE}} \left(\mathbf{L}_{\mathrm{AE}}^T \mathbf{R} \mathbf{L}_{\mathrm{AE}} \right)^{-1} \mathbf{L}_{\mathrm{AE}}^T \mathbf{P}_{\mathbf{R}} \,, \tag{4.5c}$$

$$\mathrm{FIM}_{\mathbf{u},\mathrm{H}} = \mathbf{P}_{\mathbf{R}}^T \mathbf{L}_{\mathrm{H}} \left(\mathbf{L}_{\mathrm{H}}^T \mathbf{R} \mathbf{L}_{\mathrm{H}} \right)^{-1} \mathbf{L}_{\mathrm{H}}^T \mathbf{P}_{\mathbf{R}} \,, \tag{4.5d}$$

where the subscript $\mathrm{SE_f}$ denotes SE positioning with the extra direct propagation measurement $\bar{\mathbf{m}}_{\mathrm{SE}}$. In (4.5),

$$\mathbf{L}_{\mathrm{SE}} = \left[\, \mathbf{I}_N \,,\, \mathbf{O}_{N\times N} \,\right]^T \,,\;\; \mathbf{L}_{\mathrm{AE}} = \left[\, \mathbf{I}_N \,,\, -\mathbf{I}_N \,\right]^T \,,\;\; \mathbf{L}_{\mathrm{H}} = \left[\, \mathbf{H} \,,\, \mathbf{O}_{(N-1)\times N} \,\right]^T \,. \tag{4.6}$$

Note that $\mathbf{L}_{\mathrm{SE}}$ is $2N \times N$, $\mathbf{L}_{\mathrm{AE}}$ is $2N \times N$, $\mathbf{L}_{\mathrm{H}}$ is $2N \times (N-1)$, $\mathbf{H}$ is defined below (A.22).

The matrix $\mathbf{R}$ can be decomposed as $\mathbf{R} = \mathbf{R}^{\frac{1}{2}}\mathbf{R}^{\frac{1}{2}}$ since $\mathbf{R}$ is symmetric and positive definite (PD). If we define $\widetilde{\mathbf{L}}_{\mathrm{SE}} = \mathbf{R}^{\frac{1}{2}}\mathbf{L}_{\mathrm{SE}}$, $\widetilde{\mathbf{L}}_{\mathrm{AE}} = \mathbf{R}^{\frac{1}{2}}\mathbf{L}_{\mathrm{AE}}$, $\widetilde{\mathbf{L}}_{\mathrm{H}} = \mathbf{R}^{\frac{1}{2}}\mathbf{L}_{\mathrm{H}}$ and $\widetilde{\mathbf{P}}_{\mathbf{R}} = \mathbf{R}^{-\frac{1}{2}}\mathbf{P}_{\mathbf{R}}$, (4.5) can be rewritten as

$$\mathrm{FIM}_{\mathbf{u},\mathrm{SE_f}} = \widetilde{\mathbf{P}}_{\mathbf{R}}^{T}\widetilde{\mathbf{P}}_{\mathbf{R}}\,, \tag{4.7a}$$

$$\mathrm{FIM}_{\mathbf{u},\mathrm{SE}} = \widetilde{\mathbf{P}}_{\mathbf{R}}^{T}\widetilde{\mathbf{L}}_{\mathrm{SE}}\left(\widetilde{\mathbf{L}}_{\mathrm{SE}}^{T}\widetilde{\mathbf{L}}_{\mathrm{SE}}\right)^{-1}\widetilde{\mathbf{L}}_{\mathrm{SE}}^{T}\widetilde{\mathbf{P}}_{\mathbf{R}} = \widetilde{\mathbf{P}}_{\mathbf{R}}^{T}\mathbf{P}_{\mathrm{SE}}\widetilde{\mathbf{P}}_{\mathbf{R}}\,, \tag{4.7b}$$

$$\mathrm{FIM}_{\mathbf{u},\mathrm{AE}} = \widetilde{\mathbf{P}}_{\mathbf{R}}^{T}\widetilde{\mathbf{L}}_{\mathrm{AE}}\left(\widetilde{\mathbf{L}}_{\mathrm{AE}}^{T}\widetilde{\mathbf{L}}_{\mathrm{AE}}\right)^{-1}\widetilde{\mathbf{L}}_{\mathrm{AE}}^{T}\widetilde{\mathbf{P}}_{\mathbf{R}} = \widetilde{\mathbf{P}}_{\mathbf{R}}^{T}\mathbf{P}_{\mathrm{AE}}\widetilde{\mathbf{P}}_{\mathbf{R}}\,, \tag{4.7c}$$

$$\mathrm{FIM}_{\mathbf{u},\mathrm{H}} = \widetilde{\mathbf{P}}_{\mathbf{R}}^{T}\widetilde{\mathbf{L}}_{\mathrm{H}}\left(\widetilde{\mathbf{L}}_{\mathrm{H}}^{T}\widetilde{\mathbf{L}}_{\mathrm{H}}\right)^{-1}\widetilde{\mathbf{L}}_{\mathrm{H}}^{T}\widetilde{\mathbf{P}}_{\mathbf{R}} = \widetilde{\mathbf{P}}_{\mathbf{R}}^{T}\mathbf{P}_{\mathrm{H}}\widetilde{\mathbf{G}}_{\mathbf{R}}\,, \tag{4.7d}$$

where $\mathbf{P}_{\mathrm{X}}$ is the projection matrix onto the column space of $\widetilde{\mathbf{L}}_{\mathrm{X}}$. In the following we shall simply call the subspace spanned by the columns of $\widetilde{\mathbf{L}}_{\mathrm{X}}$ as the subspace of X. Expressing the FIMs in the forms of (4.7) enables us to compare the performance of the four localization approaches directly.

We shall say a localization method A outperforms a method B if $\mathrm{CRLB_B} - \mathrm{CRLB_A} \succeq 0$, where $\succeq$ stands for positive semi-definite (PSD) and we shall use the symbol $\succ$ for PD. The condition implies $\mathrm{tr}\,(\mathrm{CRLB_B}) - \mathrm{tr}\,(\mathrm{CRLB_A}) \geq 0$. $\mathrm{tr}\,(\mathrm{CRLB})$ has the physical meaning that it is the minimum possible mean-square position error for the unknown object.

The CRLB is the inverse of the FIM and the condition $\mathrm{CRLB_B} - \mathrm{CRLB_A} \succeq 0$ is equivalent to $\mathrm{FIM_A} - \mathrm{FIM_B} \succeq 0$ from the PSD matrix property [79]. The performance study in this Section uses the FIM instead of the CRLB to simplify the derivations and

avoid the evaluation of matrix inverse. The other Sections followed will use tr (CRLB) as the performance index due to its physical meaning and the ease of comparison on the localization errors.

$\mathbf{SE_f}$ vs SE, AE and H

Let us consider SE first. The subspace of SE has a dimension of N and $\mathbf{P}_{\mathrm{SE}}$ is $2N \times 2N$. Hence,

$$\mathbf{I}_{2N} - \mathbf{P}_{\mathrm{SE}} \succeq 0\,. \tag{4.8}$$

Pre- and post-multiplying by $\widetilde{\mathbf{P}}_{\mathbf{R}}^{T}$ and $\widetilde{\mathbf{P}}_{\mathbf{R}}$ does not affect the PSD relation. Thus

$$\mathrm{FIM}_{\mathbf{u},\mathrm{SE_f}} - \mathrm{FIM}_{\mathbf{u},\mathrm{SE}} \succeq 0\,. \tag{4.9}$$

Similarly, by the same argument we have

$$\mathrm{FIM}_{\mathbf{u},\mathrm{SE_f}} - \mathrm{FIM}_{\mathbf{u},\mathrm{AE}} \succeq 0\,, \qquad \mathrm{FIM}_{\mathbf{u},\mathrm{SE_f}} - \mathrm{FIM}_{\mathbf{u},\mathrm{H}} \succeq 0\,. \tag{4.10}$$

Consequently, $\mathrm{SE_f}$ outperforms SE, AE and H. This is not unexpected because $\mathrm{SE_f}$ has the richest set of measurements.

SE vs AE

The subspace dimension of SE is N and so does that of AE. They do not span the same subspace as can be seen from (4.6) although the two subspaces overlap. We cannot conclude if $\mathrm{FIM}_{\mathbf{u},\mathrm{SE}} - \mathrm{FIM}_{\mathbf{u},\mathrm{AE}}$ is PSD or vice versa. Depending on the localization scenario, one could outperform the other but it is not always.

To illustrate, let us consider the specific case [4, 5, 27, 73] that the transmitter and receiver position errors are having $\mathbf{Q_t} = \sigma_{\mathbf{t}}^2 \mathbf{I}_K$ and $\mathbf{Q_s} = \widetilde{\mathbf{Q}}_{\mathbf{s}} \otimes \mathbf{I}_K$, with $\widetilde{\mathbf{Q}}_{\mathbf{s}} = \mathrm{diag}(\, \sigma_{\mathbf{s}_1}^2 \,,\, \sigma_{\mathbf{s}_2}^2 \,,\, \cdots \,,\, \sigma_{\mathbf{s}_N}^2 \,)$, and the measurement covariance matrices are $\mathbf{Q}_{\mathrm{SE}} = \mathrm{diag}(\, \sigma_{m_1}^2 \,,\, \sigma_{m_2}^2 \,,\, \cdots \,,\, \sigma_{m_N}^2 \,)$ and $\bar{\mathbf{Q}}_{\mathrm{SE}} = \mathrm{diag}(\, \bar{\sigma}_{m_1}^2 \,,\, \bar{\sigma}_{m_2}^2 \,,\, \cdots \,,\, \bar{\sigma}_{m_N}^2 \,)$.

After substituting (4.3) into (B.4b) and (B.6b), we have $\mathbf{R}_{\mathrm{AE}} - \mathbf{R}_{\mathrm{SE}} \succ 0$ and hence SE positioning is better than AE if the following conditions are satisfied:

$$\boldsymbol{\rho}_{\mathbf{t}^o,\mathbf{s}_1^o} = \cdots = \boldsymbol{\rho}_{\mathbf{t}^o,\mathbf{s}_N^o} \,, \qquad \boldsymbol{\rho}_{\mathbf{u}^o,\mathbf{t}^o}^T \boldsymbol{\rho}_{\mathbf{t}^o,\mathbf{s}_j^o} > -\frac{1}{2} \,, \qquad j = 1 \,,\, 2 \,,\, \ldots \,,\, N \,, \tag{4.11a}$$

$$\boldsymbol{\rho}_{\mathbf{u}^o,\mathbf{s}_j^o}^T \boldsymbol{\rho}_{\mathbf{t}^o,\mathbf{s}_j^o} < \frac{1}{2} \left(1 + \frac{\bar{\sigma}_{m_j}^2}{\sigma_{\mathbf{s}_j}^2} \right) , \qquad j = 1 \,,\, 2 \,,\, \ldots \,,\, N \,. \tag{4.11b}$$

(4.11) implies the transmitter and receivers are co-linear and the source is in the broadside far away from them. On the contrary, AE outperforms SE if

$$\boldsymbol{\rho}_{\mathbf{t}^o,\mathbf{s}_1^o} = \cdots = \boldsymbol{\rho}_{\mathbf{t}^o,\mathbf{s}_N^o} \,, \qquad \boldsymbol{\rho}_{\mathbf{u}^o,\mathbf{t}^o}^T \boldsymbol{\rho}_{\mathbf{t}^o,\mathbf{s}_j^o} < -\frac{1}{2} \,, \qquad j = 1 \,,\, 2 \,,\, \ldots \,,\, N \,, \tag{4.12a}$$

$$\boldsymbol{\rho}_{\mathbf{u}^o,\mathbf{s}_j^o}^T \boldsymbol{\rho}_{\mathbf{t}^o,\mathbf{s}_j^o} > \frac{1}{2} \left(1 + \frac{\bar{\sigma}_{m_j}^2}{\sigma_{\mathbf{s}_j}^2} \right) , \qquad j = 1 \,,\, 2 \,,\, \ldots \,,\, N \,, \tag{4.12b}$$

which happens if the source is close relative to the baseline span of the transmitter and receivers.

Fig. 4.1 gives an example geometry for the situation (4.11) in which $\boldsymbol{\rho}_{\mathbf{u}^o,\mathbf{t}^o}^T \boldsymbol{\rho}_{\mathbf{t}^o,\mathbf{s}_j^o} = \cos(105^o) \approx -0.2588$ and $\boldsymbol{\rho}_{\mathbf{u}^o,\mathbf{s}_j^o}^T \boldsymbol{\rho}_{\mathbf{t}^o,\mathbf{s}_j^o}$, $j = 1 \,,\, 2 \,,\, 3 \,,\, 4$, are $-0.0984, 0.0700, 0.3080$ and 0.5. With $\sigma_{\mathbf{t}}^2 = 0.1$, $\sigma_{\mathbf{s}_j}^2 = 0.1$, $\sigma_{m_j}^2 = 0.01$ and $\bar{\sigma}_{m_j}^2 = 0.01$, we have $\mathrm{tr}\,(\mathrm{CRLB}_{\mathbf{u},\mathrm{SE}}) = 0.5751$ and $\mathrm{tr}\,(\mathrm{CRLB}_{\mathbf{u},\mathrm{AE}}) = 0.8859$. Fig. 4.2 is an example geometry for the situation (4.12) where $\boldsymbol{\rho}_{\mathbf{u}^o,\mathbf{t}^o}^T \boldsymbol{\rho}_{\mathbf{t}^o,\mathbf{s}_j^o} = \cos(135^o) = -0.7071$ and $\boldsymbol{\rho}_{\mathbf{u}^o,\mathbf{s}_j^o}^T \boldsymbol{\rho}_{\mathbf{t}^o,\mathbf{s}_j^o}$, $j = 1 \,,\, 2 \,,\, 3 \,,\, 4$, are $0.5923, 0.7704, 0.8069$ and 0.8595. Under the same noise level settings,

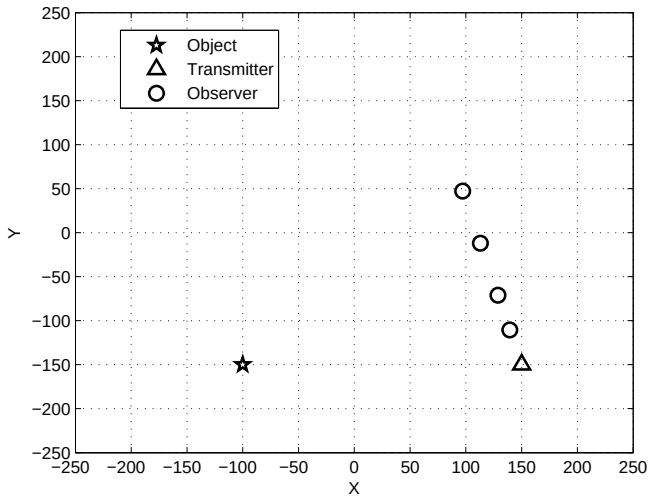

Figure 4.1: Sample configurations for SE outperforms AE.

$\mathrm{tr}\left(\mathrm{CRLB}_{\mathbf{u},\mathrm{SE}}\right) = 2.6673$ and $\mathrm{tr}\left(\mathrm{CRLB}_{\mathbf{u},\mathrm{AE}}\right) = 1.8951$.

SE vs H

The subspace dimension of H is $N-1$, 1 less than that of SE. Indeed, from (4.6) and pre-multiplying with $\mathbf{R}^{\frac{1}{2}}$,

$$\widetilde{\mathbf{L}}_{\mathrm{H}} = \widetilde{\mathbf{L}}_{\mathrm{SE}}\mathbf{H}^{T}\,. \tag{4.13}$$

The subspace of H is therefore included in the subspace of SE. As a result,

$$\mathbf{P}_{\mathrm{SE}} - \mathbf{P}_{\mathrm{H}} \succeq 0\,, \tag{4.14}$$

which yields

$$\mathrm{FIM}_{\mathbf{u},\mathrm{SE}} - \mathrm{FIM}_{\mathbf{u},\mathrm{H}} \succeq 0 \tag{4.15}$$

and SE outperforms H.

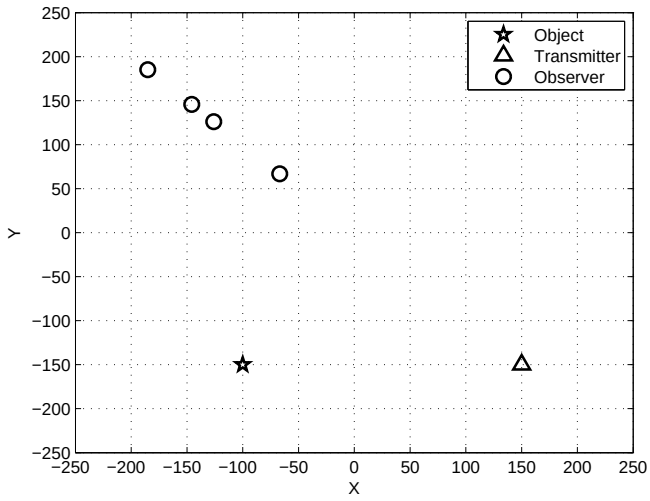

Figure 4.2: Sample configurations for AE outperforms SE.

In the specific case when there is no knowledge about the transmitter position, i.e. its prior distribution is not available, SE and H positionings will have identical performance. This is because in such situation the data model of SE is equivalent to TOA with bias where the bias is the distance between the transmitter and the object. Previous studies [7, 29] have shown that TOA positioning with a bias offset in the measurements has the same accuracy as TDOA localization.

AE vs H

The subspace dimension of AE is one more than that of H according to (4.6). However, the subspace of AE does not cover that of H although they overlap. We cannot conclude if $\mathrm{FIM}_{\mathbf{u},\mathrm{AE}} - \mathrm{FIM}_{\mathbf{u},\mathrm{H}}$ is PSD. We expect that AE would outperform H in some cases but not always.

The analysis of SE vs AE and SE vs H indicates that AE outperforms SE and

hence H when (4.12) is satisfied under the noise characteristics specified before (4.11). Fig. 4.2 is a sample geometry in which AE outperforms H positioning. Using the noise level settings as in subsection 4.1.1-2, we have $\mathrm{tr}\,(\mathrm{CRLB}_{\mathbf{u},\mathrm{AE}}) = 1.8951$ and $\mathrm{tr}\,(\mathrm{CRLB}_{\mathbf{u},\mathrm{H}}) = 401.6631$.

H is able to outperform AE on some occasions. One such scenario is for IID measurement and receiver position noise with $\mathbf{Q}_{\mathrm{SE}} = \bar{\mathbf{Q}}_{\mathrm{SE}}$ [4, 5], the localization geometry satisfies $\boldsymbol{\rho}_{\mathbf{u}^o,\mathbf{t}^o} + \boldsymbol{\rho}_{\mathbf{u}^o,\mathbf{s}_j^o} = \mathbf{0}_K$ with $j = 1\,,\,2\,,\,\ldots\,,\,\lceil M/2\rceil$ and $\boldsymbol{\rho}^T_{\mathbf{u}^o,\mathbf{s}_j^o}\boldsymbol{\rho}_{\mathbf{t}^o,\mathbf{s}_j^o} \leq 0$ for $j = \lceil M/2\rceil{+}1\,,\,\ldots\,,\,M$, where we have at least $M \geq 2K$ receivers. The simulation Section will provide more elaborations about the performance between AE and H.

Accurate Transmitter and Receiver Positions

The FIMs in this case can be obtained by setting $\mathbf{Q}_{\mathbf{t}}$ and $\mathbf{Q}_{\mathbf{s}}$ to zero in (4.4). Most of the conclusions from the general case of inaccurate transmitter and receiver positions carry but not all. We shall summarize the results and highlight the differences.

SE_{f} vs SE Putting $\mathbf{Q}_{\mathbf{t}}$ and $\mathbf{Q}_{\mathbf{s}}$ to zero in (4.4) gives $\mathbf{R} = \mathrm{diag}\,\big(\,\mathbf{Q}_{\mathrm{SE}}\,,\,\bar{\mathbf{Q}}_{\mathrm{SE}}\,\big)$. After multiplying out, (4.5a) and (4.5b) become identical and the performance of SE_{f} reduces back to SE. This is because the measurements (2.6) do not carry extra information to locate $\mathbf{u}^o$ when $\mathbf{t}^o$ and $\mathbf{s}_j^o$, $j = 1\,,\,2\,,\,\ldots\,,\,N$, are perfectly known.

SE vs AE It is more direct to use (B.4a) and (B.6a) for comparison. With accurate transmitter and receiver positions, using (2.9) we have from (B.4b) and (B.6b) that $\mathbf{R}_{\mathrm{SE}}^{-1} - \mathbf{R}_{\mathrm{AE}}^{-1} \succ 0$. Thus $\mathrm{FIM}_{\mathbf{u},\mathrm{SE}} - \mathrm{FIM}_{\mathbf{u},\mathrm{AE}}$ is PD, meaning that SE

positioning always provides better accuracy than AE positioning. This conclusion is consistent with the previous study in [20].

The conclusion is different from the situation when errors in transmitter and receiver positions are present in which SE is not necessarily better than AE.

SE vs H The analysis in subsection 4.1.1-3 remains applicable and SE outperforms H. This is consistent with the observation in [20].

AE vs H The comparison in subsection 4.1.1-4 remains valid and AE will not be definitely better than H or vice versa. One exception is that when $\mathbf{Q}_{\mathrm{SE}}^{-1}\bar{\mathbf{Q}}_{\mathrm{SE}}$ is nearly zero as in some UWB localization problems [20]. In such a case, $\mathbf{R}_{\mathrm{AE}} \approx \mathbf{R}_{\mathrm{SE}}$, (B.4a) and (B.6a) become identical, and AE will outperform H. When $\bar{\mathbf{Q}}_{\mathrm{SE}}$ increases, the possibility that H outperforms AE increases.

4.1.2 Bias

The CRLB study in the previous subsection neglects the estimation bias caused by the nonlinear nature of the localization problem. To complement the investigation, we shall examine the bias of the object location estimate for the three elliptic localization approaches, when the MLE is used. Following the steps of the derivation of (3.8) in Chapter 3, the bias of the object location estimate in the elliptic positioning problems can be computed by the formula

$$\mathbf{b_u} = -\frac{1}{2}\mathrm{FIM}_{\mathbf{u}}^{-1}\boldsymbol{\nabla}_{\mathbf{u}}^{T}\left(\mathbf{Q_m} + \boldsymbol{\nabla}_{\mathbf{t}}\mathbf{Q_t}\boldsymbol{\nabla}_{\mathbf{t}}^{T} + \boldsymbol{\nabla}_{\mathbf{s}}\mathbf{Q_s}\boldsymbol{\nabla}_{\mathbf{s}}^{T}\right)^{-1}\mathbf{k}\,. \tag{4.16}$$

(4.16) is a common formula applicable to the three elliptic localization approaches and hyperbolic positioning when substituting their $\text{FIM}_{\mathbf{u}}$ values in (4.7) and the partial derivatives in (B.1), (B.3), (B.5) and (B.7). The evaluation of $\mathbf{k}$ requires the second order derivatives and they are given in Appendix B.2.

Comparing the bias of the four localization approaches analytically is not tractable. We shall rely on numerical evaluations of the bias over a number of randomly generated geometries and the results will be presented in Section 4.3.

4.1.3 Multiple Transmitters

When multiple transmitters, say M, are present, their emitted signals are often disjoint in time or in frequency, or made orthogonal [8, 17, 18, 80, 81] such that the time measurements from different transmitters can be separated. The transmitter position vector $\mathbf{t}$ in (2.1) is a collection of all M transmitter positions and it has a length of KM. The main set of equations in (4.7) for the comparison of different localization approaches remains valid when re-defining the relevant quantities as follows. The matrix $\mathbf{R}$ in (4.4) now is $2MN \times 2MN$, the measurement noise covariance matrices $\mathbf{Q}_{\text{SE}}$ and $\bar{\mathbf{Q}}_{\text{SE}}$ are both $MN \times MN$, the transmitter correlation matrix $\mathbf{Q}_{\mathbf{t}}$ is $KM \times KM$ and $\mathbf{P}_{\mathbf{R}}$ in (4.5) is $2MN \times K$. The matrices in (4.6) become $\mathbf{L}_{\text{SE}} = [\, \mathbf{I}_M \otimes \mathbf{I}_N \,,\, \mathbf{I}_M \otimes \mathbf{O}_{N\times N} \,]^T$, $\mathbf{L}_{\text{AE}} = [\, \mathbf{I}_M \otimes \mathbf{I}_N \,,\, -\mathbf{I}_M \otimes \mathbf{I}_N \,]^T$, $\mathbf{L}_{\text{H}} = \left[\, \mathbf{I}_M \otimes \mathbf{H} \,,\, \mathbf{I}_M \otimes \mathbf{O}_{(N-1)\times N} \,\right]^T$. Their sizes are $2MN \times MN$, $2MN \times MN$ and $2MN \times M(N-1)$. Following the same derivations based on the dimensions of $\mathbf{L}_{\text{SE}}$, $\mathbf{L}_{\text{AE}}$ and $\mathbf{L}_{\text{H}}$ as in the single transmitter case, it is straightforward to verify that the conclusions about the comparisons of different localization approaches remain to be the same when we have multiple transmitters.

The formula (4.16) to examine the bias remains applicable after re-defining the

matrices and vector involved according to the multiple transmitter case.

4.2 Optimum Receiver Placement

This Section derives the optimum placement of receivers for SE and AE positionings with one transmitter. The optimization criterion is the trace of the CRLB for the object location. To make the mathematics tractable, we shall follow the noise setting as in [30, 31, 73] for obtaining the optimum geometry of hyperbolic localization, which is $\mathbf{Q}_{\mathrm{SE}} = \sigma_{\mathbf{m}}^2 \mathbf{I}_N$, $\bar{\mathbf{Q}}_{\mathrm{SE}} = \bar{\sigma}_{\mathbf{m}}^2 \mathbf{I}_N$ and zero $\mathbf{n_t}$ and $\mathbf{n_s}$. This setting implies the object has similar distances to the receivers [8], and comparable distances between the transmitter and the receivers as well for AE positioning. This situation occurs when the receivers are not close to the object and to the transmitter.

We shall look at the optimum receiver placements in 2D and 3D cases separately, starting with SE positioning. The optimum placements of AE positioning will be obtained directly from the SE's results.

4.2.1 2D

2D localization requires at least one transmitter and $N \geq 3$ receivers to uniquely identify the object location. If some prior knowledge about the region where the object lies is available to resolve the ambiguity of two possible solutions, $N \geq 2$ receivers could be sufficient. When substituting $\mathbf{Q}_{\mathrm{SE}} = \sigma_{\mathbf{m}}^2 \mathbf{I}_N$, $\mathbf{Q_t} = \mathbf{O}_K$ and $\mathbf{Q_s} = \mathbf{O}_{KN}$ into (B.4b), (B.4a) reduces to

$$\mathrm{FIM}_{\mathbf{u},\mathrm{SE}} = \sigma_{\mathbf{m}}^{-2} \left(\mathbf{P}_{\mathbf{u},\mathbf{s}} + \mathbf{P}_{\mathbf{u},\mathbf{t}}\right)^T \left(\mathbf{P}_{\mathbf{u},\mathbf{s}} + \mathbf{P}_{\mathbf{u},\mathbf{t}}\right) . \tag{4.17}$$

Using the definitions of $\mathbf{P}_{\mathbf{u},\mathbf{s}}$ and $\mathbf{P}_{\mathbf{u},\mathbf{t}}$ from (4.3), (4.17) becomes

$$\mathrm{FIM}_{\mathbf{u},\mathrm{SE}} = \sigma_{\mathbf{m}}^{-2} \sum_{j=1}^{N} \left(\boldsymbol{\rho}_{\mathbf{u}^o,\mathbf{s}_j^o} + \boldsymbol{\rho}_{\mathbf{u}^o,\mathbf{t}^o} \right) \left(\boldsymbol{\rho}_{\mathbf{u}^o,\mathbf{s}_j^o} + \boldsymbol{\rho}_{\mathbf{u}^o,\mathbf{t}^o} \right)^T . \tag{4.18}$$

Without loss of generality, we use $\boldsymbol{\rho}_{\mathbf{u}^o,\mathbf{t}^o}$ as the coordinate reference by setting $\boldsymbol{\rho}_{\mathbf{u}^o,\mathbf{t}^o} = [\,1\,,\,0\,]^T$. Let θ_j be the angle of receiver j with respect to the object. Then we have $\boldsymbol{\rho}_{\mathbf{u}^o,\mathbf{s}_j^o} = [\,\cos\theta_j\,,\,\sin\theta_j\,]^T$, $j = 1\,,\,2\,,\,\ldots\,,\,N$ and (4.18) can be expressed as

$$\mathrm{FIM}_{\mathbf{u},\mathrm{SE}} = \sigma_{\mathbf{m}}^{-2} \sum_{j=1}^{N} \begin{bmatrix} (1+\cos\theta_j)^2 & (1+\cos\theta_j)\sin\theta_j \\ (1+\cos\theta_j)\sin\theta_j & \sin^2\theta_j \end{bmatrix} . \tag{4.19}$$

The optimum receiver placement problem is to determine θ_j such that the trace of the CRLB for the object location is smallest.

Let λ_1 and λ_2 be the eigenvalues of $\mathrm{FIM}_{\mathbf{u},\mathrm{SE}}$ where $\lambda_1 \geq \lambda_2$. Then

$$\mathrm{tr}\,(\mathrm{CRLB}_{\mathbf{u},\mathrm{SE}}) = \frac{1}{\lambda_1} + \frac{1}{\lambda_2} = \frac{1}{\lambda_1} + \frac{1}{\mathrm{tr}\,(\mathrm{FIM}_{\mathbf{u},\mathrm{SE}}) - \lambda_1} . \tag{4.20}$$

It is easy to verify (4.20) is an increasing function of λ_1 by examining its derivative with respect to λ_1. As a result, $\mathrm{tr}\,(\mathrm{CRLB}_{\mathbf{u},\mathrm{SE}})$ has the smallest value when λ_1 is smallest. By the Courant-Fischer-Weyl min-max principle [79], the smallest possible value of λ_1 is the largest diagonal element, implying that $\mathrm{FIM}_{\mathbf{u},\mathrm{SE}}$ is diagonal and

$$\sum_{j=1}^{N} (1+\cos\theta_j)\sin\theta_j = 0\,, \tag{4.21}$$

making the diagonal elements of (4.19) equal to the eigenvalues.

For notation simplicity, let the variables a_j be $1+\cos\theta_j$, so that $\sum_{j=1}^{N} (1+\cos\theta_j)^2 =$

$\sum_{j=1}^{N} a_j^2$ and $\sum_{j=1}^{N} \sin^2\theta_j = \sum_{j=1}^{N} a_j\,(2 - a_j)$. Hence using the diagonal elements of $\mathrm{FIM}_{\mathbf{u},\mathrm{SE}}$ from (4.19) as the eigenvalues in (4.20) yields

$$\mathrm{tr}\,(\mathrm{CRLB}_{\mathbf{u},\mathrm{SE}}) \geq \sigma_{\mathbf{m}}^2 \frac{2\sum_{j=1}^{N} a_j}{2\sum_{j=1}^{N} a_j \sum_{j=1}^{N} a_j^2 - \sum_{j=1}^{N} a_j^2 \sum_{j=1}^{N} a_j^2}\,, \tag{4.22}$$

where $0 \leq a_j \leq 2$. We have the equality when (4.21) is fulfilled.

Given any real numbers $a_1\,,\, a_2\,,\, \ldots\,,\, a_N$, they satisfy the inequality [82]

$$\sum_{j=1}^{N} a_j^2 \geq \frac{1}{N}\left(\sum_{j=1}^{N} a_j\right)^2 \tag{4.23}$$

with the equality holds when

$$a_1 = a_2 = \cdots = a_N = a\,. \tag{4.24}$$

Thus,

$$\mathrm{tr}\,(\mathrm{CRLB}_{\mathbf{u},\mathrm{SE}}) \geq \sigma_{\mathbf{m}}^2 \frac{2N}{2N\sum_{j=1}^{N} a_j^2 - \sum_{j=1}^{N} a_j \sum_{j=1}^{N} a_j^2} \tag{4.25}$$

and the least bounding value occurs by putting (4.24) to (4.25)

$$\mathrm{tr}\,(\mathrm{CRLB}_{\mathbf{u},\mathrm{SE}}) \geq \frac{2\sigma_{\mathbf{m}}^2}{2Na^2 - Na^3}\,. \tag{4.26}$$

The right side of (4.26) gives the smallest possible value of $\mathrm{tr}\,(\mathrm{CRLB}_{\mathbf{u},\mathrm{SE}})$. It can further be optimized with respect to a. The function $2a^2 - a^3$ reaches the maximum at $a = 4/3$. Thus, $\cos\theta_j = 1/3$, $j = 1\,,\, 2\,,\, \ldots\,,\, N$. The resultant smallest error is

$$\mathrm{tr}\,(\mathrm{CRLB}_{\mathbf{u},\mathrm{SE}})_{\min} = \frac{27}{16N}\sigma_{\mathbf{m}}^2\,. \tag{4.27}$$

To satisfy the condition (4.21), we further require N is even and $\sin\theta_j = -\sin\theta_{j+1}$, $j = 1\,,\,2\,,\,\ldots\,,\,N-1$. As a result, the optimum receiver placement of the SE positioning in 2D is that

$$\boldsymbol{\rho}^T_{\mathbf{u}^o,\mathbf{t}^o}\boldsymbol{\rho}_{\mathbf{u}^o,\mathbf{s}^o_j} = \cos\theta_j = 1/3\,, \quad j = 1\,,\,2\,,\,\ldots\,,\,N\,, \tag{4.28a}$$

$$\sin\theta_j = -\sin\theta_{j+1}\,, \quad j = 1\,,\,2\,,\,\ldots\,,\,N-1\,,\ \text{ even } N\,. \tag{4.28b}$$

The optimum placement for odd N is a subject for further study. It is more difficult to derive because it does not fulfill (4.21).

Fig. 4.3 illustrates the optimum placement according to (4.28). The sensors are distributed along the two lines, with half of the sensors in each having an angle of $\cos^{-1}(1/3) = 70.53^o$ at $\mathbf{u}^o$ with respect to the axis of joining $\mathbf{u}^o$ and $\mathbf{t}^o$.

The optimum receiver arrangement depends on the object position $\mathbf{u}^o$ that is not known. It can be set according to some initial estimates of $\mathbf{u}^o$. Section 4.3 provides some study of the sensitivity of the optimum placement with respect to $\mathbf{u}^o$.

4.2.2 3D

3D localization requires $N \geq 3$ receivers. Similar with the 2D case, we set $\boldsymbol{\rho}_{\mathbf{u}^o,\mathbf{t}^o}$ as the coordinate reference such that $\boldsymbol{\rho}_{\mathbf{u}^o,\mathbf{t}^o} = [\,0\,,\,0\,,\,1\,]^T$. The sensor positions are defined by the polar and azimuth angles θ_j and ϕ_j as shown in Fig. 4.4, and $\boldsymbol{\rho}_{\mathbf{u}^o,\mathbf{s}^o_j} = [\,\sin\theta_j\cos\phi_j\,,\,\sin\theta_j\sin\phi_j\,,\,\cos\theta_j\,]^T$, $j = 1\,,\,2\,,\,\ldots\,,\,N$. We would like to optimize the performance with respect to θ_j and ϕ_j.

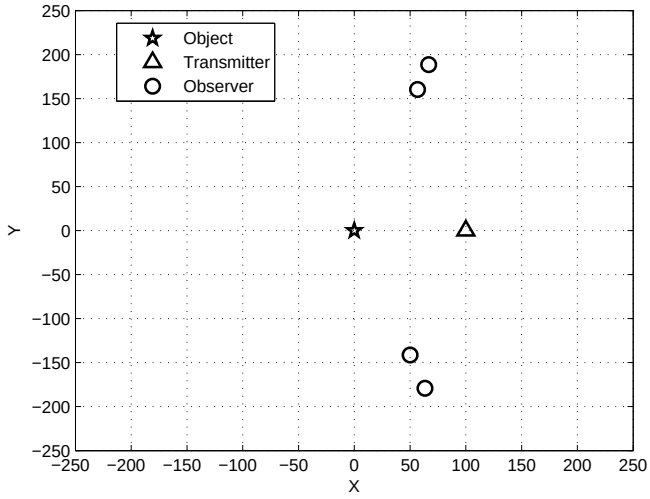

Figure 4.3: A sample configuration of the optimum receiver placement for 2D elliptic positioning.

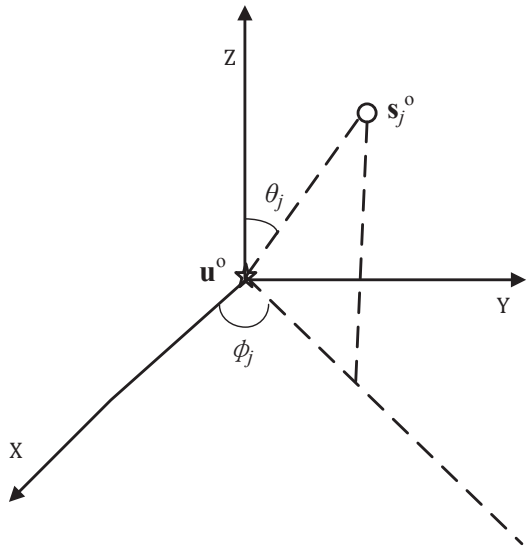

Figure 4.4: The definitions of θ_j and ϕ_j.

With $\mathbf{Q}_{\mathrm{SE}} = \sigma_{\mathbf{m}}^2 \mathbf{I}_N$, $\mathrm{FIM}_{\mathbf{u},\mathrm{SE}}$ in (4.17) is

$$\mathrm{FIM}_{\mathbf{u},\mathrm{SE}} = \sigma_{\mathbf{m}}^{-2} \sum_{j=1}^{N} \begin{bmatrix} (\sin\theta_j \cos\phi_j)^2 & \sin^2\theta_j \cos\phi_j \sin\phi_j & \sin\theta_j (1+\cos\theta_j) \cos\phi_j \\ \sin^2\theta_j \cos\phi_j \sin\phi_j & (\sin\theta_j \sin\phi_j)^2 & \sin\theta_j (1+\cos\theta_j) \sin\phi_j \\ \sin\theta_j (1+\cos\theta_j) \cos\phi_j & \sin\theta_j (1+\cos\theta_j) \sin\phi_j & (1+\cos\theta_j)^2 \end{bmatrix} . \tag{4.29}$$

Following the same argument as in the 2D case, $\mathrm{tr}\,(\mathrm{CRLB}_{\mathbf{u},\mathrm{SE}})$ is minimized when $\mathrm{FIM}_{\mathbf{u},\mathrm{SE}}$ is a diagonal matrix [79] which requires

$$\sum_{j=1}^{N} \sin^2\theta_j \cos\phi_j \sin\phi_j = 0 \,, \tag{4.30a}$$

$$\sum_{j=1}^{N} \sin\theta_j (1+\cos\theta_j) \cos\phi_j = 0 \,, \tag{4.30b}$$

$$\sum_{j=1}^{N} \sin\theta_j (1+\cos\theta_j) \sin\phi_j = 0 \,. \tag{4.30c}$$

Thus,

$$\mathrm{tr}\,(\mathrm{CRLB}_{\mathbf{u},\mathrm{SE}}) \geq \sigma_{\mathbf{m}}^2 \left(\frac{1}{\sum_{j=1}^{N} (\sin\theta_j \cos\phi_j)^2} + \frac{1}{\sum_{j=1}^{N} (\sin\theta_j \sin\phi_j)^2} + \frac{1}{\sum_{j=1}^{N} (1+\cos\theta_j)^2} \right) \tag{4.31}$$

and the equality holds when (4.30) is satisfied.

By the arithmetic and harmonic means inequality [82], we can prove that

$$\frac{1}{\sum_{j=1}^{N} (\sin\theta_j \cos\phi_j)^2} + \frac{1}{\sum_{j=1}^{N} (\sin\theta_j \sin\phi_j)^2} \geq \frac{4}{\sum_{j=1}^{N} \sin^2\theta_j} \,, \tag{4.32}$$

where it becomes strictly equal when

$$\sum_{j=1}^{N} \left(\sin\theta_j \cos\phi_j\right)^2 = \sum_{j=1}^{N} \left(\sin\theta_j \sin\phi_j\right)^2 = \frac{1}{2}\sum_{j=1}^{N} \sin^2\theta_j \,. \tag{4.33}$$

Let $a_j = 1 + \cos\theta_j$. Putting (4.32) to (4.31) gives

$$\begin{aligned} \mathrm{tr}\left(\mathrm{CRLB}_{\mathbf{u},\mathrm{SE}}\right) &\geq \sigma^2_{\mathbf{m}} \left(\frac{4}{\sum_{j=1}^{N} a_j \left(2 - a_j\right)} + \frac{1}{\sum_{j=1}^{N} a_j^2} \right) \\ &= \sigma^2_{\mathbf{m}} \frac{2\sum_{j=1}^{N} a_j + 3\sum_{j=1}^{N} a_j^2}{2\sum_{j=1}^{N} a_j \sum_{j=1}^{N} a_j^2 - \sum_{j=1}^{N} a_j^2 \sum_{j=1}^{N} a_j^2} \,. \end{aligned} \tag{4.34}$$

Upon using (4.23) and followed by (4.24), (4.34) can further be reduced to

$$\mathrm{tr}\left(\mathrm{CRLB}_{\mathbf{u},\mathrm{SE}}\right) \geq \sigma^2_{\mathbf{m}} \frac{2 + 3a}{2Na^2 - Na^3} \,. \tag{4.35}$$

The right side of (4.35) attains the minimum value at $a = 2/\sqrt{3}$. The minimum possible error is $\mathrm{tr}\left(\mathrm{CRLB}_{\mathbf{u},\mathrm{SE}}\right)_{\min} = \frac{3\sqrt{3}\left(\sqrt{3}+1\right)}{4N\left(\sqrt{3}-1\right)}\sigma^2_{\mathbf{m}}$. Noting that $a = 1 + \cos\theta_j$ and including (4.30) and (4.33), the optimum receiver placement is defined by

$$\boldsymbol{\rho}^T_{\mathbf{u}^o,\mathbf{t}^o} \boldsymbol{\rho}_{\mathbf{u}^o,\mathbf{s}^o_j} = \cos\theta_j = \frac{2}{\sqrt{3}} - 1 \,, \qquad j = 1\,,\, 2\,,\, \ldots\,,\, N \,, \tag{4.36a}$$

$$\phi_j = \frac{2\pi}{N}\left(j - 1\right) + \beta \,, \qquad j = 1\,,\, 2\,,\, \ldots\,,\, N \,, \tag{4.36b}$$

and β is any constant angle. Note that (4.30) and (4.33) define four equations for ϕ_j under (4.36a): $\sum_{j=1}^{N} \sin\phi_j = 0$, $\sum_{j=1}^{N} \cos\phi_j = 0$, $\sum_{j=1}^{N} \sin 2\phi_j = 0$ and $\sum_{j=1}^{N} \cos 2\phi_j = 0$. (4.36b) is the unique solution for ϕ_j only when $N \leq 5$ and there are other, infinite indeed, solutions if $N > 5$ [31].

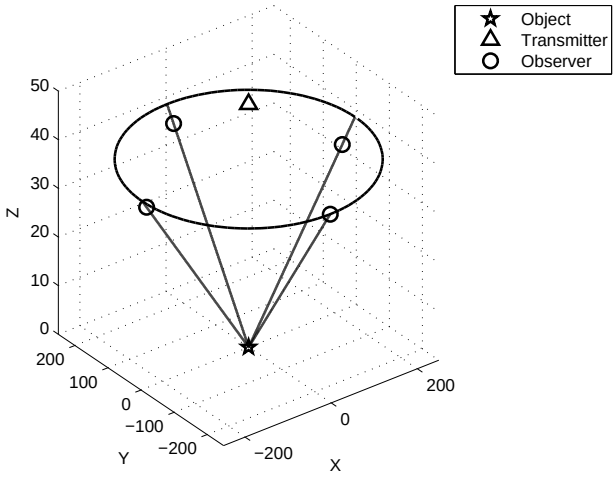

Figure 4.5: A sample configuration of the 3D optimum receiver placement.

The optimum sensor placement requires the sensors to be lying on the surface of a right cone centered at the object-transmitter axis, where the vertex is at the object location and the open angle is $2\cos^{-1}\left(2/\sqrt{3}-1\right) = 162.20^o$. The sensors should have equal angular spacings when projected onto the plane perpendicular to the object-transmitter axis. Fig. 4.5 shows an example of the 3D optimum configuration.

Under the situation that we develop the optimum sensor placement where the noise satisfies $\mathbf{Q}_{\rm SE} = \sigma_{\mathbf{m}}^2\mathbf{I}_N$, $\bar{\mathbf{Q}}_{\rm SE} = \bar{\sigma}_{\mathbf{m}}^2\mathbf{I}_N$, $\mathbf{Q_t} = \mathbf{O}_{K\times K}$ and $\mathbf{Q_s} = \mathbf{O}_{KN\times KN}$, (B.4) and (B.6) indicate that the only difference between $\text{FIM}_{\mathbf{u},\text{SE}}$ and $\text{FIM}_{\mathbf{u},\text{AE}}$ is the geometry independent scaling factor $(\sigma_{\mathbf{m}}^2 + \bar{\sigma}_{\mathbf{m}}^2)/\sigma_{\mathbf{m}}^2$. Hence, the optimum placements (4.28) and (4.36) of SE positioning are also optimum for AE positioning. The minimum value of $\text{tr}\left(\text{CRLB}_{\text{AE}}\right)$ is $\text{tr}\left(\text{CRLB}_{\mathbf{u},\text{SE}}\right)_{\min}(\sigma_{\mathbf{m}}^2 + \bar{\sigma}_{\mathbf{m}}^2)/\sigma_{\mathbf{m}}^2$.

It is rather interesting to observe that the optimum geometries of elliptic positioning are much different from the optimum geometries of circular positioning which

is either the uniform angular full or half array or hyperbolic positioning which is the uniform angular array [30, 31, 32].

The above study of the optimum receiver placement remains valid for SE positioning in the presence of IID receiver position errors but accurate transmitter position. Under this situation, we obtain from (B.4) and the definition of $\widetilde{\mathbf{P}}_{\mathbf{u},\mathbf{s}}$ in (4.3) that $\mathrm{FIM}_{\mathbf{u},\mathrm{SE}} = (\sigma_{\mathbf{m}}^{-2} + \sigma_{\mathbf{s}}^{-2}) (\mathbf{P}_{\mathbf{u},\mathbf{s}} + \mathbf{P}_{\mathbf{u},\mathbf{t}})^T (\mathbf{P}_{\mathbf{u},\mathbf{s}} + \mathbf{P}_{\mathbf{u},\mathbf{t}})$. It is identical to (4.17) apart from a scaling factor and hence we will reach the same optimum geometries (4.28) and (4.36). It does not appear possible to extend directly the results here to non-IID receiver position errors or inaccurate transmitter position and further investigations are needed. The optimum geometries derived here are for a single transmitter. Extension to the multiple transmitter case is a subject for further study.

4.3 Simulation

4.3.1 Elliptic Positioning Performance

The simulation scenario is 2D for ease of illustration. We consider two scenarios to locate an object using six receivers. One is with one transmitter only and the other is with two transmitters. The scenario of single transmitter and multiple receivers has been widely used in multistatic radar [2, 3], UWB network localization [20] and radio communications [19]. The Cartesian coordinates of the object, transmitters and receivers are chosen randomly from independent uniform distributions within an area of 500×500. To avoid degenerate localization scenario, we ensure each geometry satisfies (i) the transmitter, receivers and object are not too close where $||\mathbf{t}^o - \mathbf{u}^o||$,

$||\mathbf{s}_j^o - \mathbf{u}^o||$, and $||\mathbf{s}_j^o - \mathbf{t}^o||$, $j = 1, 2, \ldots, N$, are not smaller than 20; (ii) at least three receivers are not co-linear with the object such that

$$|\boldsymbol{\rho}^T_{\mathbf{u}^o,\mathbf{s}_i^o}\boldsymbol{\rho}_{\mathbf{u}^o,\mathbf{s}_j^o}| < 0.98\,,\ |\boldsymbol{\rho}^T_{\mathbf{u}^o,\mathbf{s}_i^o}\boldsymbol{\rho}_{\mathbf{u}^o,\mathbf{s}_k^o}| < 0.98\,,\ |\boldsymbol{\rho}^T_{\mathbf{u}^o,\mathbf{s}_j^o}\boldsymbol{\rho}_{\mathbf{u}^o,\mathbf{s}_k^o}| < 0.98\,,\ i \neq j \neq k\,. \quad (4.37)$$

Otherwise, poor MLE performance occurs and will dominate the simulation results.

The MLE implemented in the simulation uses the Gauss-Newton iteration method. It jointly estimates the unknown parameter vector $\boldsymbol{\gamma}^o = \left[\, \mathbf{u}^{oT}\,,\, \mathbf{t}^{oT}\,,\, \mathbf{s}^{oT}\,\right]^T$, with the initial guess equal to the true parameter values plus independent Gaussian noise with variances equal to twice the CRLBs for the individual unknowns. The number of ensemble runs is 10,000 for each geometry to obtain the ML object location estimates.

One Transmitter

A total of 100,000 random geometries are created. The CRLB and expected bias values reported in Figs. 4.6, 4.11 are the averages from these geometries. The localization performance of the MLE together with the corresponding CRLB and theoretical bias values in Figs. 4.7 and 4.12 are illustrated separately for 40 geometries that are obtained by sampling at regular intervals among the 100,000 geometries.

The noise settings are $\mathbf{Q}_{\rm SE} = \sigma^2_{\mathbf{m}}\mathbf{I}_N$ and $\bar{\mathbf{Q}}_{\rm SE} = \bar{\sigma}^2_{\mathbf{m}}\mathbf{I}_N$ with $\sigma^2_{\mathbf{m}} = \bar{\sigma}^2_{\mathbf{m}} = 10^{-2}$, and $\mathbf{Q}_{\rm H} = \sigma^2_{\mathbf{m}}\mathbf{H}\mathbf{H}^T$ according to (B.8). The covariance matrices of the transmitter and receiver noises are $\mathbf{Q}_{\mathbf{t}} = \sigma^2_{\mathbf{t}}\mathbf{I}_K$ and $\mathbf{Q}_{\mathbf{s}} = \sigma^2_{\mathbf{s}}\mathbf{I}_{KN}$ where $\sigma^2_{\mathbf{t}} = \sigma^2_{\mathbf{s}}$.

Fig. 4.6 shows the average performance of the four positioning approaches over the 100,000 geometries as $\sigma^2_{\mathbf{s}}/\sigma^2_{\mathbf{m}}$ increases. The $\rm SE_f$ has the best performance while the H is the worst. SE behaves close to $\rm SE_f$ when $\sigma^2_{\mathbf{s}}/\sigma^2_{\mathbf{m}}$ is small, e.g. less than

10^{-2}, as anticipated from the analysis in Section 4.1.1 since the measurement noise dominates the performance. The performance of SE deviates from $\mathrm{SE_f}$ when $\sigma_{\mathbf{s}}^2/\sigma_{\mathbf{m}}^2$ increases and gradually approaches that of AE. It appears the accuracy of AE is 3 dB worse than $\mathrm{SE_f}$.

Although the average performance of Fig. 4.6 shows that SE is always no worse than AE, it is not true that SE is always better than AE for every geometry. This is apparent in Fig. 4.7 in which we depict the localization accuracy at 40 geometries, sampled from the 100,000 geometries at regular intervals after sorting the CRLB values of $\mathrm{SE_f}$ in increasing order. The noise level is at $\sigma_{\mathbf{s}}^2/\sigma_{\mathbf{m}}^2 = 10$. In addition to the CRLBs shown by lines, the location MSEs of the MLEs for the four approaches are shown in symbols. It appears that $\mathrm{SE_f}$ is the best and SE is always better than H. However, AE occasionally outperforms SE with considerable margin for some unfavorable geometries that have larger localization errors, e.g. at geometry indices 33 and 36. Furthermore, H at times behaves better than AE as can be seen at index 23. These observations confirm the theoretical investigations in Section 4.1.

The top plots in Figs. 4.8−4.10 give the histograms of $\mathrm{tr}\,(\mathrm{CRLB_{AE}})/\mathrm{tr}\,(\mathrm{CRLB_{SE}})$, $\mathrm{tr}\,(\mathrm{CRLB_H})/\mathrm{tr}\,(\mathrm{CRLB_{SE}})$ and $\mathrm{tr}\,(\mathrm{CRLB_H})/\mathrm{tr}\,(\mathrm{CRLB_{AE}})$ over the 100,000 geometries to reassert our findings in Fig. 4.7. At the noise level $\sigma_{\mathbf{s}}^2/\sigma_{\mathbf{m}}^2 = 10$, the performance of SE and AE are comparable but AE could be better than SE, SE is always better than H but the mode of $\mathrm{tr}\,(\mathrm{CRLB_H})/\mathrm{tr}\,(\mathrm{CRLB_{SE}})$ is close to unity, and finally H could outperform AE although the chance is small.

Fig. 4.11 shows the averaged theoretical bias-squares of the ML object position estimates over the 100,000 geometries computed using (4.16). When the measurement noise dominates such that $\sigma_{\mathbf{s}}^2/\sigma_{\mathbf{m}}^2$ is small, the $\mathrm{SE_f}$ and SE have comparable and

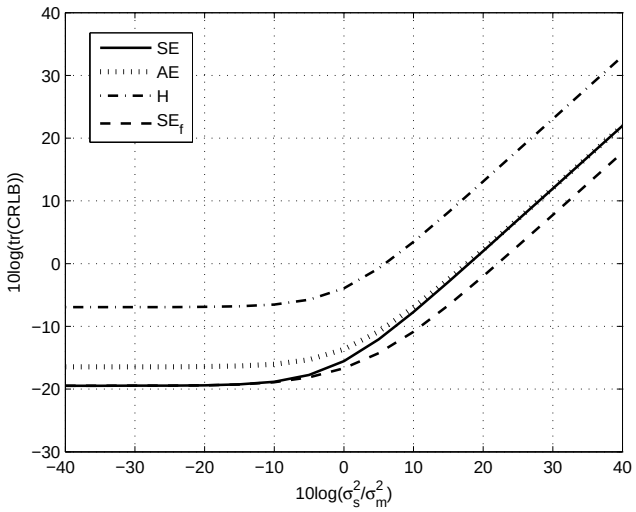

Figure 4.6: The average performance of the four positioning approaches over 100,000 randomly generated geometries with one transmitter and six receivers.

smallest bias, followed by H and AE. On the contrary as the sensor position noise dominates, AE has a much smaller bias than SE and H is the worst.

Fig. 4.12 gives the bias-squares over the same 40 geometries as in Fig. 4.7. The bias-squares are shown by lines and results from the MLEs are indicated by symbols. It is interesting that SE_f is not always the best and occasionally AE yields smaller bias as in indices 17 and 25. H is not the worst either when observing the bias at indices 5 and 13.

Two Transmitters

The performance of the four positioning approaches is further compared when two transmitters are used. A total of 100,000 geometries each having two transmitters and six receivers are randomly generated. The CRLB and expected bias values reported in Figs. 4.13, 4.15 are the averages from these geometries. The localization performance

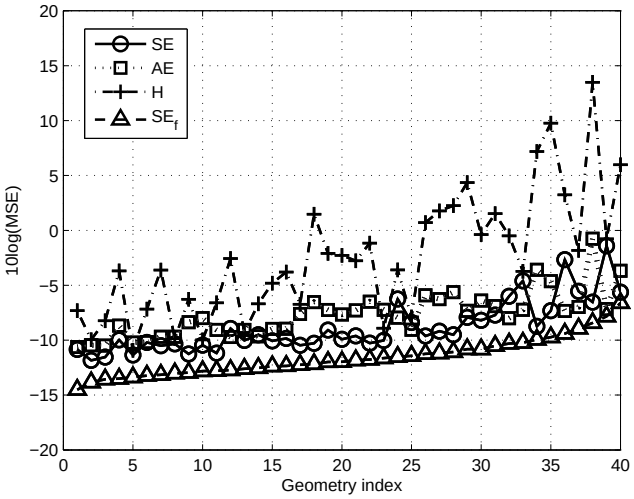

Figure 4.7: The tr(CRLB)s (lines) and the MSEs (symbols) of the four positioning approaches in a sample of 40 selected geometries with one transmitter and six receivers.

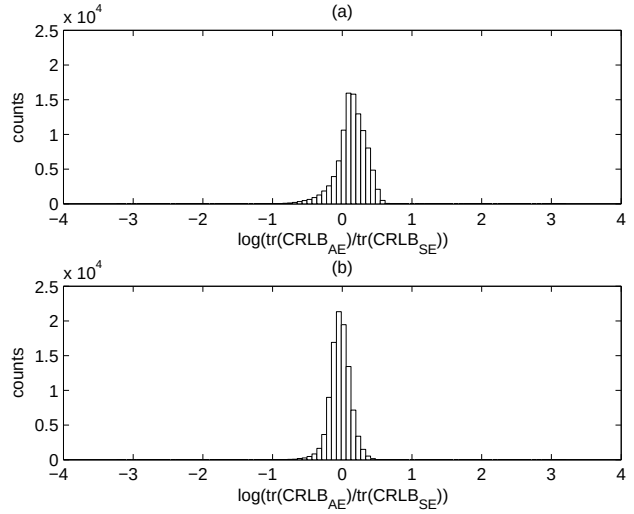

Figure 4.8: The histogram of $\log(\mathrm{tr}\,(\mathrm{CRLB}_{\mathbf{u},\mathrm{AE}})/\mathrm{tr}\,(\mathrm{CRLB}_{\mathbf{u},\mathrm{SE}}))$ when $\sigma_{\mathbf{s}}^2/\sigma_{\mathbf{m}}^2 = 10$, (a) one transmitter, (b) two transmitters.

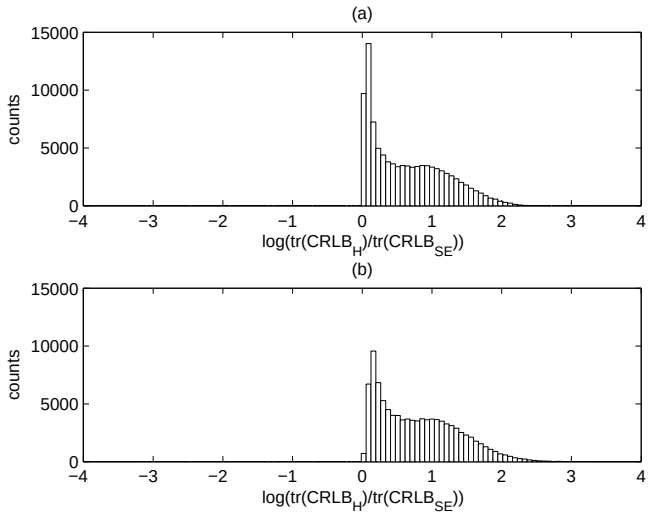

Figure 4.9: The histogram of $\log(\mathrm{tr}\,(\mathrm{CRLB}_{\mathbf{u},\mathrm{H}})/\mathrm{tr}\,(\mathrm{CRLB}_{\mathbf{u},\mathrm{SE}}))$ when $\sigma_{\mathbf{s}}^2/\sigma_{\mathbf{m}}^2 = 10$, (a) one transmitter, (b) two transmitters.

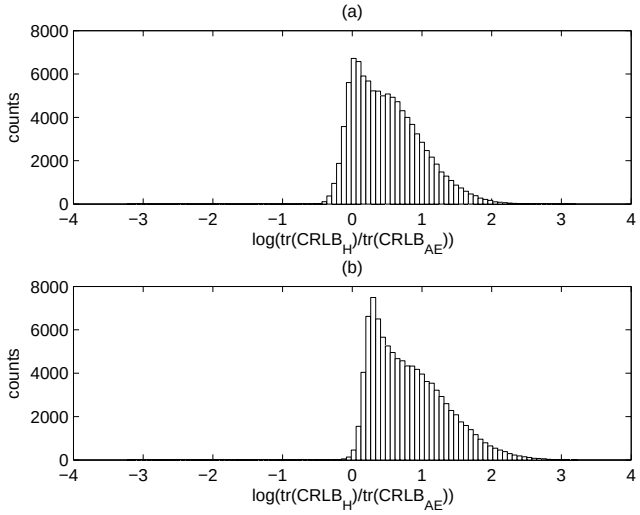

Figure 4.10: The histogram of $\log(\mathrm{tr}\,(\mathrm{CRLB}_{\mathbf{u},\mathrm{H}})/\mathrm{tr}\,(\mathrm{CRLB}_{\mathbf{u},\mathrm{AE}}))$ when $\sigma_{\mathbf{s}}^2/\sigma_{\mathbf{m}}^2 = 10$, (a) one transmitter, (b) two transmitters.

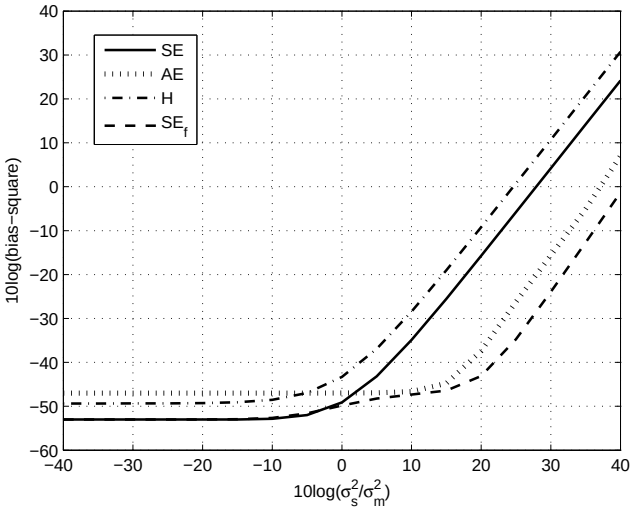

Figure 4.11: The average theoretical bias-squares of the ML object position estimates from the four positioning approaches over the 100,000 randomly generated geometries with one transmitter and six receivers.

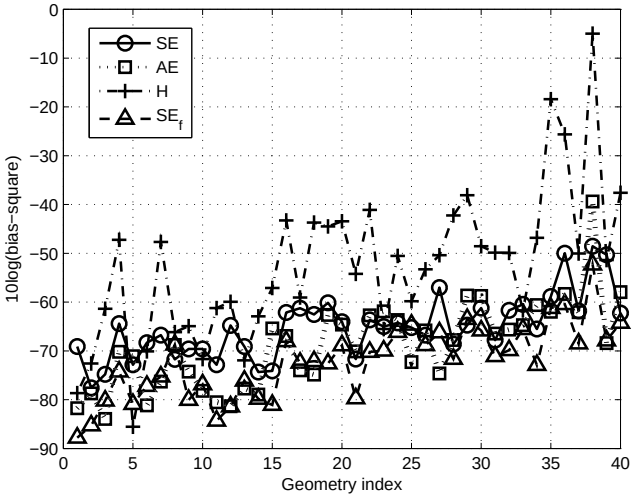

Figure 4.12: Bias behaviors of the ML object position estimates of the four positioning approaches in a sample of 40 selected geometries with one transmitter and six receivers.

of the MLE together with the corresponding CRLB and theoretical bias values in Figs. 4.14 and 4.16 are depicted separately for 40 geometries that are obtained by sampling at regular intervals among the 100,000 geometries. The measurement errors corresponding to the two different transmitters are IID, where for each transmitter $\mathbf{Q}_{\mathrm{SE}} = \sigma_{\mathbf{m}}^2 \mathbf{I}_N$ and $\bar{\mathbf{Q}}_{\mathrm{SE}} = \bar{\sigma}_{\mathbf{m}}^2 \mathbf{I}_N$, and $\sigma_{\mathbf{m}}^2 = \bar{\sigma}_{\mathbf{m}}^2 = 10^{-2}$. The covariance matrix of transmitter position errors is $\sigma_{\mathbf{t}}^2 \mathbf{I}_{2M}$ and the other simulation settings are the same as in the single transmitter case.

The bottom plots in Figs. 4.8−4.10 and Figs. 4.13, 4.14 show the CRLB results of the four positioning approaches with two transmitters. The observations are similar to the single transmitter scenario and consistent with the theoretical analysis from Sections 4.1.1 and 4.1.3. Comparing Figs. 4.8(b)−4.10(b), 4.13, 4.14 with Figs. 4.6, 4.7 and 4.8(a)−4.10(a) reveals that AE positioning has larger chance to outperform SE and H in the two-transmitter case than in the one transmitter situation.

Fig. 4.15 gives the expected bias squares averaged over the 100,000 geometries, and it indicates an additional transmitter can effectively reduce the bias of the four positioning approaches compared to the single transmitter case in Fig. 4.11, especially for the three elliptic positioning methods. Fig. 4.16 is the MLE results of the bias squares for the same 40 geometries used in Fig. 4.14. The observations from Fig. 4.16 are consistent with those from Fig. 4.12.

4.3.2 Optimum Receiver Placement

We shall validate the optimum receiver placement derived in Section 4.2, under IID measurement noise and accurate transmitter and receiver positions.

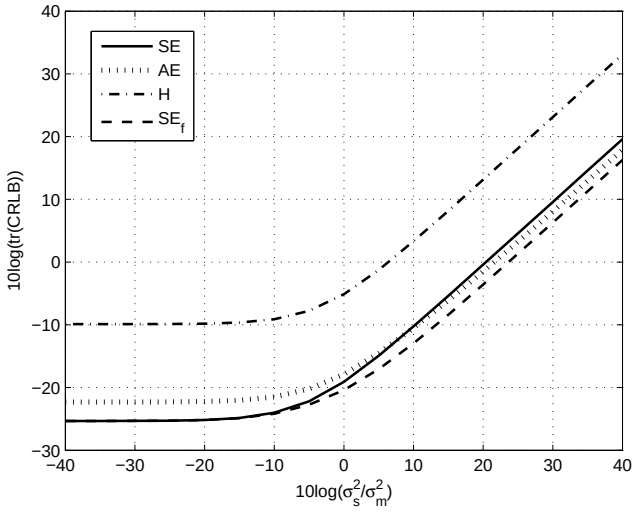

Figure 4.13: The average performance of the four positioning approaches over 100,000 randomly generated geometries with two transmitters and six receivers.

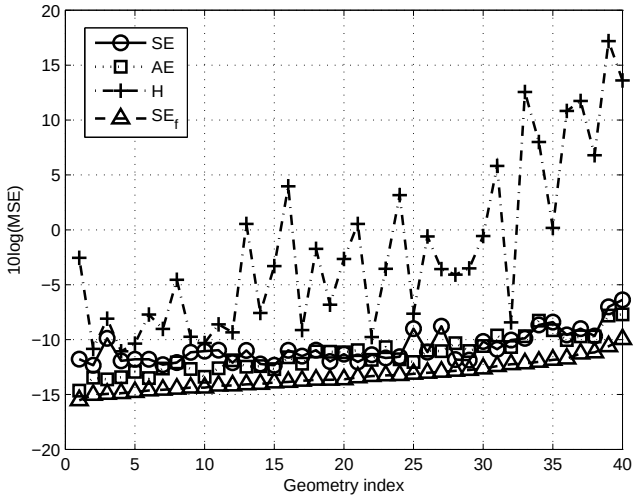

Figure 4.14: The tr(CRLB)s (lines) and the MSEs (symbols) of the four positioning approaches in a sample of 40 selected geometries with two transmitters and six receivers.

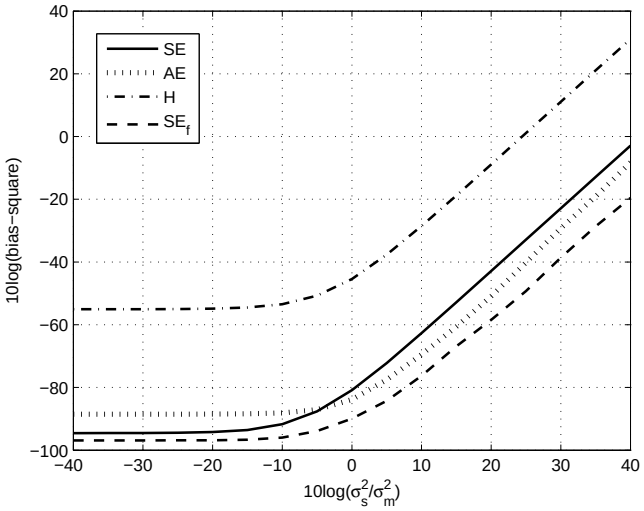

Figure 4.15: The average theoretical bias-squares of the ML object position estimates from the four positioning approaches over the 100,000 randomly generated geometries with two transmitters and six receivers.

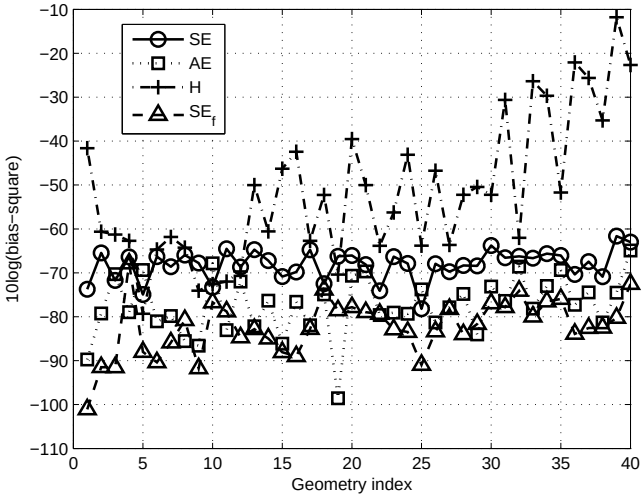

Figure 4.16: Bias behaviors of the ML object position estimates of the four positioning approaches in a sample of 40 selected geometries with two transmitters and six receivers.

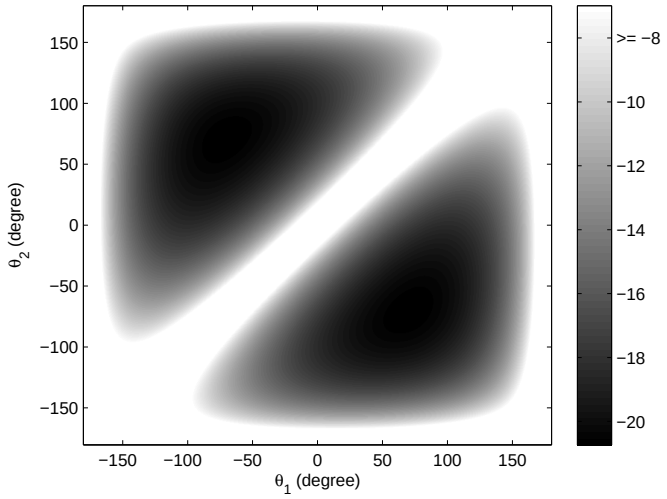

Figure 4.17: Error surface $10\log\left(\mathrm{tr}\left(\mathrm{CRLB}_{\mathbf{u},\mathrm{SE}}\right)\right)$ as a function of θ_1 and θ_2 for 2D localization with 2 receivers.

2D

Let us use two receivers to locate an object at $[\,0\,,\,0\,]^T$, where the transmitter is on the positive side of the x-axis. Figs. 4.17 and 4.18 show the image plots of $10\log\left(\mathrm{tr}\left(\mathrm{CRLB}_{\mathbf{u},\mathrm{SE}}\right)\right)$ as a function of receiver angles θ_1 and θ_2 measured with respect to the x-axis. The smallest error occurs when ($\theta_1 = 70.53^o$, $\theta_2 = -70.53^o$) or ($\theta_1 = -70.53^o$, $\theta_2 = 70.53^o$) and they fit the theoretical result (4.28) well.

Next we consider the 4 receivers case. The object and transmitter are at the same positions as before. Table 4.1 summarizes the numerical solution of the θ_j, $j = 1\,,\,2\,,\,3\,,\,4\,$, obtained from the genetic algorithm of the Matlab Global Optimization Toolbox, where the permutations for other possible solutions are eliminated. The generation number of the genetic algorithm is 1000 and the algorithm runs until the cumulative improvement in the fitness function value over 50 consecutive generations is less than 10^{-13}. The numerical solutions match Section 4.2 well.

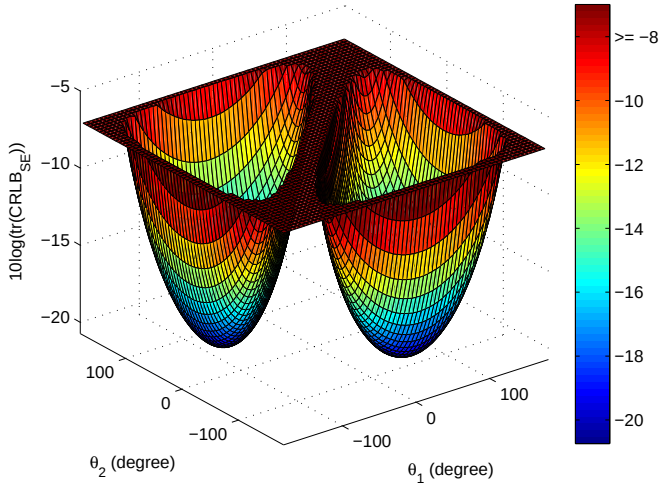

Figure 4.18: 3D plot of the error surface $10\log\left(\mathrm{tr}\left(\mathrm{CRLB}_{\mathbf{u},\mathrm{SE}}\right)\right)$ as a function of θ_1 and θ_2 for 2D localization with 2 receivers.

	$\mathbf{s}_1^o$	$\mathbf{s}_2^o$	$\mathbf{s}_3^o$	$\mathbf{s}_4^o$
θ	-70.53^o	70.53^o	-70.53^o	70.53^o

Table 4.1: The genetic algorithm solution for the 2D optimum placement of 4 receivers for elliptic positioning.

The optimum placement of the receivers requires the object location which is not known. One can only place the receivers using a coarse estimate of the object location. To examine the sensitivity of the optimum receiver placement with respect to the source positions, Figs. 4.19 and 4.20 give $10\log\left(\mathrm{tr}\left(\mathrm{CRLB}_{\mathbf{u},\mathrm{SE}}\right)\right)$ when varying the object location, where $\mathbf{s}_1^o = [\,60\,,\,-169.70\,]^T$, $\mathbf{s}_2^o = [\,56.67\,,\,160.28\,]^T$, $\mathbf{s}_3^o = [\,50\,,\,-141.42\,]^T$, $\mathbf{s}_4^o = [\,66.67\,,\,188.56\,]^T$ and $\mathbf{t}^o = [\,100\,,\,0\,]^T$ are chosen to satisfy (4.28) when $\mathbf{u}^o$ is at the origin. The smallest error occurs at the exact object location. However, the errors remain small over a large region around it. We therefore anticipate that the optimum receiver placement is not sensitive to the object location.

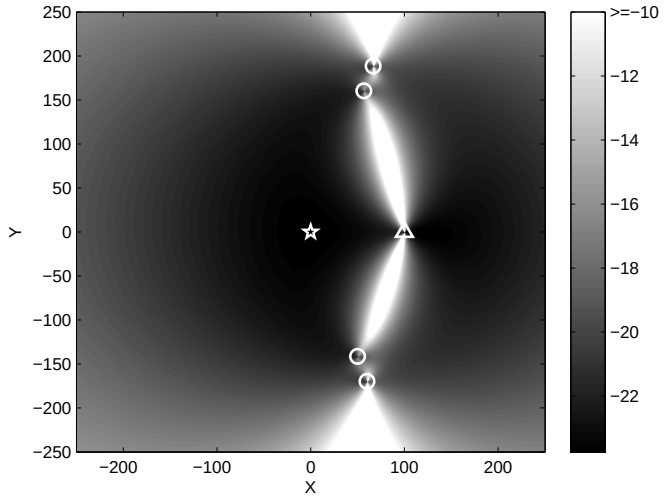

Figure 4.19: Sensitivity of the 2D 4-receiver optimum receiver placement with respect to $\mathbf{u}^o$.

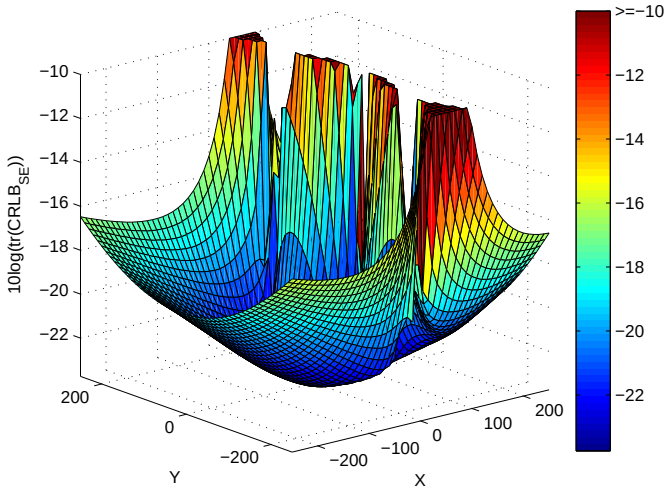

Figure 4.20: 3D plot of sensitivity of the 2D 4-receiver optimum receiver placement with respect to $\mathbf{u}^o$.

	$\mathbf{s}_1^o$	$\mathbf{s}_2^o$	$\mathbf{s}_3^o$
θ	81.10^o	81.10^o	81.10^o
ϕ	-60.07^o	59.93^o	179.93^o

Table 4.2: The genetic algorithm solution for the 3D optimum placement of 3 receivers for elliptic positioning.

	$\mathbf{s}_1^o$	$\mathbf{s}_2^o$	$\mathbf{s}_3^o$	$\mathbf{s}_4^o$
θ	81.11^o	81.09^o	81.10^o	81.10^o
ϕ	-89.96^o	0.06^o	90.03^o	180.00^o

Table 4.3: The genetic algorithm solution for the 3D optimum placement of 4 receivers for elliptic positioning

3D

In the 3D case, we keep $\mathbf{u}^o$ at the origin and $\mathbf{t}^o$ at the positive z-axis. Tables 4.2 and 4.3 summarize the numerical solutions of the optimum receiver angles for $N = 3$ and $N = 4$ from the genetic algorithm, where ϕ_j are arranged in ascending order. They match the theoretical solutions very well.

In Figs. 4.21 and 4.22, we show the error surface $10 \log (\text{tr} (\text{CRLB}_{\text{SE}}))$ with respect to the polar angles of the first and second receivers, where we fix $\theta_3 = \theta_1$ and $\theta_4 = \theta_2$ and the azimuth angles satisfy (4.36b) with $\beta = 0$. It is clear that the error surface is minimized at the expected values of $\theta_1 = \theta_2 = 81.10^o$.

4.4 Conclusion

This Chapter examines the localization performance of elliptic positioning through the CRLB in the presence of Gaussian measurement noise and sensor position errors. Both SE and AE approaches are investigated and their performance is compared with each other and with the hyperbolic positioning. Among the four localization

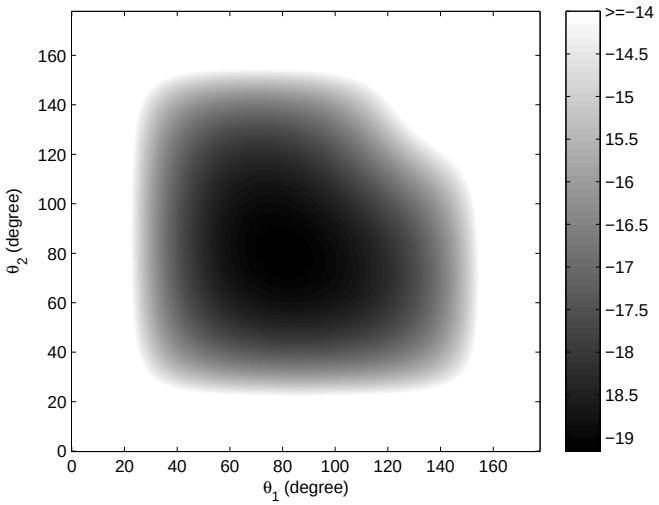

Figure 4.21: Error surface $10\log\left(\mathrm{tr}\left(\mathrm{CRLB}_{\mathbf{u},\mathrm{SE}}\right)\right)$ as a function of θ_1 and θ_2 in the 3D localization when $\theta_3 = \theta_1$, $\theta_4 = \theta_2$ and (4.36b) are satisfied with $\beta = 0$.

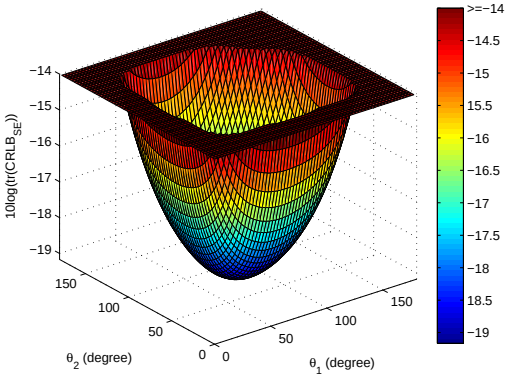

Figure 4.22: 3D plot of the error surface $10\log\left(\mathrm{tr}\left(\mathrm{CRLB}_{\mathbf{u},\mathrm{SE}}\right)\right)$ as a function of θ_1 and θ_2 in the 3D localization when $\theta_3 = \theta_1$, $\theta_4 = \theta_2$ and (4.36b) are satisfied with $\beta = 0$.

approaches SE_f, SE, AE and H, SE_f yields the best accuracy and SE is always better than H. The sensor position errors have considerable effects on the conclusion of the AE performance. While SE outperforms AE when the sensor positions are exactly known, AE could perform better than SE when transmitter and receiver position errors are present for some localization geometries. In addition, H occasionally outperforms AE in some cases. Apart from the CRLB, we have examined the bias behaviors of the MLE in obtaining the solutions of the four positioning approaches. When the sensor positions are accurate, SE_f has the smallest bias, followed in sequence by SE, H and AE. If sensor position errors are significant, SE_f remains to have the smallest bias, followed by AE, SE and then H. When the number of transmitter increases, AE positioning has more possibilities to outperform SE and H and the bias of elliptic positioning reduces.

We have also derived the optimum receiver placements for SE positioning with one transmitter that yield the best localization accuracies under IID Gaussian noise and accurate sensor positions. In 2D, the receiving sensors should be placed along two lines of $\pm 70.53^o$ at the object location with respect to the axis joining the object and the transmitter, with half of the receivers in each. In 3D, the receivers should be allocated on the surface of a right cone centered at the object-transmitter axis, with the vertex at the object position and the open angle given by 162.20^o. The optimum placements also apply to AE positioning, as well as accurate transmitter position and IID receiver position errors.

Chapter 5

Algebraic Solution for Joint Localization and Synchronization of Multiple Sensor Nodes in the Presence of Beacon Uncertainties

The previous two Chapters fundamentally investigate the performance of common positioning approaches. In this Chapter, efficient algorithms are proposed to simultaneously locate and synchronize multiple sensor nodes in a WSN while the previous works only consider similar problem for a single sensor node.

5.1 Problem Scenario

We are interested in locating and synchronizing a number of sensor nodes simultaneously using multiple beacons through message exchanges in a WSN as shown in Fig. 5.1, where the sensor nodes are represented by the cross and the beacons are denoted

by the circle symbols. A 2D scenario is used here and the extension to 3D is straightforward. We shall simply call the sensor nodes to be localized as the unknown nodes. There are M of them whose locations to be found are denoted by $\mathbf{u}_i^o = \left[\, x_{\mathbf{u}_i}^o,\, y_{\mathbf{u}_i}^o \,\right]^T$, $i = 1, 2, \ldots, M$. Each unknown node has its own non-ideal clock which has drift $\varepsilon_{\mathbf{u}_i}^o$ and offset $\omega_{\mathbf{u}_i}^o$ with respect to the global clock. The parameter vector to be solved for the joint localization and synchronization problem is

$$\boldsymbol{\eta}^o = \left[\, \boldsymbol{\eta}_1^{oT},\, \boldsymbol{\eta}_2^{oT},\, \cdots,\, \boldsymbol{\eta}_M^{oT} \,\right]^T,\ \boldsymbol{\eta}_i^o = \left[\, \varepsilon_{\mathbf{u}_i}^o,\, \omega_{\mathbf{u}_i}^o,\, \mathbf{u}_i^{oT} \,\right]^T. \tag{5.1}$$

The N beacons to assist the localization task are at $\mathbf{s}_j^o = \left[\, x_{\mathbf{s}_j}^o,\, y_{\mathbf{s}_j}^o \,\right]^T$, $j = 1, 2, \ldots, N$. Their clock drifts and offsets are $\varepsilon_{\mathbf{s}_j}^o$ and $\omega_{\mathbf{s}_j}^o$. In practice, $\mathbf{s}_j^o$, $\varepsilon_{\mathbf{s}_j}^o$ and $\omega_{\mathbf{s}_j}^o$ are not known exactly and only the noise corrupted values $\mathbf{s}_j = \mathbf{s}_j^o + \mathbf{n}_{\mathbf{s}_j}$, $\varepsilon_{\mathbf{s}_j} = \varepsilon_{\mathbf{s}_j}^o + n_{\varepsilon_{\mathbf{s}_j}}$ and $\omega_{\mathbf{s}_j} = \omega_{\mathbf{s}_j}^o + n_{\omega_{\mathbf{s}_j}}$ are available, where $\mathbf{n}_{\mathbf{s}_j}$, $n_{\varepsilon_{\mathbf{s}_j}}$ and $n_{\omega_{\mathbf{s}_j}}$ are additive noise. Collecting them together yields

$$\mathbf{b} = \left[\, \mathbf{s}^T,\, \boldsymbol{\varepsilon}_{\mathbf{s}}^T,\, \boldsymbol{\omega}_{\mathbf{s}}^T \,\right]^T = \mathbf{b}^o + \mathbf{n}_{\mathbf{b}} \tag{5.2}$$

where $\mathbf{s} = \left[\, \mathbf{s}_1^T,\, \mathbf{s}_2^T,\, \cdots,\, \mathbf{s}_N^T \,\right]^T = \mathbf{s}^o + \mathbf{n}_{\mathbf{s}}$, $\boldsymbol{\varepsilon}_{\mathbf{s}} = \left[\, \varepsilon_{\mathbf{s}_1},\, \varepsilon_{\mathbf{s}_2},\, \cdots,\, \varepsilon_{\mathbf{s}_N} \,\right]^T = \boldsymbol{\varepsilon}_{\mathbf{s}}^o + \mathbf{n}_{\boldsymbol{\varepsilon}_{\mathbf{s}}}$, and $\boldsymbol{\omega}_{\mathbf{s}} = \left[\, \omega_{\mathbf{s}_1},\, \omega_{\mathbf{s}_2},\, \cdots,\, \omega_{\mathbf{s}_N} \,\right]^T = \boldsymbol{\omega}_{\mathbf{s}}^o + \mathbf{n}_{\boldsymbol{\omega}_{\mathbf{s}}}$. We assume the noise vector $\mathbf{n}_{\mathbf{b}} = \left[\, \mathbf{n}_{\mathbf{s}}^T,\, \mathbf{n}_{\boldsymbol{\varepsilon}_{\mathbf{s}}}^T,\, \mathbf{n}_{\boldsymbol{\omega}_{\mathbf{s}}}^T \,\right]^T$ is zero mean Gaussian with covariance matrix $\mathbf{Q}_{\mathbf{b}}$.

Two-way message exchanges [83] provide the time stamp information for the estimation task. Fig. 5.2 depicts this message exchange process starting at the ith node with the jth beacon, where the number of messages exchanged is L. The first message embeds its sending time. The lth subsequent message contains the most recent receiving time $R_{i,j,l-1}$ and the present sending time $T_{i,j,l}$, where $l = 2, 3, \ldots, L$ is the

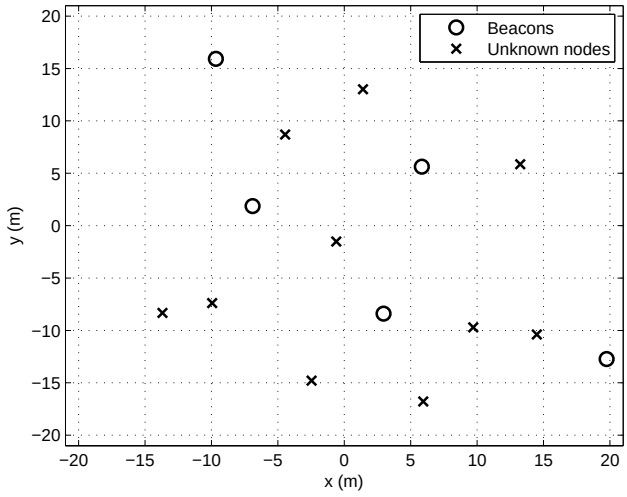

Figure 5.1: A sample configuration for joint localization and synchronization in WSN.

message index. L is supposed to be even for ease of illustration so that the message exchange ends at an unknown node. At last, the timing values $R_{i,j,l}$ and $T_{i,j,l}$ are collected by a processing centre that will jointly localize the M unknown nodes and rectify their synchronizations.

To simplify algorithm developments, we shall assume a fully connected network in which every unknown node has connection with all beacons and with all other unknown nodes. The proposed estimators do not require a fully connected network. We indeed use partially connected network in Section 5.5 Simulation.

We next derive a parametric model for the timing information. In the two-way message exchange scheme [83], the message sending time $T_{i,j,l}$ is known exactly through time calibration [84]. However, the receiving time $R_{i,j,l}$ is inaccurate because it is estimated from the incoming message. As illustrated in Fig. 5.2, due to the clock drift $\varepsilon^o_{\mathbf{u}_i}$ and clock offset $\omega^o_{\mathbf{u}_i}$, the observed time will be scaled by $\frac{1}{1+\varepsilon^o_{\mathbf{u}_i}}$ and translated

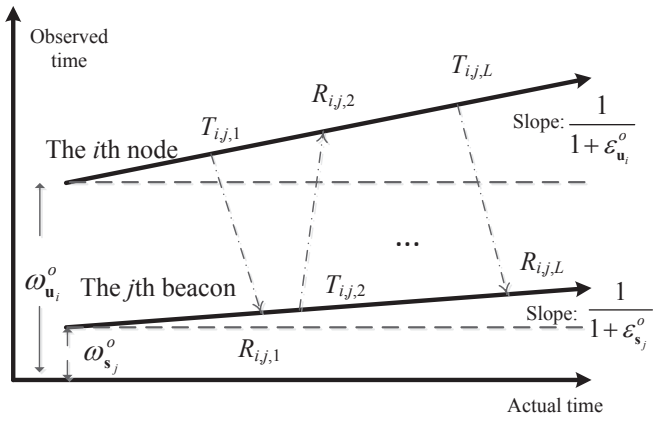

Figure 5.2: The process of the two-way message exchanges between the ith node and the jth beacon [47].

by $\omega^o_{\mathbf{u}_i}$. Hence, the sending and receiving times observed at node i are different from their true values $T^o_{i,j,l}$ and $R^o_{i,j,l}$ through [85]

$$T_{i,j,l} = \frac{T^o_{i,j,l}}{1+\varepsilon^o_{\mathbf{u}_i}} + \omega^o_{\mathbf{u}_i}, \qquad R_{i,j,l} = \frac{R^o_{i,j,l} + n_{R_{i,j,l}}}{1+\varepsilon^o_{\mathbf{u}_i}} + \omega^o_{\mathbf{u}_i}, \tag{5.3}$$

where $n_{R_{i,j,l}}$ is the observation noise. The observed and actual times at the beacons have the relationships in (5.3) as well when replacing $\varepsilon^o_{\mathbf{u}_i}$ and $\omega^o_{\mathbf{u}_i}$ by $\varepsilon^o_{\mathbf{s}_j}$ and $\omega^o_{\mathbf{s}_j}$.

Ideally, the difference in the receiving time $R_{i,j,l}$ and the sending time $T_{i,j,l}$ is proportional to the distance between the unknown node i and the beacon j. Taking into account the presence of clock drifts and offsets as described in (5.3), they are related by [46, 47]

$$T_{i,j,l} + T_{i,j,l}\varepsilon^o_{\mathbf{u}_i} - \omega^o_{\mathbf{u}_i}\left(1+\varepsilon^o_{\mathbf{u}_i}\right) = \left(R_{i,j,l} - \omega^o_{\mathbf{s}_j}\right)\left(1+\varepsilon^o_{\mathbf{s}_j}\right) - \frac{||\mathbf{u}^o_i - \mathbf{s}^o_j||}{c} - n_{R_{i,j,l}}, \tag{5.4a}$$

$$R_{i,j,l} + R_{i,j,l}\varepsilon^o_{\mathbf{u}_i} - \omega^o_{\mathbf{u}_i}\left(1+\varepsilon^o_{\mathbf{u}_i}\right) = \left(T_{i,j,l} - \omega^o_{\mathbf{s}_j}\right)\left(1+\varepsilon^o_{\mathbf{s}_j}\right) + \frac{||\mathbf{u}^o_i - \mathbf{s}^o_j||}{c} + n_{R_{i,j,l}}, \quad (5.4b)$$

where c represents the speed of light. The value l is $l = 1, 3, \ldots, L-1$ in (5.4a) and $l = 2, 4, \ldots, L$ in (5.4b). There are a total of MNL timing measurements. The corresponding noise vector from $n_{R_{i,j,l}}$ is denoted by $\mathbf{n_m}$, which is zero mean Gaussian with covariance matrix $\mathbf{Q_m}$. $\mathbf{n_m}$ is assumed independent of the beacon noise vector $\mathbf{n_b}$ for ease of illustration. (5.4) defines the measurement equations to obtain the unknowns $\mathbf{u}^o_i$, $\varepsilon^o_{\mathbf{u}_i}$ and $\omega^o_{\mathbf{u}_i}$.

When inter-node message exchanges also occur between two unknown nodes i and k, $i = 1, 2, \ldots, M-1$ and $k = i+1, i+2, \ldots, M$, an additional set of $\frac{M(M-1)}{2}L$ time stamp pairs $\check{R}_{i,k,l}$ and $\check{T}_{i,k,l}$ are available. Similar to (5.4) they follow the relationships

$$\check{T}_{i,k,l} + \check{T}_{i,k,l}\varepsilon^o_{\mathbf{u}_i} - \omega^o_{\mathbf{u}_i}\left(1+\varepsilon^o_{\mathbf{u}_i}\right) = \check{R}_{i,k,l} + \check{R}_{i,k,l}\varepsilon^o_{\mathbf{u}_k} - \omega^o_{\mathbf{u}_k}\left(1+\varepsilon^o_{\mathbf{u}_k}\right) - \frac{||\mathbf{u}^o_i - \mathbf{u}^o_k||}{c} - n_{\check{R}_{i,k,l}}, \quad (5.5a)$$

$$\check{R}_{i,k,l} + \check{R}_{i,k,l}\varepsilon^o_{\mathbf{u}_i} - \omega^o_{\mathbf{u}_i}\left(1+\varepsilon^o_{\mathbf{u}_i}\right) = \check{T}_{i,k,l} + \check{T}_{i,k,l}\varepsilon^o_{\mathbf{u}_k} - \omega^o_{\mathbf{u}_k}\left(1+\varepsilon^o_{\mathbf{u}_k}\right) + \frac{||\mathbf{u}^o_i - \mathbf{u}^o_k||}{c} + n_{\check{R}_{i,k,l}}, \quad (5.5b)$$

where $n_{\check{R}_{i,k,l}}$ represents the measurement noise whose vector form is $\mathbf{n_{\check{m}}}$. The value l is $l = 1, 3, \ldots, L-1$ in (5.5a) and $l = 2, 4, \ldots, L$ in (5.5b). The total measurement noise vector is denoted by $\mathbf{n_{\tilde{m}}} = \left[\, \mathbf{n}^T_{\mathbf{m}}, \mathbf{n}^T_{\check{\mathbf{m}}} \,\right]^T$, which is zero mean Gaussian with covariance matrix $\mathbf{Q_{\tilde{m}}}$ and is independent of $\mathbf{n_b}$. Note that $\mathbf{Q_m}$ is the upper $MNL \times MNL$ submatrix of $\mathbf{Q_{\tilde{m}}}$.

We use Gaussian errors in the work here. The Gaussian noise assumption has been confirmed by a few previous studies [47, 85] to be reasonable.

The objective is to jointly estimate the locations, clock drifts and clock offsets of the M sensor nodes collected as $\boldsymbol{\eta}^o$ in (5.1) using the time information $R_{i,j,l}$ and

$T_{i,j,l}$ from the message exchanges between the beacons and the unknown nodes, and $\check{R}_{i,k,l}$ and $\check{T}_{i,k,l}$ from the message exchanges among the unknown nodes if available, through the inaccurate knowledge of the beacon positions and their clock parameters represented by $\mathbf{b}$ in (5.2).

We would like to clarify the assumptions used before introducing the proposed solutions. The first is the geometry constraint that each sensor node has connections with at least three beacons that are not collinear. This condition is common for solving the sensor node localization problem and is not specific to the proposed solutions. The second is that the number of time measurements L between a sensor node and a beacon must be at least 2, i.e. $L \geq 2$. This is to ensure a unique solution in the stage-1 processing of the proposed method as described in the next Section. The third is that the noise is small so that the second and higher order noise terms are insignificant to be neglected.

5.2 Node Localization without Inter-node Communication

In this case the measurements are $R_{i,j,l}$ and $T_{i,j,l}$ only and the unknowns are the position $\mathbf{u}_i^o$, the clock drift $\varepsilon_{\mathbf{u}_i}^o$ and the clock offset $\omega_{\mathbf{u}_i}^o$, where $i = 1, 2, \ldots, M$, $j = 1, 2, \ldots, N$ and $l = 1, 2, \ldots, L$.

The time measurements and the unknowns are related in a highly nonlinear manner in (5.4) and solving them directly is extremely difficult. The proposed method handles the nonlinear estimation elegantly through multi-stage processing with parameter transformation and linear optimization. The proposed algorithm in this

Section can be considered as an extension of CF-WLS [46]. In the absence of beacon position and clock uncertainties and for a single unknown node, it reduces to the CF-WLS.

In the first stage of the proposed method, we introduce additional variables and consider the distances $||\mathbf{u}_i^o - \mathbf{s}_j||$ with $j = 1, 2, \ldots, N$, the node clock drift $\varepsilon_{\mathbf{u}_i}^o$ and the product term

$$\zeta_{\mathbf{u}_i}^o = \left(1 + \varepsilon_{\mathbf{u}_i}^o\right) \omega_{\mathbf{u}_i}^o \tag{5.6}$$

as independent unknown variables to be solved. The parameter space is expanded from the original 4 unknowns for node i to $N + 2$. The rationale for expanding the parameter space is that (5.4) can be viewed as linear with respect to the $N + 2$ unknowns and they can be solved by the linear WLS optimization. Afterwards, $\varepsilon_{\mathbf{u}_i}^o$ and $\omega_{\mathbf{u}_i}^o$ can be uncoupled from the stage-1 solution. The sensor position $\mathbf{u}_i^o$ remains to be recovered from the N distances $||\mathbf{u}_i^o - \mathbf{s}_j||$.

In the second stage, the distance values from the first stage solution are squared to create a new set of pseudo linear equations with unknowns r_i^{o2} and $\mathbf{u}_i^o$. $r_i^{o2} = \mathbf{u}_i^{oT}\mathbf{u}_i^o$ is an auxiliary variable in order to make the resulting equations in linear form when interpreting it as an independent variable. The parameters $\varepsilon_{\mathbf{u}_i}^o$ and $\omega_{\mathbf{u}_i}^o$ are kept as unknowns because their estimation noise is correlated with the distances in the stage-1 solution. Processing the node position estimate in stage-2 through the distances would increase their accuracy by exploiting the noise correlation.

The estimates of $\varepsilon_{\mathbf{u}_i}^o$, $\omega_{\mathbf{u}_i}^o$ and $\mathbf{u}_i^o$ in the stage-2 solution are suboptimum. This is because r_i^{o2} and $\mathbf{u}_i^o$ are assumed to be independent variables but are indeed related.

Stage-3 reduces the parameter space from 5 in stage-2 back to 4 by defining the unknowns as $\varepsilon_{\mathbf{u}_i}^o$, $\omega_{\mathbf{u}_i}^o$ and $(\mathbf{u}_i^o \odot \mathbf{u}_i^o)$. $\varepsilon_{\mathbf{u}_i}^o$ and $\omega_{\mathbf{u}_i}^o$ are carried from stage-2 to stage-3

with the same reason as before that their estimation noise is correlated with those of $\mathbf{u}_i^o$ and r_i^{o2} in the stage-2 solution. The third unknown is defined as $(\mathbf{u}_i^o \odot \mathbf{u}_i^o)$ so that a linear equation can be formed from the solution of stage-2. The stage-3 solution gives the final estimates of $\varepsilon_{\mathbf{u}_i}^o$ and $\omega_{\mathbf{u}_i}^o$. The node location estimate is obtained from a simple mapping with square-roots taken on $(\mathbf{u}_i^o \odot \mathbf{u}_i^o)$ in stage-4.

Nonlinear transformation of the parameters occurs from one stage to the next, such as squaring. Approximations are made to ignore the second and higher order noise terms in the algorithm derivation. The approximations are quite reasonable when the measurement noise is not large and the performance analysis in Section 5.4 provides further elaborations on the approximations

Each stage except the last solves the unknowns of the M nodes simultaneously. The number of unknowns in the first three stages are $M(N+2)$, $5M$ and $4M$. It is worth mentioning that the available beacon positions and clock parameters are not accurate. Their true values in (5.4) will be replaced by their noisy versions, with proper weightings applied to take their statistical noise behaviors into account. We do not estimate the beacon position and clock parameters and as a result increasing the number of beacons does not increase the number of unknowns but could potentially improve performance.

The solution from each stage is based on the WLS minimization, where the weights are chosen to minimize the variance of the unknowns to be found [22]. Hence the solution in each stage is optimum in the MSE sense. Stage-1 has $M(N+2)$ unknowns, and we reduce in subsequent stages the number of unknowns to $5M$ and $4M$ by contracting the parameter space. The estimation accuracy improves from the first to second, and from the second to third stages. The fourth stage does not improve

accuracy but rather remap the stage-3 solution to the sensor location estimates.

The WLS optimization [22] is to solve an unknown vector $\boldsymbol{\gamma}^o$ that satisfies the linear model (2.12) and can be solved by (2.14) and (2.15). The resulting covariance matrix of the parameter estimate is given in (2.16). (2.15) and (2.16) will be used repeatedly in each stage with different values of $\boldsymbol{\gamma}^o$, $\mathbf{G}$, $\mathbf{h}$ and $\mathbf{W}$. We shall now present the processing in different stages.

First Stage: From (5.2), we can express $\mathbf{s}_j^o$, $\varepsilon_{\mathbf{s}_j}^o$, and $\omega_{\mathbf{s}_j}^o$ in terms of their available noisy values as $\mathbf{s}_j - \mathbf{n}_{\mathbf{s}_j}$, $\varepsilon_{\mathbf{s}_j} - n_{\varepsilon_{\mathbf{s}_j}}$ and $\omega_{\mathbf{s}_j} - n_{\omega_{\mathbf{s}_j}}$. Putting them in (5.4), expanding and rearranging give

$$\begin{aligned} &n_{R_{i,j,l}} + \frac{\boldsymbol{\rho}_{\mathbf{u}_i^o,\mathbf{s}_j}^T \mathbf{n}_{\mathbf{s}_j}}{c} + \left(R_{i,j,l} - \omega_{\mathbf{s}_j}\right) n_{\varepsilon_{\mathbf{s}_j}} - \left(1 + \varepsilon_{\mathbf{s}_j}\right) n_{\omega_{\mathbf{s}_j}} = \\ &\left[\left(R_{i,j,l} - \omega_{\mathbf{s}_j}\right)\left(1 + \varepsilon_{\mathbf{s}_j}\right) - T_{i,j,l}\right] - T_{i,j,l}\varepsilon_{\mathbf{u}_i}^o + \zeta_{\mathbf{u}_i}^o - \frac{||\mathbf{u}_i^o - \mathbf{s}_j||}{c}, \qquad l = 1,\, 3,\, \ldots,\, L-1 \end{aligned} \tag{5.7a}$$

$$\begin{aligned} &n_{R_{i,j,l}} + \frac{\boldsymbol{\rho}_{\mathbf{u}_i^o,\mathbf{s}_j}^T \mathbf{n}_{\mathbf{s}_j}}{c} + \left(\omega_{\mathbf{s}_j} - T_{i,j,l}\right) n_{\varepsilon_{\mathbf{s}_j}} + \left(1 + \varepsilon_{\mathbf{s}_j}\right) n_{\omega_{\mathbf{s}_j}} = \\ &\left[\left(\omega_{\mathbf{s}_j} - T_{i,j,l}\right)\left(1 + \varepsilon_{\mathbf{s}_j}\right) + R_{i,j,l}\right] + R_{i,j,l}\varepsilon_{\mathbf{u}_i}^o - \zeta_{\mathbf{u}_i}^o - \frac{||\mathbf{u}_i^o - \mathbf{s}_j||}{c}, \qquad l = 2,\, 4,\, \ldots,\, L \end{aligned} \tag{5.7b}$$

where $\zeta_{\mathbf{u}_i}^o$ is defined in (5.6), the error product $n_{\varepsilon_{\mathbf{s}_j}} n_{\omega_{\mathbf{s}_j}}$ is assumed to be small enough to be neglected and we have approximated $||\mathbf{u}_i^o - \mathbf{s}_j + \mathbf{n}_{\mathbf{s}_j}||$ by the Taylor series expansion up to linear term,

$$||\mathbf{u}_i^o - \mathbf{s}_j + \mathbf{n}_{\mathbf{s}_j}|| \simeq ||\mathbf{u}_i^o - \mathbf{s}_j|| + \boldsymbol{\rho}_{\mathbf{u}_i^o,\mathbf{s}_j}^T \mathbf{n}_{\mathbf{s}_j}, \tag{5.8}$$

where $\boldsymbol{\rho}_{\mathbf{u}_i^o,\mathbf{s}_j}$ is the unit vector pointing from $\mathbf{s}_j$ to $\mathbf{u}_i^o$. The approximation is accurate

when the beacon position error relative to the distance between $\mathbf{u}_i^o$ and $\mathbf{s}_j^o$ is small.

Eq. (5.7) is highly nonlinear with respect to the unknowns $\mathbf{u}_i^o$, $\varepsilon_{\mathbf{u}_i}^o$ and $\omega_{\mathbf{u}_i}^o$. We shall consider the MN distances $||\mathbf{u}_i^o - \mathbf{s}_j||$, the M clock drifts $\varepsilon_{\mathbf{u}_i}^o$ and the M product terms $\zeta_{\mathbf{u}_i}^o$ are independent variables so that (5.7) can be interpreted as linear equations. Collecting (5.7) for $l = 1, 2, \ldots, L$ first, $j = 1, 2, \ldots, N$ next and then $i = 1, 2, \ldots, M$, we have the vector form

$$\mathbf{n_m} + \mathbf{K}_1\mathbf{n_s} + \mathbf{D}_1\mathbf{n}_{\boldsymbol{\varepsilon_s}} + \mathbf{F}_1\mathbf{n}_{\boldsymbol{\omega_s}} = \mathbf{h}_1 - \mathbf{G}_1\boldsymbol{\gamma}_1^o \tag{5.9}$$

where the overall unknown vector is

$$\boldsymbol{\gamma}_1^o = \left[\boldsymbol{\gamma}_{1_1}^{oT}, \boldsymbol{\gamma}_{1_2}^{oT}, \cdots, \boldsymbol{\gamma}_{1_M}^{oT}\right]^T, \quad \boldsymbol{\gamma}_{1_i}^o = \left[\varepsilon_{\mathbf{u}_i}^o, \zeta_{\mathbf{u}_i}^o, ||\mathbf{u}_i^o - \mathbf{s}_1||, \cdots, ||\mathbf{u}_i^o - \mathbf{s}_N||\right]^T. \tag{5.10}$$

(5.9) fits to (2.14). The definitions of the matrices and the details for the WLS solution of $\boldsymbol{\gamma}_1^o$ are given in Appendix C.1.

Second Stage: Let $\mathbf{e}_{1_i}$ be the estimation error of $\hat{\boldsymbol{\gamma}}_{1_i}$ such that $\hat{\boldsymbol{\gamma}}_{1_i} = \boldsymbol{\gamma}_{1_i}^o + \mathbf{e}_{1_i}$. The first two elements of $\hat{\boldsymbol{\gamma}}_{1_i}$ are the estimates of $\varepsilon_{\mathbf{u}_i}^o$ and $\zeta_{\mathbf{u}_i}^o$. Hence using (5.6),

$$e_{1_i}(1) = \hat{\gamma}_{1_i}(1) - \varepsilon_{\mathbf{u}_i}^o,\ e_{1_i}(2) = \hat{\gamma}_{1_i}(2) - \zeta_{\mathbf{u}_i}^o = \hat{\gamma}_{1_i}(2) - (1 + \hat{\gamma}_{1_i}(1))\,\omega_{\mathbf{u}_i}^o + \omega_{\mathbf{u}_i}^o e_{1_i}(1), \tag{5.11}$$

where $e_{1_i}(l)$ is the lth element of the vector $\mathbf{e}_{1_i}$. The last N elements of the subvector $\hat{\boldsymbol{\gamma}}_{1_i}$ are the estimates of the distances between the ith node and the inaccurate beacon positions. Squaring $\hat{\gamma}_{1_i}(j+2) = ||\mathbf{u}_i^o - \mathbf{s}_j|| + e_{1_i}(j+2)$ on both sides and neglecting

the term $e_{1_i}(j+2)^2$ yield

$$2||\mathbf{u}_i^o - \mathbf{s}_j||e_{1_i}(j+2) \simeq \hat{\gamma}_{1_i}(j+2)^2 - \mathbf{s}_j^T\mathbf{s}_j - r_i^{o2} - \left(-2\mathbf{s}_j^T\right)\mathbf{u}_i^o \tag{5.12}$$

where $r_i^{o2} = \mathbf{u}_i^{oT}\mathbf{u}_i^o$ and $j = 1, 2, \cdots, N$. Let us pretend r_i^{o2} is independent of $\mathbf{u}_i^o$ and (5.12) is linear with r_i^{o2} and $\mathbf{u}_i^o$. Stacking (5.11) and (5.12) for all M unknown nodes gives

$$\mathbf{B}_2\mathbf{e}_1 = \mathbf{h}_2 - \mathbf{G}_2\boldsymbol{\gamma}_2^o, \tag{5.13}$$

where the unknown vector $\boldsymbol{\gamma}_2^o$ is

$$\boldsymbol{\gamma}_2^o = \left[\,\boldsymbol{\gamma}_{2_1}^{oT}, \boldsymbol{\gamma}_{2_2}^{oT}, \cdots, \boldsymbol{\gamma}_{2_M}^{oT}\,\right]^T, \boldsymbol{\gamma}_{2_i}^o = \left[\,\varepsilon_{\mathbf{u}_i}^o, \omega_{\mathbf{u}_i}^o, r_i^{o2}, \mathbf{u}_i^{oT}\,\right]^T. \tag{5.14}$$

Again, (5.13) is in the form of (2.14). The definitions of the matrices and the WLS solution of $\boldsymbol{\gamma}_2^o$ are given in Appendix C.2.

Third Stage: Let $\mathbf{e}_{2_i}$ be the estimation error of $\hat{\boldsymbol{\gamma}}_{2_i}$. The second stage solution assumes r_i^{o2} and $\mathbf{u}_i^o$ are independent variables. We exploit their relationship $r_i^{o2} = \mathbf{u}_i^{oT}\mathbf{u}_i^o$ to improve the node position estimate. From (5.14), $\hat{\gamma}_{2_i}(3) - e_{2_i}(3) = r_i^{o2}$ and $\hat{\boldsymbol{\gamma}}_{2_i}(4:5) - \mathbf{e}_{2_i}(4:5) = \mathbf{u}_i^o$. Expanding $(\hat{\boldsymbol{\gamma}}_{2_i}(4:5) - \mathbf{e}_{2_i}(4:5)) \odot (\hat{\boldsymbol{\gamma}}_{2_i}(4:5) - \mathbf{e}_{2_i}(4:5)) = \mathbf{u}_i^o \odot \mathbf{u}_i^o$ and neglecting the second order error term $\mathbf{e}_{2_i}(4:5) \odot \mathbf{e}_{2_i}(4:5)$,

$$2\mathbf{u}_i^o \odot \mathbf{e}_{2_i}(4:5) \simeq \hat{\boldsymbol{\gamma}}_{2_i}(4:5) \odot \hat{\boldsymbol{\gamma}}_{2_i}(4:5) - \mathbf{u}_i^o \odot \mathbf{u}_i^o \tag{5.15}$$

Thus,

$$\mathbf{B}_3\mathbf{e}_2 = \mathbf{h}_3 - \mathbf{G}_3\boldsymbol{\gamma}_3^o. \tag{5.16}$$

The unknown vector is

$$\boldsymbol{\gamma}_3^o = \left[\boldsymbol{\gamma}_{3_1}^{oT}, \boldsymbol{\gamma}_{3_2}^{oT}, \cdots, \boldsymbol{\gamma}_{3_M}^{oT} \right]^T, \boldsymbol{\gamma}_{3_i}^o = \left[\varepsilon_{\mathbf{u}_i}^o, \omega_{\mathbf{u}_i}^o, \left(\mathbf{u}_i^o \odot \mathbf{u}_i^o\right)^T \right]^T, \tag{5.17}$$

whose WLS solution together with the relevant matrices are given in Appendix C.3.

Fourth Stage: The last step is to re-map the last two elements of $\hat{\boldsymbol{\gamma}}_{3_i}$ back to the node position estimate $\hat{\mathbf{u}}_i$ through

$$\hat{\mathbf{u}}_i = \text{diag}(\text{sgn}(\hat{\boldsymbol{\gamma}}_{2_i}^o(4:5)))\sqrt{\hat{\boldsymbol{\gamma}}_{3_i}(3:4)} \tag{5.18}$$

where $\text{diag}(\text{sgn}(\hat{\boldsymbol{\gamma}}_{2_i}^o(4:5)))$ is to remove the sign ambiguity caused by the square root operation.

The covariance of the estimated parameter vector is obtained by taking the differential of $\boldsymbol{\gamma}_{3_i}^o$,

$$\text{cov}(\hat{\boldsymbol{\eta}}) = \mathbf{B}_4^{-1}\text{cov}(\hat{\boldsymbol{\gamma}}_3)\mathbf{B}_4^{-1} \tag{5.19}$$

where $\hat{\boldsymbol{\eta}}$ is the estimate of $\boldsymbol{\eta}^o$ defined in (5.1), $\text{cov}\left(\boldsymbol{\gamma}_3\right)$ is given by (C.12), and

$$\mathbf{B}_4 = \text{diag}\left(\mathbf{B}_{4_1}, \mathbf{B}_{4_2}, \cdots, \mathbf{B}_{4_M}\right), \mathbf{B}_{4_i} = \text{diag}\left(1, 1, 2x_{\mathbf{u}_i}^o, 2y_{\mathbf{u}_i}^o\right). \tag{5.20}$$

To summarize the proposed localization algorithm, the first stage contains (C.2)−(C.3). The following two stages involve (C.6)−(C.7) and (C.10)−(C.11). The final stage gives the position estimate of the ith node through (5.18). The estimated values of $\varepsilon_{\mathbf{u}_i}^o$ and $\omega_{\mathbf{u}_i}^o$ are contained in the solution (C.10) of $\boldsymbol{\gamma}_3^o$.

5.3 Node Localization with Inter-node Communication

The unknown parameters in this case remain to be $\mathbf{u}_i^o$, $\varepsilon_{\mathbf{u}_i}^o$ and $\omega_{\mathbf{u}_i}^o$, $i = 1, 2, \ldots, M$. Apart from $R_{i,j,l}$ and $T_{i,j,l}$, the additional measurements are $\check{T}_{i,k,l}$ and $\check{R}_{i,k,l}$ and they are related to the unknowns through (5.5).

The proposed algorithm for this scenario has two stages. The first stage is an extension of the first stage processing in Section 5.2. It has a total of $M(N+2) + M(M-1)/2$ unknowns, consisting of the original $M(N+2)$ parameters and the $M(M-1)/2$ distances between each pair of nodes $||\mathbf{u}_i^o - \mathbf{u}_k^o||$, $i = 1, 2, \ldots, M-1$, $k = i+1, i+2, \ldots, M$. The introduction of the inter-node distances allows us to interpret (5.5) as pseudo linear equations. The application of the WLS optimization to (5.4) and (5.5) together would yield the stage-1 solution.

The second stage refines the estimates of $\varepsilon_{\mathbf{u}_i}^o$ and $\omega_{\mathbf{u}_i}^o$ and obtains the sensor node positions using the distances in the stage-1 solution. $\varepsilon_{\mathbf{u}_i}^o$ and $\omega_{\mathbf{u}_i}^o$ are carried from the first to the second stage because their estimation noise is correlated with those of the distances so that contracting the parameter space from $MN + M(M-1)/2$ distances to $2M$ node coordinates would also improve their accuracy.

Rather than obtaining the node positions directly in stage-2, we estimate the amount of corrections to the solution from Section 5.2 to improve the accuracy. Such a formulation would transform the solution equations to linear form so that WLS minimization can be applied. Similar to Section 5.2, the small noise conditions are applied to the algorithm derivation so that the second and higher order error terms can be ignored. This is supported by the analysis in Section 5.4.

First Stage: Introducing the extra parameters $\zeta_{\mathbf{u}_i}^o$ and $\zeta_{\mathbf{u}_k}^o$ defined in (5.6) for the

unknown nodes i and k, (5.5) can be rewritten as

$$n_{\check{R}_{i,k,l}} = \left(\check{R}_{i,k,l} - \check{T}_{i,k,l}\right) - \check{T}_{i,k,l}\varepsilon^o_{\mathbf{u}_i} + \zeta^o_{\mathbf{u}_i} + \check{R}_{i,k,l}\varepsilon^o_{\mathbf{u}_k} - \zeta^o_{\mathbf{u}_k} - \frac{||\mathbf{u}^o_i - \mathbf{u}^o_k||}{c},\ l = 1,\, 3,\, \ldots,\, L-1 \tag{5.21a}$$

$$n_{\check{R}_{i,k,l}} = \left(\check{R}_{i,k,l} - \check{T}_{i,k,l}\right) + \check{R}_{i,k,l}\varepsilon^o_{\mathbf{u}_i} - \zeta^o_{\mathbf{u}_i} - \check{T}_{i,k,l}\varepsilon^o_{\mathbf{u}_k} + \zeta^o_{\mathbf{u}_k} - \frac{||\mathbf{u}^o_i - \mathbf{u}^o_k||}{c},\ l = 2,\, 4,\, \ldots,\, L. \tag{5.21b}$$

Collecting (5.21) for $l = 1,\, 2,\, \ldots,\, L$ first, $k = i+1,\, i+2,\, \ldots,\, M$ next and then $i = 1,\, 2,\, \ldots,\, M-1$ yields the matrix equation

$$\mathbf{n}_{\check{\mathbf{m}}} = \check{\mathbf{h}}_1 - \check{\mathbf{G}}_1\widetilde{\boldsymbol{\gamma}}^o_1 \tag{5.22}$$

where $\check{\mathbf{h}}_1$ and $\check{\mathbf{G}}_1$ are given in Appendix C.4. The unknown vector is

$$\widetilde{\boldsymbol{\gamma}}^o_1 = \left[\, \boldsymbol{\gamma}^{oT}_1,\, \check{\boldsymbol{\gamma}}^{oT}_1 \,\right]^T, \tag{5.23}$$

where $\boldsymbol{\gamma}^o_1$ is defined in (5.10), $\check{\boldsymbol{\gamma}}^o_1 = \left[\, \check{\boldsymbol{\gamma}}^{oT}_{1_1},\, \check{\boldsymbol{\gamma}}^{oT}_{1_2},\, \cdots,\, \check{\boldsymbol{\gamma}}^{oT}_{1_{M-1}} \right]^T$ and $\check{\boldsymbol{\gamma}}^o_{1_i} = \left[\, ||\mathbf{u}^o_i - \mathbf{u}^o_{i+1}||,\, ||\mathbf{u}^o_i - \mathbf{u}^o_{i+2}||,\, \cdots,\, ||\mathbf{u}^o_i - \mathbf{u}^o_M|| \,\right]^T$. Eq. (5.22) can be used in conjunction with (5.9) for the timing measurements between the unknown nodes and the beacons to form

$$\mathbf{n}_{\widetilde{\mathbf{m}}} + \widetilde{\mathbf{K}}_1\mathbf{n}_{\mathbf{s}} + \widetilde{\mathbf{D}}_1\mathbf{n}_{\boldsymbol{\varepsilon}_{\mathbf{s}}} + \widetilde{\mathbf{F}}_1\mathbf{n}_{\boldsymbol{\omega}_{\mathbf{s}}} = \widetilde{\mathbf{h}}_1 - \widetilde{\mathbf{G}}_1\widetilde{\boldsymbol{\gamma}}^o_1. \tag{5.24}$$

The details of (5.24) and its solution are given in Appendix C.4.

Second Stage: The last $\frac{M(M-1)}{2}$ elements of $\hat{\widetilde{\boldsymbol{\gamma}}}_1$ are the estimates of the distances

between two unknown nodes. For example, $\hat{\tilde{\gamma}}_1((2+N)M+1) = ||\mathbf{u}_1^o - \mathbf{u}_2^o|| + \tilde{e}_1((2+N)M+1)$ is the estimated distance between the first and second unknown nodes, where $\tilde{\mathbf{e}}_1$ is the estimation error of $\hat{\tilde{\boldsymbol{\gamma}}}_1$. Let the position estimate of node i from Section 5.2 be $\mathbf{u}_i^*$, which has a difference of $\Delta\mathbf{u}_i^o = \mathbf{u}_i^o - \mathbf{u}_i^*$ with the true value $\mathbf{u}_i^o$. Similar to obtaining (5.12), we square the two sides of $\check{\gamma}_{1_i}^o(k-i) = ||\mathbf{u}_i^o - \mathbf{u}_k^o||$ and express the true node positions in terms of their previous estimates to obtain a pseudo linear equation in $\Delta\mathbf{u}_i^o$ and $\Delta\mathbf{u}_k^o$. Using $\hat{\tilde{\gamma}}_1((2+N)M+1) = \hat{\tilde{\gamma}}_{1_1}(1)$ as an example,

$$\begin{aligned} &2\tilde{\gamma}_1^o((2+N)M+1)\tilde{e}_1((2+N)M+1) \simeq \\ &\left(\hat{\tilde{\gamma}}_1((2+N)M+1)^2 - ||\mathbf{u}_1^* - \mathbf{u}_2^*||^2\right) - 2\left(\mathbf{u}_1^* - \mathbf{u}_2^*\right)^T \Delta\mathbf{u}_1^o - 2\left(\mathbf{u}_2^* - \mathbf{u}_1^*\right)^T \Delta\mathbf{u}_2^o \end{aligned} \tag{5.25}$$

where the product terms $\tilde{e}_1((2+N)M+1)^2$, $\Delta\mathbf{u}_1^{oT}\Delta\mathbf{u}_1^o$, $\Delta\mathbf{u}_2^{oT}\Delta\mathbf{u}_2^o$ and $\Delta\mathbf{u}_1^{oT}\Delta\mathbf{u}_2^o$ are relatively insignificant to be neglected when the noise is small.

The estimated distance between the ith unknown node and the jth beacon is the element $\hat{\tilde{\gamma}}_1((i-1)(2+N)+2+j)$. In terms of the amount of position correction $\Delta\mathbf{u}_i^o$, when replacing $\mathbf{u}_i^o$ by $\mathbf{u}_i^* + \Delta\mathbf{u}_i^o$,

$$\begin{aligned} &2\tilde{\gamma}_1^o((i-1)(2+N)+2+j)\tilde{e}_1((i-1)(2+N)+2+j) \simeq \\ &\hat{\tilde{\gamma}}_1((i-1)(2+N)+2+j)^2 - ||\mathbf{u}_i^* - \mathbf{s}_j||^2 - 2\left(\mathbf{u}_i^* - \mathbf{s}_j\right)^T \Delta\mathbf{u}_i^o \end{aligned} \tag{5.26}$$

where the second order terms $\tilde{e}_1((i-1)(2+N)+2+j)^2$ and $\Delta\mathbf{u}_i^{oT}\Delta\mathbf{u}_i^o$ are omitted.

Then, we stack (5.11), (5.25) and (5.26) together and form the matrix equation

$$\tilde{\mathbf{B}}_2\tilde{\mathbf{e}}_1 = \tilde{\mathbf{h}}_2 - \tilde{\mathbf{G}}_2\tilde{\boldsymbol{\gamma}}_2^o, \tag{5.27}$$

with the unknown vector defined as

$$\widetilde{\boldsymbol{\gamma}}_2^o = \left[\, \widetilde{\boldsymbol{\gamma}}_{2_1}^{oT},\, \widetilde{\boldsymbol{\gamma}}_{2_2}^{oT},\, \cdots,\, \widetilde{\boldsymbol{\gamma}}_{2_M}^{oT} \,\right]^T, \widetilde{\boldsymbol{\gamma}}_{2_i}^o = \left[\, \varepsilon_{\mathbf{u}_i}^o,\, \omega_{\mathbf{u}_i}^o,\, \Delta\mathbf{u}_i^{oT} \,\right]^T, \tag{5.28}$$

whose WLS solution is given in Appendix C.5.

The solution of $\widetilde{\boldsymbol{\gamma}}_2^o$ gives the estimates of $\varepsilon_{\mathbf{u}_i}^o$, $\omega_{\mathbf{u}_i}^o$ and $\Delta\mathbf{u}_i^o$, $i = 1,\, 2,\, \cdots,\, M$. The position estimate of the ith node is:

$$\hat{\mathbf{u}}_i = \mathbf{u}_i^* + \widetilde{\boldsymbol{\gamma}}_{2_i}(3:4), \qquad i = 1,\, 2,\, \ldots,\, M. \tag{5.29}$$

The covariance matrix of the unknown $\boldsymbol{\eta}^o$ defined in (5.1) is given in (C.20).

Inter-node communications cause error propagation and iterative approaches are typically used to suppress such error amplifications [87, 88]. The proposed method avoids error amplifications by joint estimation of all sensor nodes with proper weightings in the measurements to handle the position and clock uncertainties of the beacons. The proposed solution refines the node position estimates $\mathbf{u}_i^*$ in Section 5.2 obtained from message exchanges between the unknown nodes and beacons. Rather than using these estimates, other initial node positions can be used as well.

The solution here can be applied directly to reduce the beacon uncertainties if message exchanges among them are available. Instead of the sensor nodes, they are interpreted as the beacons. Obviously $\mathbf{u}_i^*$ is the ith noisy beacon position that is known. The prior knowledge about the uncertainties in these beacons can be included in the estimation process by expanding the matrix equation (5.27) [89].

5.4 Analysis

We shall use the CRLBs derived in Appendix C.6 as performance indices to evaluate the proposed solutions.

5.4.1 Node Localization without Inter-node Communication

The covariance matrix of the solution in this case is given by (5.19). After substituting (C.12), (C.11) and (C.7) sequentially, we have

$$\mathrm{cov}(\boldsymbol{\eta}) = \left(\mathbf{J}^T\mathbf{W}_1\mathbf{J}\right)^{-1}, \qquad \mathbf{J} = \mathbf{G}_1\mathbf{B}_2^{-1}\mathbf{G}_2\mathbf{B}_3^{-1}\mathbf{G}_3\mathbf{B}_4. \tag{5.30}$$

Note that $\mathbf{B}_3$ and $\mathbf{B}_4$ defined in (C.9a) and (5.20) are symmetric. Replacing $\mathbf{W}_1$ by (C.3) and using the Woodbury identity [22], (5.30) can be expressed as

$$\mathrm{cov}(\boldsymbol{\eta}) = \left(\mathbf{A}_{11} - \mathbf{A}_{12}\mathbf{A}_{22}^{-1}\mathbf{A}_{12}^T\right)^{-1}, \tag{5.31}$$

where the matrices are defined in Appendix C.7. (5.31) has the same form as (C.30).

To proceed further, we shall assume the following conditions are satisfied, for $i = 1, 2, \ldots, M$ and $j = 1, 2, \ldots, N$,

(C1) $|n_{\varepsilon_{\mathbf{s}_j}}| \ll 1 + \varepsilon^o_{\mathbf{s}_j}$;

(C2) $|n_{\omega_{\mathbf{s}_j}}| \ll |R^o_{i,j,l} - \omega^o_{\mathbf{s}_j}|$, $\quad l = 1, 3, \ldots, L-1$;

(C3) $|n_{\omega_{\mathbf{s}_j}}| \ll |T^o_{i,j,l} - \omega^o_{\mathbf{s}_j}|$, $\quad l = 2, 4, \ldots, L$;

(C4) $|n_{R_{i,j,l}}| \ll ||\mathbf{u}^o_i - \mathbf{s}^o_j||/c$, $\quad l = 1, 2, \ldots, L$;

(C5) $||\mathbf{n}_{\mathbf{s}_j}|| \ll ||\mathbf{u}_i^o - \mathbf{s}_j^o||$.

Condition (C1) requires the noise in the beacon clock drift to be much less than one. This condition is often satisfied in practice because the clock drift is in the order of 10^{-4} [47]. Conditions (C2)−(C3) assume the noise in the beacon clock offset is insignificant relative to the actual time stamp values. They are, again, easily satisfied in the practical networks. Condition (C4) requires the time measurement noise to be small compared to the true message propagation time [90]. Condition (C5) demands the beacon position noise to be small relative to the range between a sensor node and the beacon. This condition is reasonable because it ensures the time stamp values are large enough to be observed in the presence of beacon position error.

These conditions simply reduce to small noise requirement for the purpose of ignoring the second or higher order noise terms. In particular, (C1)−(C5) are used in (5.7), (5.12) and (5.15). In addition, (C5) ensures the approximation in (5.8) by using the Taylor series expansion up to linear term is accurate. We would like to indicate that the CRLB is a performance bound of an unbiased estimator. In nonlinear estimation, an estimator often yields a biased solution with the bias proportional to the noise power. As a result, it is only sensible to compare the performance of nonlinear estimation with the CRLB when the measurement noise is small such that the bias is negligible compared to the variance. When the noise level is large, the CRLB is not tight anymore in nonlinear estimation [91]. Even for the MLE [22], its performance can reach the CRLB only over the small noise region [91].

Appendix C.7 shows that under (C1)−(C5), (5.31) is equal to (C.30) and the proposed solution is able to achieve the CRLB accuracy.

5.4.2 Node Localization with Inter-node Communication

The covariance matrix of the unknown $\boldsymbol{\eta}$ is the same as that of $\widetilde{\boldsymbol{\gamma}}_2$ given by (C.20). Expanding (C.20) by substituting (C.19) and (C.16),

$$\mathrm{cov}\,(\boldsymbol{\eta}) = \left(\widetilde{\mathbf{J}}^T\widetilde{\mathbf{W}}_1\widetilde{\mathbf{J}}\right)^{-1}, \qquad \widetilde{\mathbf{J}} = \widetilde{\mathbf{G}}_1\widetilde{\mathbf{B}}_2^{-1}\widetilde{\mathbf{G}}_2. \tag{5.32}$$

Applying the Woodbury identity to $\widetilde{\mathbf{W}}_1$ in (C.15) reduces (5.32) to

$$\mathrm{cov}\,(\boldsymbol{\eta}) = \left(\widetilde{\mathbf{A}}_{11} - \widetilde{\mathbf{A}}_{12}\widetilde{\mathbf{A}}_{22}^{-1}\widetilde{\mathbf{A}}_{12}^T\right)^{-1} \tag{5.33}$$

where the matrices are defined in Appendix C.7.

Let us introduce two additional conditions, for $i = 1, 2, \ldots, M-1$ and $k = i+1, i+2, \ldots, M$,

(C6) $||\Delta\mathbf{u}_i^o|| \ll ||\mathbf{u}_i^o - \mathbf{u}_k^o||$ and $||\Delta\mathbf{u}_k^o|| \ll ||\mathbf{u}_i^o - \mathbf{u}_k^o||$;

(C7) $|n_{\check{R}_{i,k,l}}| \ll ||\mathbf{u}_i^o - \mathbf{u}_k^o||/c, \qquad l = 1, 2, \cdots, L.$

(C6) indicates that the differences between the true and the estimated positions from Section 5.2 are small compared to the node distances and (C7) requires the time measurement noise to be small relative to the true message propagation time. Using (C6)−(C7) together with (C1)−(C5), the approximation errors in (5.25) and (5.26) are negligible. Under these 7 small noise conditions, Appendix C.7 has shown that the proposed solution yields the CRLB accuracy.

5.5 Simulation

The MSEs of the proposed estimators are compared to those of the CF-WLS algorithm [46] and the GTLS method [47]. CF-WLS is able to attain the CRLB accuracy only when the noise level of the timing measurement is small and the beacons are without uncertainties. GTLS is designed to handle the inaccurate beacon positions and clock parameters. Although GTLS has an algebraic solution, we follow the recommendation from [47] and use iterative computation for higher algorithm stability.

The simulation results presented are the average over 100 geometries. Each geometry has 10 unknown nodes and 5 beacons. They are randomly deployed over a square area of 40 m $\times$ 40 m using a uniform distribution random number generator. The following two constraints are imposed to the randomly generated positions to obtain a reasonable WSN geometry:

$$(1) \quad ||\mathbf{s}_\alpha^o - \mathbf{s}_\beta^o|| > 10 \text{ m}; \qquad (2) \quad 15^\circ < \arccos\left(\boldsymbol{\rho}_{\mathbf{s}_\alpha^o,\mathbf{s}_\beta^o}^T \boldsymbol{\rho}_{\mathbf{s}_\alpha^o,\mathbf{s}_\gamma^o}\right) < 165^\circ;$$

where $\alpha = 1, 2, \ldots, 5$, $\beta = 1, 2, \ldots, 5$, $\gamma = 1, 2, \ldots, 5$ and $\alpha \neq \beta \neq \gamma$. Condition (1) is to ensure the beacons are not too close to have better spatial coverage. The condition (2) is to avoid three or more beacons are nearly lying on a straight line which will give a poor geometry whose results will dominate the performance from other geometries. The clock drifts and offsets of the unknown nodes and beacons are randomly drawn from uniform distribution over $[-0.002, 0.002]$ [47] and $[1, 10]$ μs [92]. The number of exchanged messages is $L = 8$. The covariance matrix of the beacon noise is $\mathbf{Q_b} = \text{diag}\,(\,\mathbf{Q_s},\, \mathbf{Q}_{\boldsymbol{\varepsilon}_\mathbf{s}},\, \mathbf{Q}_{\boldsymbol{\omega}_\mathbf{s}}\,)$, where $\mathbf{Q_s}$, $\mathbf{Q}_{\boldsymbol{\varepsilon}_\mathbf{s}}$ and $\mathbf{Q}_{\boldsymbol{\omega}_\mathbf{s}}$ are covariance matrices of beacon position, clock drift and clock offset errors. We set $\mathbf{Q_s} = \text{diag}\left(\,\sigma_{\mathbf{s}_1}^2\mathbf{I}_K,\, \cdots,\, \sigma_{\mathbf{s}_5}^2\mathbf{I}_K\,\right)$,

$\mathbf{Q}_{\boldsymbol{\varepsilon}_\mathbf{s}} = \text{diag}\left(\sigma^2_{\varepsilon_{\mathbf{s}_1}}, \cdots, \sigma^2_{\varepsilon_{\mathbf{s}_5}}\right)$ and $\mathbf{Q}_{\boldsymbol{\omega}_\mathbf{s}} = \text{diag}\left(\sigma^2_{\omega_{\mathbf{s}_1}}, \cdots, \sigma^2_{\omega_{\mathbf{s}_5}}\right)$, where in each geometry $\sigma_{\mathbf{s}_j}$, $\sigma_{\varepsilon_{\mathbf{s}_j}}$ and $\sigma_{\omega_{\mathbf{s}_j}}$, $j = 1, \cdots, 5$, are randomly generated from uniform distribution over $[\sqrt{0.1}\sigma_\mathbf{s},\ \sigma_\mathbf{s}]$ m, $[\sqrt{0.1}\sigma_{\varepsilon_\mathbf{s}},\ \sigma_{\varepsilon_\mathbf{s}}]$ and $[0.2\sigma_{\omega_\mathbf{s}}, \sigma_{\omega_\mathbf{s}}]$. The number of ensemble runs is 1000 for each geometry. We shall assume the maximum transmission range is 30 m [93]. There will be no measurements if a node and a beacon or two nodes are separated more than this limit. This effectively creates a partially connected WSN. The covariance matrix of time measurements is set as $\mathbf{Q}_{\tilde{\mathbf{m}}} = \sigma^2_\mathbf{m}\mathbf{I}_{MNL}$.

Three cases for localization and synchronization are considered. The first case performs estimation for each unknown node separately. The GTLS and CF-WLS can only work in this case. The second case performs this task for all unknown nodes simultaneously using the time stampsbetween the unknown nodes and the beacons. The third performs the simultaneous estimation by using the time measurements between the unknown nodes and the beacons, and those between two unknown nodes.

The proposed algorithms in Sections 5.2 and 5.3 are applied directly in the simulations for cases 2 and 3. For case 1, it is the estimator in Section 5.2 when setting $M = 1$. The approach to handle the dependency of the weighting matrices on the true values is described in the appendices for the individual stages and no iteration is used to re-compute the weighting matrices. To avoid the possible ill condition behavior when taking inverse to obtain $\mathbf{W}_1$ in (C.3), diagonal loading with a loading factor equal to $\frac{0.01\%}{z}$ of the trace of the matrix before the inverse is used, where z is the number of time stamp measurements (i.e. size of $\mathbf{Q}_\mathbf{m}$).

5.5.1 Performance with Respect to Time Measurement Accuracy

Fig. 5.3 shows the performance of various algorithms for the three cases as the measurement noise power increases and $\sigma^2_{\mathbf{s}}$, $\sigma^2_{\varepsilon_{\mathbf{s}}}$ and $\sigma^2_{\omega_{\mathbf{s}}}$ are kept at 0.1 m^2 [94], 10^{-7} [47] and 2.25×10^4 ns^2 [95]. The values shown are the mean-square position error averaged over the 10 sensor nodes.

We first examine the performance of the proposed algorithm in case 1. It does not reach the CRLB because it does not take into account the beacon errors are common in the time measurements of different sensor nodes. However, it performs much better than the CF-WLS and GTLS algorithms in this random geometries simulation setting. CF-WLS ignores the uncertainties of beacon positions and clocks. GTLS does not fully exploit the dependencies between the position and clock parameters of the unknown sensors in the timing measurements (5.4). The GTLS performance is worse than expected due to the fact that it is appropriate when the beacon position errors as well as clock errors are IID.

For case 2 and case 3, the proposed algorithms work quite well and attain the CRLB performance when the measurement noise power is below $10^{1.5}$ ns^2. Beyond this level, the performance starts to deviate from the CRLB due to the second order noise effect in nonlinear estimation.

Fig. 5.4 gives the results of clock drift estimation. The observations are similar to those in Fig. 5.3. Fig. 5.5 depicts the performance on clock offset estimates. The proposed algorithms show obvious improvement over CF-WLS and GTLS. Note that when the measurement noise is not significant, the CRLBs for the second and third cases are nearly identical and the estimation accuracy does not change with

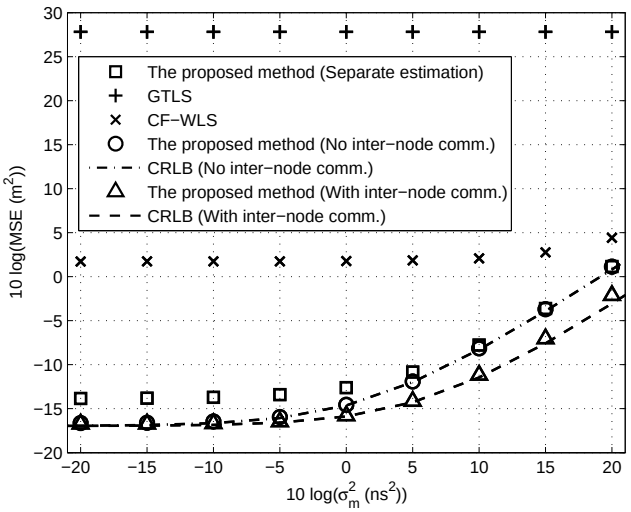

Figure 5.3: Localization performance versus the time measurement noise power.

CF-WLS	The proposed algorithms	GTLS
0.26	0.53	1

Table 5.1: Simulation times in case 1 consumed by CF-WLS and the proposed algorithm relative to that of GTLS [47]

respect to the measurement noise level. This is because the performance in clock-offset estimates is dominated by the relatively high beacon clock offset uncertainties in the simulation. The effect of measurement noise appears when it is large.

Table 5.1 tabulates the simulation times in case 1 consumed by CF-WLS and the proposed algorithm, relative to that of GTLS. GTLS takes longest while CF-WLS fastest. CF-WLS runs fastest because it ignores beacon position and clock errors and performs sequential estimation.

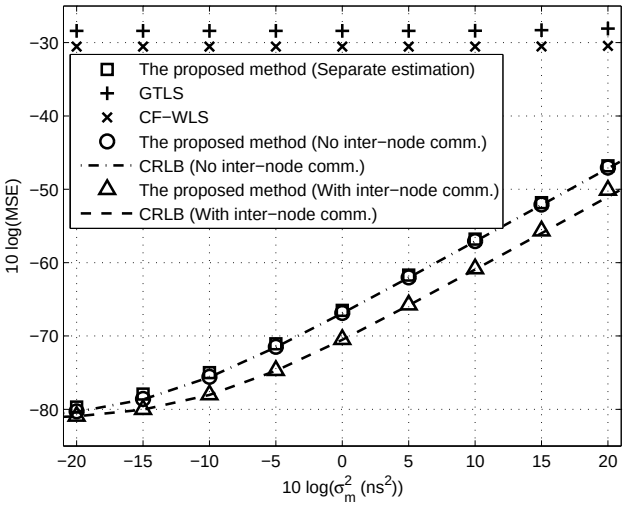

Figure 5.4: Estimation performance of the sensor node clock drifts versus the time measurement noise power, the clock drifts do not have unit [46, 47].

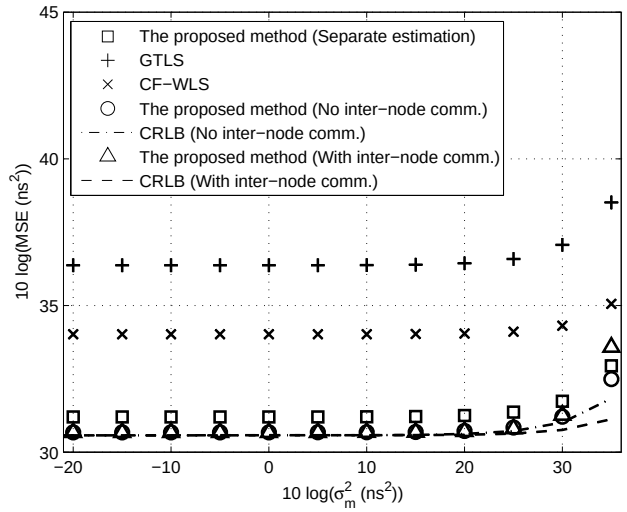

Figure 5.5: Estimation performance of the sensor node clock offsets versus the time measurement noise power.

5.5.2 Performance with Respect to Beacon Position Errors

Fig. 5.6 illustrates the results with different levels of beacon position noise power $\sigma_{\mathbf{s}}^2$ when $\sigma_{\mathbf{m}}^2$, $\sigma_{\varepsilon_{\mathbf{s}}}^2$ and $\sigma_{\omega_{\mathbf{s}}}^2$ are equal to 5 ns^2, 10^{-7} and 2.25×10^4 ns^2. The CRLB indicates that having inter-node time measurements as in case 3 provides 4 dB accuracy improvement when $\sigma_{\mathbf{s}}^2$ is small. Only the proposed algorithm is able to reach the CRLB accuracy.

Figs. 5.7 and 5.8 give the accuracy of the clock drift and offset estimates. They do not show obvious dependency of the estimation performance on the beacon position errors in this particular simulation. The dependency can be obvious and significant in a different localization scenario, as can be inferred from the CRLB shown in Appendix C.6. The proposed algorithms meet the CRLB performance quite well whilst CF-WLS and GTLS are not able to do so.

The relative processing times of the three algorithms under this simulation are the same as those in Table 5.1.

5.6 Conclusions

We have addressed the problem of joint localization and synchronization of multiple sensor nodes simultaneously in the presence of beacon position and clock uncertainties. Two computationally efficient algebraic solutions were developed. The first uses only the timing measurements from the message exchanges between the sensor nodes and beacons. The second includes the timing information from the message exchanges among the sensor nodes as well to improve performance. They were shown in theory and validated by simulations to reach the CRLB accuracy, before the nonlinear effect

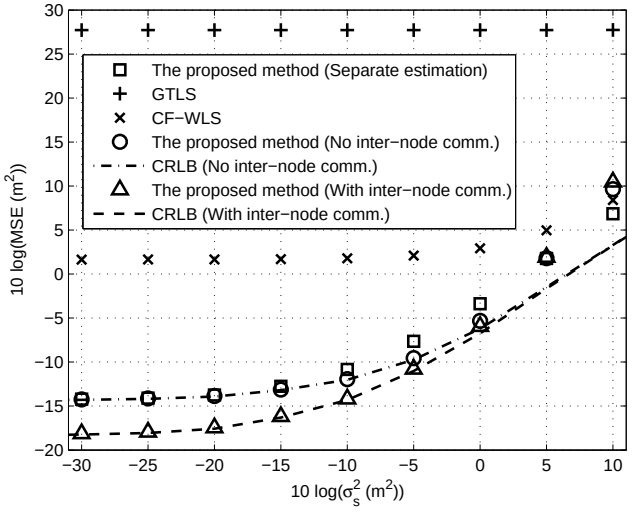

Figure 5.6: Localization performance versus the beacon position noise power.

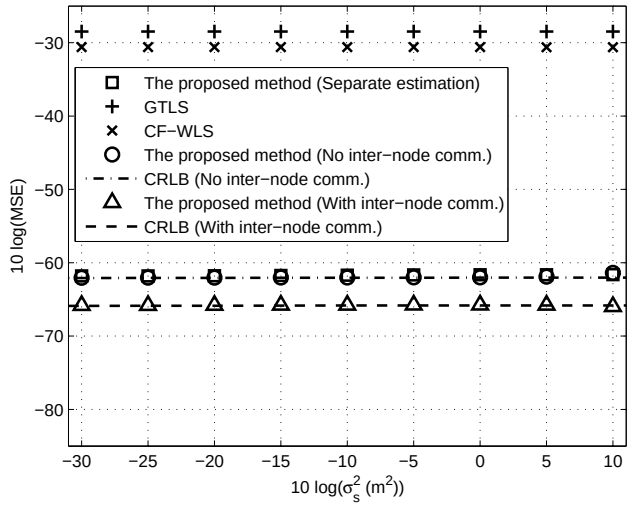

Figure 5.7: Estimation performance of the sensor node clock drifts versus the beacon position noise power.

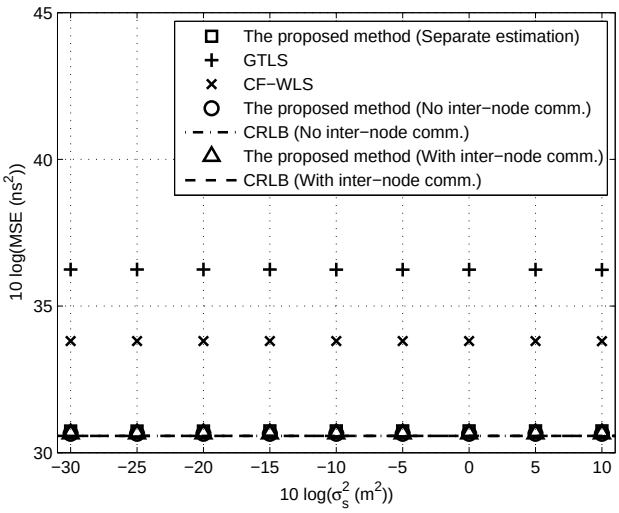

Figure 5.8: Estimation performance of the sensor node clock offsets versus the beacon position noise power.

of the measurement noise and the beacon errors occur. The proposed simultaneous estimation for multiple nodes provides a very effective way in mitigating the position and clock errors of the beacons.

The proposed solutions are derived under the condition that the noise levels in the time measurements and in the beacon parameters are small. When the noise levels become large, the proposed solutions would not have adequate performance and the results could be poor especially under bad localization geometries.

The proposed approach in jointly locating all sensor nodes does not increase communication overhead with the central processor compared to GTLS or CF-WLS that locate individual nodes one by one when the inter-node connections are not used, although we need to collect all timing measurements before the estimation can take place. The communication is increased by a factor of $(M + N)/N$ if we exploit the inter-node connections and the network is fully connected.

The proposed algorithms in their current forms require centralized processing where all the time stamp information is gathered in a processing center for the estimation task. Centralized processing ensures the optimum performance. Distributed solution such as the one in [85], even though suboptimum, can have communication and computation advantages over the centralized approach.

Chapter 6

Efficient Closed-Form Estimators for Multistatic Sonar Localization

This Chapter considers another challenging problem: multistatic sonar positioning. Comparing to the traditional sonar system, the multistatic sonar [5, 51, 55, 96] offers more flexibility and better performance. It separates the transmitters and receivers and places them at different locations. An object reflects the emitted signal from a transmitter and a receiver captures the reflected signal to locate the object after signal detection and classification. The signal propagation time defines an ellipse of possible object locations where the foci are the transmitter and receiver positions. The intersection of the ellipses yields the object location estimate. It is a kind of AE positioning problem.

6.1 Localization Scenario

We are interested in locating a single object at $\mathbf{u}^o = [\, x^o_{\mathbf{u}},\, y^o_{\mathbf{u}} \,]^T$ using M transmitters and N receivers whose positions are denoted by $\mathbf{t}_i = [\, x_{\mathbf{t}_i},\, y_{\mathbf{t}_i} \,]^T$ and $\mathbf{s}_j = \left[\, x_{\mathbf{s}_j},\, y_{\mathbf{s}_j} \,\right]^T$, $i = 1, 2, \ldots, M$, $j = 1, 2, \ldots, N$. Fig. 6.1 illustrates the scenario. Each transmitter radiates a sonar signal and all receivers observe the signals from direct propagation and from indirect reflection of the object. We shall assume the transmitter signals are disjoint either in frequency or in time [5, 51, 97] and they do not interfere with one another. Given a sufficient observation period and signal bandwidth, the autocorrelation of the signal from transmitter i at receiver j provides the arrival time difference $\tau^o_{i,j}$ between the direct and the reflected signal [50]. It is related to $\mathbf{u}^o$ by

$$\tau^o_{i,j} = \left(||\mathbf{u}^o - \mathbf{t}_i|| + ||\mathbf{u}^o - \mathbf{s}_j|| - ||\mathbf{t}_i - \mathbf{s}_j||\right)/c, i = 1, 2, \ldots, M, \;\; j = 1, 2, \ldots, N\,. \tag{6.1}$$

The time difference $\tau^o_{i,j}$ together with $\mathbf{t}_i$ and $\mathbf{s}_j$ define an ellipse in which the object lies. There is one time measurement for each combination of a transmitter and a receiver, giving a total of MN ellipses to locate the object.

In addition to the time measurements, each receiver can determine the bearing angle of the object as well [4, 5, 98]. The bearing angle, measured with respect to the x-axis, is dependent on the object location $\mathbf{u}^o$ by

$$\theta^o_j = \arctan \frac{y^o_{\mathbf{u}} - y_{\mathbf{s}_j}}{x^o_{\mathbf{u}} - x_{\mathbf{s}_j}}, \quad j = 1, 2, \ldots, N. \tag{6.2}$$

Each bearing angle θ^o_j forms a straight line that passes through the object.

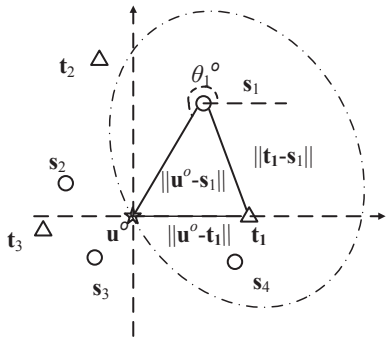

Figure 6.1: Localization geometry.

In reality, the measurements contain noise and their vector forms are

$$\boldsymbol{\tau} = \left[\, \boldsymbol{\tau}_1^T,\, \boldsymbol{\tau}_2^T,\, \cdots,\, \boldsymbol{\tau}_M^T \,\right]^T = \boldsymbol{\tau}^o + \mathbf{n}_{\boldsymbol{\tau}} \tag{6.3a}$$

$$\boldsymbol{\theta} = \left[\, \theta_1^T,\, \theta_2^T,\, \cdots,\, \theta_N^T \,\right]^T = \boldsymbol{\theta}^o + \mathbf{n}_{\boldsymbol{\theta}} \tag{6.3b}$$

where $\boldsymbol{\tau}_i = \left[\, \tau_{i,1},\, \tau_{i,2},\, \cdots,\, \tau_{i,N} \,\right]^T$, $\boldsymbol{\tau}^o$ and $\boldsymbol{\theta}^o$ are the true values. The time and bearing noise vectors are $\mathbf{n}_{\boldsymbol{\tau}}$ and $\mathbf{n}_{\boldsymbol{\theta}}$. They are independent of each other and are zero-mean Gaussian with known covariance matrices $\mathbf{Q}_{\boldsymbol{\tau}}$ and $\mathbf{Q}_{\boldsymbol{\theta}}$. For notation simplicity we shall define $\mathbf{m} = [\boldsymbol{\tau}^T, \boldsymbol{\theta}^T]^T$ as the composite measurement vector whose covariance is $\mathbf{Q}_{\mathbf{m}} = \text{diag}\,(\,\mathbf{Q}_{\boldsymbol{\tau}},\, \mathbf{Q}_{\boldsymbol{\theta}}\,)$.

The localization performance is limited by other errors in addition to measurement noise. In the sonar environment, the transmitter and receiver positions during data collection are not known and they are random realizations around their nominal positions. Randomness also appears in the signal propagation speed c as it varies with the temperature, pressure and salinity [53, 54] in the ocean. We shall model the vector

of transmitter and receiver positions $\mathbf{z} = \left[\, \mathbf{t}^T,\, \mathbf{s}^T \,\right]^T$, where $\mathbf{t} = \left[\, \mathbf{t}_1^T,\, \mathbf{t}_2^T,\, \cdots,\, \mathbf{t}_M^T \,\right]^T$ and $\mathbf{s} = \left[\, \mathbf{s}_1^T,\, \mathbf{s}_2^T,\, \cdots,\, \mathbf{s}_N^T \,\right]^T$, as Gaussian random variables [80, 81]

$$\mathbf{z} \sim \mathcal{N}\left(\, \bar{\mathbf{z}}\,,\, \mathbf{Q}_{\mathbf{z}} \,\right) \tag{6.4}$$

and so does the signal propagation speed

$$c \sim \mathcal{N}\left(\, \bar{c}\,,\, \sigma_c^2 \,\right)\,. \tag{6.5}$$

$\bar{\mathbf{z}}$ and $\bar{c}$ are the nominal positions and speed that are known. We also assume the covariance matrices are known based on prior knowledge.

We consider a 2D scenario in this study since the depth dependency on the time and bearing measurements can often be neglected [5]. We also ignore multipaths because they are insignificant when a transmitter and a receiver are not close [99]. The use of Gaussian errors are supported by the previous studies in [4, 5, 51, 49, 100].

The objective is to estimate the object location $\mathbf{u}^o$ as accurate as possible using the observations $\boldsymbol{\tau}$ and $\boldsymbol{\theta}$, and the statistical models of the sensor positions and signal propagation speed.

6.2 Hybrid CRLB

We now establish the performance bound for the multistatic sonar localization problem. The unknown parameter vector is $\boldsymbol{\gamma} = \left[\, \mathbf{u}^{oT},\, c,\, \mathbf{z}^T \,\right]^T$, where $\mathbf{u}^o$ is deterministic and the others are random. The resulting bound is the hybrid CRLB [80, 81, 101, 102], which is an integration of the classical CRLB that is for deterministic parameters and

the Bayesian bound that is for random parameters.

Let us denote the density function of the measurements given $\mathbf{z}$ and c as

$$f(\mathbf{m}|\mathbf{z},c) = C\,\exp\left(-\frac{1}{2}\left(\mathbf{m}-\mathbf{m}^o\right)^T\mathbf{Q}_{\mathbf{m}}^{-1}\left(\mathbf{m}-\mathbf{m}^o\right)\right) \tag{6.6}$$

and C is a constant independent of $\boldsymbol{\gamma}$. Let us also represent the Gaussian densities of $\mathbf{z}$ and c by $f_{\mathbf{z}}$ and f_c. According to the previous studies [80, 81, 101, 102], the hybrid bound of $\boldsymbol{\gamma}$ is the inverse of $\mathbf{F}_{\boldsymbol{\gamma}}$,

$$\begin{aligned}\mathbf{F}_{\boldsymbol{\gamma}} \triangleq\ & \mathrm{E}_{\mathbf{m},\mathbf{z},c}\left(\left(\frac{\partial \ln f}{\partial \boldsymbol{\gamma}}\right)\left(\frac{\partial \ln f}{\partial \boldsymbol{\gamma}}\right)^T\right) \\ & + \mathrm{E}_{\mathbf{z},c}\left(\left(\frac{\partial \ln f_{\mathbf{z}}}{\partial \boldsymbol{\gamma}}\right)\left(\frac{\partial \ln f_{\mathbf{z}}}{\partial \boldsymbol{\gamma}}\right)^T + \left(\frac{\partial \ln f_c}{\partial \boldsymbol{\gamma}}\right)\left(\frac{\partial \ln f_c}{\partial \boldsymbol{\gamma}}\right)^T\right).\end{aligned} \tag{6.7}$$

We use the notation $\mathrm{E}_{\mathbf{m},\mathbf{z},c}(*)$ to represent the expectation of $*$ is taken over $\mathbf{m}$, $\mathbf{z}$ and c, and $\mathrm{E}_{\mathbf{z},c}(*)$ is similarly defined.

Putting (6.6) into the first term of $\mathbf{F}_{\boldsymbol{\gamma}}$ in (6.7) and taking expectation over $\mathbf{m}$ give

$$\mathrm{E}_{\mathbf{m},\mathbf{z},c}\left(\left(\frac{\partial \ln f}{\partial \boldsymbol{\gamma}}\right)\left(\frac{\partial \ln f}{\partial \boldsymbol{\gamma}}\right)^T\right) = \mathrm{E}_{\mathbf{z},c}\left(\boldsymbol{\nabla}_{\boldsymbol{\gamma}}^T\mathbf{Q}_{\mathbf{m}}^{-1}\boldsymbol{\nabla}_{\boldsymbol{\gamma}}\right) \tag{6.8}$$

where $\boldsymbol{\nabla}_{\boldsymbol{\gamma}} = [\,\boldsymbol{\nabla}_{\mathbf{u}^o},\ \boldsymbol{\nabla}_c,\ \boldsymbol{\nabla}_{\mathbf{z}}\,] = \partial\mathbf{m}^o/\partial\boldsymbol{\gamma}^T$ whose details are given in Appendix D.1.

The levels of transmitter and receiver position uncertainties are usually small compared to the distances between transmitters and receivers as well as the distances from the object to the transmitters and to the receivers in the sonar localization problem [4, 5, 51]. In this case, the expectation over $\mathbf{z}$ in (6.8) can be approximated [80, 81, 101] by using $\bar{\mathbf{z}}$ for $\mathbf{z}$. In addition, σ_c is much less than $\bar{c}$ [5] and we have

$\mathrm{E}\,(c^{-2}) \simeq 1/\bar{c}^2$ and $\mathrm{E}\,(c^{-4}) \simeq 1/\bar{c}^4$ [103, 104]. Thus

$$\mathrm{E}_{\mathbf{m},\mathbf{z},c}\left(\left(\frac{\partial \ln f}{\partial \boldsymbol{\gamma}}\right)\left(\frac{\partial \ln f}{\partial \boldsymbol{\gamma}}\right)^T\right) \approx \bar{\boldsymbol{\nabla}}_{\boldsymbol{\gamma}}^T \mathbf{Q}_{\mathbf{m}}^{-1} \bar{\boldsymbol{\nabla}}_{\boldsymbol{\gamma}} \tag{6.9}$$

where $\bar{\boldsymbol{\nabla}}_{\boldsymbol{\gamma}}$ represents the partial derivative with $\mathbf{z}$ and c replaced by $\bar{\mathbf{z}}$ and $\bar{c}$.

Given (6.4) and (6.5), the second term in (6.7) can be readily evaluated and

$$\mathbf{F}_{\boldsymbol{\gamma}} \approx \bar{\boldsymbol{\nabla}}_{\boldsymbol{\gamma}}^T \mathbf{Q}_{\mathbf{m}}^{-1} \bar{\boldsymbol{\nabla}}_{\boldsymbol{\gamma}} + \mathrm{diag}\left(\mathbf{O}_{2\times 2},\, \sigma_c^{-2},\, \mathbf{Q}_{\mathbf{z}}^{-1}\right). \tag{6.10}$$

The hybrid CRLB of $\mathbf{u}^o$ is the upper left 2×2 block of $\mathbf{F}_{\boldsymbol{\gamma}}^{-1}$. Invoking the partitioned matrix inversion formula [80] to (6.10) and using $\bar{\boldsymbol{\nabla}}_{\boldsymbol{\gamma}} = \left[\, \bar{\boldsymbol{\nabla}}_{\mathbf{u}^o},\, \bar{\boldsymbol{\nabla}}_c,\, \bar{\boldsymbol{\nabla}}_{\mathbf{z}} \,\right]$,

$$\mathrm{HCRLB}_{\mathbf{u}^o} \approx \left(\bar{\boldsymbol{\nabla}}_{\mathbf{u}^o}^T \left(\mathbf{Q}_{\mathbf{m}} + \sigma_c^2 \bar{\boldsymbol{\nabla}}_c \bar{\boldsymbol{\nabla}}_c^T + \bar{\boldsymbol{\nabla}}_{\mathbf{z}} \mathbf{Q}_{\mathbf{z}} \bar{\boldsymbol{\nabla}}_{\mathbf{z}}^T\right)^{-1} \bar{\boldsymbol{\nabla}}_{\mathbf{u}^o}\right)^{-1}. \tag{6.11}$$

When the statistical distribution of c is not available, we model it as a deterministic unknown and represent it as c^o in $\boldsymbol{\gamma}$. In this case, there is no expectation over c and the $\partial \ln f_c / \partial \boldsymbol{\gamma}$ in (6.7) is zero. The matrix $\mathbf{F}_{\boldsymbol{\gamma}}$ remains to be given by (6.10) but with $\bar{c}$ replaced by c^o and σ_c^{-2} by zero. The hybrid bound of $\mathbf{u}^o$ and c^o is

$$\mathrm{HCRLB}_{\mathbf{u}^o,\, c^o} \approx \left(\left[\, \bar{\boldsymbol{\nabla}}_{\mathbf{u}^o},\, \bar{\boldsymbol{\nabla}}_c \,\right]^T \left(\mathbf{Q}_{\mathbf{m}} + \bar{\boldsymbol{\nabla}}_{\mathbf{z}} \mathbf{Q}_{\mathbf{z}} \bar{\boldsymbol{\nabla}}_{\mathbf{z}}^T\right)^{-1} \left[\, \bar{\boldsymbol{\nabla}}_{\mathbf{u}^o},\, \bar{\boldsymbol{\nabla}}_c \,\right]\right)^{-1}. \tag{6.12}$$

For the case when we only use the time measurements, (6.11) and (6.12) remain valid by setting $\mathbf{m}^o$ to $\boldsymbol{\tau}^o$ and $\mathbf{Q}_{\mathbf{m}}$ to $\mathbf{Q}_{\boldsymbol{\tau}}$.

We shall develop in the next Section two object location estimators using the time measurements and the statistical distributions of the transmitter and receiver positions. One is with the knowledge of the statistical distribution of signal propagation

speed and the other is without.

6.3 Localization Using Time Measurements

The nonlinear measurement equation is defined by (6.1). We shall use parameter transformation, introduce auxiliary variables and apply multi-stage processing to simplify the nonlinear estimation problem. Rather than estimating the transmitter and receiver positions and the propagation speed in conjunction with the object location, we shall replace them with their nominal values and utilize weighting to account for using their inexact values.

The use of multi-stage processing has been introduced in Chapter 5. Recently [19] applied it to solve the elliptic localization problem when there is one transmitter only, where the transmitter and receiver positions as well as the signal propagation speed are exactly known. The algorithm in [19] is a specific case of ours.

In each stage we simply utilize WLS [22] minimization to the pseudo linear equations created by introducing extra unknowns. The number of unknowns reduces from stage to stage to improve the localization accuracy. The derivations ignore the second and higher order error terms, which is justified when the measurement noise and the sensor position and speed uncertainties are not large. In particular, the following small error conditions are used:

(C1) $||\mathbf{\Delta}_{\mathbf{t}_i}|| \ll ||\mathbf{u}^o - \overline{\mathbf{t}}_i||, \qquad ||\mathbf{\Delta}_{\mathbf{t}_i}|| \ll ||\overline{\mathbf{t}}_i - \overline{\mathbf{s}}_j||$

(C2) $||\mathbf{\Delta}_{\mathbf{s}_j}|| \ll ||\mathbf{u}^o - \overline{\mathbf{s}}_j||, \qquad ||\mathbf{\Delta}_{\mathbf{s}_j}|| \ll ||\overline{\mathbf{t}}_i - \overline{\mathbf{s}}_j||$

(C3) $|n_{\boldsymbol{\tau},i,j}| \ll \tau^o_{i,j}$

(C4) $|\Delta_c| \ll \bar{c}$

where $\boldsymbol{\Delta}_{\mathbf{t}_i} = \mathbf{t}_i - \bar{\mathbf{t}}_i$, $\boldsymbol{\Delta}_{\mathbf{s}_j} = \mathbf{s}_j - \bar{\mathbf{s}}_j$, $n_{\boldsymbol{\tau},i,j} = \tau_{i,j} - \tau^o_{i,j}$ and $\Delta_c = c - \bar{c}$, for $i = 1, 2, \ldots, M$ and $j = 1, 2, \ldots, N$. (C1) means the position uncertainty of a given transmitter is small relative to its distance to the object and its distances to the receivers. Similarly, (C2) means the position uncertainty of a given receiver is small relative to its distance to the object and its distances to the transmitters. (C3) requires the relative measurement noise be small and (C4) assumes the standard deviation of the propagation speed is much less than its mean value.

6.3.1 Distribution of c Known

We shall express (6.1) in terms of the available nominal positions by substituting $\mathbf{t}_i = \bar{\mathbf{t}}_i + \boldsymbol{\Delta}_{\mathbf{t}_i}$ and $\mathbf{s}_j = \bar{\mathbf{s}}_j + \boldsymbol{\Delta}_{\mathbf{s}_j}$. Using the Taylor series expansion and the conditions (C1) and (C2),

$$\begin{aligned} ||\mathbf{u}^o - \mathbf{t}_i|| &\simeq ||\mathbf{u}^o - \bar{\mathbf{t}}_i|| - \boldsymbol{\rho}^T_{\mathbf{u}^o,\bar{\mathbf{t}}_i}\boldsymbol{\Delta}_{\mathbf{t}_i}, \\ ||\mathbf{u}^o - \mathbf{s}_j|| &\simeq ||\mathbf{u}^o - \bar{\mathbf{s}}_j|| - \boldsymbol{\rho}^T_{\mathbf{u}^o,\bar{\mathbf{s}}_j}\boldsymbol{\Delta}_{\mathbf{s}_j}, \\ ||\mathbf{t}_i - \mathbf{s}_j|| &= ||\bar{\mathbf{t}}_i - \bar{\mathbf{s}}_j + \boldsymbol{\Delta}_{\mathbf{t}_i} - \boldsymbol{\Delta}_{\mathbf{s}_j}|| \simeq ||\bar{\mathbf{t}}_i - \bar{\mathbf{s}}_j|| + \boldsymbol{\rho}^T_{\bar{\mathbf{t}}_i,\bar{\mathbf{s}}_j}\left(\boldsymbol{\Delta}_{\mathbf{t}_i} - \boldsymbol{\Delta}_{\mathbf{s}_j}\right) \end{aligned} \tag{6.13}$$

where $\boldsymbol{\rho}_{\mathbf{u}^o,\bar{\mathbf{t}}_i} = (\mathbf{u}^o - \bar{\mathbf{t}}_i)/||\mathbf{u}^o - \bar{\mathbf{t}}_i||$ is a unit vector from $\bar{\mathbf{t}}_i$ to $\mathbf{u}^o$, and $\boldsymbol{\rho}_{\mathbf{u}^o,\bar{\mathbf{s}}_j}$ and $\boldsymbol{\rho}_{\bar{\mathbf{t}}_i,\bar{\mathbf{s}}_j}$ are defined similarly. Expressing $\tau^o_{i,j} = \tau_{i,j} - n_{\boldsymbol{\tau},i,j}$ and $c = \bar{c} + \Delta_c$, using (C3) and (C4) and neglecting $\Delta_c n_{\boldsymbol{\tau},i,j}$, (6.1) becomes

$$\bar{c}\tau_{i,j} \simeq ||\mathbf{u}^o - \bar{\mathbf{t}}_i|| + ||\mathbf{u}^o - \bar{\mathbf{s}}_j|| - ||\bar{\mathbf{t}}_i - \bar{\mathbf{s}}_j|| + \epsilon_{1,i,j}, i = 1, 2, \ldots, M, \quad j = 1, 2, \ldots, N \tag{6.14}$$

where

$$\epsilon_{1,i,j} \triangleq \bar{c} n_{\boldsymbol{\tau},i,j} - \left(\boldsymbol{\rho}_{\mathbf{u}^o,\bar{\mathbf{t}}_i} + \boldsymbol{\rho}_{\bar{\mathbf{t}}_i,\bar{\mathbf{s}}_j}\right)^T \boldsymbol{\Delta}_{\mathbf{t}_i} - \left(\boldsymbol{\rho}_{\mathbf{u}^o,\bar{\mathbf{s}}_j} - \boldsymbol{\rho}_{\bar{\mathbf{t}}_i,\bar{\mathbf{s}}_j}\right)^T \boldsymbol{\Delta}_{\mathbf{s}_j} - \tau^o_{i,j}\Delta_c \,. \tag{6.15}$$

The proposed algorithm has four stages. Starting from (6.14), the first stage considers $\mathbf{u}^o$ and the distances $||\mathbf{u}^o - \bar{\mathbf{t}}_i||$, $i = 1, 2, \ldots, M$, are independent variables to be solved. The second stage squares the distance estimates from the first stage to create another set of pseudo linear equations with respect to $\mathbf{u}^o$ and $\mathbf{u}^{oT}\mathbf{u}^o$. The third stage defines its unknown as $\mathbf{u}^o \odot \mathbf{u}^o$ and uses the relation between $\mathbf{u}^o$ and $\mathbf{u}^{oT}\mathbf{u}^o$ to improve the accuracy. The last stage obtains the final solution by taking the square root on the estimates of $\mathbf{u}^o \odot \mathbf{u}^o$.

First Stage

Putting $||\mathbf{u}^o - \bar{\mathbf{t}}_i|| - ||\bar{\mathbf{t}}_i - \bar{\mathbf{s}}_j||$ from the right to the left in (6.14), squaring both sides and ignoring $\epsilon^2_{1,i,j}$ give

$$\begin{aligned} 2||\mathbf{u}^o - \bar{\mathbf{s}}_j||\epsilon_{1,i,j} \simeq\ & 2\bar{\mathbf{t}}_i^T(\bar{\mathbf{t}}_i - \bar{\mathbf{s}}_j) + 2\bar{c}\tau_{i,j}||\bar{\mathbf{t}}_i - \bar{\mathbf{s}}_j|| + \bar{c}^2\tau^2_{i,j} \\ & - 2\left(\bar{\mathbf{t}}_i - \bar{\mathbf{s}}_j\right)^T \mathbf{u}^o - 2\left(\bar{c}\tau_{i,j} + ||\bar{\mathbf{t}}_i - \bar{\mathbf{s}}_j||\right)||\mathbf{u}^o - \bar{\mathbf{t}}_i|| \end{aligned} \tag{6.16}$$

for $i = 1, 2, \ldots, M$ and $j = 1, 2, \ldots, N$. Let the unknown vector be

$$\boldsymbol{\varphi}^o_1 = \left[\mathbf{u}^{oT},\, ||\mathbf{u}^o - \bar{\mathbf{t}}_1||,\, \cdots,\, ||\mathbf{u}^o - \bar{\mathbf{t}}_M||\right]^T \tag{6.17}$$

and (6.16) is linear with respect to $\boldsymbol{\varphi}^o_1$. Collecting the MN equations together,

$$\mathbf{B}_1\boldsymbol{\epsilon}_1 = \mathbf{h}_1 - \mathbf{G}_1\boldsymbol{\varphi}^o_1 \tag{6.18}$$

where the approximation errors are ignored and the matrices and vectors are defined in (D.3) of Appendix D.2. The WLS solution to (6.18) is

$$\boldsymbol{\varphi}_1 = \left(\mathbf{G}_1^T \mathbf{W}_1 \mathbf{G}_1\right)^{-1} \mathbf{G}_1^T \mathbf{W}_1 \mathbf{h}_1 \,. \tag{6.19}$$

The weighting matrix $\mathbf{W}_1$ is given in (D.7). (D.8) is the covariance matrix of $\boldsymbol{\varphi}_1$.

Second Stage

The second stage explores the dependency in the elements of $\boldsymbol{\varphi}_1^o$ to improve the object position estimate. The stage one solution is $\boldsymbol{\varphi}_1 = \boldsymbol{\varphi}_1^o + \boldsymbol{\epsilon}_2$, where $\boldsymbol{\epsilon}_2$ is the estimation error. Let $\boldsymbol{\epsilon}_2\,(k\,:\,l)$ be the subvector of $\boldsymbol{\epsilon}_2$ from the kth element to the lth and $\epsilon_2(l)$ be the lth element of $\boldsymbol{\epsilon}_2$. Clearly,

$$\boldsymbol{\epsilon}_2\,(1\,:\,2) = \boldsymbol{\varphi}_1\,(1\,:\,2) - \mathbf{u}^o \tag{6.20a}$$

$$2\varphi_1^o(2+i)\epsilon_2(2+i) \simeq \varphi_1^2(2+i) - \overline{\mathbf{t}}_i^T \overline{\mathbf{t}}_i + 2\overline{\mathbf{t}}_i^T \mathbf{u}^o - \mathbf{u}^{oT}\mathbf{u}^o \tag{6.20b}$$

where $\epsilon_2^2(2+i)$ is small in (6.20b) and $i = 1, 2, \ldots, M$. Let the unknown vector as

$$\boldsymbol{\varphi}_2^o = \left[\, \mathbf{u}^{oT},\, \mathbf{u}^{oT}\mathbf{u}^o \,\right]^T \tag{6.21}$$

and ignore the approximation errors, the matrix form of (6.20) is

$$\mathbf{B}_2 \boldsymbol{\epsilon}_2 = \mathbf{h}_2 - \mathbf{G}_2 \boldsymbol{\varphi}_2^o \,. \tag{6.22}$$

The matrices and vector in (6.22) are defined in (D.9). The WLS solution of $\boldsymbol{\varphi}_2^o$ is

$$\boldsymbol{\varphi}_2 = \left(\mathbf{G}_2^T \mathbf{W}_2 \mathbf{G}_2\right)^{-1} \mathbf{G}_2^T \mathbf{W}_2 \mathbf{h}_2 \tag{6.23}$$

and (D.10) gives the weighting matrix $\mathbf{W}_2$.

Third Stage

It is obvious the elements of $\boldsymbol{\varphi}_2^o$ are related. We shall represent $\boldsymbol{\varphi}_2 = \boldsymbol{\varphi}_2^o + \boldsymbol{\epsilon}_3$, where $\boldsymbol{\epsilon}_3$ is the estimation noise. Expanding $(\boldsymbol{\varphi}_2(1:2) - \boldsymbol{\epsilon}_3(1:2)) \odot (\boldsymbol{\varphi}_2(1:2) - \boldsymbol{\epsilon}_3(1:2)) = \mathbf{u}^o \odot \mathbf{u}^o$ and since $\boldsymbol{\epsilon}_3(1:2) \odot \boldsymbol{\epsilon}_3(1:2)$ is small

$$2\boldsymbol{\varphi}_2^o(1:2) \odot \boldsymbol{\epsilon}_3(1:2) \simeq \boldsymbol{\varphi}_2(1:2) \odot \boldsymbol{\varphi}_2(1:2) - \boldsymbol{\varphi}_3^o \tag{6.24}$$

where

$$\boldsymbol{\varphi}_3^o = \mathbf{u}^o \odot \mathbf{u}^o \,. \tag{6.25}$$

We have

$$\epsilon_2(3) = \varphi_2(3) - \mathbf{1}_2^T \boldsymbol{\varphi}_3^o \tag{6.26}$$

from the third element of $\boldsymbol{\varphi}_2$. Thus after ignoring the approximation error,

$$\mathbf{B}_3 \boldsymbol{\epsilon}_3 = \mathbf{h}_3 - \mathbf{G}_3 \boldsymbol{\varphi}_3^o \tag{6.27}$$

and $\mathbf{B}_3$, $\mathbf{h}_3$ and $\mathbf{G}_3$ are given in (D.12). The WLS solution is

$$\boldsymbol{\varphi}_3 = \left(\mathbf{G}_3^T \mathbf{W}_3 \mathbf{G}_3\right)^{-1} \mathbf{G}_3^T \mathbf{W}_3 \mathbf{h}_3 \tag{6.28}$$

and the weighting matrix is (D.13).

Fourth Stage

The final object position estimate is

$$\hat{\mathbf{u}} = \text{diag}\left(\text{sgn}\left(\boldsymbol{\varphi}_1(1\ :\ 2)\right)\right)\sqrt{\boldsymbol{\varphi}_3} \tag{6.29}$$

where $\text{diag}\left(\text{sgn}\left(\boldsymbol{\varphi}_1(1\ :\ 2)\right)\right)$ is to remove the sign ambiguity when applying the square root operation. Taking the differential of the definition of $\boldsymbol{\varphi}_3^o$ in (6.25) relates the errors between $\boldsymbol{\varphi}_3$ and $\hat{\mathbf{u}}$. Hence we obtain

$$\text{cov}\left(\hat{\mathbf{u}}\right) = \mathbf{B}_4^{-T}\text{cov}\left(\boldsymbol{\varphi}_3\right)\mathbf{B}_4^{-1} \tag{6.30}$$

where $\text{cov}\left(\boldsymbol{\varphi}_3\right)$ is shown in (D.14) and

$$\mathbf{B}_4 = 2\text{diag}\left(\, x_{\mathbf{u}}^o,\, y_{\mathbf{u}}^o \,\right). \tag{6.31}$$

The algorithm described above assumes the number of transmitters is not more than the number of receivers, i.e. $M \leq N$. If $M > N$, the unknown vector of the first stage in (6.17) will be $\boldsymbol{\varphi}_1^o = \left[\mathbf{u}^{oT},\, ||\mathbf{u}^o - \bar{\mathbf{s}}_1||,\, \cdots,\, ||\mathbf{u}^o - \bar{\mathbf{s}}_N||\right]^T$ for the purpose to reduce the number of variables, and its WLS solution is derived in a similar manner. The $\bar{\mathbf{t}}_i$ in the second stage equations becomes $\bar{\mathbf{s}}_j$ correspondingly and the third and fourth stages are the same as before. The proposed estimator requires $MN \geq (\min(M, N) + 2)$ to ensure a unique solution because of the use of extra variables in the first stage.

6.3.2 Distribution of c Not Known

In this situation we shall express c as a deterministic unknown c^o and solve it jointly with $\mathbf{u}^o$. The processing is similar to the previous case of using four stages, however, additional auxiliary variables are needed. The first stage has $4 + 2M$ unknowns and they are $\mathbf{u}^o$, c^o, $(c^o)^2$, $||\mathbf{u}^o - \overline{\mathbf{t}}_i||$ and $c^o||\mathbf{u}^o - \overline{\mathbf{t}}_i||$, $i = 1, 2, \ldots, M$. The second reduces the unknowns to $\mathbf{u}^o$, $\mathbf{u}^{oT}\mathbf{u}^o$ and $(c^o)^2$, and the third to $\mathbf{u}^o \odot \mathbf{u}^o$ and $(c^o)^2$. The final stage removes the squares to estimate the object location and propagation speed.

First Stage

When c is the deterministic unknown c^o, (6.14) and (6.15) become

$$c^o\tau_{i,j} \simeq ||\mathbf{u}^o - \overline{\mathbf{t}}_i|| + ||\mathbf{u}^o - \overline{\mathbf{s}}_j|| - ||\overline{\mathbf{t}}_i - \overline{\mathbf{s}}_j|| + \widetilde{\epsilon}_{1,i,j}, i = 1, 2, \ldots, M, \;\; j = 1, 2, \ldots, N \tag{6.32}$$

and

$$\widetilde{\epsilon}_{1,i,j} = c^o n_{\boldsymbol{\tau},i,j} - \left(\boldsymbol{\rho}_{\mathbf{u}^o,\overline{\mathbf{t}}_i} + \boldsymbol{\rho}_{\overline{\mathbf{t}}_i,\overline{\mathbf{s}}_j}\right)^T \boldsymbol{\Delta}_{\mathbf{t}_i} - \left(\boldsymbol{\rho}_{\mathbf{u}^o,\overline{\mathbf{s}}_j} - \boldsymbol{\rho}_{\overline{\mathbf{t}}_i,\overline{\mathbf{s}}_j}\right)^T \boldsymbol{\Delta}_{\mathbf{s}_j}. \tag{6.33}$$

Moving $||\mathbf{u}^o - \overline{\mathbf{t}}_i|| - ||\overline{\mathbf{t}}_i - \overline{\mathbf{s}}_j||$ to the left, squaring both sides and dropping $\widetilde{\epsilon}^2_{1,i,j}$, (6.32) is

$$\begin{aligned} 2||\mathbf{u}^o - \overline{\mathbf{s}}_j||\widetilde{\epsilon}_{1,i,j} \simeq\; & 2\overline{\mathbf{t}}_i^T(\overline{\mathbf{t}}_i - \overline{\mathbf{s}}_j) - 2\left(\overline{\mathbf{t}}_i - \overline{\mathbf{s}}_j\right)^T \mathbf{u}^o + 2||\overline{\mathbf{t}}_i - \overline{\mathbf{s}}_j||\tau_{i,j}c^o + \tau_{i,j}^2(c^o)^2 \\ & - 2||\overline{\mathbf{t}}_i - \overline{\mathbf{s}}_j||||\mathbf{u}^o - \overline{\mathbf{t}}_i|| - 2\tau_{i,j}c^o||\mathbf{u}^o - \overline{\mathbf{t}}_i|| \end{aligned} \tag{6.34}$$

for $i = 1, 2, \ldots, M$ and $j = 1, 2, \ldots, N$. We define the unknown vector as

$$\widetilde{\boldsymbol{\varphi}}_1^o = \left[\mathbf{u}^{oT},\, c^o,\, (c^o)^2, ||\mathbf{u}^o - \overline{\mathbf{t}}_1||, \cdots, ||\mathbf{u}^o - \overline{\mathbf{t}}_M||,\, c^o||\mathbf{u}^o - \overline{\mathbf{t}}_1||, \cdots, c^o||\mathbf{u}^o - \overline{\mathbf{t}}_M||\right]^T . \tag{6.35}$$

Ignoring the approximation error, (6.34) has the linear form

$$\mathbf{B}_1 \widetilde{\boldsymbol{\epsilon}}_1 = \widetilde{\mathbf{h}}_1 - \widetilde{\mathbf{G}}_1 \widetilde{\boldsymbol{\varphi}}_1^o \tag{6.36}$$

where matrices and vectors are in (D.15) of Appendix D.3. The WLS solution is

$$\widetilde{\boldsymbol{\varphi}}_1 = \left(\widetilde{\mathbf{G}}_1^T\, \widetilde{\mathbf{W}}_1\, \widetilde{\mathbf{G}}_1\right)^{-1} \widetilde{\mathbf{G}}_1^T\, \widetilde{\mathbf{W}}_1\, \widetilde{\mathbf{h}}_1 \tag{6.37}$$

and the weighting matrix $\widetilde{\mathbf{W}}_1$ is defined in (D.16).

Second Stage

The first stage solution is $\widetilde{\boldsymbol{\varphi}}_1 = \widetilde{\boldsymbol{\varphi}}_1^o + \widetilde{\boldsymbol{\epsilon}}_2$ and $\widetilde{\boldsymbol{\epsilon}}_2$ is the estimation error. From (6.35),

$$\widetilde{\boldsymbol{\epsilon}}_2\,(1\,:\,2) = \widetilde{\boldsymbol{\varphi}}_1\,(1\,:\,2) - \mathbf{u}^o,$$

$$2\widetilde{\varphi}_1^o(3)\widetilde{\epsilon}_2(3) \simeq \widetilde{\varphi}_1^2(3) - (c^o)^2\,, \widetilde{\epsilon}_2(4) = \widetilde{\varphi}_1(4) - (c^o)^2\,,$$

$$2\widetilde{\varphi}_1^o(4+i)\widetilde{\epsilon}_2(4+i) \simeq \widetilde{\varphi}_1^2(4+i) - \overline{\mathbf{t}}_i^T\overline{\mathbf{t}}_i + 2\overline{\mathbf{t}}_i^T\mathbf{u}^o - \mathbf{u}^{oT}\mathbf{u}^o,$$

$$2\widetilde{\varphi}_1^o(4+M+i)\widetilde{\epsilon}_2(4+M+i) - ||\mathbf{u}^o - \overline{\mathbf{t}}_i||^2\widetilde{\epsilon}_2(4) \simeq$$

$$\widetilde{\varphi}_1^2(4+M+i) - \widetilde{\varphi}_1(4)\overline{\mathbf{t}}_i^T\overline{\mathbf{t}}_i + 2\widetilde{\varphi}_1(4)\overline{\mathbf{t}}_i^T\mathbf{u}^o - \widetilde{\varphi}_1(4)\mathbf{u}^{oT}\mathbf{u}^o$$

for $i = 1, 2, \ldots, M$, where $\widetilde{\epsilon}_2^2(3)$, $\widetilde{\epsilon}_2^2(4+i)$ and $\widetilde{\epsilon}_2^2(4+M+i)$ are sufficiently small. As a result after neglecting the approximation error,

$$\widetilde{\mathbf{B}}_2 \widetilde{\boldsymbol{\epsilon}}_2 = \widetilde{\mathbf{h}}_2 - \widetilde{\mathbf{G}}_2 \widetilde{\boldsymbol{\varphi}}_2^o \tag{6.38}$$

where

$$\widetilde{\boldsymbol{\varphi}}_2^o = \left[\mathbf{u}^{oT},\, \mathbf{u}^{oT}\mathbf{u}^o,\, (c^o)^2 \right]^T \tag{6.39}$$

is the unknown vector and the other vector and matrices are given in (D.18) of Appendix D.3. The WLS solution is

$$\widetilde{\boldsymbol{\varphi}}_2 = \left(\widetilde{\mathbf{G}}_2^T\, \widetilde{\mathbf{W}}_2\, \widetilde{\mathbf{G}}_2 \right)^{-1} \widetilde{\mathbf{G}}_2^T\, \widetilde{\mathbf{W}}_2\, \widetilde{\mathbf{h}}_2 \tag{6.40}$$

and the weighting matrix $\widetilde{\mathbf{W}}_2$ is (D.19).

Third Stage

This processing stage is basically the same as before for $\boldsymbol{\varphi}_2^o$, except that we include $(c^o)^2$ as an additional unknown:

$$\widetilde{\boldsymbol{\varphi}}_3^o = \left[\left(\mathbf{u}^o \odot \mathbf{u}^o \right)^T,\, (c^o)^2 \right]^T. \tag{6.41}$$

We carry $(c^o)^2$ from the second stage to the third because the estimation noise of $\widetilde{\boldsymbol{\varphi}}_2^o$ is correlated and improving the estimation accuracy for $\mathbf{u}^o$ will also improve the speed estimate. Using the same formulation as in (6.24) and (6.26), we have

$$\widetilde{\mathbf{B}}_3 \widetilde{\boldsymbol{\epsilon}}_3 = \widetilde{\mathbf{h}}_3 - \widetilde{\mathbf{G}}_3 \widetilde{\boldsymbol{\varphi}}_3^o \tag{6.42}$$

whose WLS solution is

$$\widetilde{\boldsymbol{\varphi}}_3 = \left(\widetilde{\mathbf{G}}_3^T\, \widetilde{\mathbf{W}}_3\, \widetilde{\mathbf{G}}_3\right)^{-1} \widetilde{\mathbf{G}}_3^T\, \widetilde{\mathbf{W}}_3\, \widetilde{\mathbf{h}}_3\,. \tag{6.43}$$

The matrices and vectors for (6.42) are defined in (D.21) and the weighting matrix $\widetilde{\mathbf{W}}_3$ is given in (D.22a).

Fourth Stage

The fourth stage obtains the solution of $\mathbf{u}^o$ and c^o by

$$\hat{\mathbf{u}} = \mathrm{diag}\left(\mathrm{sgn}\left(\widetilde{\boldsymbol{\varphi}}_1(1:2)\right)\right)\sqrt{\widetilde{\boldsymbol{\varphi}}_3(1:2)} \tag{6.44a}$$

$$\hat{c} = \sqrt{\widetilde{\varphi}_3(3)}. \tag{6.44b}$$

After taking the differential of (6.41), we obtain their covariance matrix,

$$\mathrm{cov}\left(\left[\,\hat{\mathbf{u}}^T,\,\hat{c}\,\right]^T\right) = \widetilde{\mathbf{B}}_4^{-T}\mathrm{cov}\left(\widetilde{\boldsymbol{\varphi}}_3\right)\widetilde{\mathbf{B}}_4^{-1} \tag{6.45}$$

where $\mathrm{cov}\left(\widetilde{\boldsymbol{\varphi}}_3\right)$ is given by (D.22b) and

$$\widetilde{\mathbf{B}}_4 = 2\mathrm{diag}\left(\,x_{\mathbf{u}}^o,\,y_{\mathbf{u}}^o,\,c^o\,\right). \tag{6.46}$$

The proposed estimator described above assumes $M \leq N$. For the situation of $M > N$ the unknowns in the first stage will be $\mathbf{u}^o$, c^o, $(c^o)^2$, $||\mathbf{u}^o - \bar{\mathbf{s}}_j||$ and $c^o||\mathbf{u}^o - \bar{\mathbf{s}}_j||$, $j = 1, 2, \ldots, N$ and the corresponding estimator can be similarly derived. It requires $MN \geq (2\min(M,N)+4)$ to ensure unique estimates for $\mathbf{u}^o$ and c^o.

We derive the two estimators under the four small error conditions given at the beginning of this Section. They can still be used when any one of these conditions is not valid. In such as case, however, (6.30) and (6.45) will not be correct in reflecting the performance of the estimators.

6.4 Analysis

We would like to examine if the proposed estimators in Section 6.3 are able to yield the hybrid CRLB performance. We shall use small error analysis and the results presented below is valid over the small error region.

6.4.1 Distribution of c Known

The conditions (C1)−(C4) are valid under small error analysis and the proposed estimator has covariance given by (6.30). After substituting (D.14), (D.13), (D.11), (D.10), and (D.7) in sequence,

$$\mathrm{cov}\left(\hat{\mathbf{u}}\right) = \left(\mathbf{G}_4^T \left(\bar{c}^2\mathbf{Q}_{\boldsymbol{\tau}} + \sigma_c^2\boldsymbol{\tau}^o\boldsymbol{\tau}^{oT} + \mathbf{D}_{\mathbf{z}}\mathbf{Q}_{\mathbf{z}}\mathbf{D}_{\mathbf{z}}^T\right)^{-1}\mathbf{G}_4\right)^{-1} \tag{6.47}$$

where $\mathbf{G}_4 = \mathbf{B}_1^{-1}\mathbf{G}_1\mathbf{B}_2^{-1}\mathbf{G}_2\mathbf{B}_3^{-1}\mathbf{G}_3\mathbf{B}_4$ is an $MN \times 2$ matrix and $\mathbf{D}_{\mathbf{z}}$ is defined in (D.6a). Besides conditions (C1)−(C4), the subsequent analysis requires the following additional conditions:

(C5) $||\boldsymbol{\Delta}_{\mathbf{t}_i}|| \ll ||\mathbf{u}^o - \bar{\mathbf{s}}_j||, \qquad |\bar{c}n_{\boldsymbol{\tau},i,j}| \ll ||\mathbf{u}^o - \bar{\mathbf{s}}_j||, \qquad |\tau_{i,j}^o\Delta_c| \ll ||\mathbf{u}^o - \bar{\mathbf{s}}_j||$

(C6) $||\boldsymbol{\Delta}_{\mathbf{s}_j}|| \ll ||\mathbf{u}^o - \bar{\mathbf{t}}_i||, \qquad |\bar{c}n_{\boldsymbol{\tau},i,j}| \ll ||\mathbf{u}^o - \bar{\mathbf{t}}_i||, \qquad |\tau_{i,j}^o\Delta_c| \ll ||\mathbf{u}^o - \bar{\mathbf{t}}_i||$

for $i = 1, 2, \ldots, M$ and $j = 1, 2, \ldots, N$. Appendix D.4 shows that, under conditions (C1)−(C5),

$$\mathbf{G}_4 \simeq \bar{c}\bar{\boldsymbol{\nabla}}_{\mathbf{u}^o}, \quad -\boldsymbol{\tau}^o \simeq \bar{c}\bar{\boldsymbol{\nabla}}_c, \quad \mathbf{D}_{\mathbf{z}} = \bar{c}\bar{\boldsymbol{\nabla}}_{\mathbf{z}}. \tag{6.48}$$

Putting (6.48) into (6.47), cancelling $\bar{c}^2$ and comparing to (6.11), we have $\mathrm{cov}\,(\mathbf{u}) \simeq \mathrm{HCRLB}_{\mathbf{u}^o}$ and the proposed estimator achieves the hybrid CRLB under (C1)−(C5).

6.4.2 Distribution of c Not Known

In this case, the joint estimation algorithm has the covariance matrix given by (6.45). After substituting (D.22b), (D.22a), (D.20), (D.19) and (D.16) to (6.45), it becomes

$$\mathrm{cov}\left(\left[\,\hat{\mathbf{u}}^T,\,\hat{c}\,\right]^T\right) = \left(\widetilde{\mathbf{G}}_4^T\left(\left(c^o\right)^2\mathbf{Q}_{\boldsymbol{\tau}} + \mathbf{D}_{\mathbf{z}}\mathbf{Q}_{\mathbf{z}}\mathbf{D}_{\mathbf{z}}^T\right)^{-1}\widetilde{\mathbf{G}}_4\right)^{-1} \tag{6.49}$$

where $\widetilde{\mathbf{G}}_4 = \mathbf{B}_1^{-1}\widetilde{\mathbf{G}}_1\widetilde{\mathbf{B}}_2^{-1}\widetilde{\mathbf{G}}_2\widetilde{\mathbf{B}}_3^{-1}\widetilde{\mathbf{G}}_3\widetilde{\mathbf{B}}_4$ is an $MN \times 3$ matrix.

Under the conditions (C1)−(C3) and (C5), we have from Appendix D.4

$$\widetilde{\mathbf{G}}_4 \simeq c^o\left[\,\bar{\boldsymbol{\nabla}}_{\mathbf{u}^o},\,\bar{\boldsymbol{\nabla}}_c\,\right]. \tag{6.50}$$

Note that $\bar{c}$ is replaced by c^o in this case. Putting (6.50) and $\mathbf{D}_{\mathbf{z}} = c^o\bar{\boldsymbol{\nabla}}_{\mathbf{z}}$ from (6.48) into (6.49) and comparing to (6.12), we immediately obtain $\mathrm{cov}\left(\left[\,\hat{\mathbf{u}}^T,\,\hat{c}\,\right]^T\right) \simeq \mathrm{HCRLB}_{\mathbf{u}^o,\,c^o}$. The proposed estimator gives the hybrid CLRB performance for the object position and signal propagation speed over the small error region.

The above proof considers the situation when $M \leq N$. If $M > N$, the stage one extra unknown variables are the distances of the object to the receivers rather than to the transmitters as explained at the end of Sections 6.3.A and 6.3.B. The analysis

applies condition (C6) instead of (C5) to validate the near hybrid CRLB performance. The conditions (C5) and (C6) are satisfied when the object is not close to the sensors, which is often the case in practice.

6.5 Localization Using Bearing and Time Measurements

Including the bearing measurements can improve the localization accuracy. The bearing angle is related to the object position through (6.2). We shall express (6.2) in terms of the noisy bearing and the nominal receiver position to create a solution equation. The N bearing equations will combine with the MN time measurement equations in Section 6.3 to obtain a better object position estimate.

In addition to the small noise conditions (C1)−(C4), the algorithm derivation here requires the bearing noise to be small as well:

(C7) $n_{\boldsymbol{\theta},j} = \theta_j - \theta_j^o \simeq 0, \qquad j = 1, 2, \ldots, N.$

Under (C7), we have $\sin(n_{\boldsymbol{\theta},j}) \simeq n_{\boldsymbol{\theta},j}$ and $\cos(n_{\boldsymbol{\theta},j}) \simeq 1$. Thus $\sin(\theta_j^o) \simeq \sin(\theta_j) - \cos(\theta_j)\, n_{\boldsymbol{\theta},j}$ and $\cos(\theta_j^o) \simeq \cos(\theta_j) + \sin(\theta_j) n_{\boldsymbol{\theta},j}$.

Let us define $\boldsymbol{\nu}_j = [-\sin(\theta_j), \cos(\theta_j)]^T$ and $\boldsymbol{\nu}_j^{\perp} = [\cos(\theta_j), \sin(\theta_j)]^T$. After taking tangent on both sides of (6.2), cross-multiplying by expressing $\tan(\theta_j^o) = \sin(\theta_j^o)/\cos(\theta_j^o)$ and $\mathbf{s}_j = \bar{\mathbf{s}}_j + \boldsymbol{\Delta}_{\mathbf{s}_j}$ and invoking (C7), we have

$$\boldsymbol{\nu}_j^{\perp T} (\mathbf{u}^o - \bar{\mathbf{s}}_j)\, n_{\boldsymbol{\theta},j} - \boldsymbol{\nu}_j^T \boldsymbol{\Delta}_{\mathbf{s}_j} \simeq \boldsymbol{\nu}_j^T \bar{\mathbf{s}}_j - \boldsymbol{\nu}_j^T \mathbf{u}^o, j = 1, 2, \ldots, N \tag{6.51}$$

where $n_{\boldsymbol{\theta},j} \boldsymbol{\Delta}_{\mathbf{s}_j}$ is neglected. In (6.51), the left side represents the equation error

and the right side contains the unknown $\mathbf{u}^o$ to be found. Collecting (6.51) for $j = 1, 2, \cdots, N$ yields the matrix pseudo linear bearing equation

$$\boldsymbol{\epsilon}_{\boldsymbol{\theta}} = \mathbf{h}_{\boldsymbol{\theta}} - \mathbf{G}_{\boldsymbol{\theta}}\mathbf{u}^o. \tag{6.52}$$

The matrix and vectors in (6.52) are defined in Appendix D.5.

When the distribution of c is available, we stack (6.18) and (6.52) by expressing it as $\boldsymbol{\epsilon}_{\boldsymbol{\theta}} = \mathbf{h}_{\boldsymbol{\theta}} - [\, \mathbf{G}_{\boldsymbol{\theta}},\, \mathbf{O}_{N\times M}\,]\, \boldsymbol{\varphi}_1^o$ to obtain a better first stage solution. The details are given in Appendix D.5. The remaining three stages are the same as before. The same procedure applies to the case when the statistical distribution of c is not available.

Following the same procedures in Section 6.4, it can be shown that the proposed estimators using both time and bearing measurements yield the hybrid CRLB performance, under the conditions (C1)−(C7). The detail steps for the proof are not presented here for brevity.

6.6 Simulation

The simulation uses three transmit and five receive sonobuoys to locate one object. Their nominal positions are $\bar{\mathbf{t}}_1 = [\,1500,\, 1500\,]^T$ m, $\bar{\mathbf{t}}_2 = [\,-900,\, 4000\,]^T$ m, $\bar{\mathbf{t}}_3 = [\,-3000,\, -4000\,]^T$ m, $\bar{\mathbf{s}}_1 = [\,-1000,\, 3000\,]^T$ m, $\bar{\mathbf{s}}_2 = [\,2500,\, -500\,]^T$ m, $\bar{\mathbf{s}}_3 = [\,-3000,\, 1000\,]^T$ m, $\bar{\mathbf{s}}_4 = [\,2000,\, -4000\,]^T$ m and $\bar{\mathbf{s}}_5 = [\,-2000,\, -2000\,]^T$ m. The object to be located is at $\mathbf{u}^o = [\,0,\, 2000\,]^T$ m. The scenario is depicted in Fig. 6.2.

In each simulation trial, the true transmitter and receiver position vector $\mathbf{z}$ is created by adding to its nominal value $\bar{\mathbf{z}}$ zero mean Gaussian random variables with covariance matrix $\mathbf{Q}_{\mathbf{z}} = \sigma_{\mathbf{z}}^2\mathbf{I}_{2(M+N)}$. The true signal propagation speed c is created in

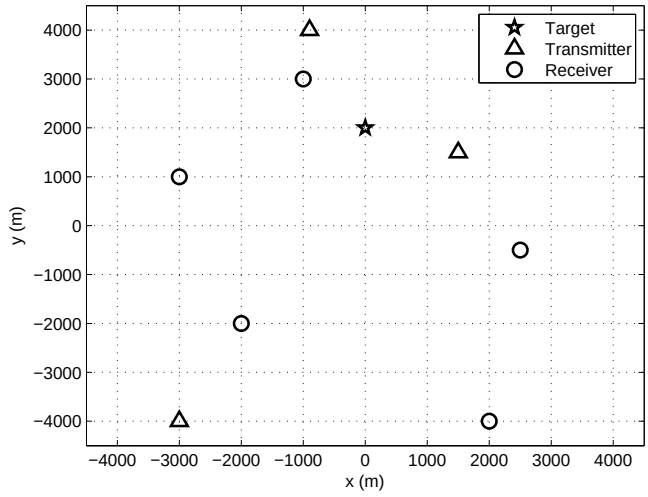

Figure 6.2: The simulation scenario.

a similar manner using $\bar{c} = 1500$ m/s and $\sigma_c = 7.5$ m/s [5]. The covariance matrices of the time and bearing measurements are set as $\mathbf{Q}_{\boldsymbol{\tau}} = \sigma_{\boldsymbol{\tau}}^2 \mathbf{I}_{MN}$ and $\mathbf{Q}_{\boldsymbol{\theta}} = \sigma_{\boldsymbol{\theta}}^2 \mathbf{I}_N$. The number of ensemble runs is 10,000.

We present the results separately for the two cases: the distribution of c known (case 1) and not known (case 2). In case 1, the MSE of the proposed estimator in Section 6.3.A is compared to that of the Bayesian method [5] and the Weiner filter method [4]. These two methods compute the individual cross fixes from two measurements first and apply filters to combine the individual object position estimates. They both require time and bearing measurements and cannot operate with time measurements only. The Weiner filter method assumes the signal propagation speed is exactly known and it uses the nominal speed $\bar{c}$ in the simulation. Case 2 applies the joint object position and signal propagation speed estimator proposed in Section 6.3.B and compares its performance with the hybrid CRLB.

6.6.1 Distribution of c Known

Fig. 6.3 illustrates the performance of the proposed estimator as the time measurement noise power increases when $\sigma_{\boldsymbol{\theta}} = 2$ degree and $\sigma_{\mathbf{z}} = 20$ m [4, 5]. The improvement by adding the bearing measurements $\boldsymbol{\theta}$ becomes apparent as $\sigma_{\boldsymbol{\tau}}$ increases. In particular, the hybrid CRLB is lowered by about 3 dB when $\sigma_{\boldsymbol{\tau}} = 0.16$ s. The proposed algorithm works well and attains the hybrid CRLB accuracy. It performs much better than the Bayesian and Weiner filter methods. The Bayesian filter method approaches the optimum performance when $\sigma_{\boldsymbol{\tau}}$ is large, but it degrades considerably at small $\sigma_{\boldsymbol{\tau}}$. The proposed algorithm deviates from the bound when $\sigma_{\boldsymbol{\tau}} > 1$ s which is not shown in Fig. 6.3. The significant MSE of the Weiner filter method is caused by a few bad individual cross fixes from two time measurements since individual fixes are more sensitive to the thresholding effect. The Wiener filter method gives reasonable accuracy if $\sigma_{\boldsymbol{\tau}}$ is sufficiently small.

Fig. 6.4 shows the results at different levels of position uncertainties $\sigma_{\mathbf{z}}$ when $\sigma_{\boldsymbol{\tau}}$ and $\sigma_{\boldsymbol{\theta}}$ are equal to 0.02 s and 2 degree [4, 5]. The proposed algorithm achieves the hybrid CRLB when $\sigma_{\mathbf{z}}$ is small and deviates slightly from the bound when $\sigma_{\mathbf{z}} \geq$ 160 m. It performs better than the Bayesian method and the Weiner filter method. In this simulation setting, the localization performance is dominated by $\sigma_{\boldsymbol{\tau}}$ and the improvement from the bearing measurement is not obvious.

6.6.2 Distribution of c Not Known

In this case, 100 different values of the signal propagation speed are randomly drawn from a uniform distribution over the interval $[\,1450,\, 1500\,]$ m/s [53]. We use 10,000 ensemble runs for each speed value and the results shown in the figures are the

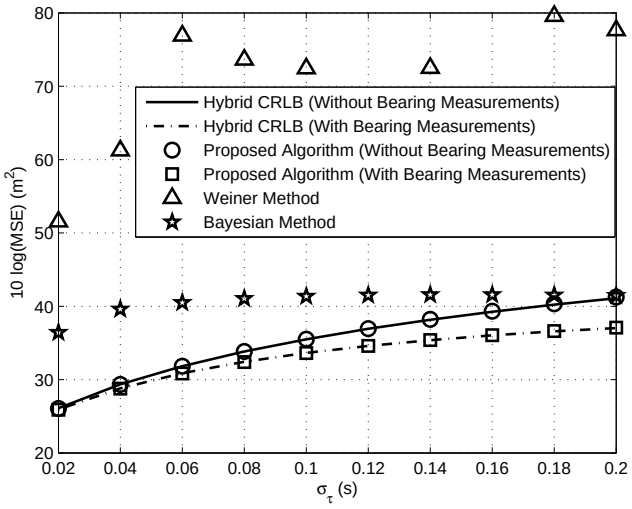

Figure 6.3: Localization performance versus $\sigma_{\boldsymbol{\tau}}$ when the distribution of c is known

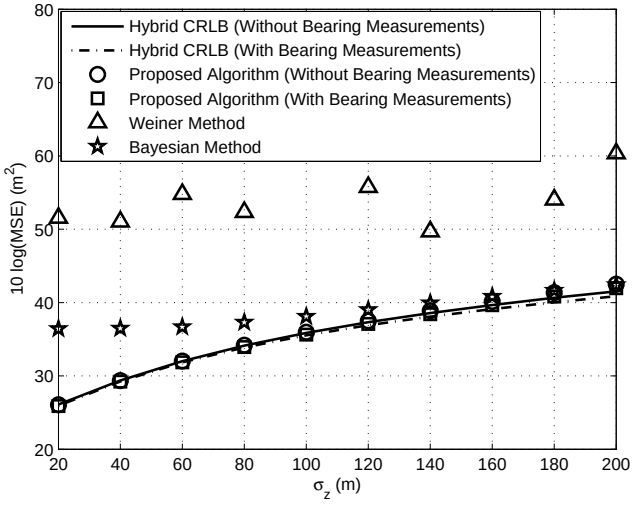

Figure 6.4: Localization performance versus $\sigma_{\mathbf{z}}$ when the distribution of c is known

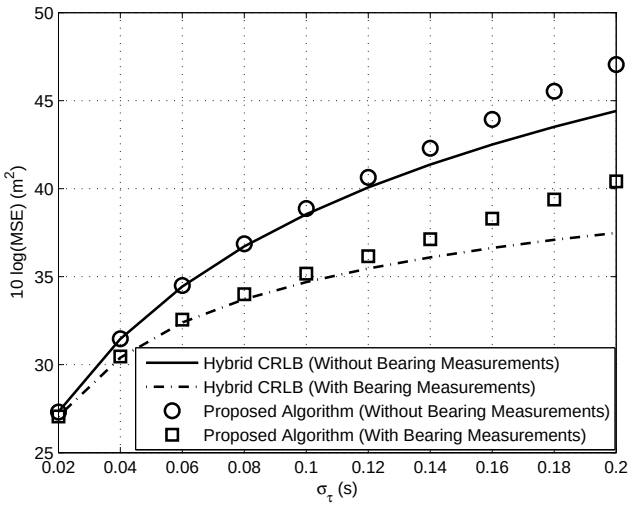

Figure 6.5: Localization performance versus $\sigma_{\boldsymbol{\tau}}$ when the distribution of c is not known.

averages from different speeds.

Fig. 6.5 illustrates the localization performance as $\sigma_{\boldsymbol{\tau}}$ varies when $\sigma_{\boldsymbol{\theta}} = 2$ degree and $\sigma_{\mathbf{z}} = 20$ m. The proposed estimator attains the hybrid CRLB accuracy when $\sigma_{\boldsymbol{\tau}} \leq 0.06$ s. Beyond this level, it deviates gradually from the bound as $\sigma_{\boldsymbol{\tau}}$ increases. Fig. 6.6 presents the accuracy of the signal propagation speed estimate and the observations are similar to those in Fig. 6.5.

Figs. 6.7 and 6.8 give the results at different levels of position uncertainties when $\sigma_{\boldsymbol{\tau}}$ and $\sigma_{\boldsymbol{\theta}}$ are equal to 0.02 s and 2 degree. The observations are consistent with those from Figs. 6.5 and 6.6.

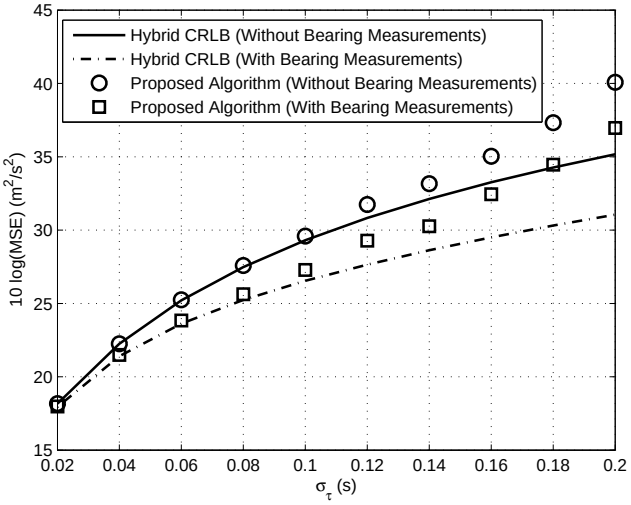

Figure 6.6: Estimation accuracy for the signal propagation speed versus $\sigma_{\boldsymbol{\tau}}$ when the distribution of c is not known.

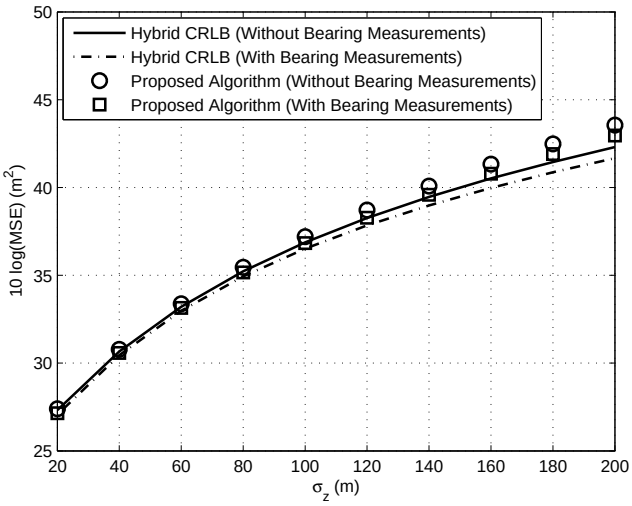

Figure 6.7: Localization performance versus $\sigma_{\mathbf{z}}$ when the distribution of c is not known.

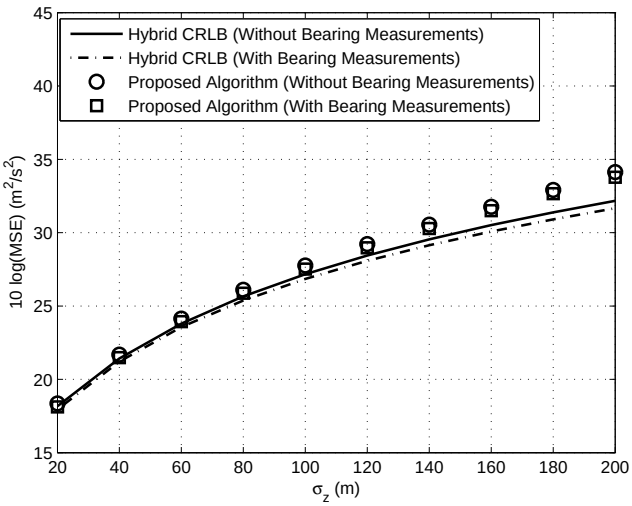

Figure 6.8: Estimation accuracy for the signal propagation speed versus $\sigma_{\mathbf{z}}$ when the distribution of c is not known.

6.7 Conclusion

We have addressed in this Chapter the optimum localization of an object using multi-static sonar in the presence of uncertainties in the transmitter and receiver positions, as well as in the signal propagation speed. Two estimators were developed when using the time measurements, one is with the statistical knowledge of the propagation speed and the other is without. They have closed-form and are derived through parameter transformation and multi-stage processing. Analysis shows that they achieve the hybrid CRLB in Gaussian noise over the small error region. The two estimators were extended to include the bearing measurements to improve the localization accuracy. Simulations collaborate the theoretical performance of the proposed estimators.

Chapter 7

A Markov Chain Monte Carlo Alternating Minimization Algorithm for Asynchronous Relay Network Localization

In this Chapter, we solves the asynchronous relay network localization problem by the alternating minimization algorithm [105]. Such network is capable to obtain multiple UWB range measurements for the unknown object by many relay or virtual anchors. The main challenge is that the association relations between the measurements and relays are unknown. To avoid the high computation burden, we proposes an efficient iterative algorithm which runs two stages until the results converge. The first stage optimally associates the range measurements to the relay nodes based on the previous object location and clock estimates. It applies the Markov Chain Monte Carlo (MCMC) method [106] to randomly generate samples of the posterior distribution of the association plan given the previous object position and clock estimates. The

second stage implements the MLE to estimate the object location and clock under the association plan from the previous stage.

7.1 Preliminary

We consider the indoor scenario where one anchor $\mathbf{s}_0^o$ localizes one unknown node $\mathbf{u}^o$ with the help from M virtual anchors $\mathbf{s}_i^o$, $i = 1, 2, \ldots, M$. The virtual anchors can be the non-regenerative relays in the relay network localization problem [70] or the reflecting points in the multipath assisted indoor positioning problem [63, 64, 65, 66]. Those anchor positions can be collected by a vector form as $\mathbf{s}^o = \left[\mathbf{s}_0^{oT}, \mathbf{s}_1^{oT}, \cdots, \mathbf{s}_M^{oT} \right]^T$. The unknown node $\mathbf{u}^o$ is asynchronous with respect to the anchor $\mathbf{s}_0^o$ with an unknown clock offset ω^o. The vector containing all unknown parameters is $\boldsymbol{\gamma}^o = \left[\mathbf{u}^{oT}, \omega^o \right]^T$.

Fig. 7.1 shows the typical network topology. The measurement signal is sent from the anchor node $\mathbf{s}_0^o$ and relayed (relay case) or reflected (multipath case) by the virtual anchors $\mathbf{s}_i^o$, $i = 1, 2, \ldots, M$. The unknown node $\mathbf{u}^o$ receives the direct and indirect signals and obtains the TOA range measurements. Since the difference between the time and range measurements is only a fixed scale factor of signal speed c, we use them interchangeably throughout the paper. The true value of the range measurement along the direct path is

$$f_0 = \| \mathbf{u}^o - \mathbf{s}_0^o \| + c\omega^o \,. \tag{7.1}$$

The noiseless indirect path range measurements are

$$f_i = \|\mathbf{u}^o - \mathbf{s}_i^o\| + \|\mathbf{s}_0^o - \mathbf{s}_i^o\| + c\omega^o, \quad i = 1, 2, \ldots, M. \tag{7.2}$$

In both relay and multipath cases, the indirect path signals are non-regenerative [63, 65, 70]. Hence, the unknown node $\mathbf{u}^o$ receives the signals from the direct and indirect paths at different time instants and collects its range measurement vector following the receiving time order as

$$\mathbf{d} = [\, d_0, d_1, \cdots, d_M \,]^T = \mathbf{B}\mathbf{f} + \mathbf{n}, \tag{7.3}$$

where $0 < d_0 < d_1 < \cdots < d_M$, $\mathbf{f} = [\, f_0, f_1, \cdots, f_M \,]^T$ and $\mathbf{n}$ is the zero mean Gaussian measurement noise with covariance $\mathbf{Q}$. The $(M+1) \times (M+1)$ matrix $\mathbf{B}$ represents the bijection relationship between $\mathbf{d}$ and $\mathbf{f}$ which satisfies

$$\sum_{j=0}^{M} B(i,j) = 1, \quad i = 0, 1, \ldots, M \tag{7.4a}$$

$$\sum_{i=0}^{M} B(i,j) = 1, \quad j = 0, 1, \ldots, M \tag{7.4b}$$

$$B(i,j) = \{0, 1\}, \quad i = 0, 1, \ldots, M, \quad j = 0, 1, \ldots, M. \tag{7.4c}$$

Eq. (7.3) indicates that the ambiguity of the measurement assignment in $\mathbf{d}$ complicates the localization problem that both $\mathbf{B}$ and $\boldsymbol{\gamma}^o$ have to be estimated. We next develop an alternating minimization algorithm which iteratively optimizes its estimates to search for the ML solution.

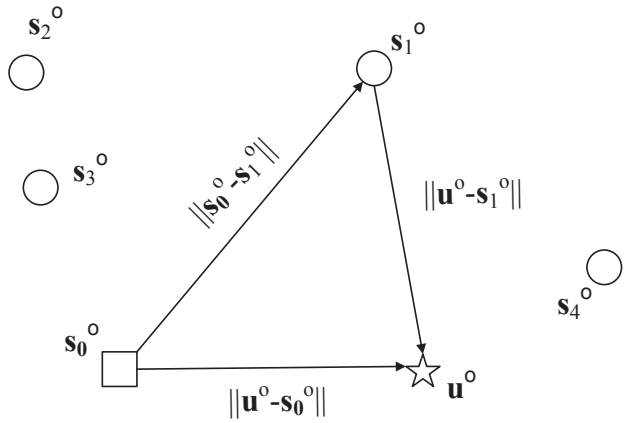

Figure 7.1: Network geometry.

7.2 Algorithm

Given (7.3), the MLE of $\mathbf{B}$ and $\boldsymbol{\gamma}^o$ is to minimize the object function

$$J\left(\mathbf{B},\, \boldsymbol{\gamma}^o\right) = \left(\mathbf{d} - \mathbf{B}\mathbf{f}\left(\boldsymbol{\gamma}^o\right)\right)^T \mathbf{Q}^{-1} \left(\mathbf{d} - \mathbf{B}\mathbf{f}\left(\boldsymbol{\gamma}^o\right)\right). \tag{7.5}$$

The proposed algorithm searches for the minimization solution by iteratively proceeding two steps: it begins with some initials $\mathbf{B}^{(0)}$ and $\boldsymbol{\gamma}^{(0)}$, and having found $\mathbf{B}^{(n)}$ and $\boldsymbol{\gamma}^{(n)}$ at the n-th iteration, it

1. minimizes $J\left(\mathbf{B},\, \boldsymbol{\gamma}^{(n)}\right)$ to get $\mathbf{B} = \mathbf{B}^{(n+1)}$, and then
2. minimizes $J\left(\mathbf{B}^{(n+1)},\, \boldsymbol{\gamma}\right)$ to get $\boldsymbol{\gamma} = \boldsymbol{\gamma}^{(n+1)}$.

It repeats the two steps until converges. Note that the algorithm performance depends on the pick of $\mathbf{B}^{(0)}$ and $\boldsymbol{\gamma}^{(0)}$. It will be shown in Section 7.4 that the algorithm can achieve good accuracy with rough initial value selections.

7.2.1 Step 1: $\boldsymbol{\gamma}^{(n)} \rightarrow \mathbf{B}^{(n+1)}$

When $\boldsymbol{\gamma}^{(n)}$ is known, the minimization problem becomes to find $\mathbf{B}^{(n+1)}$ satisfying

$$\mathbf{B}^{(n+1)} = \arg\min \left(\mathbf{d} - \mathbf{B}\mathbf{f}(\boldsymbol{\gamma}^{(n)})\right)^T \mathbf{Q}^{-1} \left(\mathbf{d} - \mathbf{B}\mathbf{f}(\boldsymbol{\gamma}^{(n)})\right), \tag{7.6}$$

where $\mathbf{B}^{(n+1)}$ subjects to the constraints (7.4). Note that minimization problem in (7.6) is equivalent to find $\mathbf{B}^{(n+1)}$ maximizing the probability $p\left(\mathbf{d} \left| \mathbf{B}, \boldsymbol{\gamma}^{(n)} \right.\right)$.

There are $(M+1)!$ candidates as the possible solution of $\mathbf{B}^{(n+1)}$ under the restriction condition (7.4). The traditional brute force algorithm is easy to implement but with extremely high computation burden, especially when M is large. We will propose an MCMC algorithm to achieve good computation efficiency. Based on the Bayesian theorem, we have

$$p\left(\mathbf{B}^{(n+1)} \left| \mathbf{d}, \boldsymbol{\gamma}^{(n)} \right.\right) = \frac{p\left(\mathbf{d} \left| \mathbf{B}^{(n+1)}, \boldsymbol{\gamma}^{(n)} \right.\right) p\left(\mathbf{B}^{(n+1)}\right)}{p\left(\mathbf{d}\right)}. \tag{7.7}$$

Suppose the prior probability $p\left(\mathbf{B}^{(n+1)}\right)$ follows uniform distribution and note that $p\left(\mathbf{d}\right)$ does not depend on $\mathbf{B}^{(n+1)}$. The minimization problem in (7.6) is equivalent to find $\mathbf{B}^{(n+1)}$ that maximizes the posterior probability $p\left(\mathbf{B} \left| \mathbf{d}, \boldsymbol{\gamma}^{(n)} \right.\right)$. However, it is hard to derive a theoretical formula of $p\left(\mathbf{B} \left| \mathbf{d}, \boldsymbol{\gamma}^{(n)} \right.\right)$. Hence, we apply the MCMC model to randomly generate samples of $\mathbf{B}$ under the posterior distribution $p\left(\mathbf{B} \left| \mathbf{d}, \boldsymbol{\gamma}^{(n)} \right.\right)$. When enough samples have been collected, the candidate which has the largest count is selected as the solution of $\mathbf{B}^{(n+1)}$.

We set all possible $\mathbf{B}$ that satisfy (7.4) as the states of a Markov process. The Markov process has one step transition between two states which only have two measurements associated differently. The random samples of $p\left(\mathbf{B} \left| \mathbf{d}, \boldsymbol{\gamma}^{(n)} \right.\right)$ are generated

by the Metropolis-Hastings algorithm [106]. Suppose we have obtain the pth sample state $\mathbf{B}_p^{(n+1)}$. A proposal distribution $g\left(\mathbf{B}_p^{(n+1)} \to \mathbf{B}_{p+1}^{(n+1)}\right)$ is used to randomly pick the next potential sample $\mathbf{B}_{p+1}^{(n+1)}$ which could be transited by one step from the current state $\mathbf{B}_p^{(n+1)}$. The transition is checked by the Acceptance-Rejection rule with the acceptance probability

$$A\left(\mathbf{B}_p^{(n+1)} \to \mathbf{B}_{p+1}^{(n+1)}\right) = \min\left(1, \frac{p\left(\mathbf{d}\left|\mathbf{B}_{p+1}^{(n+1)}\right.\right) g\left(\mathbf{B}_{p+1}^{(n+1)} \to \mathbf{B}_p^{(n+1)}\right)}{p\left(\mathbf{d}\left|\mathbf{B}_p^{(n+1)}\right.\right) g\left(\mathbf{B}_p^{(n+1)} \to \mathbf{B}_{p+1}^{(n+1)}\right)}\right). \tag{7.8}$$

If the transition is rejected, the Markov process stays at $\mathbf{B}_p^{(n+1)}$ and the $(p+1)$th sample is $\mathbf{B}_{p+1}^{(n+1)} = \mathbf{B}_p^{(n+1)}$. The Markov process continues until enough samples of $\mathbf{B}^{(n+1)}$ have been collected. Since we assume the prior distribution of $\mathbf{B}^{(n+1)}$ is uniform distribution, we set $g\left(\mathbf{B}_p^{(n+1)} \to \mathbf{B}_{p+1}^{(n+1)}\right)$ as uniform distribution as well. In summary, the work flow of the algorithm is

1. Set $\mathbf{B}^{(n)}$ as the first sample state $\mathbf{B}_p^{(n+1)}$, where $p = 1$.

2. Randomly pick two elements $\mathbf{B}_p^{(n+1)}(i,k)$ and $\mathbf{B}_p^{(n+1)}(j,l)$ from the $(M+1)$ non-zero elements in $\mathbf{B}_p^{(n+1)}$ under uniform distribution.

3. Let $\mathbf{B}_{p+1}^{(n+1)} = \mathbf{B}_p^{(n+1)}$, except $\mathbf{B}_{p+1}^{(n+1)}(i,k) = \mathbf{B}_{p+1}^{(n+1)}(j,l) = 0$ and $\mathbf{B}_{p+1}^{(n+1)}(i,l) = \mathbf{B}_{p+1}^{(n+1)}(j,k) = 1$.

4. Compute the acceptance probability $A\left(\mathbf{B}_p^{(n+1)} \to \mathbf{B}_{p+1}^{(n+1)}\right)$ by (7.8) where $g\left(\mathbf{B}_{p+1}^{(n+1)} \to \mathbf{B}_p^{(n+1)}\right) = g\left(\mathbf{B}_p^{(n+1)} \to \mathbf{B}_{p+1}^{(n+1)}\right)$.

5. Generate $\tau \sim \text{UNIF}\,(0,\,1)$. If $\tau < A\left(\mathbf{B}_p^{(n+1)} \to \mathbf{B}_{p+1}^{(n+1)}\right)$, $\mathbf{B}_{p+1}^{(n+1)}$ is accepted. Otherwise $\mathbf{B}_{p+1}^{(n+1)} = \mathbf{B}_p^{(n+1)}$.

6. $p = p + 1$. Go back to step 2 until P samples have been collected.

7. $\mathbf{B}^{(n+1)}$ is the mode of sample sequence $\mathbf{B}_p^{(n+1)}$, $p = 1, 2, \ldots, P$.

7.2.2 Step 2: $\mathbf{B}^{(n+1)} \rightarrow \boldsymbol{\gamma}^{(n+1)}$

This step minimizes the object function $J\left(\mathbf{B}^{(n+1)}, \boldsymbol{\gamma}\right)$ by updating $\boldsymbol{\gamma}^{(n+1)}$ based on the range measurement vector $\mathbf{d}$, the updated association matrix $\mathbf{B}^{(n+1)}$ and the estimates of the unknown parameters at the previous iteration $\boldsymbol{\gamma}^{(n)}$. Inspired by [107], we solve this problem by the Taylor series method. Let $\boldsymbol{\gamma}^{(n+1)} = \boldsymbol{\gamma}^{(n)} + \boldsymbol{\Delta}$, where $\boldsymbol{\Delta}$ is the correction term. Taking the Taylor series expansion of $f\left(\boldsymbol{\gamma}^{(n+1)}\right)$ at $\boldsymbol{\gamma}^{(n)}$ gives

$$\mathbf{f}\left(\boldsymbol{\gamma}^{(n+1)}\right) \simeq \mathbf{f}\left(\boldsymbol{\gamma}^{(n)}\right) + \nabla\mathbf{f}\left(\boldsymbol{\gamma}^{(n)}\right)\boldsymbol{\Delta} \tag{7.9}$$

where

$$\nabla\mathbf{f}\left(\boldsymbol{\gamma}^{(n)}\right) = \left[\frac{\partial f_0}{\partial \boldsymbol{\gamma}^o}, \frac{\partial f_1}{\partial \boldsymbol{\gamma}^o}, \cdots, \frac{\partial f_M}{\partial \boldsymbol{\gamma}^o}\right]^T\Bigg|_{\boldsymbol{\gamma}^o=\boldsymbol{\gamma}^{(n)}}, \tag{7.10}$$

$$\frac{\partial f_i}{\partial \boldsymbol{\gamma}^o} = \left[\left\|\mathbf{u}^o - \mathbf{s}_i^o\right\|^{-1}\left(\mathbf{u}^o - \mathbf{s}_i^o\right)^T, c\right]^T, \quad i = 0, 1, \ldots, M. \tag{7.11}$$

Substituting (7.9) to $\mathbf{f}\left(\boldsymbol{\gamma}^{\boldsymbol{o}}\right)$ in (7.5) and taking the differentiation with respect to $\boldsymbol{\Delta}$ give

$$\frac{\partial J}{\partial \boldsymbol{\Delta}} = -2\nabla\mathbf{f}^T\left(\boldsymbol{\gamma}^{(n)}\right)\mathbf{B}^{(n+1)^T}\mathbf{Q}^{-1}\left(\mathbf{d} - \mathbf{B}^{(n+1)}\mathbf{f}\left(\boldsymbol{\gamma}^{(n)}\right) - \mathbf{B}^{(n+1)}\nabla\mathbf{f}\left(\boldsymbol{\gamma}^{(n)}\right)\boldsymbol{\Delta}\right) \tag{7.12}$$

The minimization of the object function means $(\partial J)/(\partial \boldsymbol{\Delta}) = 0$. Putting it back

to (7.12) and rearranging the terms, we can get

$$\begin{aligned}\boldsymbol{\Delta} = &\left(\nabla \mathbf{f}^T\left(\boldsymbol{\gamma}^{(n)}\right) \mathbf{B}^{(n+1)^T} \mathbf{Q}^{-1} \mathbf{B}^{(n+1)} \nabla \mathbf{f}\left(\boldsymbol{\gamma}^{(n)}\right)\right)^{-1} \\ &\nabla \mathbf{f}^T\left(\boldsymbol{\gamma}^{(n)}\right) \mathbf{B}^{(n+1)^T} \mathbf{Q}^{-1}\left(\mathbf{d} - \mathbf{B}^{(n+1)} \mathbf{f}\left(\boldsymbol{\gamma}^{(n)}\right)\right).\end{aligned} \tag{7.13}$$

Then, the updated $\boldsymbol{\gamma}^{(n+1)}$ can be obtained by $\boldsymbol{\gamma}^{(n+1)} = \boldsymbol{\gamma}^{(n)} + \boldsymbol{\Delta}$.

The object localization algorithm iteratively executes the two steps until the object position estimates converge.

7.3 Simulation

In the simulation, 1 anchor and 9 virtual anchors are deployed to locate a single object as shown in Fig. 7.2. The unknown clock offset between the anchor and the object is 0.1 μs. We set $\mathbf{Q} = \sigma^2 \mathbf{I}_{10}$. In the measurement association step, the Metropolis-Hastings algorithm generates 10000 state samples. The proposed algorithm stops when the norm difference of object position estimates between two iterations is less the 10^{-3} m. The number of ensemble runs is 1000. For each ensemble run, the initial guess $\boldsymbol{\gamma}^{(0)}$ is randomly generated following $\mathcal{N}\left(\boldsymbol{\gamma}^o, 2\text{CRLB}\left(\boldsymbol{\gamma}^o\right)\right)$, where $\text{CRLB}\left(\boldsymbol{\gamma}^o\right)$ is the CRLB of $\boldsymbol{\gamma}^o$ [26]. The detail of the CRLB derivation is omitted here for simplicity. To construct $\mathbf{B}^{(0)}$, the noiseless range guesses $f_i\left(\boldsymbol{\gamma}^{(0)}\right)$, $i = 0, 1, \ldots, M$, are sorted in ascending order so that d_i is associated to the virtual anchor corresponding to the ith smallest range guess.

Fig. 7.3 shows the percentages of correct measurement association at different measurement noise levels. When σ^2 is small, perfect association is achievable by the proposed algorithm. However, when $\sigma^2 > 1\text{m}^2$, its performance deteriorates rapidly

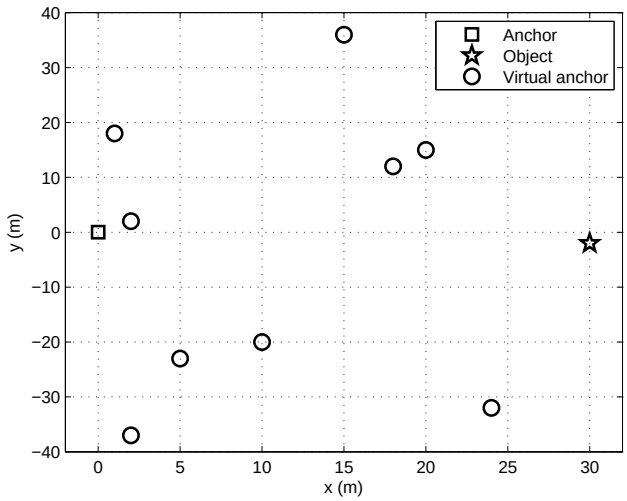

Figure 7.2: Simulation scenario.

with the increase of noise power. Note that better association ratio is achievable when greater number of the samples in the Metropolis-Hastings algorithm are used. Fig. 7.4 illustrates the estimation accuracy of the object position with respect to the increase of the TOA measurement noise power when the measurements are correctly associated. As long as the measurements are correctly associated, the algorithm attains the CRLB accuracy well. Note that there is no good measurement association when $\sigma^2 = 100\text{m}^2$, the corresponding MSE symbol at this noise level is not shown in Fig. 7.4. Fig. 7.5 gives the results of the clock offset. The observation is similar to Fig. 7.4. Usually, the proposed algorithm converges after three or four iterations in this simulation setting. In each iteration, the total random samples generated in the measurement association stage are fixed at 10000 while the brute force method computes the likelihood function 10! times.

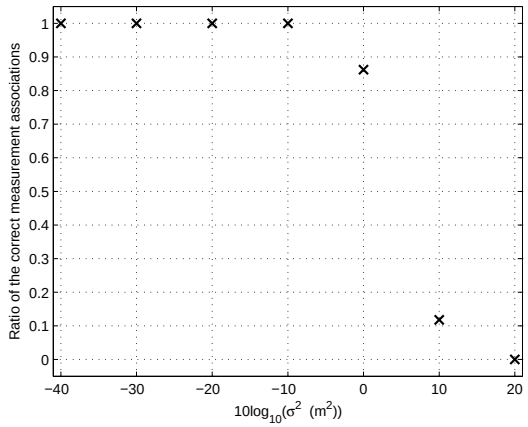

Figure 7.3: Ratio of the correct associations at different range measurement noise powers.

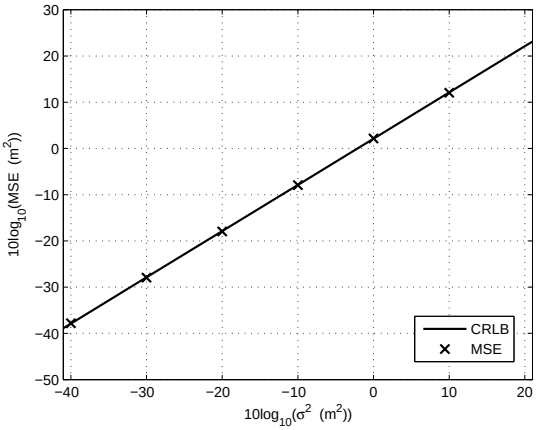

Figure 7.4: Object position estimation performance under different range measurement noise powers.

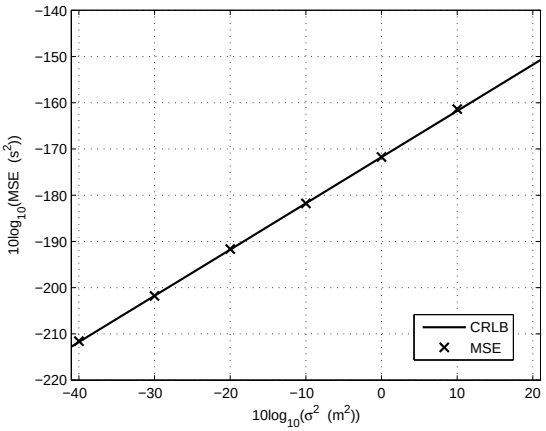

Figure 7.5: Estimation accuracy of clock offsets of the object under different range measurement noise powers.

7.4 Conclusion

We have developed an efficient solution to the relay network localization problem based on iterative minimization method. It solves the measurement association problem and object location estimation iteratively. The Metropolis-Hastings algorithm is employed to simulate the probability distribution of the measurement association plan and avoid the huge computation burden in the brute force method. The MLE is applied to estimate the object position given the measurement association results. The performance of the proposed algorithm has been shown to be close to the CRLB accuracy for Gaussian noise over the small error region.

Chapter 8

Summary

We have investigated five important topics in the object positioning area. First, the bias of the ML object position estimate is studied under a general condition that both measurement noise and the observer position errors are present. We derived a theoretical bias expression and found that the effects of the measurement noise and position error to the bias are different and the bias components caused by them are usually coupled. The bias behaviors for TOA, TDOA and AOA localizations were compared. TOA and TDOA positionings have smaller bias for a distant than a near object whilst AOA positioning has larger bias for a distant object. The bias for TOA and TDOA positionings are very vulnerable with respect to the sensor position errors. On the contrary, the bias of AOA localization is relatively resilient to sensor position errors. Simulation results showed that on average TOA positioning has the smallest bias among the three positioning methods under the same noise conditions. We also derived the geometries which yield zero bias for the three positioning methods. The developed theoretical results were applied to compensate the bias in the object

tracking problem and its effectiveness was supported by simulation experiments.

Second, we fundamentally evaluated the performance of elliptic positioning in the presence of Gaussian measurement noise and sensor position errors. The study investigated three types of elliptic positioning, SE_f, SE and AE. We compared their performance with each other and with the hyperbolic positioning (TDOA). The SE_f positioning yields the best accuracy and SE is always better than TDOA. The sensor position errors have significant effects on the conclusion of AE. In the absence of sensor position error, SE outperforms AE. When the transmitter and receiver position errors are present, AE could outperform SE for some localization geometries. In addition, TDOA occasionally outperforms AE in some cases. The bias behaviors of the ML object location estimates of the four positioning approaches have been examined by simulation. On average, SE_f always has the smallest bias. We also studied the effect of the number of transmitters to their performance. When the number of transmitter increases, AE positioning has more possibilities to outperform SE and TDOA and the bias of elliptic positioning reduces. We derived the optimum receiver placements for SE and AE positionings with one transmitter under IID Gaussian noise and accurate sensor positions. The derived optimum geometries are much different from the optimum geometries of TOA and TDOA.

Third, we have proposed two efficient solutions to the problem of joint localization and synchronization of multiple sensor nodes simultaneously in the presence of beacon position and clock uncertainties. The first one uses only the timing measurements from the message exchanges between the sensor nodes and beacons. The second one also uses timing information from the message exchanges among the sensor nodes to improve performance. Analytical study has shown they are able to reach the CRLB

accuracy under the mild noise region. Simulation experiments have been conducted to further validate the theoretical analysis. We also found from simulation experiments that using the message exchanges among the sensor node can effectively improve localization accuracy when the noise level in beacon position is small.

Fourth, the multistatic sonar localization problem is solved by efficient estimators. The proposed algorithms take into account the factors caused by the complex ocean environment such as random transmitter position, receiver position and signal propagation speed uncertainties. Two efficient closed-form solutions are developed. One is with the statistical knowledge of the propagation speed and the other is without. Theoretical analysis shows that they can achieve the hybrid CRLB performance in Gaussian noise over the small error region. Both estimators are further extended to be able to use the bearing measurements to improve the localization accuracy. Simulation results support the theoretical performance analysis.

Fifth, we have developed an efficient solution to the relay network localization problem. It iteratively optimizes the measurement association and object location estimation. The Metropolis-Hastings algorithm is employed to simulate the probability distribution of the measurement association plan and avoid the huge computation burden in the brute force method. The MLE is applied to estimate the object position given the measurement association results. The performance of the proposed algorithm has been shown to be close to the CRLB accuracy for Gaussian noise over the small error region.

Appendix A

Appendix for Chapter 3

A.1 The Derivation of (3.5)

This appendix derives the theoretical bias formula (3.5) from (3.4). Substituting the definition of $J(\boldsymbol{\gamma})$ above (2.13) into $\mathbf{p}(\boldsymbol{\gamma}^o)$ yields

$$\mathbf{p}(\boldsymbol{\gamma}^o) = \left.\frac{\partial J(\boldsymbol{\gamma})}{\partial \boldsymbol{\gamma}}\right|_{\boldsymbol{\gamma}=\boldsymbol{\gamma}^o} = -2\frac{\partial \check{\mathbf{g}}(\boldsymbol{\gamma}^o)^T}{\partial \boldsymbol{\gamma}}(\check{\mathbf{h}} - \check{\mathbf{g}}(\boldsymbol{\gamma}^o)) \tag{A.1}$$

where $\check{\mathbf{h}} = \mathbf{Q}^{-\frac{1}{2}}\mathbf{h}$, $\check{\mathbf{g}}(\boldsymbol{\gamma}^o) = \mathbf{Q}^{-\frac{1}{2}}\mathbf{g}(\boldsymbol{\gamma}^o)$ and $\mathbf{Q}^{-\frac{1}{2}}$ is the square root of $\mathbf{Q}^{-1}$ so that $\mathbf{Q}^{-\frac{1}{2}}\mathbf{Q}^{-\frac{1}{2}} = \mathbf{Q}^{-1}$. Furthermore,

$$\frac{\partial \mathbf{p}(\boldsymbol{\gamma}^o)}{\partial \boldsymbol{\gamma}^T} = \mathbf{A} - \mathbf{B}, \tag{A.2}$$

where

$$\mathbf{A} = 2\frac{\partial \check{\mathbf{g}}(\boldsymbol{\gamma}^o)^T}{\partial \boldsymbol{\gamma}}\frac{\partial \check{\mathbf{g}}(\boldsymbol{\gamma}^o)}{\partial \boldsymbol{\gamma}^T}, \tag{A.3a}$$

$$\mathbf{B} = 2\sum_{i=1}^{L+KN}(\check{h}_i - \check{g}_i(\boldsymbol{\gamma}^o))\frac{\partial^2 \check{g}_i(\boldsymbol{\gamma}^o)}{\partial\boldsymbol{\gamma}\partial\boldsymbol{\gamma}^T}. \tag{A.3b}$$

When the noise $\mathbf{n}$ is small, we have the approximation

$$\left(\frac{\partial \mathbf{p}(\boldsymbol{\gamma}^o)}{\partial\boldsymbol{\gamma}^T}\right)^{-1} = (\mathbf{I} - \mathbf{A}^{-1}\mathbf{B})^{-1}\mathbf{A}^{-1} \simeq \mathbf{A}^{-1} + \mathbf{A}^{-1}\mathbf{B}\mathbf{A}^{-1}, \tag{A.4}$$

where the higher order terms of $\mathbf{B}$ are neglected. Since $\mathbf{A}^{-1}$ is independent of noise and $\mathbf{p}(\boldsymbol{\gamma}^o)$ is zero mean, the first term in (3.4) is

$$\mathrm{E}\left(-\left(\frac{\partial \mathbf{p}(\boldsymbol{\gamma}^o)}{\partial\boldsymbol{\gamma}^T}\right)^{-1}\mathbf{p}(\boldsymbol{\gamma}^o)\right) \simeq -\mathrm{E}\left(\mathbf{A}^{-1}\mathbf{B}\mathbf{A}^{-1}\mathbf{p}(\boldsymbol{\gamma}^o)\right). \tag{A.5}$$

Putting (A.1) into (A.5), we have

$$\mathrm{E}\left(-\left(\frac{\partial \mathbf{p}(\boldsymbol{\gamma}^o)}{\partial\boldsymbol{\gamma}^T}\right)^{-1}\mathbf{p}(\boldsymbol{\gamma}^o)\right) \simeq 2\mathbf{A}^{-1}\mathrm{E}\left(\mathbf{B}\mathbf{A}^{-1}\frac{\partial \check{\mathbf{g}}(\boldsymbol{\gamma}^o)^T}{\partial\boldsymbol{\gamma}}\left(\check{\mathbf{h}} - \check{\mathbf{g}}(\boldsymbol{\gamma}^o)\right)\right).$$

After substituting (A.1) for $\mathbf{p}(\boldsymbol{\gamma}^o)$, (A.3b) for $\mathbf{B}$ and using $\mathrm{E}\left(\left(\check{\mathbf{h}} - \check{\mathbf{g}}(\boldsymbol{\gamma}^o)\right)\left(\check{\mathbf{h}} - \check{\mathbf{g}}(\boldsymbol{\gamma}^o)\right)^T\right)$ equal to identity matrix of size $L + KN$, we have

$$\mathrm{E}\left(-\left(\frac{\partial \mathbf{p}(\boldsymbol{\gamma}^o)}{\partial\boldsymbol{\gamma}^T}\right)^{-1}\mathbf{p}(\boldsymbol{\gamma}^o)\right) \simeq 4\mathbf{A}^{-1}\left(\sum_{i=1}^{L+KN}\frac{\partial^2 \check{g}_i(\boldsymbol{\gamma}^o)}{\partial\boldsymbol{\gamma}\partial\boldsymbol{\gamma}^T}\mathbf{A}^{-1}\frac{\partial \check{g}_i(\boldsymbol{\gamma}^o)}{\partial\boldsymbol{\gamma}}\right), \tag{A.6}$$

In the second term of (3.4), $\mathbf{q}(\boldsymbol{\gamma}^o)$ is

$$\mathbf{q}(\boldsymbol{\gamma}^o) = \frac{1}{2}\begin{bmatrix} \mathrm{tr}\left(\frac{\partial^2 p_1(\boldsymbol{\gamma}^o)}{\partial\boldsymbol{\gamma}\partial\boldsymbol{\gamma}^T}(\hat{\boldsymbol{\gamma}} - \boldsymbol{\gamma}^o)(\hat{\boldsymbol{\gamma}} - \boldsymbol{\gamma}^o)^T\right) \\ \vdots \\ \mathrm{tr}\left(\frac{\partial^2 p_{K(N+1)}(\boldsymbol{\gamma}^o)}{\partial\boldsymbol{\gamma}\partial\boldsymbol{\gamma}^T}(\hat{\boldsymbol{\gamma}} - \boldsymbol{\gamma}^o)(\hat{\boldsymbol{\gamma}} - \boldsymbol{\gamma}^o)^T\right) \end{bmatrix} \tag{A.7}$$

and $\frac{\partial^2 p_j(\boldsymbol{\gamma}^o)}{\partial\boldsymbol{\gamma}\partial\boldsymbol{\gamma}^T}$ has linear noise term only, $j = 1, 2, \cdots, K(N+1)$.

Note that $\hat{\boldsymbol{\gamma}} - \boldsymbol{\gamma}^o$ contains noise only. When we maintain up to second order noise components by ignoring the noise in $\frac{\partial \mathbf{p}(\boldsymbol{\gamma}^o)}{\partial\boldsymbol{\gamma}^T}$ and $\frac{\partial^2 p_j(\boldsymbol{\gamma}^o)}{\partial\boldsymbol{\gamma}\partial\boldsymbol{\gamma}^T}$,

$$\mathrm{E}\left(-\left(\frac{\partial \mathbf{p}(\boldsymbol{\gamma}^o)}{\partial\boldsymbol{\gamma}^T}\right)^{-1}\mathbf{q}(\boldsymbol{\gamma}^o)\right) \simeq -\mathbf{A}^{-1}\begin{bmatrix} \mathrm{tr}\left(\mathrm{E}\left(\frac{\partial^2 p_1(\boldsymbol{\gamma}^o)}{\partial\boldsymbol{\gamma}\partial\boldsymbol{\gamma}^T}\right)\times\mathbf{A}^{-1}\right) \\ \vdots \\ \mathrm{tr}\left(\mathrm{E}\left(\frac{\partial^2 p_{K(N+1)}(\boldsymbol{\gamma}^o)}{\partial\boldsymbol{\gamma}\partial\boldsymbol{\gamma}^T}\right)\times\mathbf{A}^{-1}\right)\end{bmatrix}, \tag{A.8}$$

where $\mathrm{E}\left((\hat{\boldsymbol{\gamma}} - \boldsymbol{\gamma}^o)(\hat{\boldsymbol{\gamma}} - \boldsymbol{\gamma}^o)^T\right) \approx \mathrm{CRLB}_{\boldsymbol{\gamma}} = 2\mathbf{A}^{-1}$ [22] has been used.

From (A.2) and (A.3),

$$\begin{aligned}\mathrm{E}\left(\frac{\partial^2 p_j(\boldsymbol{\gamma}^o)}{\partial\boldsymbol{\gamma}\partial\boldsymbol{\gamma}^T}\right) =& 2\sum_{i=1}^{L+KN}\left(\frac{\partial\check{h}_i(\boldsymbol{\gamma}^o)}{\partial\boldsymbol{\gamma}^T}\mathbf{e}_j\frac{\partial^2\check{h}_i(\boldsymbol{\gamma}^o)}{\partial\boldsymbol{\gamma}\partial\boldsymbol{\gamma}^T} + \frac{\partial^2\check{h}_i(\boldsymbol{\gamma}^o)}{\partial\boldsymbol{\gamma}\partial\boldsymbol{\gamma}^T}\mathbf{e}_j\frac{\partial\check{h}_i(\boldsymbol{\gamma}^o)}{\partial\boldsymbol{\gamma}^T}\right. \\ &\left. + \frac{\partial\check{h}_i(\boldsymbol{\gamma}^o)}{\partial\boldsymbol{\gamma}}\mathbf{e}_j^T\frac{\partial^2\check{h}_i(\boldsymbol{\gamma}^o)}{\partial\boldsymbol{\gamma}\partial\boldsymbol{\gamma}^T}\right).\end{aligned} \tag{A.9}$$

The first two terms on the right come from the derivative over $\mathbf{A}$ and the last the derivative over $\mathbf{B}$. In (A.9), $\mathbf{e}_j$ is the $K(N+1)$ length vector whose jth element is 1 and all the other elements are 0.

Putting (A.9) simplifies (A.8) to

$$\begin{aligned}&\mathrm{E}\left(-\left(\frac{\partial \mathbf{p}(\boldsymbol{\gamma}^o)}{\partial\boldsymbol{\gamma}^T}\right)^{-1}\mathbf{q}(\boldsymbol{\gamma}^o)\right) = \\ &-2\mathbf{A}^{-1}\sum_{i=1}^{L+KN}\left(\mathrm{tr}\left(\frac{\partial^2\check{h}_i(\boldsymbol{\gamma}^o)}{\partial\boldsymbol{\gamma}\partial\boldsymbol{\gamma}^T}\mathbf{A}^{-1}\right)\frac{\partial\check{h}_i(\boldsymbol{\gamma}^o)}{\partial\boldsymbol{\gamma}} + 2\frac{\partial^2\check{h}_i(\boldsymbol{\gamma}^o)}{\partial\boldsymbol{\gamma}\partial\boldsymbol{\gamma}^T}\mathbf{A}^{-1}\frac{\partial\check{h}_i(\boldsymbol{\gamma}^o)}{\partial\boldsymbol{\gamma}}\right).\end{aligned} \tag{A.10}$$

Adding (A.6) to (A.10) cancels out the last term and (3.4) becomes

$$\mathbf{b}_{\boldsymbol{\gamma}} = -2\mathbf{A}^{-1} \sum_{i=1}^{L+KN} \left(\mathrm{tr} \left(\frac{\partial^2 \check{h}_i(\boldsymbol{\gamma}^o)}{\partial \boldsymbol{\gamma} \partial \boldsymbol{\gamma}^T} \mathbf{A}^{-1} \right) \frac{\partial \check{h}_i(\boldsymbol{\gamma}^o)}{\partial \boldsymbol{\gamma}} \right). \tag{A.11}$$

Let $\mathbf{e}_i$ be a length $L + KN$ zero vector with its ith element equal to identity. By expressing $\check{h}_i(\boldsymbol{\gamma}^o) = \mathbf{e}_i^T \mathbf{Q}^{-\frac{1}{2}} \mathbf{g}(\boldsymbol{\gamma}^o)$ with $\mathbf{g}(\boldsymbol{\gamma}^o)$ defined below (3.1) and noting that $\mathbf{Q} = \mathrm{diag}\,(\,\mathbf{Q_m},\, \mathbf{Q_s}\,)$ and $\mathbf{A} = 2\mathrm{FIM}_{\boldsymbol{\gamma}}$, (A.11) can be further simplified to (3.5).

A.2 The Derivative Terms of TOA, TDOA and AOA positionings

The first and second derivatives of TOA measurement (2.4), $j = 1, 2, \ldots, N$, are

$$\frac{\partial m^o_{\mathrm{TOA},j}(\boldsymbol{\gamma}^o)}{\partial \boldsymbol{\gamma}} = \begin{bmatrix} \frac{\partial m^o_{\mathrm{TOA},j}(\boldsymbol{\gamma}^o)}{\partial \mathbf{u}^T} & \frac{\partial m^o_{\mathrm{TOA},j}(\boldsymbol{\gamma}^o)}{\partial \mathbf{s}_1^T} & \cdots & \frac{\partial m^o_{\mathrm{TOA},j}(\boldsymbol{\gamma}^o)}{\partial \mathbf{s}_N^T} \end{bmatrix}^T, \tag{A.12a}$$

$$\frac{\partial^2 m^o_{\mathrm{TOA},j}(\boldsymbol{\gamma}^o)}{\partial \boldsymbol{\gamma} \partial \boldsymbol{\gamma}^T} = \begin{bmatrix} \frac{\partial^2 m^o_{\mathrm{TOA},j}(\boldsymbol{\gamma}^o)}{\partial \mathbf{u} \partial \mathbf{u}^T} & \frac{\partial^2 m^o_{\mathrm{TOA},j}(\boldsymbol{\gamma}^o)}{\partial \mathbf{u} \partial \mathbf{s}_1^T} & \cdots & \frac{\partial^2 m^o_{\mathrm{TOA},j}(\boldsymbol{\gamma}^o)}{\partial \mathbf{u} \partial \mathbf{s}_N^T} \\ \frac{\partial^2 m^o_{\mathrm{TOA},j}(\boldsymbol{\gamma}^o)}{\partial \mathbf{s}_1 \partial \mathbf{u}^T} & \frac{\partial^2 m^o_{\mathrm{TOA},j}(\boldsymbol{\gamma}^o)}{\partial \mathbf{s}_1 \partial \mathbf{s}_1^T} & \cdots & \frac{\partial^2 m^o_{\mathrm{TOA},j}(\boldsymbol{\gamma}^o)}{\partial \mathbf{s}_1 \partial \mathbf{s}_N^T} \\ \vdots & \vdots & \ddots & \vdots \\ \frac{\partial^2 m^o_{\mathrm{TOA},j}(\boldsymbol{\gamma}^o)}{\partial \mathbf{s}_N \partial \mathbf{u}^T} & \frac{\partial^2 m^o_{\mathrm{TOA},j}(\boldsymbol{\gamma}^o)}{\partial \mathbf{s}_N \partial \mathbf{s}_1^T} & \cdots & \frac{\partial^2 m^o_{\mathrm{TOA},j}(\boldsymbol{\gamma}^o)}{\partial \mathbf{s}_N \partial \mathbf{s}_N^T} \end{bmatrix}, \tag{A.12b}$$

where

$$\frac{\partial m^o_{\mathrm{TOA},j}(\boldsymbol{\gamma}^o)}{\partial \mathbf{u}} = \boldsymbol{\rho}_{\mathbf{u}^o, \mathbf{s}_j^o}, \quad \frac{\partial m^o_{\mathrm{TOA},j}(\boldsymbol{\gamma}^o)}{\partial \mathbf{s}_j} = -\boldsymbol{\rho}_{\mathbf{u}^o, \mathbf{s}_j^o}, \tag{A.13a}$$

$$\begin{aligned} \frac{\partial^2 m^o_{\mathrm{TOA},j}(\boldsymbol{\gamma}^o)}{\partial \mathbf{u} \partial \mathbf{u}^T} &= -\frac{\partial^2 m^o_{\mathrm{TOA},j}(\boldsymbol{\gamma}^o)}{\partial \mathbf{u} \partial \mathbf{s}_j^T} = -\frac{\partial^2 m^o_{\mathrm{TOA},j}(\boldsymbol{\gamma}^o)}{\partial \mathbf{s}_j \partial \mathbf{u}^T} \\ &= \frac{\partial^2 m^o_{\mathrm{TOA},j}(\boldsymbol{\gamma}^o)}{\partial \mathbf{s}_j \partial \mathbf{s}_j^T} = \frac{1}{||\mathbf{u}^o - \mathbf{s}_j^o||} \mathbf{P}^{\perp}_{\mathbf{u}^o, \mathbf{s}_j^o}, \end{aligned} \tag{A.13b}$$

$\boldsymbol{\rho}_{\mathbf{u}^o,\mathbf{s}_j^o} = \left(\mathbf{u}^o - \mathbf{s}_j^o\right)/||\mathbf{u}^o - \mathbf{s}_j^o||$, $\mathbf{P}^{\perp}_{\mathbf{u}^o,\mathbf{s}_j^o} = \mathbf{I}_K - \boldsymbol{\rho}_{\mathbf{u}^o,\mathbf{s}_j^o}\boldsymbol{\rho}^T_{\mathbf{u}^o,\mathbf{s}_j^o}$ and all the other elements are 0.

From (2.10), for the TDOA case, $j = 2, 3, \ldots, N$,

$$\frac{\partial m^o_{\mathrm{H},j-1}(\boldsymbol{\gamma}^o)}{\partial \boldsymbol{\gamma}} = \begin{bmatrix} \frac{\partial m^o_{\mathrm{H},j-1}(\boldsymbol{\gamma}^o)}{\partial \mathbf{u}^T} & \frac{\partial m^o_{\mathrm{H},j-1}(\boldsymbol{\gamma}^o)}{\partial \mathbf{s}_1^T} & \cdots & \frac{\partial m^o_{\mathrm{H},j-1}(\boldsymbol{\gamma}^o)}{\partial \mathbf{s}_N^T} \end{bmatrix}^T, \tag{A.14a}$$

$$\frac{\partial^2 m^o_{\mathrm{H},j-1}(\boldsymbol{\gamma}^o)}{\partial \boldsymbol{\gamma}\partial \boldsymbol{\gamma}^T} = \begin{bmatrix} \frac{\partial^2 m^o_{\mathrm{H},j-1}(\boldsymbol{\gamma}^o)}{\partial \mathbf{u}\partial \mathbf{u}^T} & \frac{\partial^2 m^o_{\mathrm{H},j-1}(\boldsymbol{\gamma}^o)}{\partial \mathbf{u}\partial \mathbf{s}_1^T} & \cdots & \frac{\partial^2 m^o_{\mathrm{H},j-1}(\boldsymbol{\gamma}^o)}{\partial \mathbf{u}\partial \mathbf{s}_N^T} \\ \frac{\partial^2 m^o_{\mathrm{H},j-1}(\boldsymbol{\gamma}^o)}{\partial \mathbf{s}_1\partial \mathbf{u}^T} & \frac{\partial^2 m^o_{\mathrm{H},j-1}(\boldsymbol{\gamma}^o)}{\partial \mathbf{s}_1\partial \mathbf{s}_1^T} & \cdots & \frac{\partial^2 m^o_{\mathrm{H},j-1}(\boldsymbol{\gamma}^o)}{\partial \mathbf{s}_1\partial \mathbf{s}_N^T} \\ \vdots & \vdots & \ddots & \vdots \\ \frac{\partial^2 m^o_{\mathrm{H},j-1}(\boldsymbol{\gamma}^o)}{\partial \mathbf{s}_N\partial \mathbf{u}^T} & \frac{\partial^2 m^o_{\mathrm{H},j-1}(\boldsymbol{\gamma}^o)}{\partial \mathbf{s}_N\partial \mathbf{s}_1^T} & \cdots & \frac{\partial^2 m^o_{\mathrm{H},j-1}(\boldsymbol{\gamma}^o)}{\partial \mathbf{s}_N\partial \mathbf{s}_N^T} \end{bmatrix}, \tag{A.14b}$$

where

$$\frac{\partial m^o_{\mathrm{H},j-1}(\boldsymbol{\gamma}^o)}{\partial \mathbf{u}} = \boldsymbol{\rho}_{\mathbf{u}^o,\mathbf{s}_j^o} - \boldsymbol{\rho}_{\mathbf{u}^o,\mathbf{s}_1^o}, \quad \frac{\partial m^o_{\mathrm{H},j-1}(\boldsymbol{\gamma}^o)}{\partial \mathbf{s}_1} = \boldsymbol{\rho}_{\mathbf{u}^o,\mathbf{s}_1^o}, \quad \frac{\partial m^o_{\mathrm{H},j-1}(\boldsymbol{\gamma}^o)}{\partial \mathbf{s}_j} = -\boldsymbol{\rho}_{\mathbf{u}^o,\mathbf{s}_j^o}, \tag{A.15a}$$

$$\frac{\partial^2 m^o_{\mathrm{H},j-1}(\boldsymbol{\gamma}^o)}{\partial \mathbf{u}\partial \mathbf{u}^T} = \frac{1}{||\mathbf{u}^o - \mathbf{s}_j^o||}\mathbf{P}^{\perp}_{\mathbf{u}^o,\mathbf{s}_j^o} - \frac{1}{||\mathbf{u}^o - \mathbf{s}_1^o||}\mathbf{P}^{\perp}_{\mathbf{u}^o,\mathbf{s}_1^o}, \tag{A.15b}$$

$$\frac{\partial^2 m^o_{\mathrm{H},j-1}(\boldsymbol{\gamma}^o)}{\partial \mathbf{u}\partial \mathbf{s}_1^T} = \frac{\partial^2 m^o_{\mathrm{H},j-1}(\boldsymbol{\gamma}^o)}{\partial \mathbf{s}_1\partial \mathbf{u}^T} = -\frac{\partial^2 m^o_{\mathrm{H},j-1}(\boldsymbol{\gamma}^o)}{\partial \mathbf{s}_1\partial \mathbf{s}_1^T} = \frac{1}{||\mathbf{u}^o - \mathbf{s}_1^o||}\mathbf{P}^{\perp}_{\mathbf{u}^o,\mathbf{s}_1^o}, \tag{A.15c}$$

$$\frac{\partial^2 m^o_{\mathrm{H},j-1}(\boldsymbol{\gamma}^o)}{\partial \mathbf{u}\partial \mathbf{s}_j^T} = \frac{\partial^2 m^o_{\mathrm{H},j-1}(\boldsymbol{\gamma}^o)}{\partial \mathbf{s}_j\partial \mathbf{u}^T} = -\frac{\partial^2 m^o_{\mathrm{H},j-1}(\boldsymbol{\gamma}^o)}{\partial \mathbf{s}_j\partial \mathbf{s}_j^T} = -\frac{1}{||\mathbf{u}^o - \mathbf{s}_j^o||}\mathbf{P}^{\perp}_{\mathbf{u}^o,\mathbf{s}_j^o}, \tag{A.15d}$$

and all the other elements are 0.

From (2.11), for the AOA case, $j = 1, 2, \ldots, N$,

$$\frac{\partial m^o_{\mathrm{AOA},j}(\boldsymbol{\gamma}^o)}{\partial \boldsymbol{\gamma}} = \begin{bmatrix} \frac{\partial m^o_{\mathrm{AOA},j}(\boldsymbol{\gamma}^o)}{\partial \mathbf{u}^T} & \frac{\partial m^o_{\mathrm{AOA},j}(\boldsymbol{\gamma}^o)}{\partial \mathbf{s}_1^T} & \cdots & \frac{\partial m^o_{\mathrm{AOA},j}(\boldsymbol{\gamma}^o)}{\partial \mathbf{s}_N^T} \end{bmatrix}^T, \tag{A.16a}$$

$$\frac{\partial^2 m^o_{\mathrm{AOA},j}(\boldsymbol{\gamma}^o)}{\partial\boldsymbol{\gamma}\partial\boldsymbol{\gamma}^T} = \begin{bmatrix} \frac{\partial^2 m^o_{\mathrm{AOA},j}(\boldsymbol{\gamma}^o)}{\partial\mathbf{u}\partial\mathbf{u}^T} & \frac{\partial^2 m^o_{\mathrm{AOA},j}(\boldsymbol{\gamma}^o)}{\partial\mathbf{u}\partial\mathbf{s}_1^T} & \cdots & \frac{\partial^2 m^o_{\mathrm{AOA},j}(\boldsymbol{\gamma}^o)}{\partial\mathbf{u}\partial\mathbf{s}_N^T} \\ \frac{\partial^2 m^o_{\mathrm{AOA},j}(\boldsymbol{\gamma}^o)}{\partial\mathbf{s}_1\partial\mathbf{u}^T} & \frac{\partial^2 m^o_{\mathrm{AOA},j}(\boldsymbol{\gamma}^o)}{\partial\mathbf{s}_1\partial\mathbf{s}_1^T} & \cdots & \frac{\partial^2 m^o_{\mathrm{AOA},j}(\boldsymbol{\gamma}^o)}{\partial\mathbf{s}_1\partial\mathbf{s}_N^T} \\ \vdots & \vdots & \ddots & \vdots \\ \frac{\partial^2 m^o_{\mathrm{AOA},j}(\boldsymbol{\gamma}^o)}{\partial\mathbf{s}_N\partial\mathbf{u}^T} & \frac{\partial^2 m^o_{\mathrm{AOA},j}(\boldsymbol{\gamma}^o)}{\partial\mathbf{s}_N\partial\mathbf{s}_1^T} & \cdots & \frac{\partial^2 m^o_{\mathrm{AOA},j}(\boldsymbol{\gamma}^o)}{\partial\mathbf{s}_N\partial\mathbf{s}_N^T} \end{bmatrix}, \tag{A.16b}$$

where

$$\frac{\partial m^o_{\mathrm{AOA},j}(\boldsymbol{\gamma}^o)}{\partial\mathbf{u}} = \frac{1}{||\mathbf{u}^o-\mathbf{s}_j^o||}\mathbf{T}\boldsymbol{\rho}_{\mathbf{u}^o,\mathbf{s}_j^o}, \qquad \frac{\partial m^o_{\mathrm{AOA},j}(\boldsymbol{\gamma}^o)}{\partial\mathbf{s}_j} = -\frac{1}{||\mathbf{u}^o-\mathbf{s}_j^o||}\mathbf{T}\boldsymbol{\rho}_{\mathbf{u}^o,\mathbf{s}_j^o}, \tag{A.17a}$$

$$\begin{aligned}\frac{\partial^2 m^o_{\mathrm{AOA},j}(\boldsymbol{\gamma}^o)}{\partial\mathbf{u}\partial\mathbf{u}^T} &= -\frac{\partial^2 m^o_{\mathrm{AOA},j}(\boldsymbol{\gamma}^o)}{\partial\mathbf{u}\partial\mathbf{s}_j^T} = -\frac{\partial^2 m^o_{\mathrm{AOA},j}(\boldsymbol{\gamma}^o)}{\partial\mathbf{s}_j\partial\mathbf{u}^T} = \frac{\partial^2 m^o_{\mathrm{AOA},j}(\boldsymbol{\gamma}^o)}{\partial\mathbf{s}_j\partial\mathbf{s}_j^T} \\ &= \frac{1}{||\mathbf{u}^o-\mathbf{s}_j^o||^2}\mathbf{T}\left(\mathbf{I}_K - 2\boldsymbol{\rho}_{\mathbf{u}^o,\mathbf{s}_j^o}\boldsymbol{\rho}^T_{\mathbf{u}^o,\mathbf{s}_j^o}\right),\end{aligned} \tag{A.17b}$$

where $\mathbf{T} = \begin{bmatrix} 0 & -1 \\ 1 & 0 \end{bmatrix}$ and all the other elements are 0.

A.3 The Detail of $\mathbf{b}_{\mathbf{u},\mathbf{s}}$

After using (3.7b) and (3.9) in (3.5) and some algebraic manipulations,

$$\begin{aligned}\mathbf{b}_{\mathbf{u},\mathbf{s}} = -\frac{1}{2}\mathrm{FIM}^{-1}_{\boldsymbol{\gamma},\mathbf{uu}}\left(\nabla^T_{\mathbf{u}}\mathbf{Q}^{-1}_{\mathbf{m}}\mathbf{k}_{\mathbf{s}} + \mathrm{FIM}_{\boldsymbol{\gamma},\mathbf{us}}\times\right. \\ \left.\left(\mathrm{FIM}_{\boldsymbol{\gamma},\mathbf{ss}} - \mathrm{FIM}^T_{\boldsymbol{\gamma},\mathbf{us}}\mathrm{FIM}^{-1}_{\boldsymbol{\gamma},\mathbf{uu}}\mathrm{FIM}_{\boldsymbol{\gamma},\mathbf{us}}\right)^{-1}\left(\mathrm{FIM}^T_{\boldsymbol{\gamma},\mathbf{us}}\mathrm{FIM}^{-1}_{\boldsymbol{\gamma},\mathbf{uu}}\nabla^T_{\mathbf{u}} - \nabla^T_{\mathbf{s}}\right)\mathbf{Q}^{-1}_{\mathbf{m}}\mathbf{k}\right),\end{aligned} \tag{A.18}$$

where

$$\mathbf{k}_{\mathbf{s}} = \left[\, k_{\mathbf{s},1},\, k_{\mathbf{s},2},\, \cdots,\, k_{\mathbf{s},L}\,\right]^T, \quad k_{\mathbf{s},i} = \mathrm{tr}\left(\frac{\partial^2 m^o_i(\boldsymbol{\gamma}^o)}{\partial\boldsymbol{\gamma}\partial\boldsymbol{\gamma}^T}\mathrm{FIM}^{-1}_{\boldsymbol{\gamma}} - \begin{bmatrix} \mathrm{FIM}^{-1}_{\boldsymbol{\gamma},\mathbf{uu}} & \mathbf{O}_{K\times KN} \\ \mathbf{O}_{KN\times K} & \mathbf{O}_{KN\times KN}\end{bmatrix}\right).$$

A.4 The Bias Expressions for the Three Localization Approaches with General Form of $\mathbf{Q_m}$

For TOA localization (2.4), the components of $\mathrm{FIM}_{\boldsymbol{\gamma}}^{-1}$ in (3.7b) are

$$\mathrm{FIM}_{\mathbf{u}}^{-1} = \frac{1}{2}\left(\mathbf{P}_{\mathbf{u},\mathbf{s}}^{T}\left(\mathbf{Q}_{\mathbf{m}}+\widetilde{\mathbf{Q}}_{\mathbf{s}}\right)^{-1}\mathbf{P}_{\mathbf{u},\mathbf{s}}\right)^{-1}, \tag{A.19a}$$

$$\mathrm{FIM}_{\boldsymbol{\gamma},\mathbf{us}}\mathrm{FIM}_{\boldsymbol{\gamma},\mathbf{ss}}^{-1} = \mathbf{P}_{\mathbf{u},\mathbf{s}}^{T}\left(\mathbf{Q}_{\mathbf{m}}+\widetilde{\mathbf{Q}}_{\mathbf{s}}\right)^{-1}\widetilde{\mathbf{P}}_{\mathbf{u},\mathbf{s}}\mathbf{Q}_{\mathbf{s}}, \tag{A.19b}$$

$$\mathrm{FIM}_{\mathbf{s}}^{-1} = \frac{1}{2}\left(\mathbf{Q}_{\mathbf{s}}-\mathbf{Q}_{\mathbf{s}}\widetilde{\mathbf{P}}_{\mathbf{u},\mathbf{s}}^{T}\left(\mathbf{Q}_{\mathbf{m}}+\widetilde{\mathbf{Q}}_{\mathbf{s}}\right)^{-1}\widetilde{\mathbf{P}}_{\mathbf{u},\mathbf{s}}\mathbf{Q}_{\mathbf{s}}\right), \tag{A.19c}$$

where $\mathbf{P}_{\mathbf{u},\mathbf{s}} = \left[\,\boldsymbol{\rho}_{\mathbf{u}^o,\mathbf{s}_1^o},\,\boldsymbol{\rho}_{\mathbf{u}^o,\mathbf{s}_2^o},\,\cdots,\,\boldsymbol{\rho}_{\mathbf{u}^o,\mathbf{s}_N^o}\,\right]^T$ and $\widetilde{\mathbf{P}}_{\mathbf{u},\mathbf{s}} = \mathrm{diag}\left(\,\boldsymbol{\rho}_{\mathbf{u}^o,\mathbf{s}_1^o},\,\boldsymbol{\rho}_{\mathbf{u}^o,\mathbf{s}_2^o},\,\cdots,\,\boldsymbol{\rho}_{\mathbf{u}^o,\mathbf{s}_N^o}\,\right)^T$. (A.19a) is obtained through applying the matrix inverse lemma [22] for the inverse of $\mathrm{FIM}_{\boldsymbol{\gamma},\mathbf{ss}}$, and so does (A.19b). The Woodbury identity [22] is used to arrive at $\mathrm{FIM}_{\mathbf{s}}^{-1}$.

Putting (A.19), (A.12b) and (A.13b) into (3.6b) gives the jth element of $\mathbf{k}_{\mathrm{TOA}}$ as

$$k_{\mathrm{TOA},j} = \frac{1}{2||\mathbf{u}^o-\mathbf{s}_j^o||}\mathrm{tr}\left(\mathbf{P}_{\mathbf{u}^o,\mathbf{s}_j^o}^{\perp}\left(\mathbf{P}_{\mathbf{u},\mathbf{s}}^{T}\left(\mathbf{Q}_{\mathbf{m}}+\widetilde{\mathbf{Q}}_{\mathbf{s}}\right)^{-1}\mathbf{P}_{\mathbf{u},\mathbf{s}}\right)^{-1}\right)+\frac{\sigma_{\mathbf{s}_j}^2(K-1)}{2||\mathbf{u}^o-\mathbf{s}_j^o||}, \tag{A.20}$$

where $j = 1, 2, \ldots, N$. Using (A.19) and (A.20) in (3.5), the bias of TOA is

$$\mathbf{b}_{\mathbf{u},\mathrm{TOA}} = -\left(\mathbf{P}_{\mathbf{u},\mathbf{s}}^{T}\left(\mathbf{Q}_{\mathbf{m}}+\widetilde{\mathbf{Q}}_{\mathbf{s}}\right)^{-1}\mathbf{P}_{\mathbf{u},\mathbf{s}}\right)^{-1}\mathbf{P}_{\mathbf{u},\mathbf{s}}^{T}\left(\mathbf{Q}_{\mathbf{m}}+\widetilde{\mathbf{Q}}_{\mathbf{s}}\right)^{-1}\mathbf{k}_{\mathrm{TOA}}. \tag{A.21}$$

For the TDOA localization, the true values of TDOA in (2.10) are related to those of TOA by

$$\mathbf{m}_{\mathrm{H}}^o = \mathbf{H}\mathbf{m}_{\mathrm{TOA}}^o \tag{A.22}$$

where $\mathbf{H} = [-\mathbf{1}_{N-1},\,\mathbf{I}_{N-1}]$.

The bias of TDOA localization is, from (A.22) and using similar procedures as for the TOA case,

$$\mathbf{b}_{\mathbf{u},\mathrm{H}} = -\left(\mathbf{P}^T\mathbf{H}^T\left(\mathbf{Q}_\mathbf{m}+\mathbf{H}\widetilde{\mathbf{Q}}_\mathbf{s}\mathbf{H}^T\right)^{-1}\mathbf{H}\mathbf{P}\right)^{-1}\mathbf{P}^T\mathbf{H}^T\left(\mathbf{Q}_\mathbf{m}+\mathbf{H}\widetilde{\mathbf{Q}}_\mathbf{s}\mathbf{H}^T\right)^{-1}\mathbf{k}_\mathrm{H}, \tag{A.23}$$

where $\mathbf{k}_\mathrm{H} = \mathbf{H}\boldsymbol{\kappa}_\mathrm{H} = \mathbf{H}\left[\kappa_{\mathrm{H},1},\, \kappa_{\mathrm{H},2},\, \cdots,\, \kappa_{\mathrm{H},N}\right]^T$ and

$$\kappa_{\mathrm{H},j} = \frac{1}{2||\mathbf{u}^o-\mathbf{s}_j^o||}\mathrm{tr}\left(\mathbf{P}^\perp_{\mathbf{u}^o,\mathbf{s}_j^o}\left(\mathbf{P}^T_{\mathbf{u},\mathbf{s}}\mathbf{H}^T\left(\mathbf{Q}_\mathbf{m}+\mathbf{H}\widetilde{\mathbf{Q}}_\mathbf{s}\mathbf{H}^T\right)^{-1}\mathbf{H}\mathbf{P}_{\mathbf{u},\mathbf{s}}\right)^{-1}\right)+\frac{\sigma^2_{\mathbf{s}_j}(K-1)}{2||\mathbf{u}^o-\mathbf{s}_j^o||}. \tag{A.24}$$

When the measurement type is AOA (2.11), the bias of the ML position estimate can be similarly computed by (3.5), (3.6), (A.16) and (A.17) and it is equal to

$$\mathbf{b}_{\mathbf{u},\mathrm{AOA}} = -\left(\boldsymbol{\Gamma}^T\left(\mathbf{Q}_\mathbf{m}+\widetilde{\mathbf{Q}}_\mathbf{s}\widetilde{\mathbf{R}}^{-2}\right)^{-1}\boldsymbol{\Gamma}\right)^{-1}\boldsymbol{\Gamma}^T\left(\mathbf{Q}_\mathbf{m}+\widetilde{\mathbf{Q}}_\mathbf{s}\widetilde{\mathbf{R}}^{-2}\right)^{-1}\mathbf{k}_\mathrm{AOA}, \tag{A.25}$$

where $\boldsymbol{\Gamma} = \left[\, ||\mathbf{u}^o-\mathbf{s}_1^o||^{-1}\mathbf{T}\boldsymbol{\rho}_{\mathbf{u}^o,\mathbf{s}_1^o},\, ||\mathbf{u}^o-\mathbf{s}_2^o||^{-1}\mathbf{T}\boldsymbol{\rho}_{\mathbf{u}^o,\mathbf{s}_2^o},\, \cdots,\, ||\mathbf{u}^o-\mathbf{s}_N^o||^{-1}\mathbf{T}\boldsymbol{\rho}_{\mathbf{u}^o,\mathbf{s}_N^o}\,\right]^T$ and $\widetilde{\mathbf{R}} = \mathrm{diag}\left(\, ||\mathbf{u}^o-\mathbf{s}_1^o||,\, ||\mathbf{u}^o-\mathbf{s}_2^o||,\, \cdots,\, ||\mathbf{u}^o-\mathbf{s}_N^o||\,\right)$. The elements of $\mathbf{k}_\mathrm{AOA}$ are

$$\begin{aligned} k_{\mathrm{AOA},j} = \mathrm{tr}\Bigg(&\left(\boldsymbol{\Gamma}^T\left(\mathbf{Q}_\mathbf{m}+\widetilde{\mathbf{Q}}_\mathbf{s}\widetilde{\mathbf{R}}^{-2}\right)^{-1}\boldsymbol{\Gamma}\right)^{-1}\frac{1}{||\mathbf{u}^o-\mathbf{s}_j^o||^2}\mathbf{T}\times \\ &\left(\mathbf{I}_2-2\boldsymbol{\rho}_{\mathbf{u}^o,\mathbf{s}_j^o}\boldsymbol{\rho}^T_{\mathbf{u}^o,\mathbf{s}_j^o}\right)\left(\frac{1}{2}\mathbf{I}_2-\sigma^2_{\mathbf{s}_j}\mathbf{E}_j\widetilde{\boldsymbol{\Gamma}}^T\left(\mathbf{Q}_\mathbf{m}+\widetilde{\mathbf{Q}}_\mathbf{s}\widetilde{\mathbf{R}}^{-2}\right)^{-1}\boldsymbol{\Gamma}\right)\Bigg), \end{aligned} \tag{A.26}$$

where $\widetilde{\boldsymbol{\Gamma}} = \mathrm{diag}\left(\, ||\mathbf{u}^o-\mathbf{s}_1^o||^{-1}\mathbf{T}\boldsymbol{\rho}_{\mathbf{u}^o,\mathbf{s}_1^o},\, ||\mathbf{u}^o-\mathbf{s}_2^o||^{-1}\mathbf{T}\boldsymbol{\rho}_{\mathbf{u}^o,\mathbf{s}_2^o},\, \cdots,\, ||\mathbf{u}^o-\mathbf{s}_N^o||^{-1}\mathbf{T}\boldsymbol{\rho}_{\mathbf{u}^o,\mathbf{s}_N^o}\,\right)^T$ and $\mathbf{E}_j$ is an $2\times 2N$ matrix whose sub-matrix consisting of elements in the columns $2(j-1)+1$ to $2j$ is size 2 identity and all the other elements are 0.

Appendix B

Appendix for Chapter 4

B.1 The FIMs of the Three Elliptic Localization and Hyperbolic Positioning Approaches

B.1.1 $\mathrm{SE_f}$ Positioning

From (2.5) and (2.6) and in terms of the matrices defined in (4.3), the partial derivatives in (4.2) are

$$\boldsymbol{\nabla}_{\mathbf{u}} = -\left[\left(\mathbf{P}_{\mathbf{u},\mathbf{s}} + \mathbf{P}_{\mathbf{u},\mathbf{t}}\right)^T, \mathbf{O}_{N\times K}^T \right]^T, \quad \boldsymbol{\nabla}_{\mathbf{t}} = \left[\mathbf{P}_{\mathbf{u},\mathbf{t}}^T, -\mathbf{P}_{\mathbf{t},\mathbf{s}}^T \right]^T, \quad \boldsymbol{\nabla}_{\mathbf{s}} = \left[\widetilde{\mathbf{P}}_{\mathbf{u},\mathbf{s}}^T, \widetilde{\mathbf{P}}_{\mathbf{t},\mathbf{s}}^T \right]^T. \tag{B.1}$$

As a result,

$$\mathrm{FIM}_{\mathbf{u},\mathrm{SE_f}} = \left[\left(\mathbf{P}_{\mathbf{u},\mathbf{s}} + \mathbf{P}_{\mathbf{u},\mathbf{t}}\right)^T, \mathbf{O}_{N\times K}^T \right] \mathbf{R}^{-1} \left[\left(\mathbf{P}_{\mathbf{u},\mathbf{s}} + \mathbf{P}_{\mathbf{u},\mathbf{t}}\right)^T, \mathbf{O}_{N\times K}^T \right]^T = \mathbf{P}_{\mathbf{R}}^T \mathbf{R}^{-1} \mathbf{P}_{\mathbf{R}}, \tag{B.2}$$

where $\mathbf{R}$ is defined in (4.4) and $\mathbf{P_R}$ is below (4.4).

B.1.2 SE Positioning

From the SE measurement model (2.5), we have

$$\boldsymbol{\nabla}_{\mathbf{u}} = -\mathbf{P}_{\mathbf{u,s}} - \mathbf{P}_{\mathbf{u,t}}\,, \quad \boldsymbol{\nabla}_{\mathbf{t}} = \mathbf{P}_{\mathbf{u,t}}\,, \quad \boldsymbol{\nabla}_{\mathbf{s}} = \widetilde{\mathbf{P}}_{\mathbf{u,s}} \tag{B.3}$$

and

$$\mathrm{FIM}_{\mathbf{u},\mathrm{SE}} = \left(\,\mathbf{P}_{\mathbf{u,s}} + \mathbf{P}_{\mathbf{u,t}}\right)^T \mathbf{R}_{\mathrm{SE}}^{-1} \left(\mathbf{P}_{\mathbf{u,s}} + \mathbf{P}_{\mathbf{u,t}}\right)\,, \tag{B.4a}$$

$$\mathbf{R}_{\mathrm{SE}} = \mathbf{Q}_{\mathrm{SE}} + \mathbf{P}_{\mathbf{u,t}}\mathbf{Q}_{\mathbf{t}}\mathbf{P}_{\mathbf{u,t}}^T + \widetilde{\mathbf{P}}_{\mathbf{u,s}}\mathbf{Q}_{\mathbf{s}}\widetilde{\mathbf{P}}_{\mathbf{u,s}}^T\,. \tag{B.4b}$$

B.1.3 AE Positioning

Using the AE measurement model (2.7) gives

$$\boldsymbol{\nabla}_{\mathbf{u}} = -\mathbf{P}_{\mathbf{u,s}} - \mathbf{P}_{\mathbf{u,t}}\,, \qquad \boldsymbol{\nabla}_{\mathbf{t}} = \mathbf{P}_{\mathbf{u,t}} + \mathbf{P}_{\mathbf{t,s}}\,, \qquad \boldsymbol{\nabla}_{\mathbf{s}} = \widetilde{\mathbf{P}}_{\mathbf{u,s}} - \widetilde{\mathbf{P}}_{\mathbf{t,s}}\,. \tag{B.5}$$

Hence

$$\mathrm{FIM}_{\mathbf{u},\mathrm{AE}} = \left(\mathbf{P}_{\mathbf{u,s}} + \mathbf{P}_{\mathbf{u,t}}\right)^T \mathbf{R}_{\mathrm{AE}}^{-1} \left(\mathbf{P}_{\mathbf{u,s}} + \mathbf{P}_{\mathbf{u,t}}\right)\,, \tag{B.6a}$$

$$\mathbf{R}_{\mathrm{AE}} = \mathbf{Q}_{\mathrm{AE}} + \left(\mathbf{P}_{\mathbf{u,t}} + \mathbf{P}_{\mathbf{t,s}}\right)\mathbf{Q}_{\mathbf{t}}\left(\mathbf{P}_{\mathbf{u,t}} + \mathbf{P}_{\mathbf{t,s}}\right)^T + \left(\widetilde{\mathbf{P}}_{\mathbf{u,s}} - \widetilde{\mathbf{P}}_{\mathbf{t,s}}\right)\mathbf{Q}_{\mathbf{s}}\left(\widetilde{\mathbf{P}}_{\mathbf{u,s}} - \widetilde{\mathbf{P}}_{\mathbf{t,s}}\right)^T\,. \tag{B.6b}$$

B.1.4 H Positioning

The partial derivatives in this case are

$$\boldsymbol{\nabla}_{\mathbf{u}} = -\mathbf{H}\mathbf{P}_{\mathbf{u},\mathbf{s}}\,, \quad \boldsymbol{\nabla}_{\mathbf{t}} = \mathbf{O}_{(N-1)\times K}\,, \quad \boldsymbol{\nabla}_{\mathbf{s}} = \mathbf{H}\widetilde{\mathbf{P}}_{\mathbf{u},\mathbf{s}}\,. \tag{B.7}$$

Given the measurement functions of SE (2.5) and H (2.10), we have that

$$\mathbf{m}_{\mathrm{H}} = \mathbf{H}\mathbf{m}_{\mathrm{SE}}, \quad \mathbf{Q}_{\mathrm{H}} = \mathbf{H}\mathbf{Q}_{\mathrm{SE}}\mathbf{H}^T, \tag{B.8}$$

where $\mathbf{H}$ is defined below (A.22) and the FIM for hyperbolic positioning is

$$\mathrm{FIM}_{\mathbf{u},\mathrm{H}} = \mathbf{P}_{\mathbf{u},\mathbf{s}}^T\mathbf{H}^T \left(\mathbf{Q}_{\mathrm{H}} + \mathbf{H}\widetilde{\mathbf{P}}_{\mathbf{u},\mathbf{s}}\mathbf{Q}_{\mathbf{s}}\widetilde{\mathbf{P}}_{\mathbf{u},\mathbf{s}}^T\mathbf{H}^T\right)^{-1} \mathbf{H}\mathbf{P}_{\mathbf{u},\mathbf{s}}\,. \tag{B.9}$$

Using the equality $\mathbf{H}\mathbf{P}_{\mathbf{u},\mathbf{t}} = \mathbf{O}_{(N-1)\times K}$, (B.9) can be rewritten as

$$\mathrm{FIM}_{\mathbf{u},\mathrm{H}} = \\ \left(\mathbf{P}_{\mathbf{u},\mathbf{s}} + \mathbf{P}_{\mathbf{u},\mathbf{t}}\right)^T \mathbf{H}^T \left(\mathbf{H}\left(\mathbf{Q}_{\mathrm{SE}} + \mathbf{P}_{\mathbf{u},\mathbf{t}}\mathbf{Q}_{\mathbf{t}}\mathbf{P}_{\mathbf{u},\mathbf{t}}^T + \widetilde{\mathbf{P}}_{\mathbf{u},\mathbf{s}}\mathbf{Q}_{\mathbf{s}}\widetilde{\mathbf{P}}_{\mathbf{u},\mathbf{s}}^T\right)\mathbf{H}^T\right)^{-1} \mathbf{H}\left(\mathbf{P}_{\mathbf{u},\mathbf{s}} + \mathbf{P}_{\mathbf{u},\mathbf{t}}\right)\,. \tag{B.10}$$

Given (4.4) and (4.6), the $\mathrm{FIM}_{\mathbf{u},\mathrm{SE}}$, $\mathrm{FIM}_{\mathbf{u},\mathrm{AE}}$ and $\mathrm{FIM}_{\mathbf{u},\mathrm{H}}$ in (B.4a), (B.6a) and (B.10) can be re-expressed as (4.5b), (4.5c) and (4.5d), respectively.

B.2 The Second Order Derivatives of the Elliptic Localization Approaches

The partial derivative $\partial^2 m_j^o(\boldsymbol{\gamma}^o)/\left(\partial\boldsymbol{\gamma}\partial\boldsymbol{\gamma}^T\right)$ is characterized by $\partial^2 m_j^o(\boldsymbol{\gamma}^o)/\left(\partial\mathbf{u}\partial\mathbf{u}^T\right)$, $\partial^2 m_j^o(\boldsymbol{\gamma}^o)/\left(\partial\mathbf{t}\partial\mathbf{t}^T\right)$, $\partial^2 m_j^o(\boldsymbol{\gamma}^o)/\left(\partial\mathbf{s}_j\partial\mathbf{s}_j^T\right)$, $\partial^2 m_j^o(\boldsymbol{\gamma}^o)/\left(\partial\mathbf{u}\partial\mathbf{t}^T\right)$, $\partial^2 m_j^o(\boldsymbol{\gamma}^o)/\left(\partial\mathbf{u}\partial\mathbf{s}_j^T\right)$ and $\partial^2 m_j^o(\boldsymbol{\gamma}^o)/\left(\partial\mathbf{t}\partial\mathbf{s}_j^T\right)$. Their values for the four approaches are as follows.

B.2.1 $\mathrm{SE_f}$ Positioning

From (2.5), we have

$$\frac{\partial^2 m_{\mathrm{SE},j}^o(\boldsymbol{\gamma}^o)}{\partial\mathbf{u}\partial\mathbf{u}^T} = \frac{1}{||\mathbf{u}^o-\mathbf{t}^o||}\mathbf{P}_{\mathbf{u}^o,\mathbf{t}^o}^{\perp} + \frac{1}{||\mathbf{u}^o-\mathbf{s}_j^o||}\mathbf{P}_{\mathbf{u}^o,\mathbf{s}_j^o}^{\perp}, \tag{B.11a}$$

$$\frac{\partial^2 m_{\mathrm{SE},j}^o(\boldsymbol{\gamma}^o)}{\partial\mathbf{t}\partial\mathbf{t}^T} = -\frac{\partial^2 m_{\mathrm{SE},j}^o(\boldsymbol{\gamma}^o)}{\partial\mathbf{u}\partial\mathbf{t}^T} = \frac{1}{||\mathbf{u}^o-\mathbf{t}^o||}\mathbf{P}_{\mathbf{u}^o,\mathbf{t}^o}^{\perp}, \tag{B.11b}$$

$$\frac{\partial^2 m_{\mathrm{SE},j}^o(\boldsymbol{\gamma}^o)}{\partial\mathbf{s}_j\partial\mathbf{s}_j^T} = -\frac{\partial^2 m_{\mathrm{SE},j}^o(\boldsymbol{\gamma}^o)}{\partial\mathbf{u}\partial\mathbf{s}_j^T} = \frac{1}{||\mathbf{u}^o-\mathbf{s}_j^o||}\mathbf{P}_{\mathbf{u}^o,\mathbf{s}_j^o}^{\perp}, \tag{B.11c}$$

$$\frac{\partial^2 m_{\mathrm{SE},j}^o(\boldsymbol{\gamma}^o)}{\partial\mathbf{t}\partial\mathbf{s}_j^T} = \mathbf{O}_{K\times K}. \tag{B.11d}$$

Also, from (2.6),

$$\frac{\partial^2 \bar{m}_{\mathrm{SE},j}^o(\boldsymbol{\gamma}^o)}{\partial\mathbf{t}\partial\mathbf{t}^T} = \frac{\partial^2 \bar{m}_{\mathrm{SE},j}^o(\boldsymbol{\gamma}^o)}{\partial\mathbf{s}_j\partial\mathbf{s}_j^T} = -\frac{\partial^2 \bar{m}_{\mathrm{SE},j}^o(\boldsymbol{\gamma}^o)}{\partial\mathbf{t}\partial\mathbf{s}_j^T} = \frac{1}{||\mathbf{t}^o-\mathbf{s}_j^o||}\mathbf{P}_{\mathbf{t}^o,\mathbf{s}_j^o}^{\perp}, \tag{B.12a}$$

$$\frac{\partial^2 \bar{m}_{\mathrm{SE},j}^o(\boldsymbol{\gamma}^o)}{\partial\mathbf{u}\partial\mathbf{u}^T} = \frac{\partial^2 \bar{m}_{\mathrm{SE},j}^o(\boldsymbol{\gamma}^o)}{\partial\mathbf{u}\partial\mathbf{t}^T} = \frac{\partial^2 \bar{m}_{\mathrm{SE},j}^o(\boldsymbol{\gamma}^o)}{\partial\mathbf{u}\partial\mathbf{s}_j^T} = \mathbf{O}_{K\times K}. \tag{B.12b}$$

The index j is from 1 to N.

B.2.2 SE Positioning

For SE positioning, the second derivatives are given in (B.11).

B.2.3 AE Positioning

From the AE measurement model (2.7), we simply have

$$\frac{\partial^2 m^o_{\mathrm{AE},j}\left(\boldsymbol{\gamma}^o\right)}{\partial\boldsymbol{\gamma}\partial\boldsymbol{\gamma}^T} = \frac{\partial^2 m^o_{\mathrm{SE},j}\left(\boldsymbol{\gamma}^o\right)}{\partial\boldsymbol{\gamma}\partial\boldsymbol{\gamma}^T} - \frac{\partial^2 \bar{m}^o_{\mathrm{SE},j}\left(\boldsymbol{\gamma}^o\right)}{\partial\boldsymbol{\gamma}\partial\boldsymbol{\gamma}^T}\,, \quad j = 1\,, 2\,, \ldots\,, N\,. \tag{B.13}$$

Appendix C

Appendices for Chapter 5

C.1 The WLS Optimization of $\boldsymbol{\gamma}_1^o$

The matrices $\mathbf{K}_1$, $\mathbf{D}_1$ and $\mathbf{F}_1$ in (5.9) are defined as

$$\mathbf{K}_1 = \left[\, \mathbf{K}_{1_1}^T,\, \mathbf{K}_{1_2}^T,\, \cdots,\, \mathbf{K}_{1_M}^T \,\right]^T, \mathbf{K}_{1_i} = \mathrm{diag}\left(\, \mathbf{K}_{1_{i,1}},\, \mathbf{K}_{1_{i,2}},\, \cdots,\, \mathbf{K}_{1_{i,N}} \,\right), \mathbf{K}_{1_{i,j}} = \frac{1}{c}\mathbf{1}_L \boldsymbol{\rho}_{\mathbf{u}_i^o,\mathbf{s}_j}^T,$$

$$\mathbf{D}_1 = \left[\, \mathbf{D}_{1_1}^T,\, \mathbf{D}_{1_2}^T,\, \cdots,\, \mathbf{D}_{1_M}^T \,\right]^T, \mathbf{D}_{1_i} = \mathrm{diag}\left(\, \mathbf{d}_{1_{i,1}},\, \mathbf{d}_{1_{i,2}},\, \cdots,\, \mathbf{d}_{1_{i,N}} \right),$$

$$\mathbf{d}_{1_{i,j}} = \left[\, R_{i,j,1} - \omega_{\mathbf{s}_j},\, \omega_{\mathbf{s}_j} - T_{i,j,2},\, \cdots,\, \omega_{\mathbf{s}_j} - T_{i,j,L} \,\right]^T, \mathbf{F}_1 = \left[\, \mathbf{F}_{1_1}^T,\, \mathbf{F}_{1_2}^T,\, \cdots,\, \mathbf{F}_{1_M}^T \,\right]^T,$$

$$\mathbf{F}_{1_i} = \mathrm{diag}\left(\, \mathbf{f}_{1_{i,1}},\, \mathbf{f}_{1_{i,2}},\, \cdots,\, \mathbf{f}_{1_{i,N}} \right), \mathbf{f}_{1_{i,j}} = \left[\, -\left(1 + \varepsilon_{\mathbf{s}_j}\right),\, 1 + \varepsilon_{\mathbf{s}_j},\, \cdots,\, 1 + \varepsilon_{\mathbf{s}_j} \,\right]^T.$$

The details of the vector $\mathbf{h}_1 = \left[\, \mathbf{h}_{1_1}^T,\, \mathbf{h}_{1_2}^T,\, \cdots,\, \mathbf{h}_{1_M}^T \,\right]^T$ and the matrix $\mathbf{G}_1 =$

$\text{diag}\,(\,\mathbf{G}_{1_1},\,\mathbf{G}_{1_2},\,\cdots,\,\mathbf{G}_{1_M}\,)$ are

$$\mathbf{h}_{1_i} = \begin{bmatrix} \mathbf{h}_{1_{i,1}} \\ \mathbf{h}_{1_{i,2}} \\ \vdots \\ \mathbf{h}_{1_{i,N}} \end{bmatrix}, \quad \mathbf{h}_{1_{i,j}} = \begin{bmatrix} \left(R_{i,j,1} - \omega_{\mathbf{s}_j}\right)\left(1 + \varepsilon_{\mathbf{s}_j}\right) - T_{i,j,1} \\ \left(\omega_{\mathbf{s}_j} - T_{i,j,2}\right)\left(1 + \varepsilon_{\mathbf{s}_j}\right) + R_{i,j,2} \\ \vdots \\ \left(\omega_{\mathbf{s}_j} - T_{i,j,L}\right)\left(1 + \varepsilon_{\mathbf{s}_j}\right) + R_{i,j,L} \end{bmatrix}, \tag{C.1a}$$

$$\mathbf{G}_{1_i} = \begin{bmatrix} \mathbf{G}_{1_{i,1}} \\ \mathbf{G}_{1_{i,2}} \\ \vdots \\ \mathbf{G}_{1_{i,N}} \end{bmatrix}, \quad \mathbf{G}_{1_{i,j}} = \begin{bmatrix} T_{i,j,1} & -1 & \mathbf{O}_{1\times j-1} & \frac{1}{c} & \mathbf{O}_{1\times N-j} \\ -R_{i,j,2} & 1 & \mathbf{O}_{1\times j-1} & \frac{1}{c} & \mathbf{O}_{1\times N-j} \\ \vdots & \vdots & \vdots & \vdots & \vdots \\ -R_{i,j,L} & 1 & \mathbf{O}_{1\times j-1} & \frac{1}{c} & \mathbf{O}_{1\times N-j} \end{bmatrix}. \tag{C.1b}$$

The WLS solution to (5.9) is

$$\hat{\boldsymbol{\gamma}}_1 = \left(\mathbf{G}_1^T \mathbf{W}_1 \mathbf{G}_1\right)^{-1} \mathbf{G}_1^T \mathbf{W}_1 \mathbf{h}_1 \tag{C.2}$$

and the weighting matrix is

$$\mathbf{W}_1 = \left(\mathbf{Q_m} + [\,\mathbf{K}_1,\,\mathbf{D}_1,\,\mathbf{F}_1\,]\,\mathbf{Q_b}\,[\,\mathbf{K}_1,\,\mathbf{D}_1,\,\mathbf{F}_1\,]^T\right)^{-1}. \tag{C.3}$$

When the noises in $\mathbf{K}_1$, $\mathbf{D}_1$, $\mathbf{F}_1$ and $\mathbf{G}_1$ are relatively small,

$$\text{cov}\,(\hat{\boldsymbol{\gamma}}_1) = \left(\mathbf{G}_1^T \mathbf{W}_1 \mathbf{G}_1\right)^{-1}. \tag{C.4}$$

The size of the matrix to be inverted in (C.3) is $MNL \times MNL$, it can be large and presents difficulty in the inversion. Note that $\mathbf{Q_b}$ is $4N \times 4N$ whose inverse is

easier to compute. When $\mathbf{Q_m}$ is diagonal or block diagonal, which is often the case in practice, the inverse in (C.3) can be computed very efficiently in terms of $\mathbf{Q_m}^{-1}$ and $\mathbf{Q_b}^{-1}$ using the Matrix Inversion Lemma.

Obtaining $\mathbf{K}_1$ to form $\mathbf{W}_1$ requires the true node positions that are yet to be found. To handle this difficulty, we shall set $\mathbf{K}_1$ to zero and generate a rough solution using (C.2). This rough estimate essentially pretends the beacon positions do not have uncertainties. $\mathbf{K}_1$ is then built using this initial estimate, a more accurate $\mathbf{W}_1$ can be formed and a better stage-1 solution can be obtained. Although $\mathbf{K}_1$ is only approximated, experimental results indicate the resulting degradation in the stage-1 solution is negligible. This is because the WLS solution is insensitive to the error in the weighting matrix [108].

C.2 The WLS Optimization of $\boldsymbol{\gamma}_2^o$

The terms $\mathbf{B}_2$, $\mathbf{h}_2$ and $\mathbf{G}_2$ in (5.13) are

$$\mathbf{B}_2 = \mathrm{diag}\left(\mathbf{B}_{2_1}, \mathbf{B}_{2_2}, \cdots, \mathbf{B}_{2_M}\right), \mathbf{B}_{2_i} = \begin{bmatrix} 1 & 0 & 0 & \cdots & 0 \\ -\omega^o_{\mathbf{u}_i} & 1 & 0 & \cdots & 0 \\ 0 & 0 & 2||\mathbf{u}_i^o - \mathbf{s}_1|| & \cdots & 0 \\ \vdots & \vdots & \vdots & \ddots & \vdots \\ 0 & 0 & 0 & \cdots & 2||\mathbf{u}_i^o - \mathbf{s}_N|| \end{bmatrix}, \tag{C.5a}$$

$$\mathbf{h}_2 = \left[\mathbf{h}_{2_1}^T, \cdots, \mathbf{h}_{2_M}^T\right]^T, \mathbf{h}_{2_i} = \left[\hat{\gamma}_{1_i}(1), \hat{\gamma}_{1_i}(2), \hat{\gamma}_{1_i}(3)^2 - \mathbf{s}_1^T\mathbf{s}_1, \cdots, \hat{\gamma}_{1_i}(N+2)^2 - \mathbf{s}_N^T\mathbf{s}_N\right]^T, \tag{C.5b}$$

$$\mathbf{G}_2 = \text{diag}\left(\mathbf{G}_{2_1}, \mathbf{G}_{2_2}, \cdots, \mathbf{G}_{2_M}\right), \mathbf{G}_{2_i} = \begin{bmatrix} 1 & 0 & 0 & \mathbf{0}_2^T \\ 0 & (1+\hat{\gamma}_{1_i}(1)) & 0 & \mathbf{0}_2^T \\ 0 & 0 & 1 & -2\mathbf{s}_1^T \\ \vdots & \vdots & \vdots & \vdots \\ 0 & 0 & 1 & -2\mathbf{s}_N^T \end{bmatrix}. \quad \text{(C.5c)}$$

The WLS solution to (5.13) is

$$\hat{\boldsymbol{\gamma}}_2 = \left(\mathbf{G}_2^T \mathbf{W}_2 \mathbf{G}_2\right)^{-1} \mathbf{G}_2^T \mathbf{W}_2 \mathbf{h}_2 \quad \text{(C.6)}$$

where $\mathbf{W}_2 = \left(\mathbf{B}_2 \text{cov}\left(\hat{\boldsymbol{\gamma}}_1\right) \mathbf{B}_2^T\right)^{-1}$. Using (C.4), $\mathbf{W}_2$ can be obtained easily as

$$\mathbf{W}_2 = \mathbf{B}_2^{-T} \left(\mathbf{G}_1^T \mathbf{W}_1 \mathbf{G}_1\right) \mathbf{B}_2^{-1}. \quad \text{(C.7)}$$

When the noise components in $\mathbf{B}_2$ and $\mathbf{G}_2$ are relatively insignificant,

$$\text{cov}\left(\hat{\boldsymbol{\gamma}}_2\right) = \left(\mathbf{G}_2^T \mathbf{W}_2 \mathbf{G}_2\right)^{-1}. \quad \text{(C.8)}$$

The matrix $\mathbf{B}_2$ contains the true clock offsets and the true sensor node to beacon distances. They will be replaced by the solution from the first stage and the degradation in performance is negligible.

C.3 The WLS Optimization of $\boldsymbol{\gamma}_3^o$

The matrices and vector $\mathbf{B}_3$, $\mathbf{h}_3$ and $\mathbf{G}_3$ in (5.16) are defined as

$$\mathbf{B}_3 = \text{diag}\left(\mathbf{B}_{3_1}, \mathbf{B}_{3_2}, \cdots, \mathbf{B}_{3_M}\right), \mathbf{B}_{3_i} = \text{diag}\left(1,\, 1,\, 1,\, 2x^o_{\mathbf{u}_i},\, 2y^o_{\mathbf{u}_i}\right), \tag{C.9a}$$

$$\mathbf{h}_3 = \left[\mathbf{h}_{3_1}^T, \cdots, \mathbf{h}_{3_M}^T\right]^T, \mathbf{h}_{3_i} = \left[\hat{\boldsymbol{\gamma}}_{2_i}(1:3)^T,\, \left(\hat{\boldsymbol{\gamma}}_{2_i}(4:5) \odot \hat{\boldsymbol{\gamma}}_{2_i}(4:5)\right)^T\right]^T, \tag{C.9b}$$

$$\mathbf{G}_3 = \text{diag}\left(\mathbf{G}_{3_1}, \mathbf{G}_{3_2}, \cdots, \mathbf{G}_{3_M}\right), \mathbf{G}_{3_i} = \begin{bmatrix} 1 & 0 & 0 & 0 & 0 \\ 0 & 1 & 0 & 0 & 0 \\ 0 & 0 & 1 & 1 & 0 \\ 0 & 0 & 1 & 0 & 1 \end{bmatrix}^T. \tag{C.9c}$$

The WLS solution of $\boldsymbol{\gamma}_3^o$ is

$$\hat{\boldsymbol{\gamma}}_3 = \left(\mathbf{G}_3^T \mathbf{W}_3 \mathbf{G}_3\right)^{-1} \mathbf{G}_3^T \mathbf{W}_3 \mathbf{h}_3 \tag{C.10}$$

and the weighting matrix is

$$\mathbf{W}_3 = \left(\mathbf{B}_3 \text{cov}\left(\hat{\boldsymbol{\gamma}}_2\right) \mathbf{B}_3^T\right)^{-1} = \mathbf{B}_3^{-T} \left(\mathbf{G}_2^T \mathbf{W}_2 \mathbf{G}_2\right) \mathbf{B}_3^{-1}. \tag{C.11}$$

The covariance matrix of $\hat{\boldsymbol{\gamma}}_3$ is

$$\text{cov}\left(\hat{\boldsymbol{\gamma}}_3\right) = \left(\mathbf{G}_3^T \mathbf{W}_3 \mathbf{G}_3\right)^{-1}. \tag{C.12}$$

The matrix $\mathbf{B}_3$ depends on the true sensor node positions. They will be replaced by the solution from the second stage and the resulting loss in accuracy is negligible.

C.4 The WLS Optimization of $\widetilde{\boldsymbol{\gamma}}_1^o$

The vector $\check{\mathbf{h}}_1$ and matrix $\check{\mathbf{G}}_1$ in (5.22) are

$$\check{\mathbf{h}}_1 = \Big[\, \check{\mathbf{h}}_{1_1}^T,\, \check{\mathbf{h}}_{1_2}^T,\, \cdots,\, \check{\mathbf{h}}_{1_{M-1}}^T \,\Big]^T, \check{\mathbf{h}}_{1_i} = \Big[\, \check{\mathbf{h}}_{1_{i,i+1}}^T,\, \check{\mathbf{h}}_{1_{i,i+2}}^T,\, \cdots,\, \check{\mathbf{h}}_{1_{i,M}}^T \,\Big]^T, \tag{C.13a}$$

$$\check{\mathbf{h}}_{1_{i,k}} = \big[\, \check{R}_{i,k,1} - \check{T}_{i,k,1},\, \check{R}_{i,k,2} - \check{T}_{i,k,2},\, \cdots,\, \check{R}_{i,k,L} - \check{T}_{i,k,L} \,\big]^T, \tag{C.13b}$$

$$\check{\mathbf{G}}_1 = \Big[\, \check{\mathbf{G}}_{1_1}^T,\, \check{\mathbf{G}}_{1_2}^T,\, \cdots,\, \check{\mathbf{G}}_{1_{M-1}}^T \,\Big]^T, \check{\mathbf{G}}_{1_i} = \Big[\, \check{\mathbf{G}}_{1_{i,i+1}}^T,\, \check{\mathbf{G}}_{1_{i,i+2}}^T,\, \cdots,\, \check{\mathbf{G}}_{1_{i,M}}^T \,\Big]^T, \tag{C.13c}$$

$$\check{\mathbf{G}}_{1_{i,k}} = \begin{bmatrix} \mathbf{0}_{(2+N)(i-1)}^T & \check{T}_{i,k,1} & -1 & \mathbf{0}_{((2+N)(k-i)-2)}^T & -\check{R}_{i,k,1} & 1 & \mathbf{0}_{c_1}^T & \frac{1}{c} & \mathbf{0}_{c_2}^T \\ \mathbf{0}_{(2+N)(i-1)}^T & -\check{R}_{i,k,2} & 1 & \mathbf{0}_{((2+N)(k-i)-2)}^T & \check{T}_{i,k,2} & -1 & \mathbf{0}_{c_1}^T & \frac{1}{c} & \mathbf{0}_{c_2}^T \\ \vdots & \vdots & \vdots & \vdots & \vdots & \vdots & \vdots & \vdots & \vdots \\ \mathbf{0}_{(2+N)(i-1)}^T & -\check{R}_{i,k,L} & 1 & \mathbf{0}_{((2+N)(k-i)-2)}^T & \check{T}_{i,k,L} & -1 & \mathbf{0}_{c_1}^T & \frac{1}{c} & \mathbf{0}_{c_2}^T \end{bmatrix}. \tag{C.13d}$$

where $c_1 = (2+N)(M-k+1)+\frac{(2M-i)(i-1)}{2}+k-i-3$, $c_2 = \frac{M(M-1)}{2} - \Big(\frac{(2M-i)(i-1)}{2} + k - i\Big)$.

The matrices and vectors in (5.24) are defined as $\widetilde{\mathbf{K}}_1 = \Big[\, \mathbf{K}_1^T,\, \mathbf{O}_{\frac{M(M-1)L}{2}\times 2N}^T \,\Big]^T$, $\widetilde{\mathbf{D}}_1 = \Big[\, \mathbf{D}_1^T,\, \mathbf{O}_{\frac{M(M-1)L}{2}\times N}^T \,\Big]^T$, $\widetilde{\mathbf{F}}_1 = \Big[\, \mathbf{F}_1^T,\, \mathbf{O}_{\frac{M(M-1)L}{2}\times N}^T \,\Big]^T$, $\widetilde{\mathbf{h}}_1 = \big[\, \mathbf{h}_1^T,\, \check{\mathbf{h}}_1^T \,\big]^T$ and $\widetilde{\mathbf{G}}_1 = \Big[\, \Big[\, \mathbf{G}_1,\, \mathbf{O}_{MNL\times\frac{M(M-1)}{2}} \,\Big]^T,\ \check{\mathbf{G}}_1^T \,\Big]^T$. The solution to (5.24) is

$$\hat{\widetilde{\boldsymbol{\gamma}}}_1 = \Big(\widetilde{\mathbf{G}}_1^T \widetilde{\mathbf{W}}_1 \widetilde{\mathbf{G}}_1\Big)^{-1} \widetilde{\mathbf{G}}_1^T \widetilde{\mathbf{W}}_1 \widetilde{\mathbf{h}}_1 \tag{C.14}$$

and $\widetilde{\mathbf{W}}_1$ is

$$\widetilde{\mathbf{W}}_1 = \Big(\mathbf{Q}_{\tilde{\mathbf{m}}} + \Big[\, \widetilde{\mathbf{K}}_1,\, \widetilde{\mathbf{D}}_1,\, \widetilde{\mathbf{F}}_1 \,\Big]\, \mathbf{Q}_{\mathbf{b}} \Big[\, \widetilde{\mathbf{K}}_1,\, \widetilde{\mathbf{D}}_1,\, \widetilde{\mathbf{F}}_1 \,\Big]^T\Big)^{-1}. \tag{C.15}$$

When the timing measurement noise and beacon uncertainties are small,

$$\mathrm{cov}\left(\hat{\widetilde{\boldsymbol{\gamma}}}_1\right) = \left(\widetilde{\mathbf{G}}_1^T \widetilde{\mathbf{W}}_1 \widetilde{\mathbf{G}}_1\right)^{-1}. \tag{C.16}$$

The matrix to be inverted in (C.15) has a large size of $MNL + \frac{M(M-1)}{2}L$. In the case when $\mathbf{n_m}$ and $\mathbf{n_{\check{m}}}$ are uncorrelated, the inverse can be computed easily because it is a block diagonal matrix with diagonal blocks $\mathbf{W}_1$ and $\mathbf{Q}_{\mathbf{\check{m}}}^{-1}$, where $\mathbf{Q_{\check{m}}}$ is the lower right $\frac{M(M-1)}{2}L$ block of $\mathbf{Q_{\widetilde{m}}}$.

The matrix $\widetilde{\mathbf{K}}_1$ is formed by $\mathbf{K}_1$ and it is dependent on the true parameter values as shown in Appendix C.1. We shall use the unknown node positions from Section 5.2 to approximate the true values in $\mathbf{K}_1$ and the resulting degradation is negligible.

C.5 The WLS Optimization of $\widetilde{\boldsymbol{\gamma}}_2^o$

In the expression (5.27),

$$\widetilde{\mathbf{h}}_2 = \left[\mathbf{h}_2^{'T}, \check{\mathbf{h}}_2^T\right]^T, \mathbf{h}_2^{'} = \left[\mathbf{h}_{2_1}^{'T}, \mathbf{h}_{2_2}^{'T}, \cdots, \mathbf{h}_{2_M}^{'T}\right]^T, \tag{C.17a}$$

$$\mathbf{h}_{2_i}^{'} = \begin{bmatrix} \widetilde{\gamma}_1((i-1)(2+N)+1) \\ \widetilde{\gamma}_1((i-1)(2+N)+2) \\ \widetilde{\gamma}_1((i-1)(2+N)+3)^2 - ||\mathbf{u}_i^* - \mathbf{s}_1||^2 \\ \vdots \\ \widetilde{\gamma}_1((2+N)i)^2 - ||\mathbf{u}_i^* - \mathbf{s}_N||^2 \end{bmatrix}, \tag{C.17b}$$

$$\check{\mathbf{h}}_2 = \begin{bmatrix} \widetilde{\gamma}_1((2+N)M+1)^2 - ||\mathbf{u}_1^* - \mathbf{u}_2^*||^2 \\ \vdots \\ \widetilde{\gamma}_1\left((2+N)M + \frac{M(M-1)}{2}\right)^2 - ||\mathbf{u}_{M-1}^* - \mathbf{u}_M^*||^2 \end{bmatrix}, \tag{C.17c}$$

$$\widetilde{\mathbf{G}}_2 = \left[\mathbf{G}_2^{\prime T},\, \check{\mathbf{G}}_2^T\right]^T, \mathbf{G}_2^{\prime} = \mathrm{diag}\left(\mathbf{G}_{2_1}^{\prime},\, \mathbf{G}_{2_2}^{\prime},\, \cdots,\, \mathbf{G}_{2_M}^{\prime}\right), \tag{C.17d}$$

$$\mathbf{G}_{2_i}^{\prime} = \begin{bmatrix} 1 & 0 & \mathbf{0}_2^T \\ 0 & (1+\widetilde{\gamma}_1((i-1)(2+N)+1)) & \mathbf{0}_2^T \\ 0 & 0 & 2\left(\mathbf{u}_i^* - \mathbf{s}_1\right)^T \\ \vdots & \vdots & \vdots \\ 0 & 0 & 2\left(\mathbf{u}_i^* - \mathbf{s}_N\right)^T \end{bmatrix}, \tag{C.17e}$$

$$\check{\mathbf{G}}_2 = 2\begin{bmatrix} \check{\mathbf{g}}_{2_{1,2}}^T & \check{\mathbf{g}}_{2_{2,1}}^T & \mathbf{0}_4^T & \mathbf{0}_4^T & \cdots & \mathbf{0}_4^T & \mathbf{0}_4^T \\ \check{\mathbf{g}}_{2_{1,3}}^T & \mathbf{0}_4^T & \check{\mathbf{g}}_{2_{3,1}}^T & \mathbf{0}_4^T & \cdots & \mathbf{0}_4^T & \mathbf{0}_4^T \\ \vdots & \vdots & \vdots & \vdots & \ddots & \vdots & \vdots \\ \mathbf{0}_4^T & \mathbf{0}_4^T & \mathbf{0}_4^T & \mathbf{0}_4^T & \cdots & \check{\mathbf{g}}_{2_{M-1,M}}^T & \check{\mathbf{g}}_{2_{M,M-1}}^T \end{bmatrix}, \check{\mathbf{g}}_{2_{i,k}} = \begin{bmatrix} 0 \\ 0 \\ \mathbf{u}_i^* - \mathbf{u}_k^* \end{bmatrix}, \tag{C.17f}$$

$$\widetilde{\mathbf{B}}_2 = \mathrm{diag}\left(\mathbf{B}_2,\, \check{\mathbf{B}}_2\right), \check{\mathbf{B}}_2 = 2\mathrm{diag}\left(\check{\gamma}_1^o(1),\, \check{\gamma}_1^o(2),\, \cdots,\, \check{\gamma}_1^o\left(\frac{M(M-1)}{2}\right)\right), \tag{C.17g}$$

and $\mathbf{B}_2$ is defined in (C.5a).

The solution to (5.27) is

$$\hat{\widetilde{\gamma}}_2 = \left(\widetilde{\mathbf{G}}_2^T \widetilde{\mathbf{W}}_2 \widetilde{\mathbf{G}}_2\right)^{-1} \widetilde{\mathbf{G}}_2^T \widetilde{\mathbf{W}}_2 \widetilde{\mathbf{h}}_2 \tag{C.18}$$

and

$$\widetilde{\mathbf{W}}_2 = \left(\widetilde{\mathbf{B}}_2 \mathrm{cov}\left(\hat{\widetilde{\gamma}}_1\right) \widetilde{\mathbf{B}}_2^T\right)^{-1}. \tag{C.19}$$

When the noise in $\widetilde{\mathbf{B}}_2$ and $\widetilde{\mathbf{G}}_2$ are relatively small, the covariance matrix of $\widetilde{\boldsymbol{\gamma}}_2$ is

$$\mathrm{cov}\left(\hat{\widetilde{\boldsymbol{\gamma}}}_2\right) = \left(\widetilde{\mathbf{G}}_2^T \widetilde{\mathbf{W}}_2 \widetilde{\mathbf{G}}_2\right)^{-1}. \tag{C.20}$$

The matrix $\widetilde{\mathbf{B}}_2$ depends on the true parameter values. They will be approximated by using $\widetilde{\boldsymbol{\gamma}}_1$ to obtain $\widetilde{\mathbf{B}}_2$ and the loss in performance is negligible.

C.6 CRLB Derivation

We shall derive the CRLB of the unknown node parameter vector $\boldsymbol{\eta}^o$ defined in (5.1) using the time stamp information. For the timing measurement relationship in (5.4) between the unknown nodes and the beacons, we define the vectors $\mathbf{p} = \left[\, \mathbf{p}_1^T,\, \mathbf{p}_2^T,\, \cdots,\, \mathbf{p}_M^T \,\right]^T$ and $\mathbf{q} = \left[\, \mathbf{q}_1^T,\, \mathbf{q}_2^T,\, \cdots,\, \mathbf{q}_M^T \,\right]^T$, where

$$\mathbf{p}_i = \left[\, \mathbf{p}_{i,1}^T,\, \mathbf{p}_{i,2}^T,\, \cdots,\, \mathbf{p}_{i,N}^T \,\right]^T, \mathbf{q}_i = \left[\, \mathbf{q}_{i,1}^T,\, \mathbf{q}_{i,2}^T,\, \cdots,\, \mathbf{q}_{i,N}^T \,\right]^T, \tag{C.21}$$

$$\mathbf{p}_{i,j} = \begin{bmatrix} \left(R_{i,j,1} - \omega_{\mathbf{s}_j}^o\right)\left(1 + \varepsilon_{\mathbf{s}_j}^o\right) \\ \left(R_{i,j,2} - \omega_{\mathbf{u}_i}^o\right)\left(1 + \varepsilon_{\mathbf{u}_i}^o\right) \\ \vdots \\ \left(R_{i,j,L} - \omega_{\mathbf{u}_i}^o\right)\left(1 + \varepsilon_{\mathbf{u}_i}^o\right) \end{bmatrix}, \mathbf{q}_{i,j} = \begin{bmatrix} \left(T_{i,j,1} - \omega_{\mathbf{u}_i}^o\right)\left(1 + \varepsilon_{\mathbf{u}_i}^o\right) + \frac{||\mathbf{u}_i^o - \mathbf{s}_j^o||}{c} \\ \left(T_{i,j,2} - \omega_{\mathbf{s}_j}^o\right)\left(1 + \varepsilon_{\mathbf{s}_j}^o\right) + \frac{||\mathbf{u}_i^o - \mathbf{s}_j^o||}{c} \\ \vdots \\ \left(T_{i,j,L} - \omega_{\mathbf{s}_j}^o\right)\left(1 + \varepsilon_{\mathbf{s}_j}^o\right) + \frac{||\mathbf{u}_i^o - \mathbf{s}_j^o||}{c} \end{bmatrix}. \tag{C.22}$$

For the timing measurements between two unknown nodes, the corresponding timing vectors are $\check{\mathbf{p}} = \left[\, \check{\mathbf{p}}_1^T,\, \check{\mathbf{p}}_2^T,\, \cdots,\, \check{\mathbf{p}}_{M-1}^T \,\right]^T$ and $\check{\mathbf{q}} = \left[\, \check{\mathbf{q}}_1^T,\, \check{\mathbf{q}}_2^T,\, \cdots,\, \check{\mathbf{q}}_{M-1}^T \,\right]^T$, where

$$\check{\mathbf{p}}_i = \left[\, \check{\mathbf{p}}_{i,i+1}^T,\, \check{\mathbf{p}}_{i,i+2}^T,\, \cdots,\, \check{\mathbf{p}}_{i,M}^T \right]^T, \check{\mathbf{q}}_i = \left[\, \check{\mathbf{q}}_{i,i+1}^T,\, \check{\mathbf{q}}_{i,i+2}^T,\, \cdots,\, \check{\mathbf{q}}_{i,M}^T \right]^T, \tag{C.23}$$

$$\check{\mathbf{p}}_{i,k} = \begin{bmatrix} \left(\check{R}_{i,k,1} - \omega^o_{\mathbf{u}_k}\right)\left(1+\varepsilon^o_{\mathbf{u}_k}\right) \\ \left(\check{R}_{i,k,2} - \omega^o_{\mathbf{u}_i}\right)\left(1+\varepsilon^o_{\mathbf{u}_i}\right) \\ \vdots \\ \left(\check{R}_{i,k,L} - \omega^o_{\mathbf{u}_i}\right)\left(1+\varepsilon^o_{\mathbf{u}_i}\right) \end{bmatrix}, \check{\mathbf{q}}_{i,k} = \begin{bmatrix} \left(\check{T}_{i,k,1} - \omega^o_{\mathbf{u}_i}\right)\left(1+\varepsilon^o_{\mathbf{u}_i}\right) + \frac{||\mathbf{u}^o_i - \mathbf{u}^o_k||}{c} \\ \left(\check{T}_{i,k,2} - \omega^o_{\mathbf{u}_k}\right)\left(1+\varepsilon^o_{\mathbf{u}_k}\right) + \frac{||\mathbf{u}^o_i - \mathbf{u}^o_k||}{c} \\ \vdots \\ \left(\check{T}_{i,k,L} - \omega^o_{\mathbf{u}_k}\right)\left(1+\varepsilon^o_{\mathbf{u}_k}\right) + \frac{||\mathbf{u}^o_i - \mathbf{u}^o_k||}{c} \end{bmatrix}. \tag{C.24}$$

Using $\mathbf{b}^o = \left[\, \mathbf{s}^{oT},\, \boldsymbol{\varepsilon}^{oT}_{\mathbf{s}},\, \boldsymbol{\omega}^{oT}_{\mathbf{s}} \,\right]^T$ in (5.2) as nuisance variables and $\boldsymbol{\eta}^o = \left[\, \boldsymbol{\eta}^{oT}_1,\, \boldsymbol{\eta}^{oT}_2,\, \cdots,\, \boldsymbol{\eta}^{oT}_M \,\right]^T$ in (5.1), where $\boldsymbol{\eta}^o_i = \left[\, \varepsilon^o_{\mathbf{u}_i},\, \omega^o_{\mathbf{u}_i},\, \mathbf{u}^{oT}_i \,\right]^T$, we have the logarithm of the probability density function

$$\ln p\left(\widetilde{\mathbf{p}}, \widetilde{\mathbf{q}}, \mathbf{b}; \boldsymbol{\eta}^o, \mathbf{b}^o\right) = C - \frac{1}{2}\left(\widetilde{\mathbf{p}} - \widetilde{\mathbf{q}}\right)^T \mathbf{Q}_{\widetilde{\mathbf{m}}}{}^{-1}\left(\widetilde{\mathbf{p}} - \widetilde{\mathbf{q}}\right) - \frac{1}{2}\left(\mathbf{b} - \mathbf{b}^o\right)^T \mathbf{Q}^{-1}_{\mathbf{b}}\left(\mathbf{b} - \mathbf{b}^o\right) \tag{C.25}$$

where $\widetilde{\mathbf{p}} = \left[\, \mathbf{p}^T,\, \check{\mathbf{p}}^T \,\right]^T$ and $\widetilde{\mathbf{q}} = \left[\, \mathbf{q}^T,\, \check{\mathbf{q}}^T \,\right]^T$. The FIM is

$$\mathrm{FIM} = \begin{bmatrix} \mathrm{FIM}_{\boldsymbol{\eta}\boldsymbol{\eta}} & \mathrm{FIM}_{\boldsymbol{\eta}\mathbf{b}} \\ \mathrm{FIM}^T_{\boldsymbol{\eta}\mathbf{b}} & \mathrm{FIM}_{\mathbf{b}\mathbf{b}} \end{bmatrix} = \mathrm{E}\begin{bmatrix} \frac{\partial(\widetilde{\mathbf{p}}-\widetilde{\mathbf{q}})^T}{\partial \boldsymbol{\eta}^o}\mathbf{Q}^{-1}_{\widetilde{\mathbf{m}}}\frac{\partial(\widetilde{\mathbf{p}}-\widetilde{\mathbf{q}})}{\partial \boldsymbol{\eta}^{oT}} & \frac{\partial(\widetilde{\mathbf{p}}-\widetilde{\mathbf{q}})^T}{\partial \boldsymbol{\eta}^o}\mathbf{Q}^{-1}_{\widetilde{\mathbf{m}}}\frac{\partial(\widetilde{\mathbf{p}}-\widetilde{\mathbf{q}})}{\partial \mathbf{b}^{oT}} \\ \frac{\partial(\widetilde{\mathbf{p}}-\widetilde{\mathbf{q}})^T}{\partial \mathbf{b}^o}\mathbf{Q}^{-1}_{\widetilde{\mathbf{m}}}\frac{\partial(\widetilde{\mathbf{p}}-\widetilde{\mathbf{q}})}{\partial \boldsymbol{\eta}^{oT}} & \frac{\partial(\widetilde{\mathbf{p}}-\widetilde{\mathbf{q}})^T}{\partial \mathbf{b}^o}\mathbf{Q}^{-1}_{\widetilde{\mathbf{m}}}\frac{\partial(\widetilde{\mathbf{p}}-\widetilde{\mathbf{q}})}{\partial \mathbf{b}^{oT}} + \mathbf{Q}^{-1}_{\mathbf{b}} \end{bmatrix} \tag{C.26}$$

The partial derivative $\frac{\partial(\widetilde{\mathbf{p}}-\widetilde{\mathbf{q}})}{\partial \boldsymbol{\eta}^{oT}} = \left[\, \frac{\partial(\mathbf{p}-\mathbf{q})^T}{\partial \boldsymbol{\eta}^o},\, \frac{\partial(\check{\mathbf{p}}-\check{\mathbf{q}})^T}{\partial \boldsymbol{\eta}^o} \,\right]^T$. From (C.21) and (C.22),

$$\frac{\partial\left(\mathbf{p}-\mathbf{q}\right)}{\partial \boldsymbol{\eta}^{oT}} = \mathrm{diag}\left(\, \frac{\partial\left(\mathbf{p}_1 - \mathbf{q}_1\right)}{\partial \boldsymbol{\eta}^{oT}_1},\, \frac{\partial\left(\mathbf{p}_2 - \mathbf{q}_2\right)}{\partial \boldsymbol{\eta}^{oT}_2},\, \cdots,\, \frac{\partial\left(\mathbf{p}_M - \mathbf{q}_M\right)}{\partial \boldsymbol{\eta}^{oT}_M} \,\right), \tag{C.27a}$$

$$\frac{\partial\left(\mathbf{p}_i-\mathbf{q}_i\right)}{\partial\boldsymbol{\eta}_i^{oT}}=\begin{bmatrix}\frac{\partial(\mathbf{p}_{i,1}-\mathbf{q}_{i,1})}{\partial\boldsymbol{\eta}_i^{oT}}\\ \frac{\partial(\mathbf{p}_{i,2}-\mathbf{q}_{i,2})}{\partial\boldsymbol{\eta}_i^{oT}}\\ \vdots\\ \frac{\partial\left(\mathbf{p}_{i,N}-\mathbf{q}_{i,N}\right)}{\partial\boldsymbol{\eta}_i^{oT}}\end{bmatrix},\ \frac{\partial\left(\mathbf{p}_{i,j}-\mathbf{q}_{i,j}\right)}{\partial\boldsymbol{\eta}_i^{oT}}=\begin{bmatrix}\omega_{\mathbf{u}_i}^o-T_{i,j,1} & \left(1+\varepsilon_{\mathbf{u}_i}^o\right) & -\frac{1}{c}\boldsymbol{\rho}_{\mathbf{u}_i^o,\mathbf{s}_j^o}^T\\ R_{i,j,2}-\omega_{\mathbf{u}_i}^o & -\left(1+\varepsilon_{\mathbf{u}_i}^o\right) & -\frac{1}{c}\boldsymbol{\rho}_{\mathbf{u}_i^o,\mathbf{s}_j^o}^T\\ \vdots & \vdots & \vdots\\ R_{i,j,L}-\omega_{\mathbf{u}_i}^o & -\left(1+\varepsilon_{\mathbf{u}_i}^o\right) & -\frac{1}{c}\boldsymbol{\rho}_{\mathbf{u}_i^o,\mathbf{s}_j^o}^T\end{bmatrix} \tag{C.27b}$$

where $i=1,\,2,\ldots,M$ and $j=1,\,2,\ldots,N$. Using (C.23) and (C.24), we obtain

$$\frac{\partial\left(\check{\mathbf{p}}-\check{\mathbf{q}}\right)}{\partial\boldsymbol{\eta}^{oT}}=$$
$$\begin{bmatrix}\frac{\partial(\check{\mathbf{p}}_{1,2}-\check{\mathbf{q}}_{1,2})}{\partial\boldsymbol{\eta}_1^{oT}} & \frac{\partial(\check{\mathbf{p}}_{1,2}-\check{\mathbf{q}}_{1,2})}{\partial\boldsymbol{\eta}_2^{oT}} & \mathbf{O}_{L\times4} & \cdots & \mathbf{O}_{L\times4} & \mathbf{O}_{L\times4}\\ \frac{\partial(\check{\mathbf{p}}_{1,3}-\check{\mathbf{q}}_{1,3})}{\partial\boldsymbol{\eta}_1^{oT}} & \mathbf{O}_{L\times4} & \frac{\partial(\check{\mathbf{p}}_{1,3}-\check{\mathbf{q}}_{1,3})}{\partial\boldsymbol{\eta}_3^{oT}} & \cdots & \mathbf{O}_{L\times4} & \mathbf{O}_{L\times4}\\ \vdots & \vdots & \vdots & \ddots & \vdots & \vdots\\ \mathbf{O}_{L\times4} & \mathbf{O}_{L\times4} & \mathbf{O}_{L\times4} & \cdots & \frac{\partial\left(\check{\mathbf{p}}_{M-1,M}-\check{\mathbf{q}}_{M-1,M}\right)}{\partial\boldsymbol{\eta}_{M-1}^{oT}} & \frac{\partial\left(\check{\mathbf{p}}_{M-1,M}-\check{\mathbf{q}}_{M-1,M}\right)}{\partial\boldsymbol{\eta}_M^{oT}}\end{bmatrix}, \tag{C.28}$$

$$\frac{\partial\left(\check{\mathbf{p}}_{i,k}-\check{\mathbf{q}}_{i,k}\right)}{\partial\boldsymbol{\eta}_i^{oT}}=\begin{bmatrix}\omega_{\mathbf{u}_i}^o-\check{T}_{i,k,1} & \left(1+\varepsilon_{\mathbf{u}_i^o}\right) & -\frac{1}{c}\boldsymbol{\rho}_{\mathbf{u}_i^o,\mathbf{u}_k^o}^T\\ \check{R}_{i,k,2}-\omega_{\mathbf{u}_i}^o & -\left(1+\varepsilon_{\mathbf{u}_i^o}\right) & -\frac{1}{c}\boldsymbol{\rho}_{\mathbf{u}_i^o,\mathbf{u}_k^o}^T\\ \vdots & \vdots & \vdots\\ \check{R}_{i,k,L}-\omega_{\mathbf{u}_i}^o & -\left(1+\varepsilon_{\mathbf{u}_i^o}\right) & -\frac{1}{c}\boldsymbol{\rho}_{\mathbf{u}_i^o,\mathbf{u}_k^o}^T\end{bmatrix},$$

$$\frac{\partial\left(\check{\mathbf{p}}_{i,k}-\check{\mathbf{q}}_{i,k}\right)}{\partial\boldsymbol{\eta}_k^{oT}}=\begin{bmatrix}\check{R}_{i,k,1}-\omega_{\mathbf{u}_k}^o & -\left(1+\varepsilon_{\mathbf{u}_k^o}\right) & \frac{1}{c}\boldsymbol{\rho}_{\mathbf{u}_i^o,\mathbf{u}_k^o}^T\\ \omega_{\mathbf{u}_k}^o-\check{T}_{i,k,2} & \left(1+\varepsilon_{\mathbf{u}_k^o}\right) & \frac{1}{c}\boldsymbol{\rho}_{\mathbf{u}_i^o,\mathbf{u}_k^o}^T\\ \vdots & \vdots & \vdots\\ \omega_{\mathbf{u}_k}^o-\check{T}_{i,k,L} & \left(1+\varepsilon_{\mathbf{u}_k^o}\right) & \frac{1}{c}\boldsymbol{\rho}_{\mathbf{u}_i^o,\mathbf{u}_k^o}^T\end{bmatrix},$$

where $i = 1, 2, \ldots, M-1$ and $k = i, i+1, \ldots, M$. The partial derivative $\frac{\partial(\widetilde{\mathbf{p}}-\widetilde{\mathbf{q}})}{\partial \mathbf{b}^{oT}}$ is given by $\frac{\partial(\widetilde{\mathbf{p}}-\widetilde{\mathbf{q}})}{\partial \mathbf{b}^{oT}} = \begin{bmatrix} \frac{\partial(\mathbf{p}-\mathbf{q})}{\partial \mathbf{b}^{oT}} \\ \frac{\partial(\check{\mathbf{p}}-\check{\mathbf{q}})}{\partial \mathbf{b}^{oT}} \end{bmatrix} = \begin{bmatrix} \frac{\partial(\mathbf{p}-\mathbf{q})}{\partial \mathbf{b}^{oT}} \\ \mathbf{O}_{\frac{M(M-1)L}{2} \times 4N} \end{bmatrix}$ since the uncertainties from beacon positions and clock parameters have no effect on the time measurements of inter-node communications. From (C.21) and (C.22), the $((i-1)NL+1)$th row to the iNLth row of $\frac{\partial(\mathbf{p}-\mathbf{q})}{\partial \mathbf{b}^{oT}}$ is $\left[\frac{\partial(\mathbf{p}_i-\mathbf{q}_i)}{\partial \mathbf{s}^{oT}}, \frac{\partial(\mathbf{p}_i-\mathbf{q}_i)}{\partial \boldsymbol{\varepsilon}_{\mathbf{s}}^{oT}}, \frac{\partial(\mathbf{p}_i-\mathbf{q}_i)}{\partial \boldsymbol{\omega}_{\mathbf{s}}^{oT}} \right]$, where

$$\frac{\partial\left(\mathbf{p}_i - \mathbf{q}_i\right)}{\partial \mathbf{s}^{oT}} = \frac{1}{c}\mathrm{diag}\left(\mathbf{1}_L \boldsymbol{\rho}^T_{\mathbf{u}_i^o, \mathbf{s}_1^o}, \mathbf{1}_L \boldsymbol{\rho}^T_{\mathbf{u}_i^o, \mathbf{s}_2^o}, \cdots, \mathbf{1}_L \boldsymbol{\rho}^T_{\mathbf{u}_i^o, \mathbf{s}_N^o} \right), \tag{C.29a}$$

$$\frac{\partial\left(\mathbf{p}_i - \mathbf{q}_i\right)}{\partial \boldsymbol{\varepsilon}_{\mathbf{s}}^{oT}} = \mathrm{diag}\left(\frac{\partial\left(\mathbf{p}_{i,1} - \mathbf{q}_{i,1}\right)}{\partial \varepsilon^o_{\mathbf{s}_1}}, \frac{\partial\left(\mathbf{p}_{i,2} - \mathbf{q}_{i,2}\right)}{\partial \varepsilon^o_{\mathbf{s}_2}}, \cdots, \frac{\partial\left(\mathbf{p}_{i,N} - \mathbf{q}_{i,N}\right)}{\partial \varepsilon^o_{\mathbf{s}_N}} \right), \tag{C.29b}$$

$$\frac{\partial\left(\mathbf{p}_{i,j} - \mathbf{q}_{i,j}\right)}{\partial \varepsilon^o_{\mathbf{s}_j}} = \left[R_{i,j,1} - \omega^o_{\mathbf{s}_j}, \omega^o_{\mathbf{s}_j} - T_{i,j,2}, \cdots, \omega^o_{\mathbf{s}_j} - T_{i,j,L} \right]^T, \tag{C.29c}$$

$$\frac{\partial\left(\mathbf{p}_i - \mathbf{q}_i\right)}{\partial \boldsymbol{\omega}_{\mathbf{s}}^{oT}} = \mathrm{diag}\left(\frac{\partial\left(\mathbf{p}_{i,1} - \mathbf{q}_{i,1}\right)}{\partial \omega^o_{\mathbf{s}_1}}, \frac{\partial\left(\mathbf{p}_{i,2} - \mathbf{q}_{i,2}\right)}{\partial \omega^o_{\mathbf{s}_2}}, \cdots, \frac{\partial\left(\mathbf{p}_{i,N} - \mathbf{q}_{i,N}\right)}{\partial \omega^o_{\mathbf{s}_N}} \right), \tag{C.29d}$$

$$\frac{\partial\left(\mathbf{p}_{i,j} - \mathbf{q}_{i,j}\right)}{\partial \omega^o_{\mathbf{s}_j}} = \left[-\left(1 + \varepsilon^o_{\mathbf{s}_j}\right), \left(1 + \varepsilon^o_{\mathbf{s}_j}\right), \cdots, \left(1 + \varepsilon^o_{\mathbf{s}_j}\right) \right]^T, \tag{C.29e}$$

for $i = 1, 2, \ldots, M$ and $j = 1, 2, \ldots, N$.

The CRLB of $\boldsymbol{\eta}^o$ is the upper left $4M \times 4M$ submatrix of the inverse of the FIM. Applying the partitioned matrix inversion formula [22] to (C.26) gives

$$\mathrm{CRLB}_{\boldsymbol{\eta}} = \left(\mathrm{FIM}_{\boldsymbol{\eta}\boldsymbol{\eta}} - \mathrm{FIM}_{\boldsymbol{\eta}\mathbf{b}} \mathrm{FIM}^{-1}_{\mathbf{b}\mathbf{b}} \mathrm{FIM}^T_{\boldsymbol{\eta}\mathbf{b}} \right)^{-1}. \tag{C.30}$$

Eq. (C.30) is also applicable to the case of having message exchanges between the beacons and the unknown nodes only when setting $\mathbf{Q}^{-1}_{\widetilde{\mathbf{m}}}$ to $\mathrm{diag}\left(\mathbf{Q}^{-1}_{\mathbf{m}}, \mathbf{O}_{\frac{M(M-1)L}{2} \times \frac{M(M-1)L}{2}} \right)$.

C.7 Proof of Achieving the CRLB Performance

We shall show that the proposed solutions are able to achieve the CRLB accuracy. When there is no inter-node communications, the covariance matrix of proposed algorithm estimates is given by (5.31), where $\mathbf{A}_{11} = \mathbf{J}^T\mathbf{Q}_{\mathbf{m}}^{-1}\mathbf{J}$, $\mathbf{A}_{12} = -\mathbf{J}^T\mathbf{Q}_{\mathbf{m}}^{-1}[\,\mathbf{K}_1,\,\mathbf{D}_1,\,\mathbf{F}_1\,]$, and $\mathbf{A}_{22} = [\,\mathbf{K}_1,\,\mathbf{D}_1,\,\mathbf{F}_1\,]^T\mathbf{Q}_{\mathbf{m}}^{-1}[\,\mathbf{K}_1,\,\mathbf{D}_1,\,\mathbf{F}_1\,] + \mathbf{Q}_{\mathbf{b}}^{-1}$. Substituting (C.1b), (C.5a), (C.5c), (C.9a), (C.9c) and (5.20), the matrix $\mathbf{J}$ defined in (5.30) can be expressed as

$$\mathbf{J} = \mathrm{diag}\,(\,\mathbf{J}_1,\,\mathbf{J}_2,\,\cdots,\,\mathbf{J}_M\,) \tag{C.31}$$

where

$$\mathbf{J}_i = \mathbf{G}_{1_i}\mathbf{B}_{2_i}^{-1}\mathbf{G}_{2_i}\mathbf{B}_{3_i}^{-1}\mathbf{G}_{3_i}\mathbf{B}_{4_i} = \left[\,\mathbf{J}_{i,1}^T,\,\mathbf{J}_{i,2}^T,\,\cdots,\,\mathbf{J}_{i,N}^T\,\right]^T. \tag{C.32}$$

The lth row of $\mathbf{J}_{i,j}$ is $\left[-\left(\omega_{\mathbf{u}_i}^o - T_{i,j,l}\right),\,-\left(1+\hat{\gamma}_{1_i}(1)\right),\,\frac{1}{c}\boldsymbol{\rho}_{\mathbf{u}_i^o,\mathbf{s}_j}^T\right]$ and the $(l+1)$th is $\left[-\left(R_{i,j,l+1} - \omega_{\mathbf{u}_i}^o\right),\,\left(1+\hat{\gamma}_{1_i}(1)\right),\,\frac{1}{c}\boldsymbol{\rho}_{\mathbf{u}_i^o,\mathbf{s}_j}^T\right]$, where $l = 1,\,3,\,\ldots,\,L-1$.

Applying the approximation $1+\hat{\gamma}_{1_i}(1) \simeq 1+\varepsilon_{\mathbf{u}_i}^o$ and comparing with (C.27) gives

$$\mathbf{J}_{i,j} \simeq -\frac{\partial\,(\mathbf{p}_{i,j} - \mathbf{q}_{i,j})}{\partial\boldsymbol{\eta}_i^{oT}}, \quad \mathbf{J} \simeq -\frac{\partial\,(\mathbf{p}-\mathbf{q})}{\partial\boldsymbol{\eta}^{oT}} \tag{C.33}$$

which is valid under conditions (C1)−(C5). Also, comparing $\mathbf{K}_1$, $\mathbf{D}_1$ and $\mathbf{F}_1$ in Appendix C.1 with (C.29) gives

$$[\,\mathbf{K}_1,\,\mathbf{D}_1,\,\mathbf{F}_1\,] \simeq \frac{\partial\,(\mathbf{p}-\mathbf{q})}{\partial\mathbf{b}^{oT}} \tag{C.34}$$

under conditions (C1)−(C5). Substituting (C.33) and (C.34) into (5.31) gives (C.30). The proof is completed.

When the inter-node communications are available, the matrices in (5.33) are $\widetilde{\mathbf{A}}_{11} = \widetilde{\mathbf{J}}^T \mathbf{Q}_{\widetilde{\mathbf{m}}}^{-1} \widetilde{\mathbf{J}}$, $\widetilde{\mathbf{A}}_{12} = -\widetilde{\mathbf{J}}^T \mathbf{Q}_{\widetilde{\mathbf{m}}}^{-1} \left[\widetilde{\mathbf{K}}_1, \widetilde{\mathbf{D}}_1, \widetilde{\mathbf{F}}_1 \right]$, $\widetilde{\mathbf{A}}_{22} = \left[\widetilde{\mathbf{K}}_1, \widetilde{\mathbf{D}}_1, \widetilde{\mathbf{F}}_1 \right]^T \mathbf{Q}_{\widetilde{\mathbf{m}}}^{-1} \left[\widetilde{\mathbf{K}}_1, \widetilde{\mathbf{D}}_1, \widetilde{\mathbf{F}}_1 \right] + \mathbf{Q}_{\mathbf{b}}^{-1}$, and $\widetilde{\mathbf{K}}_1$, $\widetilde{\mathbf{D}}_1$ and $\widetilde{\mathbf{F}}_1$ are defined in Appendix C.4.

Using the matrix $\widetilde{\mathbf{G}}_1$ given above (C.14) and the definitions of $\widetilde{\mathbf{G}}_2$ and $\widetilde{\mathbf{B}}_2$ in (C.17), $\widetilde{\mathbf{J}}$ in (5.32) becomes

$$\widetilde{\mathbf{J}} = \begin{bmatrix} \begin{bmatrix} \mathbf{G}_1 & \mathbf{O}_{MNL \times \frac{M(M-1)}{2}} \\ & \check{\mathbf{G}}_1 \end{bmatrix} \end{bmatrix} \operatorname{diag}\left(\mathbf{B}_2^{-1}, \check{\mathbf{B}}_2^{-1} \right) \begin{bmatrix} \mathbf{G}_2' \\ \check{\mathbf{G}}_2 \end{bmatrix} = \begin{bmatrix} \mathbf{G}_1 \mathbf{B}_2^{-1} \mathbf{G}_2' \\ \check{\mathbf{G}}_1 \begin{bmatrix} \mathbf{B}_2^{-1} \mathbf{G}_2' \\ \check{\mathbf{B}}_2^{-1} \check{\mathbf{G}}_2 \end{bmatrix} \end{bmatrix} = \begin{bmatrix} \mathbf{J} \\ \check{\mathbf{J}} \end{bmatrix}, \tag{C.35}$$

where

$$\check{\mathbf{J}} = \begin{bmatrix} \check{\mathbf{J}}_{1,2} & \check{\mathbf{J}}_{2,1} & \mathbf{O}_{L\times 4} & \cdots & \mathbf{O}_{L\times 4} & \mathbf{O}_{L\times 4} \\ \check{\mathbf{J}}_{1,3} & \mathbf{O}_{L\times 4} & \check{\mathbf{J}}_{3,1} & \cdots & \mathbf{O}_{L\times 4} & \mathbf{O}_{L\times 4} \\ \vdots & \vdots & \vdots & \ddots & \vdots & \vdots \\ \mathbf{O}_{L\times 4} & \mathbf{O}_{L\times 4} & \mathbf{O}_{L\times 4} & \cdots & \check{\mathbf{J}}_{M-1,M} & \check{\mathbf{J}}_{M,M-1} \end{bmatrix}. \tag{C.36}$$

The lth row of $\check{\mathbf{J}}_{i,k}$ is $\left[-\left(\omega_{\mathbf{u}_i}^o - \check{T}_{i,k,l} \right), -\left(1 + \hat{\gamma}_{1_i}(1) \right), \frac{1}{c} \boldsymbol{\rho}_{\mathbf{u}_i^*, \mathbf{u}_k^*}^T \right]$ and the $(l+1)$th is $\left[-\left(\check{R}_{i,k,l+1} - \omega_{\mathbf{u}_i}^o \right), \left(1 + \hat{\gamma}_{1_i}(1) \right), \frac{1}{c} \boldsymbol{\rho}_{\mathbf{u}_i^*, \mathbf{u}_k^*}^T \right]$, $l = 1, 3, \ldots, L-1$. For $\check{\mathbf{J}}_{k,i}$, its lth row is $\left[-\left(\check{R}_{i,k,l} - \omega_{\mathbf{u}_k}^o \right), \left(1 + \hat{\gamma}_{1_k}(1) \right), -\frac{1}{c} \boldsymbol{\rho}_{\mathbf{u}_i^*, \mathbf{u}_k^*}^T \right]$ and the $(l+1)$th row is $\left[-\left(\omega_{\mathbf{u}_k}^o - \check{T}_{i,k,l+1} \right), -\left(1 + \hat{\gamma}_{1_k}(1) \right), -\frac{1}{c} \boldsymbol{\rho}_{\mathbf{u}_i^*, \mathbf{u}_k^*}^T \right]$, $l = 1, 3, \ldots, L-1$.
Note $i = 1, 2, \ldots, M-1$ and $k = i, i+1, \ldots, M$. Again, using the conditions (C1)−(C7), it is straightforward to verify that

$$\check{\mathbf{J}} \simeq -\frac{\partial \left(\check{\mathbf{p}} - \check{\mathbf{q}} \right)}{\partial \boldsymbol{\eta}^{oT}} \tag{C.37}$$

where $\frac{\partial(\check{\mathbf{p}}-\check{\mathbf{q}})}{\partial \boldsymbol{\eta}^{oT}}$ is defined in (C.28). Substituting (C.33), (C.34) and (C.37) into (5.33), comparing with (C.30), we obtain $\mathrm{cov}\,(\boldsymbol{\eta}) = \mathrm{CRLB}_{\boldsymbol{\eta}}$.

Appendix D

Appendix for Chapter 6

D.1 The Derivative Term $\boldsymbol{\nabla}_{\boldsymbol{\gamma}}$

From (6.1)−(6.3), the partial derivative terms in $\boldsymbol{\nabla}_{\boldsymbol{\gamma}} = [\, \boldsymbol{\nabla}_{\mathbf{u}^o}, \boldsymbol{\nabla}_c, \boldsymbol{\nabla}_{\mathbf{z}} \,]$ are

$$\boldsymbol{\nabla}_{\mathbf{u}^o} = \begin{bmatrix} \partial \boldsymbol{\tau}^o / \partial \mathbf{u}^{oT} \\ \partial \boldsymbol{\theta}^o / \partial \mathbf{u}^{oT} \end{bmatrix} = \begin{bmatrix} \Big[\left(\partial \boldsymbol{\tau}_1^o / \partial \mathbf{u}^{oT} \right)^T, \cdots, \left(\partial \boldsymbol{\tau}_M^o / \partial \mathbf{u}^{oT} \right)^T \Big]^T \\ \partial \boldsymbol{\theta}^o / \partial \mathbf{u}^{oT} \end{bmatrix} \tag{D.1a}$$

$$\boldsymbol{\nabla}_c = \Big[\left(\partial \boldsymbol{\tau}^o / \partial c \right)^T, \left(\partial \boldsymbol{\theta}^o / \partial c \right)^T \Big]^T = \Big[\left(\partial \boldsymbol{\tau}_1^o / \partial c \right)^T, \cdots, \left(\partial \boldsymbol{\tau}_M^o / \partial c \right)^T, \left(\partial \boldsymbol{\theta}^o / \partial c \right)^T \Big]^T \tag{D.1b}$$

$$\boldsymbol{\nabla}_{\mathbf{z}} = \begin{bmatrix} \partial \boldsymbol{\tau}^o / \partial \mathbf{t}^T & \partial \boldsymbol{\tau}^o / \partial \mathbf{s}^T \\ \partial \boldsymbol{\theta}^o / \partial \mathbf{t}^T & \partial \boldsymbol{\theta}^o / \partial \mathbf{s}^T \end{bmatrix} = \begin{bmatrix} \operatorname{diag}\left(\partial \boldsymbol{\tau}_1^o / \partial \mathbf{t}_1^T, \cdots, \partial \boldsymbol{\tau}_M^o / \partial \mathbf{t}_M^T \right)^T & \left(\partial \boldsymbol{\theta}^o / \partial \mathbf{t}^T \right)^T \\ \Big[\left(\partial \boldsymbol{\tau}_1^o / \partial \mathbf{s}^T \right)^T, \cdots, \left(\partial \boldsymbol{\tau}_M^o / \partial \mathbf{s}^T \right)^T \Big] & \left(\partial \boldsymbol{\theta}^o / \partial \mathbf{s}^T \right)^T \end{bmatrix}^T \tag{D.1c}$$

where

$$\partial \boldsymbol{\tau}_i^o / \partial \mathbf{u}^{oT} = \left[\boldsymbol{\rho}_{\mathbf{u}^o,\mathbf{t}_i} + \boldsymbol{\rho}_{\mathbf{u}^o,\mathbf{s}_1},\ \boldsymbol{\rho}_{\mathbf{u}^o,\mathbf{t}_i} + \boldsymbol{\rho}_{\mathbf{u}^o,\mathbf{s}_2},\ \cdots,\ \boldsymbol{\rho}_{\mathbf{u}^o,\mathbf{t}_i} + \boldsymbol{\rho}_{\mathbf{u}^o,\mathbf{s}_N} \right]^T / c \tag{D.2a}$$

$$\partial \boldsymbol{\theta}^o / \partial \mathbf{u}^{oT} = \left[\mathbf{T}\boldsymbol{\rho}_{\mathbf{u}^o,\mathbf{s}_1} / ||\mathbf{u}^o - \mathbf{s}_1||,\ \mathbf{T}\boldsymbol{\rho}_{\mathbf{u}^o,\mathbf{s}_2} / ||\mathbf{u}^o - \mathbf{s}_2||,\ \cdots,\ \mathbf{T}\boldsymbol{\rho}_{\mathbf{u}^o,\mathbf{s}_N} / ||\mathbf{u}^o - \mathbf{s}_N|| \right]^T \tag{D.2b}$$

$$\partial \boldsymbol{\tau}_i^o / \partial c = -\left[\tau_{i,1}^o,\ \tau_{i,2}^o,\ \cdots,\ \tau_{i,N}^o \right]^T / c,\ \partial \boldsymbol{\theta}^o / \partial c = \mathbf{0}_N \tag{D.2c}$$

$$\partial \boldsymbol{\tau}_i^o / \partial \mathbf{t}_i^T = -\left[\boldsymbol{\rho}_{\mathbf{u}^o,\mathbf{t}_i} + \boldsymbol{\rho}_{\mathbf{t}_i,\mathbf{s}_1},\ \boldsymbol{\rho}_{\mathbf{u}^o,\mathbf{t}_i} + \boldsymbol{\rho}_{\mathbf{t}_i,\mathbf{s}_2},\ \cdots,\ \boldsymbol{\rho}_{\mathbf{u}^o,\mathbf{t}_i} + \boldsymbol{\rho}_{\mathbf{t}_i,\mathbf{s}_N} \right]^T / c \tag{D.2d}$$

$$\partial \boldsymbol{\tau}_i^o / \partial \mathbf{s}^T = -\mathrm{diag}\left(\boldsymbol{\rho}_{\mathbf{u}^o,\mathbf{s}_1} - \boldsymbol{\rho}_{\mathbf{t}_i,\mathbf{s}_1},\ \boldsymbol{\rho}_{\mathbf{u}^o,\mathbf{s}_2} - \boldsymbol{\rho}_{\mathbf{t}_i,\mathbf{s}_2},\ \cdots,\ \boldsymbol{\rho}_{\mathbf{u}^o,\mathbf{s}_N} - \boldsymbol{\rho}_{\mathbf{t}_i,\mathbf{s}_N} \right)^T / c \tag{D.2e}$$

$$\partial \boldsymbol{\theta}^o / \partial \mathbf{s}^T = -\mathrm{diag}\left(\mathbf{T}\boldsymbol{\rho}_{\mathbf{u}^o,\mathbf{s}_1} / ||\mathbf{u}^o - \mathbf{s}_1||,\ \mathbf{T}\boldsymbol{\rho}_{\mathbf{u}^o,\mathbf{s}_2} / ||\mathbf{u}^o - \mathbf{s}_2||, \cdots,\ \mathbf{T}\boldsymbol{\rho}_{\mathbf{u}^o,\mathbf{s}_N} / ||\mathbf{u}^o - \mathbf{s}_N|| \right)^T \tag{D.2f}$$

$\partial \boldsymbol{\theta}^o / \partial \mathbf{t}^T = \mathbf{O}_{N \times 2M}$ and $\mathbf{T} = \begin{bmatrix} 0 & -1 \\ 1 & 0 \end{bmatrix}$.

D.2 The Detail of the Estimator in Section 6.3.A

D.2.1 The WLS Optimization of $\boldsymbol{\varphi}_1^o$

In (6.18), the matrices $\mathbf{B}_1$, $\mathbf{G}_1$ and the vectors $\mathbf{h}_1$ and $\boldsymbol{\epsilon}_1$ are defined as

$$\mathbf{B}_1 = 2\mathbf{I}_M \otimes \mathrm{diag}\left(||\mathbf{u}^o - \bar{\mathbf{s}}_1||,\ ||\mathbf{u}^o - \bar{\mathbf{s}}_2||,\ \cdots,\ ||\mathbf{u}^o - \bar{\mathbf{s}}_N|| \right) \tag{D.3a}$$

$$\mathbf{h}_1 = \begin{bmatrix} \mathbf{h}_{1,1} \\ \mathbf{h}_{1,2} \\ \vdots \\ \mathbf{h}_{1,M} \end{bmatrix}, \quad \mathbf{h}_{1,i} = \begin{bmatrix} 2\bar{\mathbf{t}}_i^T\bar{\mathbf{t}}_i - 2\bar{\mathbf{t}}_i^T\bar{\mathbf{s}}_1 + 2\bar{c}\tau_{i,1}||\bar{\mathbf{t}}_i - \bar{\mathbf{s}}_1|| + \bar{c}^2\tau_{i,1}^2 \\ 2\bar{\mathbf{t}}_i^T\bar{\mathbf{t}}_i - 2\bar{\mathbf{t}}_i^T\bar{\mathbf{s}}_2 + 2\bar{c}\tau_{i,2}||\bar{\mathbf{t}}_i - \bar{\mathbf{s}}_2|| + \bar{c}^2\tau_{i,2}^2 \\ \vdots \\ 2\bar{\mathbf{t}}_i^T\bar{\mathbf{t}}_i - 2\bar{\mathbf{t}}_i^T\bar{\mathbf{s}}_N + 2\bar{c}\tau_{i,N}||\bar{\mathbf{t}}_i - \bar{\mathbf{s}}_N|| + \bar{c}^2\tau_{i,N}^2 \end{bmatrix} \tag{D.3b}$$

$$\mathbf{G}_1 = \begin{bmatrix} \mathbf{G}_{1,1} \\ \mathbf{G}_{1,2} \\ \vdots \\ \mathbf{G}_{1,M} \end{bmatrix}, \quad \mathbf{G}_{1,i} = 2\begin{bmatrix} (\bar{\mathbf{t}}_i - \bar{\mathbf{s}}_1)^T & \mathbf{0}_{i-1}^T & \bar{c}\tau_{i,1} + ||\bar{\mathbf{t}}_i - \bar{\mathbf{s}}_1|| & \mathbf{0}_{M-i}^T \\ (\bar{\mathbf{t}}_i - \bar{\mathbf{s}}_2)^T & \mathbf{0}_{i-1}^T & \bar{c}\tau_{i,2} + ||\bar{\mathbf{t}}_i - \bar{\mathbf{s}}_2|| & \mathbf{0}_{M-i}^T \\ \vdots & \vdots & \vdots & \vdots \\ (\bar{\mathbf{t}}_i - \bar{\mathbf{s}}_N)^T & \mathbf{0}_{i-1}^T & \bar{c}\tau_{i,N} + ||\bar{\mathbf{t}}_i - \bar{\mathbf{s}}_N|| & \mathbf{0}_{M-i}^T \end{bmatrix} \tag{D.3c}$$

$$\boldsymbol{\epsilon}_1 = \left[\boldsymbol{\epsilon}_{1,1}^T,\, \boldsymbol{\epsilon}_{1,2}^T,\, \cdots,\, \boldsymbol{\epsilon}_{1,M}^T\right]^T, \boldsymbol{\epsilon}_{1,i} = \left[\epsilon_{1,i,1},\, \epsilon_{1,i,2},\, \cdots,\, \epsilon_{1,i,N}\right]^T \tag{D.3d}$$

and $\epsilon_{1,i,j}$ is defined in (6.15).

The weighting matrix $\mathbf{W}_1$ in (6.19) is

$$\mathbf{W}_1 = \mathrm{E}\left(\mathbf{B}_1\boldsymbol{\epsilon}_1\boldsymbol{\epsilon}_1^T\mathbf{B}_1^T\right)^{-1} = \mathbf{B}_1^{-T}\mathrm{E}\left(\boldsymbol{\epsilon}_1\boldsymbol{\epsilon}_1^T\right)^{-1}\mathbf{B}_1^{-1}. \tag{D.4}$$

From (6.15), $\boldsymbol{\epsilon}_1$ in (D.3d) can be expressed as

$$\boldsymbol{\epsilon}_1 = \bar{c}\mathbf{n}_{\boldsymbol{\tau}} + \mathbf{D}_{\mathbf{t}}\boldsymbol{\Delta}_{\mathbf{t}} + \mathbf{D}_{\mathbf{s}}\boldsymbol{\Delta}_{\mathbf{s}} - \Delta_c\boldsymbol{\tau}^o = \bar{c}\mathbf{n}_{\boldsymbol{\tau}} + \mathbf{D}_{\mathbf{z}}\boldsymbol{\Delta}_{\mathbf{z}} - \Delta_c\boldsymbol{\tau}^o \tag{D.5}$$

where

$$\mathbf{D}_{\mathbf{z}} = \left[\,\mathbf{D}_{\mathbf{t}},\, \mathbf{D}_{\mathbf{s}}\,\right], \quad \mathbf{D}_{\mathbf{t}} = \mathrm{diag}\left(\,\mathbf{D}_{\mathbf{t},1},\, \mathbf{D}_{\mathbf{t},2},\, \cdots,\, \mathbf{D}_{\mathbf{t},M}\,\right), \mathbf{D}_{\mathbf{s}} = \left[\,\mathbf{D}_{\mathbf{s},1}^T,\, \mathbf{D}_{\mathbf{s},2}^T,\, \cdots, \mathbf{D}_{\mathbf{s},M}^T\,\right]^T \tag{D.6a}$$

$$\mathbf{D}_{\mathbf{t},i} = -\left[\,\boldsymbol{\rho}_{\mathbf{u}^o,\bar{\mathbf{t}}_i} + \boldsymbol{\rho}_{\bar{\mathbf{t}}_i,\bar{\mathbf{s}}_1},\, \boldsymbol{\rho}_{\mathbf{u}^o,\bar{\mathbf{t}}_i} + \boldsymbol{\rho}_{\bar{\mathbf{t}}_i,\bar{\mathbf{s}}_2},\ \cdots,\, \boldsymbol{\rho}_{\mathbf{u}^o,\bar{\mathbf{t}}_i} + \boldsymbol{\rho}_{\bar{\mathbf{t}}_i,\bar{\mathbf{s}}_N}\,\right]^T \tag{D.6b}$$

$$\mathbf{D}_{\mathbf{s},i} = -\text{diag}\left(\boldsymbol{\rho}_{\mathbf{u}^o,\bar{\mathbf{s}}_1} - \boldsymbol{\rho}_{\bar{\mathbf{t}}_i,\bar{\mathbf{s}}_1},\, \boldsymbol{\rho}_{\mathbf{u}^o,\bar{\mathbf{s}}_2} - \boldsymbol{\rho}_{\bar{\mathbf{t}}_i,\bar{\mathbf{s}}_2},\ \cdots,\, \boldsymbol{\rho}_{\mathbf{u}^o,\bar{\mathbf{s}}_N} - \boldsymbol{\rho}_{\bar{\mathbf{t}}_i,\bar{\mathbf{s}}_N} \right)^T. \tag{D.6c}$$

Thus, $\text{E}\left(\boldsymbol{\epsilon}_1\boldsymbol{\epsilon}_1^T\right) = \bar{c}^2\mathbf{Q}_{\boldsymbol{\tau}} + \mathbf{D}_{\mathbf{z}}\mathbf{Q}_{\mathbf{z}}\mathbf{D}_{\mathbf{z}}^T + \sigma_c^2\boldsymbol{\tau}^o\boldsymbol{\tau}^{oT}$ since $\mathbf{n}_{\boldsymbol{\tau}}$, $\mathbf{z}$, and c are independent. Putting it into (D.4) gives

$$\mathbf{W}_1 = \mathbf{B}_1^{-T}\left(\bar{c}^2\mathbf{Q}_{\boldsymbol{\tau}} + \mathbf{D}_{\mathbf{z}}\mathbf{Q}_{\mathbf{z}}\mathbf{D}_{\mathbf{z}}^T + \sigma_c^2\boldsymbol{\tau}^o\boldsymbol{\tau}^{oT}\right)^{-1}\mathbf{B}_1^{-1}. \tag{D.7}$$

Based on the WLS theory [22], when the noise is small,

$$\text{cov}(\boldsymbol{\varphi}_1) \simeq \left(\mathbf{G}_1^T\mathbf{W}_1\mathbf{G}_1\right)^{-1}. \tag{D.8}$$

The weighting matrix $\mathbf{W}_1$ in (D.7) depends on the true time measurement vector $\boldsymbol{\tau}^o$ and target position $\mathbf{u}^o$. For implementation $\boldsymbol{\tau}^o$ is replaced by $\boldsymbol{\tau}$. To approximate $\mathbf{u}^o$, we shall first generate $\mathbf{W}_1$ by setting $\mathbf{B}_1$ to identity and $\mathbf{D}_{\mathbf{z}}$ to zero so that we can obtain an initial estimate of $\mathbf{u}^o$. Such an initial estimate ignores the transmitter and receiver position errors and the effect of localization geometry. A better $\mathbf{W}_1$ can be generated from the initial estimate. The approximation for $\mathbf{W}_1$ is reasonable because WLS is not sensitive to the error in the weighting matrix [108].

D.2.2 The WLS Optimization of $\boldsymbol{\varphi}_2^o$

The matrices and vector in (6.22) are given as

$$\mathbf{B}_2 = \text{diag}\left(1,\, 1,\, 2\varphi_1^o(3),\ \cdots,\, 2\varphi_1^o(2+M)\right) \tag{D.9a}$$

$$\mathbf{h}_2 = \left[\, \varphi_1(1),\, \varphi_1(2),\, \varphi_1^2(3) - \bar{\mathbf{t}}_1^T\bar{\mathbf{t}}_1,\, \cdots,\, \varphi_1^2(2+M) - \bar{\mathbf{t}}_M^T\bar{\mathbf{t}}_M \right]^T,$$
$$\mathbf{G}_2 = \begin{bmatrix} \mathbf{I}_2 & -2\bar{\mathbf{t}}_1 & \cdots & -2\bar{\mathbf{t}}_M \\ \mathbf{0}_2^T & 1 & \cdots & 1 \end{bmatrix}^T. \tag{D.9b}$$

The weighting matrix $\mathbf{W}_2$ in (6.23) is

$$\mathbf{W}_2 = \mathrm{E}\left(\mathbf{B}_2\boldsymbol{\epsilon}_2\boldsymbol{\epsilon}_2^T\mathbf{B}_2^T\right)^{-1} = \mathbf{B}_2^{-T}\left(\mathbf{G}_1^T\mathbf{W}_1\mathbf{G}_1\right)\mathbf{B}_2^{-1} \tag{D.10}$$

where (D.8) has been used. The covariance of $\boldsymbol{\varphi}_2$ is, from the WLS theory,

$$\mathrm{cov}\left(\boldsymbol{\varphi}_2\right) = \left(\mathbf{G}_2^T\mathbf{W}_2\mathbf{G}_2\right)^{-1}. \tag{D.11}$$

The true solution $\boldsymbol{\varphi}_1^o$ in $\mathbf{B}_2$ will be approximated by $\boldsymbol{\varphi}_1$ in the implementation.

D.2.3 The WLS Optimization of $\boldsymbol{\varphi}_3^o$

In (6.27),

$$\mathbf{B}_3 = \mathrm{diag}\left(2\varphi_2^o(1),\, 2\varphi_2^o(2),\, 1\right), \mathbf{h}_3 = \begin{bmatrix} \left(\boldsymbol{\varphi}_2(1:2) \odot \boldsymbol{\varphi}_2(1:2)\right) \\ \varphi_2(3) \end{bmatrix}, \mathbf{G}_3 = \begin{bmatrix} 1 & 0 & 1 \\ 0 & 1 & 1 \end{bmatrix}^T. \tag{D.12}$$

The weighting matrix is

$$\mathbf{W}_3 = \mathrm{E}\left(\mathbf{B}_3\boldsymbol{\epsilon}_3\boldsymbol{\epsilon}_3^T\mathbf{B}_3^T\right)^{-1} = \mathbf{B}_3^{-T}\mathrm{cov}\left(\boldsymbol{\varphi}_2\right)^{-1}\mathbf{B}_3^{-1} \tag{D.13}$$

and

$$\mathrm{cov}\left(\boldsymbol{\varphi}_3\right) = \left(\mathbf{G}_3^T\mathbf{W}_3\mathbf{G}_3\right)^{-1}. \tag{D.14}$$

$\boldsymbol{\varphi}_2$ is to approximate $\boldsymbol{\varphi}_2^o$ in $\mathbf{B}_3$ (D.12) in practice.

D.3 The Detail of the Estimator in Section 6.3.B

D.3.1 The WLS Optimization of $\widetilde{\boldsymbol{\varphi}}_1^o$

In (6.36), $\mathbf{B}_1$ is defined in (D.3a) and

$$\begin{aligned} \widetilde{\mathbf{h}}_1 &= \left[\widetilde{\mathbf{h}}_{1,1}^T, \widetilde{\mathbf{h}}_{1,2}^T, \cdots, \widetilde{\mathbf{h}}_{1,M}^T \right]^T, \\ \widetilde{\mathbf{h}}_{1,i} &= 2 \left[\overline{\mathbf{t}}_i^T \overline{\mathbf{t}}_i - \overline{\mathbf{t}}_i^T \overline{\mathbf{s}}_1, \overline{\mathbf{t}}_i^T \overline{\mathbf{t}}_i - \overline{\mathbf{t}}_i^T \overline{\mathbf{s}}_2, \cdots, \overline{\mathbf{t}}_i^T \overline{\mathbf{t}}_i - \overline{\mathbf{t}}_i^T \overline{\mathbf{s}}_N \right]^T. \end{aligned} \tag{D.15a}$$

$$\begin{aligned} \widetilde{\mathbf{G}}_1 &= \left[\widetilde{\mathbf{G}}_{1,1}^T, \widetilde{\mathbf{G}}_{1,2}^T, \cdots, \widetilde{\mathbf{G}}_{1,M}^T \right]^T, \\ \widetilde{\mathbf{G}}_{1,i} &= 2 \begin{bmatrix} (\overline{\mathbf{t}}_i - \overline{\mathbf{s}}_1) & \cdots & (\overline{\mathbf{t}}_i - \overline{\mathbf{s}}_N) \\ -||\overline{\mathbf{t}}_i - \overline{\mathbf{s}}_1|| \tau_{i,1} & \cdots & -||\overline{\mathbf{t}}_i - \overline{\mathbf{s}}_N|| \tau_{i,N} \\ -\tau_{i,1}^2/2 & \cdots & -\tau_{i,N}^2/2 \\ \mathbf{0}_{i-1} & \cdots & \mathbf{0}_{i-1} \\ ||\overline{\mathbf{t}}_i - \overline{\mathbf{s}}_1|| & \cdots & ||\overline{\mathbf{t}}_i - \overline{\mathbf{s}}_N|| \\ \mathbf{0}_{M-1} & \cdots & \mathbf{0}_{M-1} \\ \tau_{i,1} & \cdots & \tau_{i,N} \\ \mathbf{0}_{M-i} & \cdots & \mathbf{0}_{M-i} \end{bmatrix}^T. \end{aligned} \tag{D.15b}$$

$\widetilde{\boldsymbol{\epsilon}}_1$ is $\boldsymbol{\epsilon}_1$ in (D.5) with $\bar{c}$ replaced by c^o and Δ_c by 0.

$\widetilde{\mathbf{W}}_1$ in (6.37) is, from (D.7),

$$\widetilde{\mathbf{W}}_1 = \mathrm{E}\left(\mathbf{B}_1 \widetilde{\boldsymbol{\epsilon}}_1 \widetilde{\boldsymbol{\epsilon}}_1^T \mathbf{B}_1^T \right)^{-1} = \mathbf{B}_1^{-T} \left((c^o)^2 \mathbf{Q}_{\boldsymbol{\tau}} + \mathbf{D}_{\mathbf{z}} \mathbf{Q}_{\mathbf{z}} \mathbf{D}_{\mathbf{z}}^T \right)^{-1} \mathbf{B}_1^{-1}. \tag{D.16}$$

When the noise in $\widetilde{\mathbf{G}}_1$ is small, the covariance of $\widetilde{\boldsymbol{\varphi}}_1$ can be expressed as

$$\mathrm{cov}(\widetilde{\boldsymbol{\varphi}}_1) \simeq \left(\widetilde{\mathbf{G}}_1^T\, \widetilde{\mathbf{W}}_1\, \widetilde{\mathbf{G}}_1\right)^{-1}. \tag{D.17}$$

D.3.2 The WLS Optimization of $\widetilde{\boldsymbol{\varphi}}_2^o$

The matrices and vector in (6.38) are

$$\widetilde{\mathbf{B}}_2 = \begin{bmatrix} \widetilde{\mathbf{B}}_{2,1} & \mathbf{O}_{(4+M)\times M} \\ \widetilde{\mathbf{B}}_{2,2} & 2\mathrm{diag}\left(\widetilde{\varphi}_1^o(5+M),\, \cdots,\, \widetilde{\varphi}_1^o(4+2M)\right) \end{bmatrix} \tag{D.18a}$$

$$\widetilde{\mathbf{B}}_{2,1} = \mathrm{diag}\left(1,\, 1,\, 2\widetilde{\varphi}_1^o(3),\, 1,\, 2\mathrm{diag}\left(\widetilde{\varphi}_1^o(5),\, \cdots,\, \widetilde{\varphi}_1^o(4+M)\right)\right) \tag{D.18b}$$

$$\widetilde{\mathbf{B}}_{2,2} = \begin{bmatrix} \mathbf{O}_{M\times 3},\, -\begin{bmatrix} ||\mathbf{u}^o - \overline{\mathbf{t}}_1||^2 \\ \vdots \\ ||\mathbf{u}^o - \overline{\mathbf{t}}_M||^2 \end{bmatrix},\, \mathbf{O}_{M\times M} \end{bmatrix} \tag{D.18c}$$

$$\widetilde{\mathbf{h}}_2 = \left[\, \widetilde{\boldsymbol{\varphi}}_1^T(1:2),\, \widetilde{\varphi}_1^2(3),\, \widetilde{\varphi}_1(4), \widetilde{\mathbf{h}}_{2,1}^T,\, \widetilde{\mathbf{h}}_{2,2}^T \,\right]^T \tag{D.18d}$$

$$\widetilde{\mathbf{h}}_{2,1} = \left[\, \widetilde{\varphi}_1^2(5) - \overline{\mathbf{t}}_1^T\overline{\mathbf{t}}_1,\, \cdots,\, \widetilde{\varphi}_1^2(4+M) - \overline{\mathbf{t}}_M^T\overline{\mathbf{t}}_M \,\right]^T \tag{D.18e}$$

$$\widetilde{\mathbf{h}}_{2,2} = \begin{bmatrix} \widetilde{\varphi}_1^2(5+M) - \widetilde{\varphi}_1(4)\overline{\mathbf{t}}_1^T\overline{\mathbf{t}}_1 \\ \vdots \\ \widetilde{\varphi}_1^2(4+2M) - \widetilde{\varphi}_1(4)\overline{\mathbf{t}}_M^T\overline{\mathbf{t}}_M \end{bmatrix} \tag{D.18f}$$

$$\widetilde{\mathbf{G}}_2 = \begin{bmatrix} \mathbf{I}_2 & \mathbf{0}_2 & \mathbf{0}_2 \\ \mathbf{0}_2^T & 0 & 1 \\ \mathbf{0}_2^T & 0 & 1 \\ -2\bar{\mathbf{t}}_1^T & 1 & 0 \\ \vdots & \vdots & \vdots \\ -2\bar{\mathbf{t}}_M^T & 1 & 0 \\ -2\widetilde{\varphi}_1(4)\bar{\mathbf{t}}_1^T & \widetilde{\varphi}_1(4) & 0 \\ \vdots & \vdots & \vdots \\ -2\widetilde{\varphi}_1(4)\bar{\mathbf{t}}_M^T & \widetilde{\varphi}_1(4) & 0 \end{bmatrix}. \tag{D.18g}$$

The weighting matrix $\widetilde{\mathbf{W}}_2$ in (6.40) is

$$\widetilde{\mathbf{W}}_2 = \mathrm{E}\left(\widetilde{\mathbf{B}}_2\widetilde{\boldsymbol{\epsilon}}_2\widetilde{\boldsymbol{\epsilon}}_2^T\widetilde{\mathbf{B}}_2^T\right)^{-1} = \widetilde{\mathbf{B}}_2^{-T}\left(\widetilde{\mathbf{G}}_1^T\ \widetilde{\mathbf{W}}_1\ \widetilde{\mathbf{G}}_1\right)\widetilde{\mathbf{B}}_2^{-1} \tag{D.19}$$

where (D.17) has been used.

The covariance of $\widetilde{\boldsymbol{\varphi}}_2$ is

$$\mathrm{cov}\left(\widetilde{\boldsymbol{\varphi}}_2\right) = \left(\widetilde{\mathbf{G}}_2^T\ \widetilde{\mathbf{W}}_2\ \widetilde{\mathbf{G}}_2\right)^{-1}. \tag{D.20}$$

D.3.3 The WLS Optimization of $\widetilde{\boldsymbol{\varphi}}_3^o$

In (6.42), the matrices and vectors are

$$\widetilde{\mathbf{B}}_3 = \mathrm{diag}\left(2\widetilde{\varphi}_2^o(1),\, 2\widetilde{\varphi}_2^o(2),\, 1,\, 1\right),$$
$$\widetilde{\mathbf{h}}_3 = \begin{bmatrix} \widetilde{\boldsymbol{\varphi}}_2(1:2) \odot \widetilde{\boldsymbol{\varphi}}_2(1:2) \\ \widetilde{\varphi}_2(3) \\ \widetilde{\varphi}_2(4) \end{bmatrix}, \quad \widetilde{\mathbf{G}}_3 = \begin{bmatrix} 1 & 0 & 1 & 0 \\ 0 & 1 & 1 & 0 \\ 0 & 0 & 0 & 1 \end{bmatrix}^T \tag{D.21}$$

and $\widetilde{\boldsymbol{\epsilon}}_3$ is the error in $\widetilde{\boldsymbol{\varphi}}_2$. Furthermore,

$$\widetilde{\mathbf{W}}_3 = \mathrm{E}\left(\widetilde{\mathbf{B}}_3\widetilde{\boldsymbol{\epsilon}}_3\widetilde{\boldsymbol{\epsilon}}_3^T\widetilde{\mathbf{B}}_3^T\right)^{-1} = \widetilde{\mathbf{B}}_3^{-T}\mathrm{cov}\left(\widetilde{\boldsymbol{\varphi}}_2\right)^{-1}\widetilde{\mathbf{B}}_3^{-1} \tag{D.22a}$$

$$\mathrm{cov}\left(\widetilde{\boldsymbol{\varphi}}_3\right) = \left(\widetilde{\mathbf{G}}_3^T\, \widetilde{\mathbf{W}}_3\, \widetilde{\mathbf{G}}_3\right)^{-1}. \tag{D.22b}$$

The formation of $\widetilde{\mathbf{W}}_1$, $\widetilde{\mathbf{W}}_2$ and $\widetilde{\mathbf{W}}_3$ defined in (D.16), (D.19) and (D.22a) follows similar steps explained in Appendix B.

D.4 Proof of (6.48) and (6.50)

We begin with the matrix $\mathbf{G}_4$ defined below (6.47). Substituting $\mathbf{B}_4$ by (6.31), $\mathbf{G}_3$ and $\mathbf{B}_3$ in (D.12), $\mathbf{G}_2$ in (D.9b), $\mathbf{B}_2$ by (D.9a), $\mathbf{G}_1$ in (D.3c), $\mathbf{B}_1$ in (D.3a), and after some direct algebraic manipulations, we have

$$\mathbf{G}_4 = \left[\, \mathbf{G}_{4,1}^T,\, \mathbf{G}_{4,2}^T,\, \cdots,\, \mathbf{G}_{4,M}^T \,\right]^T \tag{D.23}$$

where

$$\mathbf{G}_{4,i} = \begin{bmatrix} \left(\bar{\mathbf{t}}_i - \bar{\mathbf{s}}_1 + \left(\bar{c}\tau_{i,1} + ||\bar{\mathbf{t}}_i - \bar{\mathbf{s}}_1||\right)\boldsymbol{\rho}_{\mathbf{u}^o,\bar{\mathbf{t}}_i}\right)^T / ||\mathbf{u}^o - \bar{\mathbf{s}}_1|| \\ \vdots \\ \left(\bar{\mathbf{t}}_i - \bar{\mathbf{s}}_N + \left(\bar{c}\tau_{i,N} + ||\bar{\mathbf{t}}_i - \bar{\mathbf{s}}_N||\right)\boldsymbol{\rho}_{\mathbf{u}^o,\bar{\mathbf{t}}_i}\right)^T / ||\mathbf{u}^o - \bar{\mathbf{s}}_N|| \end{bmatrix}. \tag{D.24}$$

When the conditions (C1)−(C4) are satisfied, we have from (6.14) $\bar{c}\tau_{i,j} + ||\bar{\mathbf{t}}_i - \bar{\mathbf{s}}_j|| \simeq ||\mathbf{u}^o - \bar{\mathbf{t}}_i|| + ||\mathbf{u}^o - \bar{\mathbf{s}}_j|| + \epsilon_{1,i,j}$, where $\epsilon_{1,i,j}$ is defined in (6.15). Under (C2) and (C5), $\epsilon_{1,i,j}/||\mathbf{u}^o - \bar{\mathbf{s}}_j||$ is negligible. Putting it back to (D.24) and ignoring the approximation errors

$$\mathbf{G}_{4,i} = \left[\, \boldsymbol{\rho}_{\mathbf{u}^o,\bar{\mathbf{t}}_i} + \boldsymbol{\rho}_{\mathbf{u}^o,\bar{\mathbf{s}}_1},\ \boldsymbol{\rho}_{\mathbf{u}^o,\bar{\mathbf{t}}_i} + \boldsymbol{\rho}_{\mathbf{u}^o,\bar{\mathbf{s}}_2},\ \cdots,\ \boldsymbol{\rho}_{\mathbf{u}^o,\bar{\mathbf{t}}_i} + \boldsymbol{\rho}_{\mathbf{u}^o,\bar{\mathbf{s}}_N} \,\right]^T. \tag{D.25}$$

Comparing (D.23) and (D.25) with (D.1a) and (D.2a) when only time measurements are used and noting $\bar{\boldsymbol{\nabla}}_{\mathbf{u}^o}$ is $\boldsymbol{\nabla}_{\mathbf{u}^o}$ with $\mathbf{z}$ and c replaced by $\bar{\mathbf{z}}$ and $\bar{c}$, we arrive at $\mathbf{G}_4 \simeq \bar{c}\bar{\boldsymbol{\nabla}}_{\mathbf{u}^o}$.

The matrix $\mathbf{D}_{\mathbf{z}}$ is defined in (D.6). Comparing it with (D.1c), (D.2d) and (D.2e) when only time measurements are used gives $\mathbf{D}_{\mathbf{z}} = \bar{c}\bar{\boldsymbol{\nabla}}_{\mathbf{z}}$. Similarly, we have from (6.13), (D.1b) and (D.2c) $-\boldsymbol{\tau}^o \simeq \bar{c}\bar{\boldsymbol{\nabla}}_c$ under (C1), (C2) and (C4). Hence (6.48) is valid.

To prove (6.50), we substitute (D.3a), (D.15b), (D.18a), (D.18g), (D.21) and (6.46) into $\widetilde{\mathbf{G}}_4$ defined below (6.49) and obtain

$$\widetilde{\mathbf{G}}_4 = \left[\, \widetilde{\mathbf{G}}_{4,1}^T,\ \widetilde{\mathbf{G}}_{4,2}^T,\ \cdots,\ \widetilde{\mathbf{G}}_{4,M}^T \,\right]^T \tag{D.26}$$

where $\widetilde{\mathbf{G}}_{4,i}$ is defined in (D.27) on the top of next page. Given the definition of $\widetilde{\boldsymbol{\varphi}}_1^o$

$$\widetilde{\mathbf{G}}_{4,i} = \begin{bmatrix} \frac{\left(\bar{\mathbf{t}}_i - \bar{\mathbf{s}}_1 + (\widetilde{\varphi}_1(4)\tau_{i,1}/c^o + ||\bar{\mathbf{t}}_i - \bar{\mathbf{s}}_1||)\boldsymbol{\rho}_{\mathbf{u}^o,\bar{\mathbf{t}}_i}\right)^T}{||\mathbf{u}^o - \bar{\mathbf{s}}_1||} & \frac{\tau_{i,1}(-c^o\tau_{i,1} - ||\bar{\mathbf{t}}_i - \bar{\mathbf{s}}_1|| + ||\mathbf{u}^o - \bar{\mathbf{t}}_i||)}{||\mathbf{u}^o - \bar{\mathbf{s}}_1||} \\ \vdots & \vdots \\ \frac{\left(\bar{\mathbf{t}}_i - \bar{\mathbf{s}}_N + \left(\widetilde{\varphi}_1(4)\tau_{i,N}/c^o + ||\bar{\mathbf{t}}_i - \bar{\mathbf{s}}_N||\right)\boldsymbol{\rho}_{\mathbf{u}^o,\bar{\mathbf{t}}_i}\right)^T}{||\mathbf{u}^o - \bar{\mathbf{s}}_N||} & \frac{\tau_{i,N}\left(-c^o\tau_{i,N} - ||\bar{\mathbf{t}}_i - \bar{\mathbf{s}}_N|| + ||\mathbf{u}^o - \bar{\mathbf{t}}_i||\right)}{||\mathbf{u}^o - \bar{\mathbf{s}}_N||} \end{bmatrix} . \quad \text{(D.27)}$$

in (6.35), $\widetilde{\varphi}_1(4)/c^o \simeq c^o$ over the small error region. Using the conditions (C1)−(C3), we have from (6.32) $c^o\tau_{i,j} + ||\bar{\mathbf{t}}_i - \bar{\mathbf{s}}_j|| \simeq ||\mathbf{u}^o - \bar{\mathbf{t}}_i|| + ||\mathbf{u}^o - \bar{\mathbf{s}}_j|| + \widetilde{\epsilon}_{1,i,j}$ where $\widetilde{\epsilon}_{1,i,j}$ is defined in (6.33). Under (C2) and (C5), $\widetilde{\epsilon}_{1,i,j}/||\mathbf{u}^o - \bar{\mathbf{s}}_j||$ is sufficiently small. We can verify (6.50) by using (D.26) and (D.27) and following similar steps to obtain (6.48) above.

D.5 The Detail of the Solution Using Both Bearing and Time Measurements

Given (6.3b) and (6.51), the matrix and vectors in (6.52) are

$$\begin{aligned} \mathbf{h}_{\boldsymbol{\theta}} &= \left[\, \boldsymbol{\nu}_1^T\bar{\mathbf{s}}_1,\, \boldsymbol{\nu}_2^T\bar{\mathbf{s}}_2,\, \cdots,\, \boldsymbol{\nu}_N^T\bar{\mathbf{s}}_N \,\right]^T, \\ \mathbf{G}_{\boldsymbol{\theta}} &= \left[\, \boldsymbol{\nu}_1,\, \boldsymbol{\nu}_2,\, \cdots,\, \boldsymbol{\nu}_N \,\right]^T, \quad \boldsymbol{\epsilon}_{\boldsymbol{\theta}} = \mathbf{B}_{\boldsymbol{\theta}}\mathbf{n}_{\boldsymbol{\theta}} + \mathbf{D}_{\boldsymbol{\theta}}\boldsymbol{\Delta}_{\mathbf{z}} \end{aligned} \quad \text{(D.28)}$$

where

$$\mathbf{B}_{\boldsymbol{\theta}} = \text{diag}\left(\boldsymbol{\nu}_1^{\perp T}\left(\mathbf{u}^o - \bar{\mathbf{s}}_1\right),\, \boldsymbol{\nu}_2^{\perp T}\left(\mathbf{u}^o - \bar{\mathbf{s}}_2\right),\, \cdots,\, \boldsymbol{\nu}_N^{\perp T}\left(\mathbf{u}^o - \bar{\mathbf{s}}_N\right) \right) \quad \text{(D.29a)}$$

$$\mathbf{D}_{\boldsymbol{\theta}} = \left[\, \mathbf{O}_{N\times 2M},\, -\text{diag}\left(\boldsymbol{\nu}_1^T,\, \boldsymbol{\nu}_2^T,\, \cdots,\, \boldsymbol{\nu}_N^T \right) \right] . \quad \text{(D.29b)}$$

When the distribution of c is known, stacking (6.18) and (6.52) together yields

the matrix equation

$$\breve{\boldsymbol{\epsilon}}_1 = \breve{\mathbf{h}}_1 - \breve{\mathbf{G}}_1 \boldsymbol{\varphi}_1^o \tag{D.30}$$

where $\breve{\mathbf{h}}_1 = \left[\, \mathbf{h}_1^T,\, \mathbf{h}_{\boldsymbol{\theta}}^T \,\right]^T$, $\breve{\mathbf{G}}_1 = \left[\, \mathbf{G}_1^T,\, [\mathbf{G}_{\boldsymbol{\theta}},\, \mathbf{O}_{N\times M}]^T \,\right]^T$, $\breve{\boldsymbol{\epsilon}}_1 = \left[\, (\mathbf{B}_1 \boldsymbol{\epsilon}_1)^T,\, \boldsymbol{\epsilon}_{\boldsymbol{\theta}}^T \,\right]^T$ and $\boldsymbol{\varphi}_1^o$ is defined in (6.17). The WLS solution is

$$\boldsymbol{\varphi}_1 = \left(\breve{\mathbf{G}}_1^T \breve{\mathbf{W}}_1 \breve{\mathbf{G}}_1 \right)^{-1} \breve{\mathbf{G}}_1^T \breve{\mathbf{W}}_1 \breve{\mathbf{h}}_1 \tag{D.31}$$

and $\breve{\mathbf{W}}_1$ is, when the bearing and time measurements are independent,

$$\breve{\mathbf{W}}_1 = \begin{bmatrix} \mathbf{W}_1^{-1} & \mathbf{B}_1 \mathbf{D}_{\mathbf{z}} \mathbf{Q}_{\mathbf{z}} \mathbf{D}_{\boldsymbol{\theta}}^T \\ \mathbf{D}_{\boldsymbol{\theta}} \mathbf{Q}_{\mathbf{z}} \mathbf{D}_{\mathbf{z}}^T \mathbf{B}_1^T & \mathbf{W}_{\boldsymbol{\theta}}^{-1} \end{bmatrix}^{-1}$$

where $\mathbf{W}_1$, $\mathbf{B}_1$, $\mathbf{D}_{\mathbf{z}}$, and $\mathbf{D}_{\boldsymbol{\theta}}$ are defined in (D.7), (D.3a), (D.6), and (D.29b). Under (C2) and (C7),

$$\mathbf{W}_{\boldsymbol{\theta}} \triangleq \mathrm{E}\left(\boldsymbol{\epsilon}_{\boldsymbol{\theta}} \boldsymbol{\epsilon}_{\boldsymbol{\theta}}^T \right)^{-1} \simeq \left(\mathbf{B}_{\boldsymbol{\theta}} \mathbf{Q}_{\boldsymbol{\theta}} \mathbf{B}_{\boldsymbol{\theta}}^T + \mathbf{D}_{\boldsymbol{\theta}} \mathbf{Q}_{\mathbf{z}} \mathbf{D}_{\boldsymbol{\theta}}^T \right)^{-1}$$

where $\mathbf{B}_{\boldsymbol{\theta}}$ is defined in (D.29a). Furthermore, when (C1)$-$(C4) and (C7) are valid,

$$\mathrm{cov}(\boldsymbol{\varphi}_1) = \left(\breve{\mathbf{G}}_1^T \breve{\mathbf{W}}_1 \breve{\mathbf{G}}_1 \right)^{-1}.$$

The subsequent stages are the same as those in the Section 6.3.A. The generation of $\breve{\mathbf{W}}_1$ follows similar steps in Appendix D.2. The algorithm for the case when the statistical distribution of c is unknown can be similarly developed.

Bibliography

[1] A. Farina and E. Hanle, "Position accuracy in netted monostatic and bistatic radar," *IEEE Trans. Aerosp. Electron. Syst.*, vol. AES-19, no. 4, pp. 513-520, Jul. 1983.

[2] V. S. Chernyak, *Fundamentals of Multisite Radar Systems: Multistatic Radars and Multistatic Radar Systems*. CRC Press, 1998.

[3] E. Hanle, "Survey of bistatic and multistatic radar," *IEE Proc.*, vol. 133, no. 7, pp. 587-595, Dec. 1986.

[4] S. Simakov, "Localization in airborne multistatic sonars," *IEEE J. Ocean. Eng.*, vol. 33, no. 3, pp. 278-288, Jul. 2008.

[5] S. Coraluppi, "Multistatic sonar localization," *IEEE J. Ocean. Eng.*, vol. 31, no. 4, pp. 964–974, Oct. 2006.

[6] J. J. Caffery and G. L. Stuber, "Overview of radiolocation in CDMA cellular systems," *IEEE Commun. Mag.*, vol. 36, no. 4, pp. 38-45, Apr. 1998.

[7] A. Urruela, J. Sala, and J. Riba, "Average performance analysis of circular and hyperbolic geolocation," *IEEE Trans. Veh. Technol.*, vol. 55, no. 1, pp. 52-66, Jan. 2006.

[8] N. Patwari, J. N. Ash, S. Kyperountas, A. O. Hero, III, R. L. Moses, and N. S. Correal, "Locating the nodes: cooperative localization in wireless sensor networks," *IEEE Signal Process. Mag.*, vol. 22, no. 4, pp. 54-69, Jul. 2005.

[9] U. A. Khan, S. Kar, and J. M. F. Moura, "Distributed sensor localization in random environments using minimal number of anchor nodes," *IEEE Trans. Signal Process.*, vol. 57, no. 5, pp. 2000-2016, May 2009.

[10] P. Addesso, S. Marano, and V. Matta, "Estimation of target location via likelihood approximation in sensor networks," *IEEE Trans. Signal Process.*, vol. 58, no. 3, pp. 1358-1368, Mar. 2010.

[11] H. Qi, N. Xiu, and X. Yuan, "A Lagrangian dual approach to the single-source localization problem," *IEEE Trans. Signal Process.*, vol. 61, no. 15, pp. 3815-3826, Aug. 2013.

[12] S. Chen and K. C. Ho, "Achieving asymptotic efficient performance for squared range and squared range difference localizations," *IEEE Trans. Signal Process.*, vol. 61, no. 11, pp. 2836-2849, Jun. 2013.

[13] K. C. Ho, "Bias reduction for an explicit solution of source localization using TDOA," *IEEE Trans. Signal Process.*, vol. 60, no. 5, pp. 2101-2104, May 2012.

[14] S. Kay and N. Vankayalapati, "Improvement of TDOA position fixing using the likelihood curvature," *IEEE Trans. Signal Process.*, vol. 61, no. 8, pp. 1910-1914, Apr. 2013.

[15] M. Gavish and A. J. Weiss, "Performance analysis of bearing-only target location algorithms," *IEEE Trans. Aerosp. Electron. Syst.*, vol. AES-28, no. 3, pp. 817-828, Jul. 1992.

[16] C. H. Knapp and G. C. Carter, "The generalized correlation method for estimation of time delay," *IEEE Trans. Acoust., Speech, Signal Process.*, vol. ASSP-24, no. 4, pp. 320-327, Aug. 1976.

[17] H. Godrich, A. M. Haimovich, and R. S. Blum, "Target localization accuracy gain in MIMO radar-based systems," *IEEE Trans. Inf. Theory*, vol. 56, no. 6, pp. 2783-2803, Jun. 2010.

[18] A. M. Haimovich, R. S. Blum, and L. J. Cimini, "MIMO radar with widely separated antennas," *IEEE Signal Process. Mag.*, vol. 25, no. 1, pp. 116-129, Jan. 2008.

[19] J. Shen, A. Molisch, and J. Salmi, "Accurate passive location estimation using TOA measurements," *IEEE Trans. Wireless Commun.*, vol. 11, no. 6, pp. 2182-2192, Jun. 2012.

[20] Y. Zhou, C. L. Law, Y. L. Guan, and F. Chin, "Indoor elliptical localization based on asynchronous UWB range measurement," *IEEE Trans. Instrum. Meas.*, vol. 60, no. 1, pp. 248-257, Jan. 2011.

[21] U. D. Hanebeck and G. Schmidt, "Closed-form elliptic location with an arbitrary array topology," in *Proc. IEEE Int. Conf. on Acoust., Speech, and Signal Process.*, vol. 6, Atlanta, GA, May 1996, pp. 3069-3072.

[22] S. M. Kay, *Fundamentals of Statistical Signal Process., Estimation Theory.* Englewood Cliffs, NJ: Prentice-Hall, 1993.

[23] N. Patwari, A. O. Hero, III, M. Perkins, N. S. Correal, and R. J. O'Dea, "Relative location estimation in wireless sensor networks," *IEEE Trans. Signal Process.*, vol. 51, no. 8, pp. 2137-2148, Aug. 2003.

[24] W. H. Foy, "Position-location solutions by Taylor-series estimation," *IEEE Trans. Aerosp. Electron. Syst.*, vol. AES-12, no. 2, pp. 187-194, Mar. 1976.

[25] Y. T. Chan and K. C. Ho, "A simple and efficient estimator for hyperbolic location," *IEEE Trans. Signal Process.*, vol. 42, no. 8, pp. 1905-1915, Aug. 1994.

[26] Z. Ma and K. C. Ho, "TOA localization in the presence of random sensor position errors," in *Proc. IEEE Int. Conf. Acoust., Speech, Signal Process.*, Prague, Czech Republic, May 2011, pp. 2468-2471.

[27] K. C. Ho, X. Lu, and L. Kovavisaruch, "Source localization using TDOA and FDOA measurements in the presence of receiver location errors: analysis and solution," *IEEE Trans. Signal Process.*, vol. 55, no. 2, pp. 684-696, Feb. 2007.

[28] M. Sun and K. C. Ho, "An asymptotically efficient estimator for TDOA and FDOA positioning of multiple disjoint sources in the presence of sensor location uncertainties," *IEEE Trans. Signal Process.*, vol. 59, pp. 3434-3440, Jul. 2011.

[29] D.-H. Shin and T.-K. Sung, "Comparisons of error characteristics between TOA and TDOA positioning," *IEEE Trans. Aerosp. Electron. Syst.*, vol. 38, no. 1, pp. 307-311, Jan. 2002.

[30] B. Yang and J. Scheuing, "Cramer-Rao bound and optimum sensor array for source localization from time differences of arrival," in *Proc. IEEE Int. Conf. on Acoust., Speech, and Signal Process.,* Philadelphia, PA, Mar. 2005, pp. 961-964.

[31] A. N. Bishop, B. Fidan, B. D. O. Anderson, K. Dogancay, and P. N. Pathirana, "Optimality analysis of sensor-target localization geometries," *Automat.*, vol. 46, no. 3, pp. 479-492, Mar. 2010.

[32] K. W. K. Lui and H. C. So, "A study of two-dimensional sensor placement using time-difference-of-arrival measurements," *Digital Signal Process.*, vol. 19, no. 4, pp. 650-659, Jul. 2009.

[33] R. J. Barton and D. Rao, "Performance capabilities of long-range UWB-IR TDOA localization systems," *EURASIP J. Adv. Signal Process.*, vol. 2008, 2008.

[34] K. Dogancay, "Bias compensation for the bearings-only pseudolinear target track estimator," *IEEE Trans. Signal Process.*, vol. 54, no. 1, pp. 59-68, Jan. 2006.

[35] M. Schlosser and K. Kroschel, "Limits in tracking with extended Kalman filter," *IEEE Trans. Aerosp. Electron. Syst.*, vol. 40, no. 4, pp. 1351-1359, Oct. 2004.

[36] Z. Zhao, X. R. Li, and V. P. Jilkov, "Best linear unbiased filtering with nonlinear measurements for target tracking," *IEEE Trans. Aerosp. Electron. Syst.*, vol. 40, no. 4, pp. 1324-1336, Oct. 2004.

[37] Y. Huang, J. Benesty, G. Elko, and R. Mersereau, "Real-time passive source localization: a practical linear-correction least-squares approach," *IEEE Trans. Speech Audio Process.*, vol. 9, no. 8, pp. 943-956, Nov. 2001.

[38] Y. Ji, C. Yu, and B. D. O. Anderson, "Localization bias correction in n-dimensional space," *Proc. IEEE Int. Conf. on Acoust., Speech, and Signal Process.,* Dallas, TX, Mar. 2010, pp. 2854-2857.

[39] M. S. Bartlett, "Approximate confidence intervals.II. more than one unknown parameter," *Biometrika*, vol. 40, pp. 306-317, Dec. 1953.

[40] J. B. Haldane, "The estimation of two parameters from a sample," *Sankhya*, vol. 12, no. 4, pp. 313-320, Sep. 1953.

[41] D. R. Cox and E. J. Snell, "A general definition of residuals," *J. of the Royal Statistical Society, Series B (Methodological)*, vol. 30, pp. 248-275, 1968.

[42] M. J. Box, "Bias in nonlinear estimation," *J. of the Royal Statistical Society, Series B (Methodological)*, vol. 33, pp. 171-201, 1971.

[43] P. J. G. Teunissen, "First and second moments of non-linear least-squares estimators," *J. Geodesy*, vol. 63, no. 3, pp. 253-262, Aug. 1989.

[44] P. J. G. Teunissen, "Nonlinear inversion of geodetic and geophysical data: diagnosing nonlinearity," in *Developments in Four-Dimensional Geodesy, Lecture Notes in Earth Sciences*, vol. 29, Springer, 1989, pp. 241-264.

[45] J. Zheng and Y. C. Wu, "Localization and time synchronization in wireless sensor networks: A unified approach," in *Proc. IEEE Asia Pacific Conf. on Circuits and Sys.*, Macao, China, Nov.-Dec. 2008, pp. 594-597.

[46] V. Y. Zhang and A. K. Wong, "Closed-form solution for joint localization and time synchronization in wireless sensor networks," in *Proc. IEEE ICC*, Cape Town, South Africa, May 2010, pp. 1-5.

[47] J. Zheng and Y. C. Wu, "Joint time synchronization and localization of an unknown node in wireless sensor networks," *IEEE Trans. Signal Process.*, vol. 58, no. 3, pp. 1309-1320, Mar. 2010.

[48] S. Van Huffel and J. Vandewalle, "Analysis and properties of the generalized total least squares problem $AX \approx B$ when some or all columns in A are subject to error," *SIAM J. Matrix Anal. Appl.*, vol. 10, no. 3, pp. 294-315, Jul. 1989.

[49] Sandys-Wunsch, M., and Hazen, M. G. "Multistatic localization error due to receiver positioning errors," *IEEE J. Ocean. Eng.*, vol. 27, no. 2, pp. 328-334, Apr. 2002.

[50] McIntyre, M., Wang, J., and Kelly, L. "The effect of position uncertainty in multistatic acoustic localisation," in *Proc. IEEE Int. Symp. Inform., Decision and Control*, Adelaide, Australia, Feb. 1999, pp. 347-352.

[51] Coraluppi, S. "Localization and fusion in multistatic sonar," in *Proc. IEEE Int. Conf. Inform. Fusion*, Philadelphia, PA, Jul. 2005, pp. 303-310.

[52] Malanowski, M., and Kulpa, K. "Two methods for target localization in multistatic passive radar," *IEEE Trans. Aerosp. Electron. Syst.*, vol. 48, no. 1, pp. 572-580, Jan. 2012.

[53] Chen, C.-T., and Millero, F. "Speed of sound in seawater at high pressures," *J. Acoust. Soc. Amer.*, vol. 62, no. 5, pp. 1129-1135, 1977.

[54] MacKenzie, K. V. "Nine-term equation of sound speed in the oceans," *J. Acoust. Soc. Amer.*, vol. 70, pp. 807-812, 1981.

[55] Grimmett, D., and Coraluppi, S. "Contact-level multistatic sonar data simulator for tracker performance assessment," in *Proc. IEEE Int. Conf. Inform. Fusion*, Florence, Italy, Jul. 2006, pp. 1-7.

[56] Grimmett, D. "SPECSweb multistatic tracking on a truth-blind simulated scenario of the MSTWG," in *Proc. IEEE Int. Conf. Inform. Fusion*, Seattle, WA, Jul. 2009, pp. 1568-1575.

[57] Reed, C. W., Hudson, R., and Yao, K. "Direct joint source localization and propagation speed estimation," in *Proc. IEEE Int. Conf. on Acoust., Speech, and Signal Process.*, Phoenix, AZ, Mar. 1999, pp. 1169-1172.

[58] Mahajan, A., and Walworth, M. "3-D position sensing using the differences in the time-of-flights from a wave source to various receivers," *IEEE Trans. Robot. Autom.*, vol. 17, pp. 91-94, Feb. 2001.

[59] Zheng, J., Lui, K. W. K., and So, H. C. "Accurate three-step algorithm for joint source position and propagation speed estimation," *Signal Process.*, vol. 87, pp. 3096-3100, Dec. 2007.

[60] Y. Qi, H. Kobayashi, and H. Suda, "Analysis of wireless geolocation in a non-line-of-sight environment," *IEEE Trans. Wireless Commun.*, vol. 5, no. 3, pp. 672-681, Mar. 2006.

[61] S. Gezici, H. Kobayashi, and H. Poor, "Nonparametric non-line-of-sight identification," in *Proc. IEEE Veh. Tech. Conf.*, Orlando, FL, Oct. 2003, pp. 2544-2548.

[62] J. Borras, P. Hatrack, and N. B. Mandayam, "Decision theoretic framework for NLOS identification," in *Proc. IEEE Veh. Tech. Conf.*, Ottawa, Canada, May, 1998, pp. 1583-1587.

[63] P. Meissner, C. Steiner, and K. Witrisal, "UWB positioning with virtual anchors and floor plan information," in *Proc. Workshop on Positioning, Navigation and Commun.*, Dresden, Germany, Mar. 2010, pp. 150-156.

[64] V. La Tosa, B. Denis, and B. Uguen, "Joint anchor-less tracking and room dimensions estimation through IR-UWB peer-to-peer communications," in *Proc. IEEE Int. Conf. on Utra-Wideband*, Bologna, Italy, Sep. 2011, pp. 575-579.

[65] P. Meissner, T. Gigl, and K. Witrisal, "UWB sequential Monte Carlo positioning using virtual anchors," in *Proc. Int. Conf. on Indoor Positioning and Indoor Navigation*, Zurich, Switzerland, Sep. 2010, pp. 1-10.

[66] M. Shimizu, T. Fujiwara, and S. Uebayashi, "Study of TOA positioning using UWB reflected waves," in *Proc. IEEE Veh. Tech. Conf.*, Yokohama, Japan, May 2012, pp. 1-5.

[67] L. W. Fullerton, M. D. Roberts, W. M. Einhorn, K. Loum, I. Dodoukh, and S. S. O'Hanian, "Method and system for extensible position location," U.S. Patent US 7,602,339 B2, Oct. 13, 2009.

[68] M. Rydstrom, E. Strom, A. Svensson, and L. Reggiani, "An algorithm for positioning relays and point scatterers in wireless systems," *IEEE Signal Process. Lett.*, vol. 15, pp. 381-384, Mar. 2008.

[69] L. Reggiani, M. Rydstrom, G. Tiberi, E. G. Strom, and A. Monorchio, "Ultra-wide band sensor networks for tracking point scatterers or relays," in *Proc. 2009 Int. Symp. on Wireless Commun. Syst.*, Tuscany, Italy, Sep. 2009, pp. 1-5.

[70] N. Decarli, A. Guerra, A. Conti, R. D'Errico, A. Sibille, D. Dardari, "Non-regenerative relaying for network localization," *IEEE Trans. Wireless Commun.*, vol. 13, no. 1, pp. 174-185, Jan. 2014.

[71] M. Sandys-Wunsch and M. G. Hazen, "Multistatic localization error due to receiver positioning errors," *IEEE J. Ocean. Eng.*, vol. 27, no. 2, pp. 328-334, Apr. 2002.

[72] D. S. Bernstein, *Matrix Mathematics: Theory, Facts, and Formulas.* Princeton, NJ: Princeton University Press, 2005.

[73] K. W. K. Lui, W. Ma, H. C. So, and F. K. W. Chan, "Semi-definite programming algorithms for sensor network node localization with uncertainties in anchor positions and/or propagation speed," *IEEE Trans. Signal Process.*, vol. 57, no. 2, pp. 752-763, Feb. 2009.

[74] L. M. Kaplan, "Global node selection for localization in a distributed sensor network," *IEEE Trans. Aerosp. Electron. Syst.*, vol. 42, no. 1, pp. 113-135, Jan. 2006.

[75] L. M. Kaplan, "Local node selection for localization in a distributed sensor network," *IEEE Trans. Aerosp. Electron. Syst.*, vol. 42, no. 1, pp. 136-146, Jan. 2006.

[76] X. Wang, M. Fu, and H. Zhang, "Target tracking in wireless sensor networks based on the combination of KF and MLE using distance measurements," *IEEE Trans. Mobile Computing*, vol. 11, no. 4, pp. 567-576, Apr. 2012.

[77] P. Suchomski, "Explicit expressions for debiased statistics of 3D converted measurements," *IEEE Trans. Aerosp. Electron. Syst.*, vol. 35, no. 1, pp. 368-370, Jan. 1999.

[78] K. Dogancay, "UAV path planning for passive emitter localization," *IEEE Trans. Aerosp. Electron. Syst.*, vol. 48, no. 2, pp. 1150-1166, Apr. 2012.

[79] R. Bellman, *Introduction to Matrix Analysis.* New York, NY: McGraw-Hill, 1960.

[80] Y. Rockah and P. M. Schultheiss, "Array shape calibration using source in unknown locations - part I: Far-field sources," *IEEE Trans. Acoust., Speech, Signal Process.*, vol. ASSP-35, no. 3, pp. 286-299, Mar. 1987.

[81] Y. Rockah and P. M. Schultheiss, "Array shape calibration using source in unknown locations - part II: Near-field sources and estimator implementation," *IEEE Trans. Acoust., Speech, Signal Process.*, vol. ASSP-35, no. 6, pp. 724-735, Jun. 1987.

[82] P. S. Bullen, *Handbook of Means and Their Inequalities.* Portland, OR: Book News, 2004.

[83] K. Noh, Q. M. Chaudhari, E. Serpedin, and B. W. Suter, "Novel clock phase offset and skew estimation using two-way timing message exchanges for wireless sensor networks," *IEEE Trans. Commun.*, vol. 55, pp. 766-777, Apr. 2007.

[84] Z. Sahinoglu, "Improving range accuracy of IEEE 802.15.4a radios in the presence of clock frequency offsets," *IEEE Commun. Lett.*, vol. 15, no. 2, pp. 244-246, Feb. 2011.

[85] B. Denis, J.-B. Pierrot, and C. Abou-Rjeily, "Joint distributed synchronization and positioning in UWB ad hoc networks using ToA," *IEEE Trans. Microw. Theory Tech.*, vol. 54, no. 4, pp. 1896-1911, Jun. 2006.

[86] A. J. Weiss and J. S. Picard, "Network localization with biased range measurements," *IEEE Trans. Wireless Commun.*, vol. 7, no. 1, pp. 298-304, Jan. 2008.

[87] J. Liu, Y. Zhang, and F. Zhao, "Robust distributed node localization with error management," in *Proc. ACM Int. Symp. Mobile Ad Hoc Networking and Computing*, Florence, Italy, May 2006, pp. 250-261.

[88] S. Srirangarajan, A. H. Tewfik, and Z. Luo, "Distributed sensor network localization using SOCP relaxation," *IEEE Trans. Wireless Commun.*, vol. 7, no. 12, pp. 4886-4895, Dec. 2008.

[89] L. Yang and K. C. Ho, "An approximately efficient TDOA localization algorithm in closed-form for locating multiple disjoint sources with erroneous sensor positions," *IEEE Trans. Signal Process.*, vol. 57, pp. 4598-4615, Dec. 2009.

[90] S. Gezici, Z. Tian, G. B. Giannakis, H. Kobayashi, A. F. Molisch, H. V. Poor, and Z. Sahinoglu, "Localization via ultra-wideband radios," *IEEE Signal Process. Mag.*, vol. 22, no. 4, pp. 70-84, Jul. 2005.

[91] H. L. Van Trees and K. L. Bell, *Bayesian Bounds for Parameter Estimation and Nonlinear Filtering/Tracking*. IEEE Press, John Wiley & Sons, 2007.

[92] M. Maroti, B. Kusy, G. Simon, and A. Ledeczi, "The flooding time synchronization protocol," in *Proc. SenSys 04*, Baltimore, MD, Nov. 2004, pp. 39-49.

[93] Q. Zou, A. Tarighat, and A. H. Sayed, "Performance analysis and range improvement in multiband-OFDM UWB communications," in *Proc. IEEE ICASSP*, Toulouse, France, May 2006, pp. 629-632.

[94] J. Farrell, T. Givargis, and M. Barth, "Real-time differential carrier phase GPS-aided INS," *IEEE Trans. Contr. Syst. Technol.*, vol. 8, pp. 709-721, Jul. 2000.

[95] J. Mannermaa, K. Kalliomaki, T. Mansten, and S. Turunen, "Timing performance of various GPS receivers," in *Proc. IEEE Int. Frequency Contr. Symp., 1999*, Besancon, France, Apr. 1999, pp. 287-290.

[96] Coraluppi, S., and Carthel, C. "Distributed tracking in multistatic sonar", *IEEE Trans. Aerosp. Electron. Syst.*, vol. 41, no. 3, pp. 1138-1147, Jul. 2005.

[97] Kim, S., Ku, B., Hong, W., and Ko, H. "Performance comparison of target localization for active sonar systems," *IEEE Trans. Aerosp. Electron. Syst.*, vol. 44, no. 4, pp. 1371-1380, Oct. 2008.

[98] Bishop, A., Anderson, B. D. O., Fidan, B., Pathirana, P. N., and Mao, G. "Bearing-only localization using geometrically constrained optimization," *IEEE Trans. Aerosp. Electron. Syst.*, vol. 45, no. 1, pp. 308-320, Jan. 2009.

[99] Owsley, N. L. "Source location with an adaptively focused array," in *Proc. IEEE Conf. on Decision and Control including the Symp. on Adaptive Process.*, Albuquerque, NM, Dec. 1980, pp. 945-948.

[100] Ehlers, F., Daun, M., and Ulmke, M. "System design and fusion techniques for multistatic active sonar," in *Proc. OCEANS - EUROPE*, Bremen, Germany, May 2009, pp. 1-10.

[101] Messer, H. "The hybrid Cramer-Rao lower bound−from practice to theory," in *Proc. IEEE Workshop Sensor Array Multichannel Process.*, Waltham, MA, Jul. 2006, pp. 304-307.

[102] Noam, Y., and Messer, H. "The hybrid Cramer-Rao bound and the generalized Gaussian linear estimation problem," in *Proc. IEEE Workshop Sensor Array Multichannel Process.*, Darmstadt, Germany, Jul. 2008, pp. 395-399.

[103] Hall, R. L. "Inverse moments for a class of truncated normal distributions," *Sankhya*, vol. 41, pp. 66-76, May 1979.

[104] Lai, C. D., Wood, G. R., and Qiao, C. G. "The mean of the inverse of a punctured normal distribution and its application," *J. Biometrical*, vol. 46, no. 4, pp. 420-429, 2004.

[105] U. Niesen, D. Shah, and G. W. Wornell, "Adaptive Alternating Minimization Algorithms," *IEEE Trans. Inf. Theory*, vol.55, no.3, pp. 1423-1429, Mar. 2009.

[106] B. A. Berg, *Markov Chain Monte Carlo Simulations and Their Statistical Analysis.* Hackensack, NJ: World Scientific, 2004.

[107] X. Lu and K. C. Ho, "Taylor-series technique for source localization using AoAs in the presence of sensor location errors," in *Proc. IEEE Sensor Array and Multichannel Process. Workshop*, Waltham, MA, Jul. 2006, pp. 190-194.

[108] Stoica, P., and Sharman, K. "Maximum likelihood methods for direction of arrival estimation," *IEEE Trans. Acoust., Speech, Signal Process.*, vol. ASSP-38, pp. 1132-1143, Jul. 1990.

VITA

Liyang Rui was born in Tianjin, China. He received the Bachelor of Engineering and Master of Engineering both in Electrical Engineering, from Beihang University, Beijing, China in 2006 and 2009 respectively. He received the PhD degree in Electrical and Computer Engineering from University of Missouri in 2015. His research interests include source localization, detection and estimation, audio signal processing, statistical and digital signal processing theory, and their applications to the health care industry.